SANDIA REPORT

SAND2009-7189
Unlimited Release
Printed November 2009

Reduced Order Modeling of Fluid/Structure Interaction

Matthew F. Barone, Irina Kalashnikova, Matthew R. Brake, and
Daniel J. Segalman

Prepared by
Sandia National Laboratories
Albuquerque, New Mexico 87185 and Livermore, California 94550

Sandia is a multiprogram laboratory operated by Sandia Corporation,
a Lockheed Martin Company, for the United States Department of Energy's
National Nuclear Security Administration under Contract DE-AC04-94-AL85000.

Issued by Sandia National Laboratories, operated for the United States Department of Energy by Sandia Corporation.

Available to DOE and DOE contractors from
U.S. Department of Energy
Office of Scientific and Technical Information
P.O. Box 62
Oak Ridge, TN 37831

Telephone: (865) 576-8401
Facsimile: (865) 576-5728
E-Mail: reports@adonis.osti.gov
Online ordering: http://www.osti.gov/bridge

Available to the public from
U.S. Department of Commerce
National Technical Information Service
5285 Port Royal Rd
Springfield, VA 22161

Telephone: (800) 553-6847
Facsimile: (703) 605-6900
E-Mail: orders@ntis.fedworld.gov
Online ordering: http://www.ntis.gov/help/ordermethods.asp?loc=7-4-0#online

SAND2009-7189
Unlimited Release
Printed November 2009

Reduced Order Modeling of Fluid/Structure Interaction

Matthew F. Barone – Wind Energy Technology Department
Irina Kalashnikova [*]– Aerosciences Department
Matthew R. Brake – Component Science and Mechanics Department
Daniel J. Segalman – Strategic Initiatives Department

Sandia National Laboratories
P.O. Box 5800
Albuquerque, NM 87185

Abstract

This report describes work performed from October 2007 through September 2009 under the Sandia Laboratory Directed Research and Development project titled "Reduced Order Modeling of Fluid/Structure Interaction." This project addresses fundamental aspects of techniques for construction of predictive Reduced Order Models (ROMs). A ROM is defined as a model, derived from a sequence of high-fidelity simulations, that preserves the essential physics and predictive capability of the original simulations but at a much lower computational cost. Techniques are developed for construction of provably stable linear Galerkin projection ROMs for compressible fluid flow, including a method for enforcing boundary conditions that preserves numerical stability. A convergence proof and error estimates are given for this class of ROM, and the method is demonstrated on a series of model problems. A reduced order method, based on the method of quadratic components, for solving the von Karman nonlinear plate equations is developed and tested. This method is applied to the problem of nonlinear limit cycle oscillations encountered when the plate interacts with an adjacent supersonic flow. A stability-preserving method for coupling the linear fluid ROM with the structural dynamics model for the elastic plate is constructed and tested. Methods for constructing efficient ROMs for nonlinear fluid equations are developed and tested on a one-dimensional convection-diffusion-reaction equation. These methods are combined with a symmetrization approach to construct a ROM technique for application to the compressible Navier-Stokes equations.

[*]Also with the Institute for Computational and Mathematical Engineering, Stanford University, Stanford, CA 94305

Acknowledgments

The authors gratefully acknowledge Thuan Lieu and Charbel Farhat of Stanford University for providing the AERO-F code along with generous amounts of user-support. This work was funded by Sandia National Laboratories' Laboratory Directed Research and Development (LDRD) program from Fiscal Year 2007 through Fiscal Year 2009.

Contents

Figures

1 Introduction

The contemporary engineering analyst has at his or her disposal an increasingly sophisticated collection of computational tools. These "high-fidelity" simulation tools include finite element, finite volume, and finite difference codes for computing three-dimensional fluid flows and dynamics of complex structures. Yet, even as such tools mature and expansion of computational resources makes them more accessible, these tools are often still computationally expensive for use in a design or analysis setting. Modern engineered systems are often complex, possessing many design variables and/or uncertainties. There is a continuing push within the Department of Energy laboratories and other scientific and engineering communities to address the quantification of uncertainties in models of physical systems. Emphasis on uncertainty quantification, optimal design, or parametric studies leads to requirements for relatively large numbers of analysis points, which is often not compatible with the computational expense of high-fidelity simulation approaches.

This situation has led researchers in mathematics and engineering to propose simulation techniques that retain the essential physics and dynamics captured by a high-fidelity model, but at a much lower computational cost. These efforts have created a large and growing area of research termed Reduced Order Modeling, also called Model Reduction. The basic idea in most Reduced Order Modeling approaches is to use a relatively small number of solutions generated by a high-fidelity model to construct a computationally cheaper model. In order to be successful, the Reduced Order Model (ROM) must be predictive across the design or parameter space of interest. In this discussion we assume that the high-fidelity model itself meets the requirements for accuracy and predictive capability for the problem of interest.

In order for a ROM of a dynamical system to be predictive, it must retain the essential dynamics contained within the high-fidelity simulations. In most applications of ROMs to date, this requirement is evaluated *a posteriori*. That is, the ROM is constructed, then used to predict some dynamical behavior. If the solutions generated by the ROM are numerically stable and accurately reproduce expected behavior, the model is declared a success. This "try and see" approach to model reduction certainly has many success stories. However, for ROMs to serve as reliable predictive tools, their numerical properties must be better characterized, and methods for building numerically stable and convergent ROMs must be developed.

The present research program was initiated under the Sandia National Laboratories' Laboratory Directed Research and Development (LDRD) program to address reduced order modeling for coupled fluid-structure systems. Such physical systems are of interest in many Sandia applications, including analysis of flight vehicle aero-elastic stability, space vehicle vibrations during atmospheric flight, and wind turbine aero-elastic modeling. The overall approach of this effort was to use existing techniques for ROM construction of such systems as a starting point, and to explore whether these techniques could be modified to create ROMs with improved predictive capability. This research was carried out under two parallel tracks: one for creating ROMs for fluid dynamics problems, and the other for creating ROMs for thin shelled, nonlinear structures. Methods for coupling the two fluid and structural ROMs were also developed. Each chapter of this report describes one element of this research.

In Section 2, the problem of constructing a numerically stable ROM for linearized, compressible flow is addressed. ROMs of fluid systems linearized about some (non-linear) base flow are useful when used as a component of an aero-elastic stability analysis, or for some other types of small-perturbation analyses, including aero-acoustic problems. A new method for creating a projection ROM is developed that preserves numerical stability and allows for the development of error estimates for the ROM.

In Section 3, a new technique is developed for model reduction of thin plates with nonlinear in-plane stresses. The method of Quadratic Components is introduced to reduce the number of required degrees of freedom while still capturing the essential non-linear plate dynamics. This model is coupled with a simple aerodynamic model and with a method to compute nonlinear limit cycle behavior of an unstable panel flutter solution.

In Section 4, the numerical stability of a coupled ROM combining the linearized fluid/structure ROMs of Sections 2 and 3 is studied using energy methods. Stability is proven for the coupled linearized system when a specific penalty term is introduced.

Section 5 returns to techniques for building fluid ROMs, but now with a focus on the compressible Navier-Stokes equations. The nonlinearity of the Navier-Stokes equations presents a challenge for developing provably stable ROMs. This challenge is addressed by the introduction of a ROM projection technique that leads to a model that obeys the second law of thermodynamics. In this way, the ROM preserves an essential stability property of the governing equations, that of non-decreasing entropy in the solution. The treatment of the nonlinear terms in the Navier-Stokes equations is handled using a Best-Points interpolation algorithm. This approach is tested on a model convection-diffusion-reaction system of equations.

2 Stable Reduced Order Models for Linearized Compressible Flow

2.1 Introduction

Simulation of time-varying, three-dimensional fluid flow remains, and will continue to remain for some time, an expensive endeavor. This reality has motivated efforts to seek reduced order models (ROMs) that capture the essential dynamics of the full simulations, but at a much lower computational cost. Many ROM techniques in fluid mechanics are derived from the Proper Orthogonal Decomposition (POD)/Galerkin projection approach [1, 2, 3]. The original intent of this approach was to develop low-dimensional models, containing only a few degrees of freedom, to enable and enhance understanding of the nonlinear dynamics of turbulent flows. Since then, other approaches to building ROMs have been proposed, each with its own inherent strengths, including the reduced basis method [4], balanced truncation [5, 6], and goal-oriented ROMs [7]. The potential usefulness of ROMs has also since expanded to include predictive applications; for example, ROMs have been used in flow controller design [8], shape optimization [9], and aeroelastic stability analysis [10, 11].

The use of POD/Galerkin ROMs in a predictive setting raises fundamental questions regarding numerical properties of the resulting models. In this setting the ROM may be viewed as an alternative discretization of the governing partial differential equations. As such, the essential properties of any such discretization are stability, consistency, and convergence. In many situations satisfaction of the first two properties guarantees convergence. General results for any of the three properties are lacking for POD/Galerkin models of compressible fluid flow. This leads to practical limitations; for example, a ROM might be stable for a given number of modes, but unstable for other choices of basis size (see an example of this for a POD model in Bui-Thanh *et al.* [7]).

The present section addresses numerical stability of linear ROMs for compressible flow. Convergence of the ROM solutions is also examined, which reveals certain requirements on consistency of the basis. A POD basis, or any other empirical basis, is not usually complete, which complicates a general consistency analysis. Not addressed herein is the related question of the behavior of a ROM when applied to a parameter space region not included in the ROM construction. There are promising developments in this area which can be applied; see, for example, Lieu and Farhat [12]. Despite the lack of a comprehensive numerical theory, it is still desirable to be able to generate a stable ROM regardless of the quality of the POD basis used to generate it. This is analagous to being able to run computational fluid dynamics (CFD) simulations on a series of meshes, from coarse to fine, and having confidence that the simulations will remain stable regardless of the mesh spacing.

Stable formulations for reduced order models have been proposed in other settings. Stability of reduced order models for electrical circuit analysis is considered by Freund and co-workers [13]. Preservation of the passivity, or energy dissipation, of the circuit system guarantees stability of the reduced order model. In fluid dynamics, Kwasniok [14] recognized the role of energy conservation in ROMs of nonlinear, incompressible fluid flow for atmospheric modeling applications.

The Galerkin projection approach is constructed so that the nonlinear terms in the ROM conserve turbulent kinetic energy or turbulent enstrophy.

These works and others demonstrate the importance of maintaining the proper energy balance in a reduced order model. Mathematically, the energy is expressed as an inner product, so that the stability of a reduced order model is often tied to the definition of this inner product. Rowley *et al.* [15] examined different choices for the inner product that approximately conserve total energy or total enthalpy for compressible flow. Rowley [6] has shown how balanced truncation may be viewed as a particular form of the POD, using the observability Gramian as an inner product. Balanced truncation and balanced POD methods are guaranteed to be stable for linear systems, and also preserve the stability of an equilibrium point at the origin for nonlinear systems.

Although these and other advancements have led to a better understanding of the stability properties of reduced order models, error quantification and convergence analysis of ROMs has yet to be placed on a complete mathematical footing. One difficulty in quantifying the error in a ROM is that the span of the POD basis is not complete in the Hilbert space to which the exact solution belongs; it is only complete in the space defined by the numerical solutions used to generate it, and only in an *average* sense. Since the POD basis contains only information of the kinematics of the flow field that were already encoded in the observations, it cannot be expected to contain all the features present in the exact analytical solution. Several attempts at error estimation in the context of ROMs have been made. A general convergence result can be found in [16], where it is shown that as the reduced basis is enriched, the state error in a steady reduced model is strictly monotone decreasing. More specific convergence estimates are derived in [17, 18]. In [17], Rathinam and Petzold provide an error analysis of the POD method applied to a general non-linear dynamical system. In [18], Kunisch and Volkwein propose a strategy to describe and analyze convergence approximations based on POD approximation in space and backwards Euler discretization in time for nonlinear parabolic systems arising in fluid dynamics.

In the present work, described also in [19] and [20], we again demonstrate that the inner product used to define the Galerkin projection is closely tied to the stability of the resulting model. We further show how it is possible to construct stable ROMs for *any* choice of basis using Galerkin projection. An energy stability analysis is carried out for Galerkin methods applied to the linearized Euler equations, resulting in an inner product that guarantees certain stability bounds satisfied by the ROM. We show that appropriate boundary treatment is crucial to ensuring a well-posed initial boundary value problem (IBVP) for the governing equations, and we give sufficient conditions for a set of boundary conditions for a ROM to be well-posed and stable. Solid wall and non-reflecting far-field boundary conditions are formulated, and a means of implementing these boundary conditions in a way that preserves the stability of the ROM is developed. *A priori* error estimates for the computed ROM solution relative to the CFD solution and the exact analytical solution are then derived. Numerical implementation of the ROM is defined in terms of finite element representations of the simulation data and of the POD modes. Along with numerical quadrature rules of sufficient accuracy, this approach ensures that the continuous stability estimates are satisfied by the discrete computer implementation. ROMs are then constructed for several model fluid flows using the schemes developed from the numerical analysis.

2.2 The Proper Orthogonal Decomposition (POD)/Galerkin Method for Model Reduction

Before turning our attention to the equations of interest, namely the linearized compressible Euler equations (Section 2.3), we give an overview of the Proper Orthogonal Decomposition (POD)/Galerkin method for reducing the order of a complex physical system governed by a general set of PDEs. The approach consists of two steps:

Step 1: Calculation of a reduced basis using the POD of an ensemble of flow-field realizations.

Step 2: Galerkin projection of the governing (continuous) PDEs onto the basis of POD modes in some appropriate inner product.

In the first step, kinematic information is transferred from the high-fidelity simulation to a relatively small number of modes. In the second step, the full-system dynamics are translated to the implied dynamics of these modes. When successful, the result is a set of time-dependent ordinary differential equations (ODEs) in the modal amplitudes (also referred to as the ROM coefficients) that accurately describes the flow dynamics of the full system of PDEs for some limited set of flow conditions.

Proper Orthogonal Decomposition (POD) and the Method of Snapshots

Discussed in detail in Lumley [21] and Holmes *et. al.* [3], POD is a mathematical procedure that, given an ensemble of data, constructs a basis for that ensemble that is optimal in a well-defined sense. Let $\mathcal{H}(\Omega)$ be a Hilbert space with associated inner product $(\cdot,\cdot)$, and let $\{\mathbf{u}^k(\mathbf{x})\} \subset \mathcal{H}(\Omega)$ be an ensemble of real vector fields on a domain $\Omega \subset \mathbb{R}^3$. In the present context, the ensemble $\{\mathbf{u}^k(\mathbf{x}) : k = 1,\ldots,N\}$ is a set of N instantaneous snapshots (in time) of a CFD numerical solution field. A POD basis of order $M << N$ is a set of functions $\{\boldsymbol{\phi}_i : i = 1,2,\ldots,M\}$ that is the "best" linear basis for describing the original ensemble. Mathematically, POD seeks an M-dimensional ($M << N$) subspace $\mathcal{H}^M(\Omega) \subset \mathcal{H}(\Omega)$ spanned by the set $\{\boldsymbol{\phi}_i\}$ such that the projection of the difference between the ensemble $\mathbf{u}^k$ and its projection onto $\mathcal{H}^M(\Omega)$ is minimized on average; that is, it seeks the set $\{\boldsymbol{\phi}_i\}$ that solves the following constrained optimization problem:

$$\begin{array}{ll} \min_{\{\boldsymbol{\phi}_i\}_{i=1}^M} & \langle ||\mathbf{u}^k - \Pi_M \mathbf{u}^k||^2 \rangle \\ \text{subject to} & (\boldsymbol{\phi}_i, \boldsymbol{\phi}_j) = \delta_{ij},\ 1 \le i \le M, 1 \le j \le i \end{array} . \tag{1}$$

Here, $\langle\cdot\rangle$ is a discrete averaging operator, e.g., $\langle ||\mathbf{u}^k||^2 \rangle \equiv \frac{1}{N}\sum_{k=1}^N ||\mathbf{u}^k||^2$, and $\Pi_M : \mathcal{H}(\Omega) \to \mathcal{H}^M(\Omega)$ is an orthogonal projection operator onto the subspace $\mathcal{H}^M(\Omega)$, satisfying properties 1–6 in Section A.1 of the Appendix. In the context of the ROM, a natural definition of Π_M is, for $\mathbf{u} \in \mathcal{H}(\Omega)$,

$$\Pi_M \mathbf{u} = \sum_{k=1}^{M} (\boldsymbol{\phi}_k, \mathbf{u})\, \boldsymbol{\phi}_k. \tag{2}$$

The numerical ROM solution $\mathbf{u}_M$ can be represented as a linear combination of POD modes

$$\mathbf{u}_M(\mathbf{x},t) = \sum_{j=1}^{M} a_j(t)\boldsymbol{\phi}_j(\mathbf{x}), \tag{3}$$

where the $a_j(t)$ are the temporally-varying ROM coefficients, to be solved for in the linear dynamical system arising in the ROM (Section 2.2).

It is a well-known result [3] that the solution to (1) reduces to the eigenvalue problem

$$\mathcal{R}\boldsymbol{\phi} = \lambda\boldsymbol{\phi}, \tag{4}$$

where

$$\mathcal{R} \equiv \langle \mathbf{u}^k \otimes \mathbf{u}^k \rangle = \frac{1}{N}\sum_{k=1}^{N} \left(\mathbf{u}^k \otimes \mathbf{u}^k \right) \tag{5}$$

The operator $\mathcal{R}$ is self-adjoint and positive semi-definite. If one further assumes that $\mathcal{R}$ is compact, then there exists a countable set of non-negative eigenvalues λ_i with associated eigenfunctions $\boldsymbol{\phi}_i$. These eigenfunctions form an orthonormal subspace of $\mathcal{H}(\Omega)$, namely $\mathcal{H}^M(\Omega)$. In building a ROM, one is interested in truncating the POD basis and retaining only the $M << N$ most energetic modes. It can be shown [3, 21] that the set of M eigenfunctions, or POD modes, $\{\boldsymbol{\phi}_i : i = 1,2,\ldots,M\}$ corresponding to the M largest eigenvalues of $\mathcal{R}$ is precisely the set of $\{\boldsymbol{\phi}_i\}$ that solves (1), and that the minimum value of the objective function in (1) is

$$\langle ||\mathbf{u}^k - \Pi_M \mathbf{u}^k||^2 \rangle = \frac{1}{N}\sum_{k=1}^{N} ||\mathbf{u}^k - \Pi_M \mathbf{u}^k||^2 = \sum_{j=M+1}^{N} \lambda_j. \tag{6}$$

Here, $\lambda_1 \geq \cdots \geq \lambda_M \geq \cdots \geq \lambda_N$ are the ordered eigenvalues of $\mathcal{R}$, so that λ_N is the smallest non-zero eigenvalue of $\mathcal{R}$. The truncated basis $\{\boldsymbol{\phi}_i : i = 1,2,\ldots,M\}$ is optimal in the sense that it describes more energy (on average) of the ensemble than any other linear basis of the same dimension M. The compression of the ensemble energy into a minimum number of modes is what makes the POD basis attractive for reduced order modeling. We emphasize that the POD basis $\{\boldsymbol{\phi}_i : i = 1,2,\ldots,M\}$ just described is *not* complete in $\mathcal{H}(\Omega)$. It is, however, complete in an average sense, that is $\left\langle \left|\left| \mathbf{u}^k - \sum_j (\mathbf{u}^k, \boldsymbol{\phi}_j)\boldsymbol{\phi}_j \right|\right| \right\rangle = 0$ for $M = N$.

Note that bases other than POD could be used in constructing the ROM using the present model reduction technique, and in fact, the stability results presented in this work do not depend on the choice of basis. To show convergence of the ROM to an exact solution, however, one must choose a basis whose span contains the exact solution.

Galerkin Projection

The second step in constructing a ROM involves projecting the governing system of PDEs onto the POD basis $\{\boldsymbol{\phi}_i\}$ in the inner product $(\cdot,\cdot)$ defining the Hilbert space $\mathcal{H}(\Omega)$. Suppose the governing system of equations for the state variable vector $\mathbf{u}$ has the form

$$\frac{\partial \mathbf{u}}{\partial t} = \mathcal{L}\mathbf{u} + \mathcal{N}_2(\mathbf{u},\mathbf{u}) + \mathcal{N}_3(\mathbf{u},\mathbf{u},\mathbf{u}), \tag{7}$$

where $\mathcal{L}$ is a linear differential operator, and $\mathcal{N}_2$ and $\mathcal{N}_3$ are (non-linear) quadratic and cubic operators respectively. Then, the Galerkin projection of (7) onto the POD mode $\boldsymbol{\phi}_j$ for $j = 1, 2, ..., M$ is

$$\left(\boldsymbol{\phi}_j, \frac{\partial \mathbf{u}}{\partial t}\right) = \left(\boldsymbol{\phi}_j, \mathcal{L}\mathbf{u}\right) + \left(\boldsymbol{\phi}_j, \mathcal{N}_2(\mathbf{u}, \mathbf{u})\right) + \left(\boldsymbol{\phi}_j, \mathcal{N}_3(\mathbf{u}, \mathbf{u}, \mathbf{u})\right). \tag{8}$$

Substituting the POD decomposition of $\mathbf{u}$ (3) into (8) and applying the orthonormality property of the basis functions $\boldsymbol{\phi}_i$ gives, for $j = 1, 2, \ldots, M$

$$\dot{a}_j = \sum_{l=1}^{M} a_l(\boldsymbol{\phi}_j, \mathcal{L}(\boldsymbol{\phi}_l)) + \sum_{l=1}^{M}\sum_{m=1}^{M} a_l a_m(\boldsymbol{\phi}_j, \mathcal{N}_2(\boldsymbol{\phi}_l, \boldsymbol{\phi}_m)) + \sum_{l=1}^{M}\sum_{m=1}^{M}\sum_{n=1}^{M} a_l a_m a_n(\boldsymbol{\phi}_j, \mathcal{N}_3(\boldsymbol{\phi}_l, \boldsymbol{\phi}_m, \boldsymbol{\phi}_n)), \tag{9}$$

where the "$\cdot$" operator denotes differentiation in time $\left(\text{that is, } \dot{a}_j \equiv \frac{da_j}{dt}\right)$. (9) is a non-linear time-dependent system of M ODEs for the time-dependent ROM coefficients; it is the reduced order model for (7) by the POD/Galerkin method. In practice, the inner products in (9) will be integrals of products of the known, time-independent POD modes $\boldsymbol{\phi}_j$ and may be precomputed before time-integration of the ROM.

We emphasize that, in the ROM presented herein, the Galerkin projection step is applied to the *continuous* system of PDEs. In many applications of reduced order modeling, a *discrete* approximation of the equations is projected onto the POD modes. This discrete approach has the advantage that, depending on the implementation, boundary condition terms present in the discretized equation set are inherited by the ROM. Additionally, certain properties of the numerical scheme used to solve the full equations may be inherited by the ROM. The continuous approach, on the other hand, is appealing in that it does not require an intrusive or code-specific implementation. It is also similar in procedure to spectral numerical approximation methods, allowing the use of analysis techniques employed by the spectral methods community.

2.3 The Governing Fluid Equations

Linearized Euler Equations for Compressible Flow

Let $\mathbf{q}^T \equiv \begin{pmatrix} u_1 & u_2 & u_3 & \zeta & p \end{pmatrix} \in \mathbb{R}^5$ denote the vector of fluid state variables. Here, u_1, u_2 and u_3 are the x_1-, x_2-, and x_3-components of the velocity vector $\mathbf{u}^T \equiv \begin{pmatrix} u_1 & u_2 & u_3 \end{pmatrix}$, p is the fluid pressure, and $\zeta \equiv 1/\rho$ is the specific volume of the fluid (ρ denoting the fluid density).

The governing fluid equations are the compressible Euler equations, linearized about a base state $\bar{\mathbf{q}}$. Splitting the state variable vector $\mathbf{q}$ into a steady mean plus a fluctuation ($\mathbf{q}(\mathbf{x}, t) = \bar{\mathbf{q}}(\mathbf{x}) + \mathbf{q}'(\mathbf{x}, t)$), substitution of this form into the full Euler equations, and retaining only first order terms in the fluctuating quantities results in

$$\frac{\partial \mathbf{q}'}{\partial t} + \underbrace{\mathbf{A}_i \frac{\partial \mathbf{q}'}{\partial x_i} + \mathbf{C}\mathbf{q}'}_{\equiv \mathcal{L}\mathbf{q}'} = \mathbf{0} \tag{10}$$

where

$$\mathbf{A}_1 \equiv \mathbf{A}_1(\bar{\mathbf{q}}) = \begin{pmatrix} \bar{u}_1 & 0 & 0 & 0 & \bar{\zeta} \\ 0 & \bar{u}_1 & 0 & 0 & 0 \\ 0 & 0 & \bar{u}_1 & 0 & 0 \\ -\bar{\zeta} & 0 & 0 & \bar{u}_1 & 0 \\ \gamma\bar{p} & 0 & 0 & 0 & \bar{u}_1 \end{pmatrix}, \quad \mathbf{A}_2 \equiv \mathbf{A}_2(\bar{\mathbf{q}}) = \begin{pmatrix} \bar{u}_2 & 0 & 0 & 0 & 0 \\ 0 & \bar{u}_2 & 0 & 0 & \bar{\zeta} \\ 0 & 0 & \bar{u}_2 & 0 & 0 \\ 0 & -\bar{\zeta} & 0 & \bar{u}_2 & 0 \\ 0 & \gamma\bar{p} & 0 & 0 & \bar{u}_2 \end{pmatrix}, \tag{11}$$

$$\mathbf{A}_3 \equiv \mathbf{A}_3(\bar{\mathbf{q}}) = \begin{pmatrix} \bar{u}_3 & 0 & 0 & 0 & 0 \\ 0 & \bar{u}_3 & 0 & 0 & 0 \\ 0 & 0 & \bar{u}_3 & 0 & \bar{\zeta} \\ 0 & 0 & -\bar{\zeta} & \bar{u}_3 & 0 \\ 0 & 0 & \gamma\bar{p} & 0 & \bar{u}_3 \end{pmatrix}$$

$$\mathbf{C} \equiv \mathbf{C}(\bar{\mathbf{q}}, \nabla\bar{\mathbf{q}}) = \begin{pmatrix} \frac{\partial\bar{u}_1}{\partial x_1} & \frac{\partial\bar{u}_1}{\partial x_2} & \frac{\partial\bar{u}_1}{\partial x_3} & \frac{\partial\bar{p}}{\partial x_1} & 0 \\ \frac{\partial\bar{u}_2}{\partial x_1} & \frac{\partial\bar{u}_2}{\partial x_2} & \frac{\partial\bar{u}_2}{\partial x_3} & \frac{\partial\bar{p}}{\partial x_2} & 0 \\ \frac{\partial\bar{u}_3}{\partial x_1} & \frac{\partial\bar{u}_3}{\partial x_2} & \frac{\partial\bar{u}_3}{\partial x_3} & \frac{\partial\bar{p}}{\partial x_3} & 0 \\ \frac{\partial\bar{\zeta}}{\partial x_1} & \frac{\partial\bar{\zeta}}{\partial x_2} & \frac{\partial\bar{\zeta}}{\partial x_3} & -\nabla\cdot\bar{\mathbf{u}} & 0 \\ \frac{\partial\bar{p}}{\partial x_1} & \frac{\partial\bar{p}}{\partial x_2} & \frac{\partial\bar{p}}{\partial x_3} & 0 & \gamma\nabla\cdot\bar{\mathbf{u}} \end{pmatrix} \tag{12}$$

Here, $\mathbf{0} \in \mathbb{R}^5$ is the zero vector, $\gamma = C_P/C_V$ is the ratio of specific heats and $\mathcal{L}$ is a linear operator. The $\{\mathbf{A}_i : i = 1,2,3\}$ matrices are functions of the base flow vector $\bar{\mathbf{q}}$; the matrix $\mathbf{C}$ is a function of $\nabla\bar{\mathbf{q}}$. In the case of uniform base flow, $\nabla\bar{\mathbf{q}} \equiv \mathbf{0}$, so that $\frac{\partial\mathbf{A}_i}{\partial x_i} \equiv \mathbf{0}$ and $\mathbf{C} \equiv \mathbf{0}$.

An initial boundary value problem (IBVP) for (10) on an open bounded domain $\Omega \subset \mathbb{R}^3$ with a connected boundary $\partial\Omega$ will be formulated in Sections 2.4 and 2.5. In typical applications, Ω may contain a fixed or moving solid wall over which the fluid flows. In this context, it is useful to introduce the following partition of $\partial\Omega$

$$\partial\Omega = \partial\Omega_F \cup \partial\Omega_W, \quad \partial\Omega_F \cap \partial\Omega_W = \emptyset \tag{13}$$

into a far-field boundary ($\partial\Omega_F$) and a solid wall boundary ($\partial\Omega_W$).

The Characteristic Variables

It is a well-known fact that the system (10) is hyperbolic. This implies that the tensor $\mathbf{A}_n \equiv \mathbf{A}_1 n_1 + \mathbf{A}_2 n_2 + \mathbf{A}_3 n_3$, for some spatial orientation $\mathbf{n}^T = \begin{pmatrix} n_1 & n_2 & n_3 \end{pmatrix}$, is diagonalizable:

$$\mathbf{A}_n = \mathbf{S}\mathbf{\Lambda}_n\mathbf{S}^{-1}. \tag{14}$$

Here $\mathbf{S}$ is the matrix that diagonalizes $\mathbf{A}_n$ and $\mathbf{\Lambda}_n$ is a diagonal matrix containing the eigenvalues of $\mathbf{A}_n$ (also referred to as the characteristic speeds):

$$\mathbf{\Lambda}_n = \begin{pmatrix} \bar{u}_n & & & & \\ & \bar{u}_n & & & \\ & & \bar{u}_n & & \\ & & & \bar{u}_n + \bar{c} & \\ & & & & \bar{u}_n - \bar{c} \end{pmatrix}, \tag{15}$$

with $\bar{c} = \sqrt{\gamma \bar{p} \bar{\zeta}}$ denoting the speed of sound. Defining $\mathbf{V}' \equiv \mathbf{S}^{-1}\mathbf{q}'$, the linearized Euler equations (10) in these so-called "characteristic" variables are[1]

$$\frac{\partial \mathbf{V}'}{\partial t} + \mathbf{S}^{-1}\mathbf{A}_i\mathbf{S}\frac{\partial \mathbf{V}'}{\partial x_i} + \mathbf{S}^{-1}\mathbf{C}\mathbf{S}\mathbf{V}' = \mathbf{0}. \tag{16}$$

The Symmetrized Equations

A key property of the hyperbolic system (10) is that it is symmetrizable[2]; that is, there exists a symmetric, positive definite matrix $\mathbf{H}$ such that $\{\mathbf{H}\mathbf{A}_i : i = 1,2,3\}$ are all symmetric. The symmetrizer of (10) is given by

$$\mathbf{H} \equiv \mathbf{H}(\bar{\mathbf{q}}) = \begin{pmatrix} \bar{\rho} & 0 & 0 & 0 & 0 \\ 0 & \bar{\rho} & 0 & 0 & 0 \\ 0 & 0 & \bar{\rho} & 0 & 0 \\ 0 & 0 & 0 & \alpha^2\gamma\bar{\rho}^2\bar{p} & \bar{\rho}\alpha^2 \\ 0 & 0 & 0 & \bar{\rho}\alpha^2 & \frac{(1+\alpha^2)}{\gamma\bar{p}} \end{pmatrix}, \tag{17}$$

where α^2 is an arbitrary real, nonzero parameter. Pre-multiplying (10) by the matrix $\mathbf{H}$ yields the following symmetrized system:

$$\frac{\partial(\mathbf{H}\mathbf{q}')}{\partial t} + \mathbf{H}\mathbf{A}_i\frac{\partial \mathbf{q}'}{\partial x_i} + \mathbf{H}\mathbf{C}\mathbf{q}' = \mathbf{0}. \tag{18}$$

Similarly, there exists a positive definite symmetrizer for the governing system of PDEs in the characteristic variables (16), denoted here by $\mathbf{Q}$, which has the property that the matrices

[1]The reader is referred to Section A.2 of the Appendix for explicit expressions of $\mathbf{S}$, $\mathbf{S}^{-1}$ and $\mathbf{V}'$.

[2]Among other hyperbolic systems of interest that are symmetrizable are the nonlinear Euler equations [22], the compressible Navier-Stokes equations [23], and the shallow water equations [24]. Most hyperbolic systems derived from conservation laws can be symmetrized; see Chapter 6 of [25]. A (non-unique) symmetrizer of a matrix (or set of matrices) can be derived using the eigenvectors of the matrix (or matrices), following techniques presented by Gustafsson in [26, 27]. Other symmetric forms of both the linearized Euler and linearized Navier-Stokes equations can be found in Oliger and Sundstrom [28] and in Abarbanel and Gottlieb [29].

$\{\mathbf{QS}^{-1}\mathbf{A}_i\mathbf{S} : i = 1,2,3\}$ are all symmetric:

$$\mathbf{Q} \equiv \mathbf{S}^T\mathbf{HS} = \begin{pmatrix} \bar{\rho} - \bar{\rho}n_1^2(1-\alpha^2\bar{\rho}\bar{p}) & \bar{\rho}n_1n_2(1-\alpha^2\bar{\rho}\bar{p}) & -\bar{\rho}n_1n_3(1-\alpha^2\bar{\rho}\bar{p}) & 0 & 0 \\ \bar{\rho}n_1n_2(1-\alpha^2\bar{\rho}\bar{p}) & \bar{\rho} - \bar{\rho}n_2^2(1-\alpha^2\bar{\rho}\bar{p}) & \bar{\rho}n_2n_3(1-\alpha^2\bar{\rho}\bar{p}) & 0 & 0 \\ -\bar{\rho}n_1n_3(1-\alpha^2\bar{\rho}\bar{p}) & \bar{\rho}n_2n_3(1-\alpha^2\bar{\rho}\bar{p}) & \bar{\rho} - \bar{\rho}n_3^2(1-\alpha^2\bar{\rho}\bar{p}) & 0 & 0 \\ 0 & 0 & 0 & \frac{1}{2}\bar{\rho} & 0 \\ 0 & 0 & 0 & 0 & \frac{1}{2}\bar{\rho} \end{pmatrix}. \tag{19}$$

One may check positive-definiteness of $\mathbf{Q}$ by computing its eigenvalues: $\frac{1}{2}\bar{\rho}, \bar{\rho}, \bar{\rho}, \frac{\gamma\bar{p}}{2\bar{c}^2}, \alpha^2\bar{\rho}^2\bar{p}\gamma$. All of these eigenvalues are necessarily positive, meaning $\mathbf{Q}$ is positive definite for any choice of $\alpha \neq 0$. The symmetrized system in the characteristic variables (16) is

$$\frac{\partial(\mathbf{QV}')}{\partial t} + \mathbf{QS}^{-1}\mathbf{A}_i\mathbf{S}\frac{\partial \mathbf{V}'}{\partial x_i} + \mathbf{QS}^{-1}\mathbf{CSV}' = \mathbf{0}. \tag{20}$$

Symmetry Inner Products

The inner product serves several purposes in the POD/Galerkin procedure. Fundamentally, it helps define the Hilbert space on which the analysis proceeds. It defines the projection of a solution onto the POD basis, and thereby also defines the mathematical quantity that the POD basis optimally represents. It also defines the projection of the governing equations onto the POD basis, which leads to the POD/Galerkin dynamical model.

The inner product is also a mathematical expression for the solution "energy." The majority of POD/Galerkin models for fluid flow use as the governing equation set the incompressible Navier-Stokes equations. For these equations, the natural choice of inner product is the $L^2(\Omega)$ inner product (23). This is because in these models the solution vector is taken to be the velocity vector $\mathbf{u}$, so that $||\mathbf{u}||_{L^2(\Omega)}$ is a measure of the global kinetic energy on the domain Ω. The $L^2(\Omega)$ inner product is therefore physically sensible: the POD modes optimally represent the kinetic energy present in the ensemble from which they are generated. The same is *not* true for the compressible linearized Euler equations (10) with solution vector $\mathbf{q}'$ as defined in Section 2.3. This raises the question of whether there exists a suitable energy inner product for the Euler equations.

As we will show in Section 2.4, an appropriate choice of inner product for the system (10) is a "symmetry inner product". For any symmetric positive definite matrix $\mathbf{M} \in \mathbb{R}^{n\times n}$ and bounded domain $\Omega \subset \mathbb{R}^3$, define the $(\mathbf{M},\Omega)$–inner product and $(\mathbf{M},\Omega)$–norm by:

$$(\mathbf{v}_1,\mathbf{v}_2)_{(\mathbf{M},\Omega)} \equiv \int_\Omega \mathbf{v}_1^T\mathbf{M}\mathbf{v}_2 d\Omega, \quad ||\mathbf{v}||_{(\mathbf{M},\Omega)} \equiv \sqrt{(\mathbf{v},\mathbf{v})_{(\mathbf{M},\Omega)}} \tag{21}$$

for $\mathbf{v}_1,\mathbf{v}_2,\mathbf{v} \in \mathbb{R}^n$. Note that

$$(\mathbf{v}_1,\mathbf{v}_2)_{(\mathbf{M},\Omega)} = (\mathbf{M}^{1/2}\mathbf{v}_1, \mathbf{M}^{1/2}\mathbf{v}_2)_{L^2(\Omega)} \tag{22}$$

where

$$(\mathbf{v}_1,\mathbf{v}_2)_{L^2(\Omega)} \equiv \int_\Omega \mathbf{v}_1^T\mathbf{v}_2 d\Omega \tag{23}$$

is the usual L^2 inner product on Ω and $\mathbf{M}^{1/2}$ is the "square root" factor of $\mathbf{M}$, which exists since $\mathbf{M}$ is positive definite. The set of functions $\mathbf{f}:\Omega\rightarrow\mathbb{R}^n$ such that $||\mathbf{f}||_{(\mathbf{M},\Omega)}<\infty$ taken together with the $(\mathbf{M},\Omega)$–inner product forms a Hilbert space. In the case when $\mathbf{M}=\mathbf{I}_n$, the $n\times n$ identity matrix, this space is the usual $L^2(\Omega)$ Hilbert space of square-integrable functions; for a non-trivial $\mathbf{M}$, the space is a weighted $L^2(\Omega)$ space.

In the context of the equations (10) and (16), we will consider the $(\mathbf{H},\Omega)$– and $(\mathbf{Q},\Omega)$–inner products respectively, with $\mathbf{H}$ defined in (17) and $\mathbf{Q}$ in (19). Given $\mathbf{H}$ (17), the expression for the symmetry inner product with respect to $\mathbf{H}$ over Ω is

$$(\mathbf{q}'^{(1)},\mathbf{q}'^{(2)})_{(\mathbf{H},\Omega)}= \int_\Omega\left[\bar{\rho}\mathbf{u}'^{(1)}\cdot\mathbf{u}'^{(2)}+\alpha^2\gamma\bar{\rho}^2\zeta'^{(1)}\zeta'^{(2)}+\frac{1+\alpha^2}{\gamma\bar{p}}+\alpha^2\bar{\rho}(\zeta'^{(2)}p'^{(1)}+\zeta'^{(1)}p'^{(2)})\right]d\Omega \tag{24}$$

The $(\mathbf{H},\Omega)$– and $(\mathbf{Q},\Omega)$–inner products are equivalent in the sense that

$$(\mathbf{q}'^{(1)},\mathbf{q}'^{(2)})_{(\mathbf{H},\Omega)}=(\mathbf{V}'^{(1)},\mathbf{V}'^{(2)})_{(\mathbf{Q},\Omega)} \tag{25}$$

where $\mathbf{V}'^{(1)}=\mathbf{S}^{-1}\mathbf{q}'^{(1)}$, and similarly for $\mathbf{V}'^{(2)}$. Using the relationship (19), it is straightforward to show that, denoting $\boldsymbol{\phi}_k^S\equiv\mathbf{S}^{-1}\boldsymbol{\phi}_k$,

$$\Pi_M\mathbf{q}'=\sum_{k=1}^M(\boldsymbol{\phi}_i,\mathbf{q}')_{(\mathbf{H},\Omega)}\boldsymbol{\phi}_k=\mathbf{S}\sum_{k=1}^M(\boldsymbol{\phi}_i^S,\mathbf{V}')_{(\mathbf{Q},\Omega)}\boldsymbol{\phi}_k^S\equiv\mathbf{S}(\Pi_M\mathbf{V}') \tag{26}$$

Another inner product to be utilized herein is the so-called "time-averaged" $(\mathbf{H},\Omega)$–inner product with corresponding "time-averaged" $(\mathbf{H},\Omega)$–norm:

$$(\mathbf{q}'^{(1)},\mathbf{q}'^{(2)})^{avg}_{(\mathbf{H},\Omega)}\equiv\frac{1}{T}\int_0^T(\mathbf{q}'^{(1)},\mathbf{q}'^{(2)})_{(\mathbf{H},\Omega)}dt,\quad ||\mathbf{q}'||^{avg}_{(\mathbf{H},\Omega)}\equiv\sqrt{\frac{1}{T}\int_0^T||\mathbf{q}'||^2_{(\mathbf{H},\Omega)}dt} \tag{27}$$

Similarly, one can speak of the "time-averaged" $(\mathbf{Q},\Omega)$–inner product and norm. (27) is simply the continuous time-average of (20). It can be shown that the expressions in (27) satisfy the properties of an inner product and norm respectively.

Solution Spaces

There are three solutions one can speak of in connection to the ROM, belonging to the following three Hilbert spaces:

$$\mathbf{q}'(\mathbf{x},t)\in\mathcal{H}(\Omega)\subset\mathbb{R}^5 \tag{28}$$

$$\mathbf{q}'_h(\mathbf{x},t)\in\mathcal{H}^h(\Omega)\subset\mathbb{R}^5 \tag{29}$$

$$\mathbf{q}'_M(\mathbf{x},t)\in\mathcal{H}^M(\Omega)\subset\mathbb{R}^5 \tag{30}$$

$\mathbf{q}'$ is the exact solution to the IBVP for (10), $\mathbf{q}'_h$ is the computed CFD solution, from which snapshots are extracted to construct a POD basis, and $\mathbf{q}'_M$ is the computed ROM solution. The Hilbert spaces $\mathcal{H}(\Omega)$ are essentially weighted $L^2(\Omega)$ spaces, formed by equipping the vector space of functions $\mathbf{f}:\Omega\rightarrow\mathbb{R}^5$ such that $||\mathbf{f}||_{(\mathbf{H},\Omega)}<\infty$ with the $(\mathbf{H},\Omega)$–inner product (20).

The ROM solution $\mathbf{q}'_M(\mathbf{x},t) \in \mathcal{H}^M(\Omega)$

In Section 2.6, the ROM solution $\mathbf{q}'_M$ will be defined more precisely as the solution of a penalty-formulated IBVP. For now, it is sufficient to think of it as the numerical solution obtained by applying the Galerkin/POD method described in Section 2.2 to an IBVP for (10). Expanded in its modal basis (recalling that $\boldsymbol{\phi}_k^S \equiv \mathbf{S}^{-1}\boldsymbol{\phi}_k$)

$$\mathbf{q}'_M(\mathbf{x},t) = \sum_{k=1}^{M} a_k(t)\boldsymbol{\phi}_k(\mathbf{x}), \quad \mathbf{V}'_M(\mathbf{x},t) = \sum_{k=1}^{M} a_k(t)\boldsymbol{\phi}_k^S(\mathbf{x}) \tag{31}$$

The components of the 5-vector $\boldsymbol{\phi}_k$ are denoted ϕ_k^i for $i = 1,\ldots,5$, that is

$$\boldsymbol{\phi}_k^T = \begin{pmatrix} \phi_k^1 & \phi_k^2 & \phi_k^3 & \phi_k^4 & \phi_k^5 \end{pmatrix}.$$

The Galerkin projection of the system of equations (10) onto the j^{th} POD mode in the $(\mathbf{H},\Omega)$–inner product is

$$\left(\boldsymbol{\phi}_j, \frac{\partial \mathbf{q}'_M}{\partial t}\right)_{(\mathbf{H},\Omega)} + \left(\boldsymbol{\phi}_j, \mathbf{A}_i \frac{\partial \mathbf{q}'_M}{\partial x_i}\right)_{(\mathbf{H},\Omega)} + (\boldsymbol{\phi}_j, \mathbf{C}\mathbf{q}'_M)_{(\mathbf{H},\Omega)} = 0 \tag{32}$$

(32) is the analog of (8) for the specific hyperbolic IBVP that is being considered here. Substituting the modal basis (31) into (32) gives the following set of M linear ODEs for the time-dependent ROM coefficients $\{a_j(t) : j = 1,2,\ldots,M\}$:

$$\dot{a}_j(t) = -\sum_{k=1}^{M} a_k(t)\left(\boldsymbol{\phi}_j, \mathbf{A}_i \frac{\partial \boldsymbol{\phi}_k}{\partial x_i}\right)_{(\mathbf{H},\Omega)} - \sum_{k=1}^{M} a_k(t)(\boldsymbol{\phi}_j, \mathbf{C}\boldsymbol{\phi}_k)_{(\mathbf{H},\Omega)} \tag{33}$$

2.4 Well-Posedness and Stability of the POD/Galerkin Approach for the Linearized Euler Equations

As a first step in the numerical analysis of a ROM for (10), we show that the IBVP for this set of equations is well-posed and that the Galerkin projection in the chosen inner product is stable. Consider a linear hyperbolic IBVP constructed from (10) :

$$\begin{aligned} &\tfrac{\partial \mathbf{q}'}{\partial t} + \underbrace{\mathbf{A}_i \frac{\partial \mathbf{q}'}{\partial x_i} + \mathbf{C}\mathbf{q}'}_{\equiv \mathcal{L}\mathbf{q}'} = \mathbf{0}, \quad \mathbf{x} \in \Omega, i = 1,2,3, \quad 0 < t < T \\ &\mathbf{P}\mathbf{q}' = \mathbf{h}, \qquad \mathbf{x} \in \partial\Omega_W, \qquad 0 < t < T \\ &\mathbf{R}\mathbf{q}' = \mathbf{g}, \qquad \mathbf{x} \in \partial\Omega_F, \qquad 0 < t < T \\ &\mathbf{q}'(\mathbf{x},0) = \mathbf{f}(\mathbf{x}), \qquad \mathbf{x} \in \Omega \end{aligned} \tag{34}$$

where $\mathbf{P}$ and $\mathbf{h}$ specify the solid wall boundary conditions, $\mathbf{R}$ and $\mathbf{g}$ specify the far-field boundary conditions and $\mathbf{f} : \Omega \to \mathbb{R}^5$ is a given vector-valued function. The well-posedness of (34) depends on the boundary conditions on $\partial\Omega = \partial\Omega_W \cup \partial\Omega_F$. Only after the well-posedness of this IBVP and the stability of the Galerkin projection method used in constructing the ROM are established is it possible to study the convergence properties of the ROM.

Theorem 2.1 below gives sufficient conditions on the boundary conditions for well-posedness of the IBVP (34) and shows that the $(\mathbf{H},\Omega)$–norm is an energy measure. The proof is based on the energy approach [26]: an IBVP is well-posed if the energy associated with the analogous homogeneous IBVP (that is, the original IBVP but with homogeneous Dirichlet boundary conditions and no source term) is bounded[3]. The notation is as follows:

$$\begin{array}{ll} \mathbf{q}'_w = \mathbf{P}\mathbf{q}' - \mathbf{h} \text{ on } \partial\Omega_W, & \mathbf{q}'_{w0} = \mathbf{P}\mathbf{q}' \text{ on } \partial\Omega_W \\ \mathbf{q}'_f = \mathbf{R}\mathbf{q}' - \mathbf{g} \text{ on } \partial\Omega_F, & \mathbf{q}'_{f0} = \mathbf{R}\mathbf{q}' \text{ on } \partial\Omega_F. \end{array} \tag{35}$$

In other words, $\mathbf{q}'_w$ is the vector of boundary conditions on $\partial\Omega_W$ as specified in (34) and $\mathbf{q}'_{w0}$ is the vector of boundary conditions on $\partial\Omega_W$ as specified in (34) but with $\mathbf{h} = \mathbf{0}$ (and similarly for $\mathbf{q}'_f$ and $\mathbf{q}'_{f0}$ on $\partial\Omega_F$).

Theorem 2.1. *Consider a bounded domain $\Omega \subset \mathbb{R}^3$ with connected boundary $\partial\Omega = \partial\Omega_W \cup \partial\Omega_F$, $\partial\Omega_W \cap \partial\Omega_F = \emptyset$. Let $\mathbf{n}^T \equiv \begin{pmatrix} n_1 & n_2 & n_3 \end{pmatrix}$ denote the outward-pointing unit normal vector to $\partial\Omega$, and let $\mathbf{\Lambda}_n \equiv diag\{\lambda_i\} = \mathbf{S}^{-1}\mathbf{A}_n\mathbf{S}$ be the diagonal matrix containing the eigenvalues of $\mathbf{A}_n \equiv \mathbf{A}_1 n_1 + \mathbf{A}_2 n_2 + \mathbf{A}_3 n_3$. The linear hyperbolic IBVP* (34) *is well-posed if*

$$\sum_{i=1}^{5} \lambda_i [(V_{w0})_i]^2 \geq 0 \quad \textit{and} \quad \sum_{i=1}^{5} \lambda_i [(V_{f0})_i]^2 \geq 0, \tag{36}$$

with energy estimate

$$||\mathbf{q}'(\cdot,T)||_{(\mathbf{H},\Omega)} \leq e^{\frac{1}{2}\beta T} ||\mathbf{f}(\cdot)||_{(\mathbf{H},\Omega)}, \tag{37}$$

where β is an upper bound on the eigenvalues of the matrix[4]

$$\mathbf{B} \equiv \mathbf{H}^{-T/2} \frac{\partial(\mathbf{H}\mathbf{A}_i)}{\partial x_i} \mathbf{H}^{-1/2} - \mathbf{H}^{1/2}\mathbf{C}\mathbf{H}^{-1/2} - (\mathbf{H}^{1/2}\mathbf{C}\mathbf{H}^{-1/2})^T \tag{38}$$

and $\mathbf{V}_{w0} = \mathbf{S}^{-1}\mathbf{q}'_{w0}$, $\mathbf{V}_{f0} = \mathbf{S}^{-1}\mathbf{q}'_{f0}$, with $\mathbf{q}'_{w0}$ and $\mathbf{q}'_{f0}$ given by (35).

Proof. By Definition 2.8 in [30], to show well-posedness of (34), it is sufficient to show that the energy of the analogous homogeneous IBVP is bounded in some valid norm. Selecting the $(\mathbf{H},\Omega)$–

[3]Refer to Section A.3 of Appendix A for formal definitions of well-posedness, quoted from [30].

[4]The shorthand $(\mathbf{M}^{1/2})^T \equiv \mathbf{M}^{T/2}$ is employed, where $\mathbf{M}$ is a positive definite matrix and $\mathbf{M}^{1/2}$ is its square root factor, so that $\mathbf{M} = \mathbf{M}^{T/2}\mathbf{M}^{1/2}$.

norm:

$$\begin{aligned}
\frac{1}{2}\frac{d}{dt}||\mathbf{q}'||^2_{(\mathbf{H},\Omega)} &= \frac{1}{2}\frac{d}{dt}\int_\Omega \mathbf{q}'^T\mathbf{H}\mathbf{q}'\,d\Omega \\
&= \int_\Omega \mathbf{q}'^T\mathbf{H}\frac{\partial \mathbf{q}'}{\partial t}\,d\Omega \\
&= -\int_\Omega \mathbf{q}'^T\mathbf{H}\left[\mathbf{A}_i\frac{\partial \mathbf{q}'}{\partial x_i}+\mathbf{C}\mathbf{q}'\right]\,d\Omega \\
&= -\frac{1}{2}\int_\Omega\left[\frac{\partial}{\partial x_i}(\mathbf{q}'^T\mathbf{H}\mathbf{A}_i\mathbf{q}') - \mathbf{q}'^T\frac{\partial(\mathbf{H}\mathbf{A}_i)}{\partial x_i}+2\mathbf{q}'^T\mathbf{H}\mathbf{C}\right]\mathbf{q}'\,d\Omega \qquad (39)\\
&= -\frac{1}{2}\int_\Omega\frac{\partial}{\partial x_i}(\mathbf{q}'^T\mathbf{H}\mathbf{A}_i\mathbf{q}')\,d\Omega+\frac{1}{2}\int_\Omega\mathbf{q}'^T\left[\frac{\partial(\mathbf{H}\mathbf{A}_i)}{\partial x_i}-\mathbf{H}\mathbf{C}-\mathbf{C}^T\mathbf{H}\right]\mathbf{q}'\,d\Omega \\
&= -\frac{1}{2}\int_{\partial\Omega}\mathbf{q}'^T\mathbf{H}\mathbf{A}_n\mathbf{q}'\,dS+\frac{1}{2}\int_\Omega\mathbf{q}'^T\mathbf{H}^{T/2}\mathbf{B}\mathbf{H}^{1/2}\mathbf{q}'\,d\Omega \\
&\le -\frac{1}{2}\int_{\partial\Omega_W}\mathbf{q}'^T_{w0}\mathbf{H}\mathbf{A}_n\mathbf{q}'_{w0}\,dS-\frac{1}{2}\int_{\partial\Omega_F}\mathbf{q}'^T_{f0}\mathbf{H}\mathbf{A}_n\mathbf{q}'_{f0}\,dS+\frac{1}{2}\beta\int_\Omega\mathbf{q}'^T\mathbf{H}\mathbf{q}'\,d\Omega,
\end{aligned}$$

where $\mathbf{B}$ is defined in (38) and β is an upper bound on the eigenvalues of $\mathbf{B}$. By (25),

$$\begin{aligned}
-\tfrac{1}{2}\textstyle\int_{\partial\Omega_W}\mathbf{q}'^T_{w0}\mathbf{H}\mathbf{A}_n\mathbf{q}'_{w0}\,dS-\tfrac{1}{2}\int_{\partial\Omega_F}\mathbf{q}'^T_{f0}\mathbf{H}\mathbf{A}_n\mathbf{q}'_{f0}\,dS &= -\tfrac{1}{2}\textstyle\int_{\partial\Omega_F}\mathbf{V}'^T_{f0}\mathbf{Q}\mathbf{\Lambda}_n\mathbf{V}'_{f0}\,dS \\
&\quad -\tfrac{1}{2}\textstyle\int_{\partial\Omega_W}\mathbf{V}'^T_{w0}\mathbf{Q}\mathbf{\Lambda}_n\mathbf{V}'_{w0}\,dS,
\end{aligned} \qquad (40)$$

where $\mathbf{V}'_{f0}=\mathbf{S}\mathbf{q}'_{f0}$ and similarly for $\mathbf{V}'_{w0}$. It follows from the property that $\mathbf{Q}$ is symmetric positive definite and $\mathbf{Q}\mathbf{\Lambda}_n=\mathbf{\Lambda}_n\mathbf{Q}$ that

$$\mathbf{V}'^T\mathbf{Q}\mathbf{\Lambda}_n\mathbf{V}'=\mathbf{Q}^{T/2}[\mathbf{V}'^T\mathbf{\Lambda}_n\mathbf{V}']\mathbf{Q}^{1/2}=(\mathbf{Q}^{1/2})^T\left[\sum_{i=1}^5\lambda_i(V'_i)^2\right]\mathbf{Q}^{1/2}. \qquad (41)$$

If the conditions (36) hold, the last line of (39) thus reduces to

$$\frac{d}{dt}||\mathbf{q}'||^2_{(\mathbf{H},\Omega)}\le\beta||\mathbf{q}'||^2_{(\mathbf{H},\Omega)}. \qquad (42)$$

Applying Gronwall's lemma to (42) gives (37). □

An immediate consequence of Theorem 2.1 is that, provided the IBVP (34) is well-posed, the Galerkin projection of the approximation $\mathbf{q}'_M$ in the $(\mathbf{H},\Omega)$–inner product is stable. Introducing a modal approximation $\mathbf{q}'_M=\sum_{j=1}^M a_j(t)\boldsymbol{\phi}_j(\mathbf{x})$ into (34) and taking the inner product with the numerical approximation $\mathbf{q}'_M$, one has that

$$\frac{1}{2}\frac{d}{dt}||\mathbf{q}'_M||^2_{(\mathbf{H},\Omega)}=-\int_\Omega\mathbf{q}'^T_M\mathbf{H}\mathcal{L}\mathbf{q}'_M d\Omega\equiv-\left(\mathbf{q}'_M,\mathcal{L}\mathbf{q}'_M\right)_{(\mathbf{H},\Omega)} \qquad (43)$$

and the analyis proceeds exactly as in (39)–(42) but with $\mathbf{q}'$ replaced with $\mathbf{q}'_M$. It follows that if (36) holds, that is, if the IBVP (34) is well-posed, the semi-discrete Galerkin approximation satisfies the definition of stability (Appendix A.4), with energy estimate

$$||\mathbf{q}'_M(\cdot,T)||_{(\mathbf{H},\Omega)} \leq e^{\frac{1}{2}\beta T}||\mathbf{q}'_M(\cdot,0)||_{(\mathbf{H},\Omega)} \tag{44}$$

or, in terms of the ROM coefficients,

$$\sum_{j=1}^{M} a_j^2(T) \leq e^{\beta T}\sum_{j=1}^{M} a_j^2(0) \tag{45}$$

Note that, in the uniform base flow case ($\beta \equiv 0$), (44) reduces to the following strong stability condition:

$$||\mathbf{q}'_M(\cdot,T)||_{(\mathbf{H},\Omega)} \leq ||\mathbf{q}_M(\cdot,0)||_{(\mathbf{H},\Omega)} \tag{46}$$

or

$$\sum_{j=1}^{M} a_j^2(T) \leq \sum_{j=1}^{M} a_j^2(0) \tag{47}$$

The energy estimate (44) establishes the semi-boundedness of the governing spatial differential operator $\mathcal{L}$ defined in (10) in the $(\mathbf{H},\Omega)$–norm, from which it follows that $(\cdot,\cdot)_{(\mathbf{H},\Omega)}$ is an energy inner product, with corresponding energy norm $||\cdot||_{(\mathbf{H},\Omega)}$. As a consequence, the Galerkin projection step using the symmetry inner product is guaranteed to produce a stable ROM, provided well-posed boundary conditions are prescribed. The same is *not* true if the Galerkin projection is performed using the $L^2(\Omega)$ inner product. In Section 2.8 and [31], it is shown for several test cases that the symmetry inner product with appropriate boundary conditions leads to a stable ROM for the linearized compressible Euler equations, whereas the $L^2(\Omega)$ ROM with the same boundary conditions is unstable.

2.5 Boundary Treatment

An efficient implementation of boundary conditions for a Galerkin ROM is through a weak formulation. The system of PDEs (10) is projected onto the j^{th} POD mode in the $(\mathbf{H},\Omega)$–inner product, as in (32). The second term in (32) is integrated by parts, and the vector specifying the boundary condition is inserted into the boundary integral over $\partial\Omega$ that arises:

$$\begin{aligned}\left(\boldsymbol{\phi}_j, \frac{\partial \mathbf{q}'_M}{\partial t}\right)_{(\mathbf{H},\Omega)} = &-\underbrace{\int_{\partial\Omega_W} \boldsymbol{\phi}_j^T \mathbf{H}\mathbf{A}_n \mathbf{q}'_w dS}_{\equiv I_{W_j}} - \underbrace{\int_{\partial\Omega_F} \boldsymbol{\phi}_j^T \mathbf{H}\mathbf{A}_n \mathbf{q}'_f dS}_{\equiv I_{F_j}} + \\ &\int_\Omega \left[\frac{\partial}{\partial x_i}[\boldsymbol{\phi}_j^T \mathbf{H}\mathbf{A}_i] - \boldsymbol{\phi}_j^T \mathbf{H}\mathbf{C}\right]\mathbf{q}'_M d\Omega\end{aligned} \tag{48}$$

Performing an additional integration by parts on the first term in the volume integral in (48) yields

$$\int_\Omega \frac{\partial}{\partial x_i}[\boldsymbol{\phi}_j^T \mathbf{H}\mathbf{A}_i]\mathbf{q}'_M d\Omega = \int_{\partial\Omega_W} \boldsymbol{\phi}_j^T \mathbf{H}\mathbf{A}_n \mathbf{q}'_M dS + \int_{\partial\Omega_F} \boldsymbol{\phi}_j^T \mathbf{H}\mathbf{A}_n \mathbf{q}'_M dS - \int_\Omega \boldsymbol{\phi}_j^T \mathbf{H}\mathbf{A}_i \frac{\partial \mathbf{q}'_M}{\partial x_i} d\Omega \tag{49}$$

so that (48) is equivalent to

$$\left(\boldsymbol{\phi}_j, \frac{\partial \mathbf{q}'_M}{\partial t}\right)_{(\mathbf{H},\Omega)} = -\left(\boldsymbol{\phi}_j, \mathbf{A}_i \frac{\partial \mathbf{q}'_M}{\partial x_i} + \mathbf{C}\mathbf{q}'_M\right)_{(\mathbf{H},\Omega)} + \int_{\partial\Omega_W} \boldsymbol{\phi}_j^T \mathbf{H}\mathbf{A}_n(\mathbf{q}'_M - \mathbf{q}'_w)dS + \int_{\partial\Omega_F} \boldsymbol{\phi}_j^T \mathbf{H}\mathbf{A}_n(\mathbf{q}'_M - \mathbf{q}'_f)dS \tag{50}$$

Inviscid, compressible flow boundary conditions are most often implemented in terms of the characteristic variables $\mathbf{V}'_w$, so that $\mathbf{q}'_w \leftarrow \mathbf{S}\mathbf{V}'_w$ (and similarly for $\mathbf{q}'_f$) in the appropriate boundary integral in (50). The elements of the vector $\mathbf{V}'_w$ (and $\mathbf{V}'_f$) can be viewed as incoming and outgoing waves, depending on the sign of the characteristic speeds in the matrix $\boldsymbol{\Lambda}_n$ in (15). Next, the modal representation $\mathbf{q}'_M \leftarrow \sum_{k=1}^{M} a_k(t)\boldsymbol{\phi}_k$ is inserted into the boundary integrals in (50) to yield the following boundary integral expressions appearing in the j^{th} ROM equation:

$$I_{Wu_{jk}} \equiv \int_{\partial\Omega_W} \boldsymbol{\phi}_j^T \mathbf{H}\mathbf{A}_n \boldsymbol{\phi}_k dS, \quad I_{Fu_{jk}} \equiv \int_{\partial\Omega_F} \boldsymbol{\phi}_j^T \mathbf{H}\mathbf{A}_n \boldsymbol{\phi}_k dS \tag{51}$$

$$I_{W_j} \equiv \int_{\partial\Omega_W} \boldsymbol{\phi}_j^T \mathbf{H}\mathbf{S}\boldsymbol{\Lambda}_n \mathbf{V}'_w dS, \quad I_{F_j} \equiv \int_{\partial\Omega_F} \boldsymbol{\phi}_j^T \mathbf{H}\mathbf{S}\boldsymbol{\Lambda}_n \mathbf{V}'_f dS \tag{52}$$

Substituting this notation into (50) and simplifying the resulting expression using the orthonormality of the $\boldsymbol{\phi}_j$, one arrives at the following system of M ODEs for the ROM coefficients:

$$\dot{a}_j(t) = -\sum_{k=1}^{M} a_k(t)\left(\boldsymbol{\phi}_j, \mathbf{A}_i \frac{\partial \boldsymbol{\phi}_k}{\partial x_i} + \mathbf{C}\boldsymbol{\phi}_k\right)_{(\mathbf{H},\Omega)} + \sum_{k=1}^{M}\left[a_k(t) I_{Wu_{jk}} - I_{W_j}\right] + \sum_{k=1}^{M}\left[a_k(t) I_{Fu_{jk}} - I_{F_j}\right] \tag{53}$$

where $j = 1, \ldots, M$. To solve for the ROM coefficients, (53) is advanced in time using a time-integration scheme. Note that the boundary conditions may also be implemented weakly using a penalty method (Section 2.5).

Far-field Non-Reflecting Boundary Condition

Since the computational domain Ω is by necessity finite, boundary conditions should be prescribed on the artificial far-field boundary $\partial\Omega_F$. Without far-field boundary conditions, non-physical reflections of unsteady waves will be observed at the far-field. These unwanted reflections can affect the accuracy of the simulation and possibly lead to numerical instability. An appropriate far-field boundary condition is one that will suppress the reflection of waves from the outer computational boundaries. This is the so-called non-reflecting boundary condition on $\partial\Omega_F$, specified in the characteristic variables $\mathbf{V}'$. All outgoing unsteady characteristic waves are allowed to exit the flow domain at the far-field boundary without reflection, that is, without being allowed to re-enter the domain through the boundary. This is accomplished by setting the components of $\mathbf{V}'$ corresponding to characteristic waves traveling into Ω (those corresponding to negative eigenvalues of $\mathbf{A}_n$) to zero:

$$V_i \leftarrow (V_f)_i \equiv \begin{cases} 0, & \text{if } \lambda_i < 0 \\ V_i, & \text{if } \lambda_i \geq 0 \end{cases} \tag{54}$$

for $i = 1, \ldots, 5$. As in Theorem 2.1, $\{\lambda_i : i = 1, ..., 5\}$ denote the five eigenvalues of the matrix $\mathbf{A}_n$ (the diagonal entries of $\mathbf{\Lambda}_n$). The terms in the integrand of the boundary integral I_{F_j} in (48) are re-cast in terms of the modal representation (31), which leads to boundary terms in the ROM[5]. In matrix form, the far-field condition can be written as

$$\mathbf{R}^S \mathbf{V}' = \mathbf{0} \quad \text{on} \quad \partial\Omega_F \tag{55}$$

where

$$\mathbf{R}^S \equiv \mathbf{RS} = \begin{cases} \mathbf{I}_5, & \text{if } \bar{u}_n < -\bar{c} \\ \text{diag}\{1,1,1,0,1\}, & \text{if } -\bar{c} < \bar{u}_n < 0 \\ \text{diag}\{0,0,0,0,1\}, & \text{if } 0 < \bar{u}_n < \bar{c} \\ \mathbf{0}_5, & \text{if } \bar{u}_n > \bar{c} \end{cases} \tag{56}$$

Here $\mathbf{0}_5$ is the 5×5 zero matrix and $\mathbf{I}_5$ is the 5×5 identity matrix. The ranges in (56) correspond to the four cases that can occur at the far-field: supersonic inflow ($\bar{u}_n < -\bar{c}$), subsonic inflow ($-\bar{c} < \bar{u}_n < 0$), subsonic outflow ($0 < \bar{u}_n < \bar{c}$), and supersonic outflow ($\bar{u}_n > \bar{c}$).

Solid Wall Acoustically-Reflecting Boundary Condition

In practical applications, the domain Ω may contain a stationary or moving solid wall. The natural choice of boundary condition at the solid wall boundary is a linearized version of the no-penetration boundary condition, $\mathbf{u} \cdot \mathbf{n} = -\dot{w}$:

$$u'_n = -\bar{\mathbf{u}} \cdot \nabla w - \dot{w} \equiv u'_w \quad \text{on} \quad \partial\Omega_W \tag{57}$$

Here, w and $\dot{w}$ are respectively the solid wall displacement and velocity in the $-\mathbf{n}$ direction, with $\mathbf{n}$ denoting the outward unit normal to the solid wall boundary $\partial\Omega_W$ and $u'_n \equiv \mathbf{u}' \cdot \mathbf{n}$.

The linearized no-penetration condition (57) is posed in the characteristic variables $\mathbf{V}'$ as an acoustically-reflecting condition. Assuming the base flow satisfies a no-penetration condition at the wall ($\bar{u}_n \equiv 0$ on $\partial\Omega_W$), the characteristic speeds are $\{0,0,0,\bar{c},-\bar{c}\}$. In particular, the fourth characteristic is outgoing and the fifth characteristic is incoming. For a stationary wall, specifying the acoustically-reflecting boundary condition amounts to setting the incoming characteristic, V'_5, equal to the outgoing characteristic, V'_4. When the wall velocity is $u'_w \equiv u'_w(x,y,t)$, the following relation satisfies (57):

$$V'_5 = V'_4 - 2u'_w \quad \text{on} \quad \partial\Omega_W \tag{58}$$

That is, (58) and (57) are algebraically equivalent. (58) can be written in matrix form as

$$\mathbf{P}^S \mathbf{V}' = \mathbf{h} \quad \text{on} \quad \partial\Omega_W \tag{59}$$

with

$$\mathbf{P}^S \equiv \mathbf{PS} = \begin{pmatrix} 0 & & & & \\ & 0 & & & \\ & & 0 & & \\ & & & 0 & \\ & & & -1 & 1 \end{pmatrix}, \quad \mathbf{h} = \begin{pmatrix} 0 \\ 0 \\ 0 \\ 0 \\ -2u'_w \end{pmatrix} \tag{60}$$

[5]Explicit expressions of the integrals I_{F_j} in terms of the ROM coefficients and basis functions are given in the Appendix of [31].

or

$$\mathbf{V}' \leftarrow \mathbf{V}'_w \equiv \begin{pmatrix} V'_1 \\ V'_2 \\ V'_3 \\ V'_4 \\ V'_4 - 2u'_w \end{pmatrix} \quad \text{on} \quad \partial\Omega_W \tag{61}$$

The solid wall boundary condition is implemented by substituting the vector $\mathbf{V}'_w$ in (61) into the integrand of I_{W_j} defined in (52). The integrand that appears in I_{W_j} in (48) is

$$\boldsymbol{\phi}_j^T \mathbf{H}\mathbf{A}_n \mathbf{q}'_w = \underbrace{\bar{\rho}\bar{c}\boldsymbol{\phi}_j^n (u'_{n,M} - u'_w)}_{\text{penalty-like term}} + \underbrace{\phi_j^n p'_M + \phi_j^5 u'_w}_{=\boldsymbol{\phi}_j^T \mathbf{H}\mathbf{A}_n \mathbf{q}'_M} \tag{62}$$

The last two terms in (62) are the same as the unaltered integrand $\boldsymbol{\phi}_j^T \mathbf{H}\mathbf{A}_n \mathbf{q}'_M$. In fact, the entire integrand (62) is precisely the unaltered integrand $\boldsymbol{\phi}_j^T \mathbf{H}\mathbf{A}_n \mathbf{q}'_M$ when $u'_{n,M} = u'_w$, that is, when the linearized no-penetration condition (57) is satisfied exactly on $\partial\Omega_W$. The first term in (62) can be viewed as a penalty term that forces the normal velocity to the prescribed boundary value. This idea is explored further in Section 2.5.

Well-Posedness and Stability of the Galerkin Scheme with Boundary Conditions

Having selected specific boundary conditions on $\partial\Omega = \partial\Omega_W \cup \partial\Omega_F$, we now apply the general results and conditions derived in Section 2.4 to show the well-posedness of the IBVP (34) with $\mathbf{R}$ defined in (56), $\mathbf{g} = \mathbf{0}$, and $\mathbf{P}$ and $\mathbf{h}$ defined in (60), as well as the stability of the corresponding Galerkin approximation $\mathbf{q}'_M$ in the $(\mathbf{H}, \Omega)$–inner product.

Corollary 2.5.1. *Let $\Omega \subset \mathbb{R}^3$ be an open bounded domain with connected boundary $\partial\Omega = \partial\Omega_W \cup \Omega_F$, $\partial\Omega_W \cap \partial\Omega_F = \emptyset$. Assume $\bar{u}_n = 0$ on $\partial\Omega_W$. Then the IBVP* (34) *with the acoustically-reflecting boundary condition* (58) *on $\partial\Omega_W$ and the non-reflecting condition* (54) *on $\partial\Omega_F$ is well-posed, with energy estimate given by* (37)*, and the corresponding Galerkin approximation $\mathbf{q}'_M$ is stable with energy estimate* (44)*. In the case of uniform base flow ($\nabla\bar{\mathbf{q}} \equiv 0$), these energy estimates simplify to*

$$||\mathbf{q}'(\cdot,T)||_{(\mathbf{H},\Omega)} \leq ||\mathbf{f}(\cdot)||_{(\mathbf{H},\Omega)}, \quad ||\mathbf{q}'_M(\cdot,T)||_{(\mathbf{H},\Omega)} \leq ||\mathbf{q}_M(\cdot,0)||_{(\mathbf{H},\Omega)} \tag{63}$$

(that is, $\beta = 0$ in (37) *and* (44)*).*

Proof. Substituting the components of (61) into the left-hand side of (36) and using the fact that $\bar{u}_n = 0$ at the wall:

$$\sum_{i=1}^{5} \lambda_i [(V_w)'_i]^2 = \bar{c}(V'_4)^2 - \bar{c}(V'_4 - 2u'_w)^2 \tag{64}$$

The right-most expression in (64) is identically zero if $u'_w = 0$, that is, if one considers V'_{w0}. By condition (36), the acoustically-reflecting boundary condition (61) on $\partial\Omega_W$ is well-posed. For the

far-field non-reflecting boundary condition, observe from (54) that, by construction,

$$\lambda_i[(V'_{f0})_i]^2 = \begin{cases} 0, & \text{if } \lambda_i < 0 \\ \geq 0, & \text{if } \lambda_i \geq 0 \end{cases} \tag{65}$$

as incoming characteristics (those for which $\lambda_i < 0$) are zeroed out whereas outgoing characteristics (those for which $\lambda_i > 0$) are left unaltered. Since (36) is satisfied, the far-field condition (65) is well-posed. By Theorem 2.1, the corresponding energy estimate in the $(\mathbf{H}, \Omega)$–norm is (37). When the base flow is uniform $\frac{\partial(\mathbf{H}\mathbf{A}_i)}{\partial x_i} \equiv \mathbf{0}$ and $\mathbf{C} \equiv \mathbf{0}$, so that $\mathbf{B} \equiv 0$ (38), meaning $\beta = 0$. Thus, (37) reduces to the first expression in (63).

Noting that $\mathbf{q}'_M$ satisfies the same set of equations as $\mathbf{q}'$, by Theorem 2.1, well-posedness of (34) with boundary conditions (58) and (54), shown above using the $(\mathbf{H}, \Omega)$–norm, implies stability of the Galerkin approximation $\mathbf{q}'_M$ in the $(\mathbf{H}, \Omega)$–norm, with energy estimate (44). When $\beta = 0$, this estimate reduces to the second expression in (63). □

One can see from Corollary 2.5.1 that the uniform mean flow assumption yields a clean stability analysis, since the mean flow supports only neutral or decaying disturbances. In the non-uniform base flow case, there may exist exponentially growing instabilities, an example of which is the Kelvin-Helmholtz shear layer instability. It may then be difficult to distinguish between natural instability modes supported by the continuous equations and spurious instabilities generated by the numerical discretization.

A Stable Penalty-Like Formulation of the Boundary Conditions

The usual way to weakly enforce boundary conditions in a numerical scheme is by applying them directly into the boundary integral (Section 2.5). It has been argued [32] that this approach does not take into account the fact that the equation should be obeyed arbitrarily close to the boundary. To address this potential issue, a number of works, including for example [32, 33], have developed penalty and penalty-like enforcements of boundary conditions. Formulating a boundary condition using the penalty method amounts to rewriting the given boundary value problem as:

$$\begin{cases} \mathcal{L}\mathbf{u} - \mathbf{f} = 0, & \text{in } \Omega \\ \mathbf{B}\mathbf{u} = \mathbf{h}, & \text{on } \partial\Omega \end{cases} \quad \rightarrow \quad \mathcal{L}\mathbf{u} - \mathbf{f} = -\boldsymbol{\Gamma}(\mathbf{B}\mathbf{u} - \mathbf{h})\delta_{\partial\Omega}, \quad \text{in } \Omega \cup \partial\Omega \tag{66}$$

Here $\boldsymbol{\Gamma} = \text{diag}\{\gamma_i : i = 1, \ldots \dim(\mathbf{u})\}$ is a diagonal matrix of positive penalty parameters selected such that stability is preserved, $\mathbf{B}$ and $\mathbf{h}$ are generic operators specifying the boundary conditions on $\partial\Omega$, $\mathbf{f}$ is a generic source, and $\delta_{\partial\Omega}$ is an indicator function marking the boundary $\partial\Omega$, that is

$$\delta_{\partial\Omega} \equiv \begin{cases} 1, & \text{for } \mathbf{x} \in \partial\Omega \\ 0, & \text{otherwise.} \end{cases} \tag{67}$$

A penalty-like expression associated with the solid wall boundary condition has already been exhibited in (62). Remark that (50), repeated below (68) for emphasis, can also be viewed as a

specific penalty formulation of the projected equations with boundary conditions:

$$\left(\boldsymbol{\phi}, \frac{\partial \mathbf{q}'_M}{\partial t} + \mathbf{A}_i \frac{\partial \mathbf{q}'_M}{\partial x_i} + \mathbf{C}\mathbf{q}'_M\right)_{(\mathbf{H},\Omega)} = \int_{\partial\Omega_W} \boldsymbol{\phi}^T \mathbf{H}\mathbf{A}_n(\mathbf{q}'_M - \mathbf{q}'_w)dS + \int_{\partial\Omega_F} \boldsymbol{\phi}^T \mathbf{H}\mathbf{A}_n(\mathbf{q}'_M - \mathbf{q}'_f)dS \quad (68)$$

(68) is the projection in the $(\mathbf{H},\Omega)$–inner product of

$$\frac{\partial \mathbf{q}'_M}{\partial t} + \mathbf{A}_i \frac{\partial \mathbf{q}'_M}{\partial x_i} + \mathbf{C}\mathbf{q}'_M = \mathbf{A}_n(\mathbf{q}'_M - \mathbf{q}'_w)\delta_{\partial\Omega_W} + \mathbf{A}_n(\mathbf{q}'_M - \mathbf{q}'_f)\delta_{\partial\Omega_F} \quad (69)$$

onto the POD mode $\boldsymbol{\phi}$. In the characteristic variables, (69) is equivalent to

$$\frac{\partial \mathbf{V}'_M}{\partial t} + \mathbf{S}^{-1}\mathbf{A}_i\mathbf{S}\frac{\partial \mathbf{V}'_M}{\partial x_i} + \mathbf{S}^{-1}\mathbf{C}\mathbf{S}\mathbf{V}'_M = \boldsymbol{\Lambda}_n(\mathbf{V}'_M - \mathbf{V}'_w)\delta_{\partial\Omega_W} + \boldsymbol{\Lambda}_n(\mathbf{V}'_M - \mathbf{V}'_f)\delta_{\partial\Omega_F} \quad (70)$$

Comparing (70) with (66), one can see that the diagonal matrix $-\boldsymbol{\Lambda}_n$ plays the role of the penalty matrix $\boldsymbol{\Gamma}$. (70) is a *specific* penalty enforcement; that is the "penalty parameter" matrix $-\boldsymbol{\Lambda}_n$ is *fixed*. The natural question to ask is whether a fixed penalty matrix is required for stability of the Galerkin scheme with a penalty boundary treatment.

Theorem 2.5.2. *Consider the following penalty enforcement of the far-field and solid wall boundary conditions:*

$$\frac{\partial \mathbf{V}'_M}{\partial t} + \mathbf{S}^{-1}\mathbf{A}_i\mathbf{S}\frac{\partial \mathbf{V}'_M}{\partial x_i} + \mathbf{S}^{-1}\mathbf{C}\mathbf{S}\mathbf{V}'_M = -\boldsymbol{\Gamma}_W(\mathbf{P}^S\mathbf{V}'_M - \mathbf{h})\delta_{\partial\Omega_W} - \boldsymbol{\Gamma}_F\mathbf{R}^S\mathbf{V}'_M\delta_{\partial\Omega_F} \quad (71)$$

where $\mathbf{P}^S$ *and* $\mathbf{h}$ *are defined in* (60), $\mathbf{R}^S$ *is defined in* (56) *and* $\boldsymbol{\Gamma}_W$ *and* $\boldsymbol{\Gamma}_F$ *are positive definite, diagonal matrices of penalty parameters* γ_i*. The penalty-like enforcement of the boundary conditions* (71) *is stable if*

$$\boldsymbol{\Gamma}_W = \bar{c}\mathbf{I}_5 \quad \textit{and} \quad \boldsymbol{\Gamma}_F > \bar{c}\mathbf{I}_5 \quad (72)$$

where $\mathbf{I}_5$ *denotes that* 5×5 *identity matrix.*

Proof. (71) is stable if $||\mathbf{V}'_M||^2_{(\mathbf{Q},\Omega)}$ is non-increasing in time for $\mathbf{h}\equiv\mathbf{0}$. From (71), exploiting the symmetry of the $\mathbf{Q}\mathbf{S}^{-1}\mathbf{A}_i\mathbf{S}$ matrices,

$$\begin{aligned}
\frac{1}{2}\frac{d}{dt}||\mathbf{V}'_M||_{(\mathbf{Q},\Omega)} =& -\frac{1}{2}\int_{\partial\Omega_F}\mathbf{V}'^T_M\mathbf{Q}^{T/2}\left(\boldsymbol{\Lambda}_n + 2\Gamma_F\mathbf{R}^S\right)\mathbf{Q}^{1/2}\mathbf{V}'_M dS - \\
& \frac{1}{2}\int_{\partial\Omega_W}\mathbf{V}'^T_M\mathbf{Q}^{T/2}\left(\boldsymbol{\Lambda}_n + 2\boldsymbol{\Gamma}_W\mathbf{P}^S\right)\mathbf{Q}^{1/2}\mathbf{V}'_M dS + \\
& \frac{1}{2}\int_{\Omega}\mathbf{V}'^T_M\mathbf{Q}^{T/2}\left[\mathbf{Q}^{-T/2}\frac{\partial(\mathbf{Q}\mathbf{S}^{-1}\mathbf{A}_i\mathbf{S})}{\partial x_i}\mathbf{Q}^{-1/2} - \mathbf{Q}^{1/2}\mathbf{C}\mathbf{S}\mathbf{Q}^{-1/2} - \right. \\
& \left.(\mathbf{Q}^{1/2}\mathbf{C}\mathbf{S}\mathbf{Q}^{-1/2})^T\right]\mathbf{Q}^{1/2}\mathbf{V}'_M d\Omega \\
\leq& -\frac{1}{2}\int_{\partial\Omega_F}\mathbf{V}'^T_M\mathbf{Q}^{T/2}\left(\boldsymbol{\Lambda}_n + 2\boldsymbol{\Gamma}_F\mathbf{R}^S\right)\mathbf{Q}^{1/2}\mathbf{V}'_M dS - \\
& \frac{1}{2}\int_{\partial\Omega_W}\mathbf{V}'^T_M\mathbf{Q}^{T/2}\left(\boldsymbol{\Lambda}_n + 2\boldsymbol{\Gamma}_W\mathbf{P}^S\right)\mathbf{Q}^{1/2}\mathbf{V}'_M dS + \frac{1}{2}\beta||\mathbf{V}'_M||^2_{(\mathbf{Q},\Omega)},
\end{aligned} \quad (73)$$

where β is an upper bound on the eigenvalues of the matrix

$$\mathbf{Q}^{-T/2}\frac{\partial(\mathbf{Q}\mathbf{S}^{-1}\mathbf{A}_i\mathbf{S})}{\partial x_i}\mathbf{Q}^{-1/2} - \mathbf{Q}^{1/2}\mathbf{C}\mathbf{S}\mathbf{Q}^{-1/2} - (\mathbf{Q}^{1/2}\mathbf{C}\mathbf{S}\mathbf{Q}^{-1/2})^T. \tag{74}$$

(71) is stable if $\mathbf{\Lambda}_n + 2\mathbf{\Gamma}_F\mathbf{R}^S$ and $\mathbf{\Lambda}_n + 2\mathbf{\Gamma}_W\mathbf{P}^S$ are positive semi-definite. Note that $\mathbf{P}^S$ is asymmetric, meaning $\mathbf{\Lambda}_n + 2\mathbf{\Gamma}_W\mathbf{P}^S$ is asymmetric. To study this matrix's positive semi-definiteness, we therefore examine the eigenvalues of its symmetric part:

$$(\mathbf{\Lambda}_n + 2\mathbf{\Gamma}_W\mathbf{P}^S)^{symm} \equiv \mathbf{\Lambda}_n + \mathbf{\Gamma}_W\mathbf{P}^S + (\mathbf{P}^S)^T\mathbf{\Gamma}_W = \begin{pmatrix} 0 & & & & \\ & 0 & & & \\ & & 0 & & \\ & & & \bar{c} & -\gamma_5 \\ & & & -\gamma_5 & -\bar{c}+2\gamma_5 \end{pmatrix} \tag{75}$$

The eigenvalues of the matrix (75) are $0,0,0,\ -\gamma_5 \pm \sqrt{2\gamma_5^2 + \bar{c}^2 - 2\bar{c}\gamma_5}$. The only one of these eigenvalues that can be non-negative is the fourth one; in fact, it is strictly positive unless $\gamma_5 = \bar{c}$. It follows that stability is ensured if $\gamma_5 = \bar{c}$. The only requirement on the other penalty parameters is that they be positive. Thus, setting $\mathbf{\Gamma}_W = \bar{c}\mathbf{I}_5$ guarantees stability.

For the far-field boundary condition, there are four cases to consider. Suppose $\bar{u}_n < -\bar{c}$. Then $\mathbf{R}^S = \mathbf{I}_5$ and $\mathbf{\Lambda}_n + 2\mathbf{\Gamma}_F\mathbf{R}^S = \text{diag}\{\bar{u}_n + 2\gamma_1, \bar{u}_n + 2\gamma_2, \bar{u}_n + 2\gamma_3, \bar{u}_n + \bar{c} + 2\gamma_4, \bar{u}_n - \bar{c} + 2\gamma_5\}$. Since $\bar{u}_n < -\bar{c}$, to ensure stability, we require that

$$\gamma_1, \gamma_2, \gamma_3 > \frac{1}{2}\bar{c}, \gamma_4 > 0, \gamma_5 > \bar{c} \tag{76}$$

When $-\bar{c} < \bar{u}_n < 0$, from (56), $\mathbf{\Lambda}_n + 2\mathbf{\Gamma}_F\mathbf{R}^S = \text{diag}\{\bar{u}_n + 2\gamma_1, \bar{u}_n + 2\gamma_2, \bar{u}_n + 2\gamma_3, \bar{u}_n + \bar{c}, \bar{u}_n - \bar{c} + 2\gamma_5\}$. It follows that we have stability if

$$\gamma_1, \gamma_2, \gamma_3 > 0, \gamma_5 > \frac{1}{2}\bar{c} \tag{77}$$

If $0 < \bar{u}_n < \bar{c}$, $\mathbf{\Lambda}_n + 2\mathbf{\Gamma}_F\mathbf{R}^S = \text{diag}\{\bar{u}_n, \bar{u}_n, \bar{u}_n, \bar{u}_n + \bar{c}, \bar{u}_n - \bar{c} + 2\gamma_5\}$ and the only requirement on the γ_i is that $\gamma_5 > 0$. Finally, when $\bar{u}_n > \bar{c}$, $\mathbf{R}^S = \mathbf{0}$, so that the penalty parameters are only required to be positive. It follows that if $\mathbf{\Gamma}_W > \bar{c}\mathbf{I}_5$, a stable enforcement of the far-field boundary condition is guaranteed for any of the flow conditions that can occur at the far-field. □

Theorem 2.5.2 shows that the penalty enforcement of the solid wall boundary condition is only guaranteed to be stable for a fixed penalty matrix, whereas the penalty-like formulation of the far-field boundary condition is stable for a range of penalty parameters. The penalty-like treatment of the solid wall boundary condition therefore does not yield a "true" penalty method, in which the constraints (in this case, the boundary conditions) are more strongly enforced as the γ_i are increased. It is straightforward to check that the penalty-like formulation (70) satisfies the stability condition (72), that is, $-\mathbf{\Lambda}_n(\mathbf{V}'_M - \mathbf{V}'_w) = \bar{c}(\mathbf{P}^S\mathbf{V}'_M - \mathbf{h})$ and $-\mathbf{\Lambda}_n(\mathbf{V}'_M - \mathbf{V}'_f) > \bar{c}\mathbf{R}^S\mathbf{V}'_M$.

As mentioned earlier, the boundary conditions may be implemented using the penalty approach. A penalty-like implementation of the boundary conditions is similar to the weak implementation. The main difference between the two implementations is in the second step (48), which is replaced by

$$\begin{aligned}\left(\boldsymbol{\phi}_j, \frac{\partial \mathbf{q}'_M}{\partial t}\right)_{(\mathbf{H},\Omega)} = &- \left(\boldsymbol{\phi}_j, \mathbf{A}_i \frac{\partial \mathbf{q}'_M}{\partial x_i} + \mathbf{C}\mathbf{q}'_M\right)_{(\mathbf{H},\Omega)} \\ &- \underbrace{\int_{\partial\Omega_W} \boldsymbol{\phi}_j^T \mathbf{H}\mathbf{S}\tilde{\boldsymbol{\Gamma}}_W(\mathbf{V}'_M - \mathbf{V}'_w)dS}_{I_{W_j}} - \underbrace{\int_{\partial\Omega_F} \boldsymbol{\phi}_j^T \mathbf{H}\mathbf{S}\tilde{\boldsymbol{\Gamma}}_F(\mathbf{V}'_M - \mathbf{V}'_f)dS}_{I_{F_j}}.\end{aligned} \tag{78}$$

No integration by parts or substitutions are performed on the second term in (78); instead the boundary conditions are enforced by the added penalty-like terms, where the penalty matrices $\tilde{\boldsymbol{\Gamma}}_F$ and $\tilde{\boldsymbol{\Gamma}}_W$ are specified such that stability is preserved (Theorem 2.5.2). In practice, one may include a subroutine in the algorithm, in which the penalty parameters enforcing the far-field constraints are increased slightly during each iteration. It is emphasized that, if one selects $\tilde{\boldsymbol{\Gamma}}_W = \tilde{\boldsymbol{\Gamma}}_F = -\boldsymbol{\Lambda}_n$, the penalty-like implementation (78) and the weak implementation (50) of the boundary conditions are *identical*.

2.6 Convergence Analysis and *A Priori* Error Estimates

We are now ready to present a key result of this work, namely *a priori* error estimates for the Galerkin ROM with boundary conditions in the Hilbert space $\mathcal{H}(\Omega)$. These error bounds are derived by adapting techniques traditionally used in the numerical analysis of spectral approximations to PDEs [33], and by making use of the stable penalty-like formulation (69). The estimates (Theorem 2.6.3) show that the ROM solution is bounded for finite time and give insight into the conditions for convergence of the ROM solution to the exact solution. This error bound is computable, provided the error in the CFD solution used to derive the ROM, $||\mathbf{q}'_h - \mathbf{q}'||_{(\mathbf{H},\Omega)}$, can be estimated in some way.

Mathematical Preliminaries and Formulation

Recall from Section 2.3 that the three solutions of interest here, the exact solution, the CFD solution and the ROM solution were denoted $\mathbf{q}'$, $\mathbf{q}'_h$ and $\mathbf{q}'_M$ respectively. In preparation for the analysis below, let us be more precise in defining these solutions. We will say the exact solution in the characteristic variables $\mathbf{q}' \in \mathcal{H}(\Omega)$ satisfies

$$\begin{aligned} \tfrac{\partial \mathbf{q}'}{\partial t} + \mathbf{A}_i \tfrac{\partial \mathbf{q}'}{\partial x_i} + \mathbf{C}\mathbf{q}' = 0, &\quad \mathbf{x} \in \Omega, &\quad 0 < t < T \\ \mathbf{q}' - \mathbf{q}'_w = \mathbf{0}, &\quad \mathbf{x} \in \partial\Omega_W, &\quad 0 < t < T \\ \mathbf{q}' - \mathbf{q}'_f = \mathbf{0}, &\quad \mathbf{x} \in \partial\Omega_F, &\quad 0 < t < T \\ \mathbf{q}'(\mathbf{x},0) = \mathbf{f}(\mathbf{x}), &\quad \mathbf{x} \in \Omega \end{aligned} \tag{79}$$

Here $\mathbf{f}:\Omega\rightarrow\mathbb{R}$ is a given vector-valued function, $\mathbf{q}'_w=\mathbf{S}\mathbf{V}'_w$ is the vector defining the solid-wall boundary condition (61) and $\mathbf{q}'_f=\mathbf{S}\mathbf{V}'_f$ is the vector defining the far-field boundary condition (54). Motivated primarily by [33], the ROM solution $\mathbf{q}'_M$ is defined as the solution to the following IBVP with a penalty-type boundary treatment:

$$\begin{array}{ll}\frac{\partial\mathbf{q}'_M}{\partial t}+\mathbf{A}_i\frac{\partial\mathbf{q}'_M}{\partial x_i}+\mathbf{C}\mathbf{q}'_M=\mathbf{A}_n[\mathbf{q}'_M-\mathbf{q}'_w]\delta_{\partial\Omega_W}+\mathbf{A}_n[\mathbf{q}'_M-\mathbf{q}'_f]\delta_{\partial\Omega_F}, & \mathbf{x}\in\Omega\cup\partial\Omega_W\cup\partial\Omega_F,\ 0<t<T\\ \mathbf{q}'_M(\mathbf{x},0)=\mathbf{f}(\mathbf{x}), & \mathbf{x}\in\Omega\end{array} \tag{80}$$

(80) is precisely the penalty-like formulation (69) exhibited in Section 2.5, which is stable by Theorem 2.5.2.

Let $\mathbf{q}'\in\mathcal{H}(\Omega)$ and $\mathbf{q}'_M\in\mathcal{H}^M(\Omega)$. Denote $\mathbf{E}\equiv\Pi_M\mathbf{q}'-\mathbf{q}'_M$, where $\Pi_M:\mathcal{H}(\Omega)\rightarrow\mathcal{H}^M(\Omega)$ is an orthogonal projection operator satisfying properties 1–6 listed in Section A.1 of Appendix A. In the context of the ROM, the natural definition of Π_M is (26). Applying Π_M to (79) gives

$$\begin{array}{c}\frac{\partial(\Pi_M\mathbf{q}')}{\partial t}+\mathbf{A}_i\frac{\partial(\Pi_M\mathbf{q}')}{\partial x_i}+\mathbf{C}\Pi_M\mathbf{q}'\\ +\left[\Pi_M\left(\mathbf{A}_i\frac{\partial\mathbf{q}'}{\partial x_i}+\mathbf{C}\mathbf{q}'\right)-\left(\mathbf{A}_i\frac{\partial(\Pi_M\mathbf{q}')}{\partial x_i}+\mathbf{C}\Pi_M\mathbf{q}'\right)\right]=\mathbf{0},\ \ \mathbf{x}\in\Omega,\ 0<t<T\\ \Pi_M(\mathbf{q}'-\mathbf{q}'_w)=\mathbf{0},\ \ \mathbf{x}\in\partial\Omega_W,0<t<T\\ \Pi_M(\mathbf{q}'-\mathbf{q}'_f)=\mathbf{0},\ \ \mathbf{x}\in\partial\Omega_F,0<t<T\\ \Pi_M\mathbf{q}'(\mathbf{x},0)=\Pi_M\mathbf{f}(\mathbf{x}),\ \ \mathbf{x}\in\Omega\end{array} \tag{81}$$

Now, subtracting (80) from (81), one has that

$$\begin{array}{ll}\frac{\partial\mathbf{E}}{\partial t}+\mathbf{A}_i\frac{\partial\mathbf{E}}{\partial x_i}+\mathbf{C}\mathbf{E}+\mathbf{W}=\mathbf{A}_n[\mathbf{E}-\mathbf{E}_w]\delta_{\partial\Omega_W}+\mathbf{A}_n[\mathbf{E}-\mathbf{E}_f]\delta_{\partial\Omega_F}, & \mathbf{x}\in\Omega\cup\partial\Omega_W\cup\partial\Omega_F,\ 0<t<T\\ \mathbf{E}(\mathbf{x},0)=\Pi_M\mathbf{f}(\mathbf{x})-\mathbf{f}(\mathbf{x}), & \mathbf{x}\in\Omega\end{array} \tag{82}$$

where $\mathbf{E}_w\equiv\Pi_M\mathbf{q}'_w-\mathbf{q}'_w$, $\mathbf{E}_f\equiv\Pi_M\mathbf{q}'_f-\mathbf{q}'_f$ and

$$\mathbf{W}\equiv\Pi_M\left(\mathbf{A}_i\frac{\partial\mathbf{q}'}{\partial x_i}+\mathbf{C}\mathbf{q}'\right)-\left(\mathbf{A}_i\frac{\partial(\Pi_M\mathbf{q}')}{\partial x_i}+\mathbf{C}\Pi_M\mathbf{q}'\right)=\Pi_M(\mathcal{L}\mathbf{q}')-\mathcal{L}(\Pi_M\mathbf{q}') \tag{83}$$

In the upcoming proofs, the short-hand

$$\mathbf{V}'_M\equiv\begin{pmatrix}V'_{1,M}\\V'_{2,M}\\V'_{3,M}\\V'_{3,M}\\V'_{5,M}\end{pmatrix},\quad \Pi_M\mathbf{V}'\equiv\begin{pmatrix}V'_{1,\Pi}\\V'_{2,\Pi}\\V'_{3,\Pi}\\V'_{4,\Pi}\\V'_{5,\Pi}\end{pmatrix} \tag{84}$$

will be employed, where, as expected $\mathbf{V}'_M=\mathbf{S}^{-1}\mathbf{q}'_M$ and, from (26), $\Pi_M\mathbf{V}'=\mathbf{S}^{-1}\Pi_M\mathbf{q}'$. In particular, note that that these relations imply that

$$\mathbf{E}=\mathbf{S}(\Pi_M\mathbf{V}'-\mathbf{V}'_M)\equiv\mathbf{S}\mathbf{E}^S \tag{85}$$

and similarly for $\mathbf{E}_w$ and $\mathbf{E}_f$.

Error Estimates in the $\mathcal{H}(\Omega)$ Hilbert Space

We begin by proving the following two lemmas.

Lemma 2.6.1. *Let* $\mathbf{q}' \in \mathcal{H}(\Omega)$ *satisfy* (79) *and let* $\mathbf{q}'_M \in \mathcal{H}^M(\Omega)$ *satisfy* (80). *Denote* $\mathbf{E} \equiv \Pi_M \mathbf{q}' - \mathbf{q}'_M$, $\mathbf{E}_w \equiv \Pi_M \mathbf{q}'_w - \mathbf{q}'_w$, $\mathbf{E}_f \equiv \Pi_M \mathbf{q}'_f - \mathbf{q}'_f$ *with* $\mathbf{E}$ *satisfying* (82). *Then*

$$||\mathbf{E}(\cdot,T)||^2_{(\mathbf{H},\Omega)} \leq e^{1+\beta T}||\mathbf{E}(\cdot,0)||^2_{(\mathbf{H},\Omega)} + T\int_0^T ||\mathbf{W}(\cdot,t)||^2_{(\mathbf{H},\Omega)}dt \tag{86}$$

where $\mathbf{W}$ *is defined in* (83) *and* β *is an upper bound on the eigenvalues of the matrix*

$$\mathbf{B} \equiv \mathbf{H}^{-T/2}\frac{\partial(\mathbf{H}\mathbf{A}_i)}{\partial x_i}\mathbf{H}^{-1/2} - \mathbf{H}^{1/2}\mathbf{C}\mathbf{H}^{-1/2} - (\mathbf{H}^{1/2}\mathbf{C}\mathbf{H}^{-1/2})^T \tag{87}$$

Proof. Begin with (82). Taking the inner product with $\mathbf{E}$, integrating by parts and exploiting the symmetry property of the $\mathbf{H}\mathbf{A}_i$ matrices gives

$$\begin{aligned}
\frac{1}{2}\frac{d}{dt}||\mathbf{E}||^2_{(\mathbf{H},\Omega)} &= \frac{1}{2}\int_\Omega \mathbf{E}^T\mathbf{H}^{T/2}\mathbf{B}\mathbf{H}^{1/2}\mathbf{E}d\Omega + \int_{\partial\Omega_W}\mathbf{E}^T\mathbf{H}\mathbf{A}_n\left(\frac{1}{2}\mathbf{E}-\mathbf{E}_w\right)dS \\
&\quad + \int_{\partial\Omega_F}\mathbf{E}^T\mathbf{H}\mathbf{A}_n\left(\frac{1}{2}\mathbf{E}-\mathbf{E}_f\right)dS - (\mathbf{W},\mathbf{E})_{(\mathbf{H},\Omega)} \\
&\leq \frac{1}{2}\beta||\mathbf{E}||^2_{(\mathbf{H},\Omega)} + \int_{\partial\Omega_W}\mathbf{E}^T\mathbf{H}\mathbf{A}_n\left(\frac{1}{2}\mathbf{E}-\mathbf{E}_w\right)dS \\
&\quad + \int_{\partial\Omega_F}\mathbf{E}^T\mathbf{H}\mathbf{A}_n\left(\frac{1}{2}\mathbf{E}-\mathbf{E}_f\right)dS - (\mathbf{W},\mathbf{E})_{(\mathbf{H},\Omega)}
\end{aligned} \tag{88}$$

where β is an upper bound on the eigenvalues of the matrix $\mathbf{B}$ defined in (87). By (85) and employing the relations (14) and (19),

$$\int_{\partial\Omega_W}\mathbf{E}^T\mathbf{H}\mathbf{A}_n\left(\frac{1}{2}\mathbf{E}-\mathbf{E}_w\right)dS = \int_{\partial\Omega_W}(\mathbf{E}^S)^T\mathbf{Q}\mathbf{\Lambda}_n\left(\frac{1}{2}\mathbf{E}^S-\mathbf{E}^S_w\right)dS \tag{89}$$

$$\int_{\partial\Omega_F}\mathbf{E}^T\mathbf{H}\mathbf{A}_n\left(\frac{1}{2}\mathbf{E}-\mathbf{E}_f\right)dS = \int_{\partial\Omega_F}(\mathbf{E}^S)^T\mathbf{Q}\mathbf{\Lambda}_n\left(\frac{1}{2}\mathbf{E}^S-\mathbf{E}^S_f\right)dS \tag{90}$$

Exploiting the fact that $\mathbf{Q}$ is positive definite, (88) can be written as

$$\begin{aligned}
\frac{1}{2}\frac{d}{dt}||\mathbf{E}||^2_{(\mathbf{H},\Omega)} &= \int_{\partial\Omega_W}\mathbf{Q}^{T/2}\left[\sum_{i=1}^5\lambda_i\left(\frac{1}{2}(E^S_i)^2 - E^S_i[(E^S_w)_i]\right)\right]\mathbf{Q}^{1/2}dS \\
&\quad + \int_{\partial\Omega_F}\mathbf{Q}^{T/2}\left[\sum_{i=1}^5\lambda_i\left(\frac{1}{2}(E^S_i)^2 - E^S_i[(E^S_f)_i]\right)\right]\mathbf{Q}^{1/2}dS \\
&\quad - (\mathbf{W},\mathbf{E})_{(\mathbf{H},\Omega)} + \frac{1}{2}\beta||\mathbf{E}||^2_{(\mathbf{H},\Omega)}
\end{aligned} \tag{91}$$

Then, from the solid wall boundary condition (61) and employing the short-hand (84),

$$\begin{aligned}\textstyle\sum_{i=1}^{5}\lambda_i\left(\frac{1}{2}(E_i^S)^2-E_i^S[(E_w^S)_i]\right) &= c\left[\tfrac{1}{2}(E_4^S)^2-E_4^S(E_w^S)_4-\tfrac{1}{2}(E_5^S)^2+E_5^S(E_w^S)_5\right]\\ &= \tfrac{1}{2}c\Big[-(V'_{4,\Pi}-V'_{4,M})^2-(V'_{5,\Pi}-V'_{5,M})^2+\\ &\qquad 2(V'_{5,\Pi}-V'_{5,M})(V'_{4,\Pi}-V'_{4,M})\Big]\end{aligned} \tag{92}$$

By Young's inequality,

$$2(V'_{5,\Pi}-V'_{5,M})(V'_{4,\Pi}-V'_{4,M})\leq (V'_{5,\Pi}-V'_{5,M})^2+(V'_{4,\Pi}-V'_{4,M})^2 \tag{93}$$

Substituting this bound into the right hand side of (92) gives

$$\sum_{i=1}^{5}\lambda_i\left(\frac{1}{2}(E_i^S)^2-E_i^S[(E_w^S)_i]\right)\leq 0 \tag{94}$$

(94) implies that the term (89) can be omitted from (91), as it is non-positive. Turning our attention to the integral over $\partial\Omega_F$, remark that, from (54),

$$(E_f^S)_i=\begin{cases}0, & \text{if } \lambda_i<0\\ E_i^S, & \text{if } \lambda_i\geq 0\end{cases} \tag{95}$$

It follows that

$$\textstyle\sum_{i=1}^{5}\lambda_i\left(\frac{1}{2}(E_i^S)^2-E_i^S[(E_f^S)_i]\right) = -\frac{1}{2}\sum_{i=1}^{5}\sum_{\lambda_i\geq 0}\lambda_i(E_i^S)^2\leq 0 \tag{96}$$

which implies that the expression (90) is also non-positive and can be omitted from (91). Thus, (91) simplifies to

$$\frac{d}{dt}||\mathbf{E}||^2_{(\mathbf{H},\Omega)}\leq -2(\mathbf{W},\mathbf{E})_{(\mathbf{H},\Omega)}+\beta||\mathbf{E}||^2_{(\mathbf{H},\Omega)}\leq\left(\frac{1}{T}+\beta\right)||\mathbf{E}||^2_{(\mathbf{H},\Omega)}+T||\mathbf{W}||^2_{(\mathbf{H},\Omega)} \tag{97}$$

Applying Gronwall's Lemma to (97) gives (86). □

Lemma 2.6.2. *Let* $\mathbf{W}$ *be as defined in* (83)*. Let* $\mathbf{q}'_h\in\mathcal{H}^h(\Omega)$ *be the CFD solution. Then the following is a bound for* $||\mathbf{W}(\cdot,T)||^{avg}_{(\mathbf{H},\Omega)}=\left(\frac{1}{T}\int_0^T||\mathbf{W}(\cdot,t)||^2_{(\mathbf{H},\Omega)}dt\right)^{1/2}$*:*

$$\begin{aligned}||\mathbf{W}(\cdot,T)||^{avg}_{(\mathbf{H},\Omega)}\leq\ & ||\Pi_M(\mathcal{L}\{\mathbf{q}'-\mathbf{q}'_h\})(\cdot,T)||^{avg}_{(\mathbf{H},\Omega)}+||\mathcal{L}\{\Pi_M(\mathbf{q}'-\mathbf{q}'_h)\}(\cdot,T)||^{avg}_{(\mathbf{H},\Omega)}\\ &+||\{\Pi_M(\mathcal{L}\mathbf{q}'_h)-\mathcal{L}(\Pi_M\mathbf{q}'_h)\}(\cdot,T)||^{avg}_{(\mathbf{H},\Omega)}\end{aligned} \tag{98}$$

Proof. Let $\mathbf{q}'_h\in\mathcal{H}^h(\Omega)$ be the CFD solution. From (83) and applying the Minkoswki inequality,

$$\begin{aligned}||\mathbf{W}(\cdot,T)||^{avg}_{(\mathbf{H},\Omega)} &= \left(\tfrac{1}{T}\int_0^T||\Pi_M(\mathcal{L}\mathbf{q}')-\mathcal{L}(\Pi_M\mathbf{q}')||^2_{(\mathbf{H},\Omega)}dt\right)^{1/2}\\ &= \Big(\tfrac{1}{T}\int_0^T||\Pi_M(\mathcal{L}\mathbf{q}')-\Pi_M(\mathcal{L}\mathbf{q}'_h)+\Pi_M(\mathcal{L}\mathbf{q}'_h)-\mathcal{L}(\Pi_M\mathbf{q}')+\mathcal{L}(\Pi_M\mathbf{q}'_h)-\\ &\qquad \mathcal{L}(\Pi_M\mathbf{q}'_h)||^2_{(\mathbf{H},\Omega)}dt\Big)^{1/2}\\ &\leq \sqrt{\tfrac{1}{T}\int_0^T||\Pi_M(\mathcal{L}\{\mathbf{q}'-\mathbf{q}'_h\})||^2_{(\mathbf{H},\Omega)}dt}+\sqrt{\tfrac{1}{T}\int_0^T||\mathcal{L}\{\Pi_M(\mathbf{q}'-\mathbf{q}'_h)\}||^2_{(\mathbf{H},\Omega)}dt}\\ &+\sqrt{\tfrac{1}{T}\int_0^T||\Pi_M(\mathcal{L}\mathbf{q}'_h)-\mathcal{L}(\Pi_M\mathbf{q}'_h)||^2_{(\mathbf{H},\Omega)}dt}\end{aligned} \tag{99}$$

Recognizing the expressions in (99) as time-averaged $(\mathbf{H},\Omega)$–norms gives (98). □

Lemmas 2.6.1 and 2.6.2 lead to the following theorem, in which the error in the ROM solution $||(\mathbf{q}' - \mathbf{q}'_M)(\cdot,T)||_{(\mathbf{H},\Omega)}$ is bounded in the space $\mathcal{H}(\Omega)$.

Theorem 2.6.3. *Let* $\mathbf{q}' \in \mathcal{H}(\Omega)$ *satisfy* (79) *and* $\mathbf{q}'_M \in \mathcal{H}^M(\Omega)$ *satisfy* (80). *Let* $\Pi_M : \mathcal{H}(\Omega) \to \mathcal{H}^M(\Omega)$ *be an orthogonal projection operator satisfying properties 1–6 of Section A.1 of Appendix A, and let* $\mathbf{E} \equiv \Pi_M \mathbf{q}' - \mathbf{q}'_M$. *Let* $\mathbf{q}'_h \in \mathcal{H}^h(\Omega)$ *be the CFD solution. Then*

$$\begin{aligned} ||(\mathbf{q}' - \mathbf{q}'_M)(\cdot,T)||_{(\mathbf{H},\Omega)} \leq \quad & e^{\frac{1}{2}(1+\beta T)}||\mathbf{E}(\cdot,0)||_{(\mathbf{H},\Omega)} + ||(\mathbf{q}'_h - \Pi_M \mathbf{q}'_h)(\cdot,T)||_{(\mathbf{H},\Omega)} \\ & + T||\{\Pi_M(\mathcal{L}\mathbf{q}'_h) - \mathcal{L}(\Pi_M \mathbf{q}'_h)\}(\cdot,T)||^{avg}_{(\mathbf{H},\Omega)} \\ & + 2||(\mathbf{q}' - \mathbf{q}'_h)(\cdot,T)||_{(\mathbf{H},\Omega)} + T||\Pi_M(\mathcal{L}\{\mathbf{q}' - \mathbf{q}'_h\})(\cdot,T)||^{avg}_{(\mathbf{H},\Omega)} \\ & + T||\mathcal{L}\{\Pi_M(\mathbf{q}' - \mathbf{q}'_h)\}(\cdot,T)||^{avg}_{(\mathbf{H},\Omega)} \end{aligned} \tag{100}$$

where β *is an upper bound on the eigenvalues of the matrix*

$$\mathbf{B} \equiv \mathbf{H}^{-T/2} \frac{\partial(\mathbf{H}\mathbf{A}_i)}{\partial x_i} \mathbf{H}^{-1/2} - \mathbf{H}^{1/2}\mathbf{C}\mathbf{H}^{-1/2} - (\mathbf{H}^{1/2}\mathbf{C}\mathbf{H}^{-1/2})^T \tag{101}$$

Proof. Note that $\mathbf{q}' - \mathbf{q}'_M = \mathbf{q}' - \Pi_M \mathbf{q}' + \Pi_M \mathbf{q}' - \mathbf{q}'_M = (\mathbf{q}' - \Pi_M \mathbf{q}') + \mathbf{E}$. By the triangle inequality,

$$||(\mathbf{q}' - \mathbf{q}'_M)(\cdot,T)||_{(\mathbf{H},\Omega)} \leq ||(\Pi_M \mathbf{q}' - \mathbf{q}')(\cdot,T)||_{(\mathbf{H},\Omega)} + ||\mathbf{E}(\cdot,T)||_{(\mathbf{H},\Omega)} \tag{102}$$

where $||\mathbf{E}(\cdot,T)||^2_{(\mathbf{H},\Omega)}$ is bounded according to (86). Applying again the triangle inequality and using the fact that $||\Pi_M||_{(\mathbf{H},\Omega)} = 1$, Π_M being an orthogonal projector (see Section A.1 of Appendix A),

$$\begin{aligned} ||\mathbf{q}' - \Pi_M \mathbf{q}'||_{(\mathbf{H},\Omega)} &= ||\mathbf{q}' - \Pi_M \mathbf{q}' + \mathbf{q}'_h - \Pi_M \mathbf{q}'_h - \mathbf{q}'_h + \Pi_M \mathbf{q}'_h||_{(\mathbf{H},\Omega)} \\ &\leq ||\mathbf{q}'_h - \Pi_M \mathbf{q}'_h||_{(\mathbf{H},\Omega)} + ||\mathbf{q}' - \mathbf{q}'_h||_{(\mathbf{H},\Omega)} + ||\Pi_M(\mathbf{q}' - \mathbf{q}'_h)||_{(\mathbf{H},\Omega)} \\ &\leq ||\mathbf{q}'_h - \Pi_M \mathbf{q}'_h||_{(\mathbf{H},\Omega)} + (1 + ||\Pi_M||_{(\mathbf{H},\Omega)})||\mathbf{q}' - \mathbf{q}'_h||_{(\mathbf{H},\Omega)} \\ &\leq ||\mathbf{q}'_h - \Pi_M \mathbf{q}'_h||_{(\mathbf{H},\Omega)} + 2||\mathbf{q}' - \mathbf{q}'_h||_{(\mathbf{H},\Omega)} \end{aligned} \tag{103}$$

Substituting (103) into (102) gives

$$\begin{aligned} ||(\mathbf{q}' - \mathbf{q}'_M)(\cdot,T)||_{(\mathbf{H},\Omega)} \leq \quad & ||(\mathbf{q}'_h - \Pi_M \mathbf{q}'_h)(\cdot,T)||_{(\mathbf{H},\Omega)} + 2||(\mathbf{q}' - \mathbf{q}'_h)(\cdot,T)||_{(\mathbf{H},\Omega)} \\ & + ||\mathbf{E}(\cdot,T)||_{(\mathbf{H},\Omega)} \end{aligned} \tag{104}$$

Using the fact that $\int_\Omega f^2 d\Omega \leq (\int_\Omega |f| d\Omega)^2$ and the inequalities (86) and (98),

$$\begin{aligned} ||\mathbf{E}(\cdot,T)||_{(\mathbf{H},\Omega)} &\leq \left\{ e^{1+\beta T}||\mathbf{E}(\cdot,0)||^2_{(\mathbf{H},\Omega)} + T^2 \left(||\mathbf{W}(\cdot,t)||^{avg}_{(\mathbf{H},\Omega)} \right)^2 \right\}^{1/2} \\ &\leq e^{\frac{1}{2}(1+\beta T)}||\mathbf{E}(\cdot,0)||_{(\mathbf{H},\Omega)} + T||\mathbf{W}(\cdot,T)||^{avg}_{(\mathbf{H},\Omega)} \\ &\leq e^{\frac{1}{2}(1+\beta T)}||\mathbf{E}(\cdot,0)||_{(\mathbf{H},\Omega)} + T||\Pi_M(\mathcal{L}\{\mathbf{q}' - \mathbf{q}'_h\})(\cdot,T)||^{avg}_{(\mathbf{H},\Omega)} \\ &\quad + T||\mathcal{L}\{\Pi_M(\mathbf{q}' - \mathbf{q}'_h)\}(\cdot,T)||^{avg}_{(\mathbf{H},\Omega)} + T||\{\Pi_M(\mathcal{L}\mathbf{q}'_h) \\ &\quad - \mathcal{L}(\Pi_M \mathbf{q}'_h)\}(\cdot,T)||^{avg}_{(\mathbf{H},\Omega)} \end{aligned} \tag{105}$$

Substituting (105) into (102) gives (100).

□

Let us analyze the estimate (100), repeated below for clarification and emphasis:

$$\begin{aligned}\underbrace{||(\mathbf{q}'-\mathbf{q}'_M)(\cdot,T)||_{(\mathbf{H},\Omega)}}_{\varepsilon_{ROM}} \leq\ & e^{\frac{1}{2}(1+\beta T)}\underbrace{||\mathbf{E}(\cdot,0)||_{(\mathbf{H},\Omega)}}_{\varepsilon_0}+\underbrace{||(\mathbf{q}'_h-\Pi_M\mathbf{q}'_h)(\cdot,T)||_{(\mathbf{H},\Omega)}}_{\varepsilon_{rep}} \\ & +T\underbrace{||\{\Pi_M(\mathcal{L}\mathbf{q}'_h)-\mathcal{L}(\Pi_M\mathbf{q}'_h)\}(\cdot,T)||^{avg}_{(\mathbf{H},\Omega)}}_{\varepsilon_{Lrep}}+2\underbrace{||(\mathbf{q}'-\mathbf{q}'_h)(\cdot,T)||_{(\mathbf{H},\Omega)}}_{\varepsilon_{CFD}} \\ & +T\underbrace{\left[||\Pi_M(\mathcal{L}\{\mathbf{q}'-\mathbf{q}'_h\})(\cdot,T)||^{avg}_{(\mathbf{H},\Omega)}+||\mathcal{L}\{\Pi_M(\mathbf{q}'-\mathbf{q}'_h)\}(\cdot,T)||^{avg}_{(\mathbf{H},\Omega)}\right]}_{\varepsilon_L}\end{aligned} \tag{106}$$

The error terms comprising (106) are named in Table 1 for ease of reference.

Table 1. Nomenclature for the terms present in the error estimate (106)

Term	Name	Symbol
$\|\|(\mathbf{q}'-\mathbf{q}'_M)(\cdot,T)\|\|_{(\mathbf{H},\Omega)}$	ROM solution error	ε_{ROM}
$\|\|\mathbf{E}(\cdot,0)\|\|_{(\mathbf{H},\Omega)}$	Initial ROM subspace error	ε_0
$\|\|(\mathbf{q}'_h-\Pi_M\mathbf{q}'_h)(\cdot,T)\|\|_{(\mathbf{H},\Omega)}$	CFD representation error	ε_{rep}
$\|\|\{\Pi_M(\mathcal{L}\mathbf{q}'_h)-\mathcal{L}(\Pi_M\mathbf{q}'_h)\}(\cdot,T)\|\|^{avg}_{(\mathbf{H},\Omega)}$	CFD operator representation error	ε_{Lrep}
$\|\|(\mathbf{q}'-\mathbf{q}'_h)(\cdot,T)\|\|_{(\mathbf{H},\Omega)}$	CFD solution error	ε_{CFD}
$\|\|\Pi_M\quad(\mathcal{L}\{\mathbf{q}'-\mathbf{q}'_h\})(\cdot,T)\|\|^{avg}_{(\mathbf{H},\Omega)}+$ $\|\|\mathcal{L}\{\Pi_M(\mathbf{q}'-\mathbf{q}'_h)\}(\cdot,T)\|\|^{avg}_{(\mathbf{H},\Omega)}$	CFD operator error	ε_L
$e^{\frac{1}{2}(1+\beta T)}\varepsilon_0+\varepsilon_{rep}+T\varepsilon_{Lrep}+2\varepsilon_{CFD}+T\varepsilon_L$	Total error estimate	ε_{tot}

The initial error ε_0 is the difference (85) between the ROM solution and the projection of the exact solution onto the POD subspace at time $t=0$. For non-uniform mean flow ($\beta\neq 0$), this "initial subspace error" is amplified by the time-dependent factor $e^{\frac{1}{2}\beta T}$. The last three terms in (106) $2\varepsilon_{CFD}+T\varepsilon_L$ are essentially estimates of the error in the CFD solution. These terms converge, provided the error in the CFD solution $\mathbf{q}'_h$ relative to the exact solution $\mathbf{q}'$ is bounded as the CFD mesh is refined. A consequence of the POD approach for model reduction is that the second term in (106), the "CFD representation error" ε_{rep} also converges: that is $\Pi_M\mathbf{q}'_h\rightarrow\mathbf{q}'_h$ provided both N (the number of snapshots used in constructing the ROM) $\rightarrow\infty$ and M (the basis size) $\rightarrow\infty$.

It turns out that some additional analysis is required to show rigorously the convergence of the third term in (106), the "CFD operator representation error" ε_{Lrep}. As it stands, convergence of this term is not apparent. This is because in the POD approach, the ROM basis is constructed to represent well $\mathbf{q}'_h$, *not* to represent $\mathcal{L}\mathbf{q}'_h$. Representing $\mathcal{L}\mathbf{q}'_h$ is nonetheless critical to the performance of the ROM. Recalling that, from the governing equations, $\mathcal{L}\mathbf{q}'=-\frac{d\mathbf{q}'}{dt}$, and characterizing the numerical time integration error for the CFD solution with time step increment Δt as $\mathcal{L}\mathbf{q}'_h=-\frac{d\mathbf{q}'_h}{dt}+\Delta t^r$ for some $r\geq 1$, it can be shown (Lemma 2.6.4) that as the time increment between CFD snapshots

and the representation error of the snapshots by the POD basis both decrease to zero, $\varepsilon_{L_{rep}}$ also converges, as desired.

Lemma 2.6.4. *Let $\mathbf{q}'_h \in \mathcal{H}^h(\Omega)$ be the CFD solution, with time derivative $\dot{\mathbf{q}}'_h \equiv \frac{d\mathbf{q}'_h}{dt}$. Consider the case where P equally spaced CFD snapshots are used to construct the POD basis, with time increment Δt_p separating each snapshot, so that the time derivative of the CFD solution can be estimated using a polynomial approximation of the form*

$$\dot{\mathbf{q}}'_h = \frac{1}{\Delta t_p^{P-1}} \sum_{j=1}^{P} g_j \mathbf{q}'^j_h + O(\Delta t_p^{P-1}) \tag{107}$$

for some weights $g_j \in \mathbb{R}$, $j = 1,...,P$. Let $\Pi_M : \mathcal{H}(\Omega) \to \mathcal{H}^M(\Omega)$ be an orthogonal projection operator satisfying properties 1–6 of Section A.1 of Appendix A and characterize the numerical time integration error in the CFD solution by

$$\dot{\mathbf{q}}'_h + \mathcal{L}\mathbf{q}'_h = O(\Delta t^r), \quad r \geq 1 \tag{108}$$

where Δt is the time step increment. Then

$$\begin{aligned} ||\{\Pi_M(\mathcal{L}\mathbf{q}'_h) - \mathcal{L}(\Pi_M\mathbf{q}'_h)\}(\cdot,T)||^{avg}_{(\mathbf{H},\Omega)} \leq\ & ||\mathcal{L}\{\Pi_M\mathbf{q}'_h - \mathbf{q}'_h\}(\cdot,T)||^{avg}_{(\mathbf{H},\Omega)} \\ & + \tfrac{1}{\Delta t_P^{P-1}} \textstyle\sum_{j=1}^{P} g_j ||(\Pi_M\mathbf{q}'_h - \mathbf{q}'_h)(\cdot,t_j)||^{avg}_{(\mathbf{H},\Omega)} \\ & + \max\{O(\Delta t^r), O(\Delta t_p^{P-1})\} \end{aligned} \tag{109}$$

Proof. Consider the two terms in

$$||\Pi_M(\mathcal{L}\mathbf{q}'_h) - \mathcal{L}(\Pi_M\mathbf{q}'_h)||^{avg}_{\mathbf{H},\Omega} \tag{110}$$

separately. The first term can be written

$$\Pi_M(\mathcal{L}\mathbf{q}'_h) = \Pi_M\left(-\dot{\mathbf{q}}'_h + \dot{\mathbf{q}}'_h + \mathcal{L}\mathbf{q}'_h\right) = -\Pi_M\dot{\mathbf{q}}'_h + \Pi_M(\dot{\mathbf{q}}'_h + \mathcal{L}\mathbf{q}'_h) \tag{111}$$

Here, $O(\Delta t^r)$ with $r \geq 1$ is a measure of the projection of the temporal error in the CFD solution, which depends on the time step used in the CFD calculation and the order r of the CFD time integration scheme.

The second term in (110) can be re-written as:

$$\begin{aligned} \mathcal{L}(\Pi_M\mathbf{q}'_h) =& \mathcal{L}(\Pi_M\mathbf{q}'_h - \mathbf{q}'_h + \mathbf{q}'_h) \\ =& \mathcal{L}(\Pi_M\mathbf{q}'_h - \mathbf{q}'_h) + \mathcal{L}\mathbf{q}'_h \\ =& \mathcal{L}(\Pi_M\mathbf{q}'_h - \mathbf{q}'_h) - \dot{\mathbf{q}}'_h + \dot{\mathbf{q}}'_h + \mathcal{L}\mathbf{q}'_h \\ =& \mathcal{L}(\Pi_M\mathbf{q}'_h - \mathbf{q}'_h) - \dot{\mathbf{q}}'_h + O(\Delta t^r) \end{aligned} \tag{112}$$

Taking the norm of the difference between (112) and (111), applying the triangle inequality, and invoking the fact that $||\Pi_M||^{avg}_{(\mathbf{H},\Omega)} = 1$ (Section A.1 of Appendix A) gives

$$\begin{aligned} ||\Pi_M(\mathcal{L}\mathbf{q}'_h) - \mathcal{L}(\Pi_M\mathbf{q}'_h)||^{avg}_{(\mathbf{H},\Omega)} &= ||\mathcal{L}(\Pi_M\mathbf{q}'_h - \mathbf{q}'_h) + \Pi_M\dot{\mathbf{q}}'_h - \dot{\mathbf{q}}'_h - \Pi_M(\dot{\mathbf{q}}'_h + \mathcal{L}\mathbf{q}'_h) + O(\Delta t^r)||^{avg}_{(\mathbf{H},\Omega)} \\ &\leq ||\mathcal{L}(\Pi_M\mathbf{q}'_h - \mathbf{q}'_h)||^{avg}_{(\mathbf{H},\Omega)} + ||\Pi_M\dot{\mathbf{q}}'_h - \dot{\mathbf{q}}'_h||^{avg}_{(\mathbf{H},\Omega)} \\ &\quad + ||\Pi_M||^{avg}_{(\mathbf{H},\Omega)}||\dot{\mathbf{q}}'_h - \mathcal{L}\mathbf{q}'_h||^{avg}_{(\mathbf{H},\Omega)} + O(\Delta t^r) \\ &\leq ||\mathcal{L}(\Pi_M\mathbf{q}'_h - \mathbf{q}'_h)||^{avg}_{(\mathbf{H},\Omega)} + ||\Pi_M\dot{\mathbf{q}}'_h - \dot{\mathbf{q}}'_h||^{avg}_{(\mathbf{H},\Omega)} + O(\Delta t^r) \end{aligned} \tag{113}$$

Consider the case where P equally spaced CFD snapshots are used to construct the POD basis, with time increment Δt_p separating each snapshot, so that the time derivative of the CFD solution can be estimated using a polynomial approximation of the form (107). The projection of this approximation onto $\mathcal{H}^M(\Omega)$ is

$$\Pi_M \dot{\mathbf{q}}'_h = \frac{1}{\Delta t_p^{P-1}} \sum_{j=1}^{P} g_j \Pi_M \mathbf{q}'^j_h + O(\Delta t_p^{P-1}) \tag{114}$$

Taking the difference between (114) and $\dot{\mathbf{q}}'_h$:

$$\Pi_M \dot{\mathbf{q}}'_h - \dot{\mathbf{q}}'_h = \frac{1}{\Delta t_p^{P-1}} \sum_{j=1}^{P} g_j \left(\Pi_M \mathbf{q}'^j_h - \mathbf{q}'^j_h \right) + O(\Delta t_p^{P-1}) \tag{115}$$

Substituting (115) into (113) and applying the triangle inequality gives

$$\begin{aligned} &||\Pi_M(\mathcal{L}\mathbf{q}'_h) - \mathcal{L}(\Pi_M \mathbf{q}'_h)||^{avg}_{(\mathbf{H},\Omega)} \leq \\ &\qquad ||\mathcal{L}(\Pi_M \mathbf{q}'_h - \mathbf{q}'_h)||^{avg}_{(\mathbf{H},\Omega)} + \frac{1}{\Delta t_p^{P-1}} \sum_{j=1}^{P} g_j ||\Pi_M \mathbf{q}'^j_h - \mathbf{q}'^j_h||^{avg}_{(\mathbf{H},\Omega)} + O(\Delta t_p^{P-1}) + O(\Delta t^r) \end{aligned} \tag{116}$$

which implies the bound (109). □

Lemma 2.6.4 demonstrates that the "CFD operator representation error" $\mathcal{E}_{L_{rep}}$ is indeed bounded, and makes clear the conditions under which this term converges. The expression $\mathcal{L}(\Pi_M \mathbf{q}'_h - \mathbf{q}'_h)$ in (113) converges to zero as the size of the POD basis increases to infinity; the $O(\Delta t^r)$ term converges to zero as the CFD time step is decreased to zero. The remaining term in (113), $\Pi_M \dot{\mathbf{q}}'_h - \dot{\mathbf{q}}'_h$, is now required to converge; but this follows from (115), which shows that the projection of the time derivative converges as both the time increment between CFD snapshots decreases to zero *and* the representation error of the snapshots by the POD basis decreases to zero (that is, as the size of the basis increases to infinity). The boundedness of the right hand side of (106) implies convergence of $\mathbf{q}' \rightarrow \mathbf{q}'_M$ in the $(\mathbf{H},\Omega)$–norm, with error estimate (106). This estimate is computable, provided an *a posteriori* estimator of the error in the CFD solution $\mathbf{q}'_h$ relative to the exact solution $\mathbf{q}'$ is available.

2.7 Approximation Space and Numerical Quadrature

Thus far, the stability analysis and error estimates, along with the associated inner products for Galerkin ROMs, have only been given in continuous form. They are valid only if the relevant integrals are evaluated exactly. This is similar to the situation occurring in numerical analysis of spectral methods. With spectral methods, this problem is generally resolved by applying a high-precision numerical quadrature that is able to integrate exactly the spectral projections. We borrow from this approach in the following way. The POD basis is first described by a finite element

representation on the computational mesh. This is fairly general, as long as the simulation code can output data to a nodal mesh, and the mesh can be cast as a collection of finite elements. In the present work we use piecewise-linear (C^0) finite elements to represent the snapshot data and the POD modes. It is then possible to construct a numerical quadrature operator that exactly integrates the inner product of the finite element representations. The introduction of C^0 finite elements requires a relaxation of the smoothness requirements on $\mathbf{q}'$, $\mathbf{H}$, and $\mathbf{A_i}$, $i = 1,2,3$. The projection integrals are then to be interpreted in the sense of distributions.

Consider the d-dimensional spatial domain Ω, subdivided into N_e elements, $\Omega_e, e = 1,\ldots,N_e$. The finite element representation of the state variable $\mathbf{q}'$ is

$$\mathbf{q}_e'^{\,h}(\mathbf{x}) = \sum_{i=1}^{N_n} N_i(\mathbf{x})\mathbf{q}_i', \quad \mathbf{x} \in \Omega_e \tag{117}$$

where N_n is the number of nodes that define the element Ω_e, and N_i are the linear shape functions. Consider the case of linear tetrahedral elements, where $N_n = 4$ and the shape functions span the space of all possible linear functions on the element. A quadratic function $f(\mathbf{x})$ can be integrated exactly over an element by a quadratic Gauss quadrature rule of the form

$$\int_\Omega f(\mathbf{x})\ \mathrm{d}\Omega_e = \sum_{j=1}^{4} \omega'_{j_e} f(\mathbf{x}_{j_e}), \tag{118}$$

where ω'_{j_e} are the integration weights and the $\mathbf{x}_{j_e}$ are the Gauss integration points of the element.

Now suppose the integral to be computed is a weighted inner product of two state vector realizations $\mathbf{u}(\mathbf{x})$ and $\mathbf{v}(\mathbf{x})$,

$$(\mathbf{u},\mathbf{v})_{(\mathbf{H},\Omega)} = \int_\Omega \mathbf{u}^T \mathbf{H}\mathbf{v}\ \mathrm{d}\Omega. \tag{119}$$

The discrete representations of the vectors $\mathbf{u}$ and $\mathbf{v}$ are written as $\mathbf{u}^h$ and $\mathbf{v}^h$, respectively, with length equal to the number of mesh nodes N times the dimension of the vector, r. Let $\mathbf{H}_e^h(\bar{\mathbf{q}})$ be the $r \times r$ element inner product matrix, taken to be piecewise constant over each element. The formula for numerical integration can be written

$$(\mathbf{u},\mathbf{v})_H = \mathbf{u}^{h^T} \mathbf{W} \mathbf{v}^h \tag{120}$$

where $\mathbf{W}$ is a sparse block matrix comprised of $N \times N$ blocks of dimension $r \times r$. The k-l^{th} block of $\mathbf{W}$ is $w_{kl}\ \mathbf{I}$, with

$$w_{kl} = \sum_{e=1}^{N_{kl}^e} \mathbf{H}_e^h \sum_{j=1}^{4} N_{k_e}(\mathbf{x}_{j_e}) N_{l_e}(\mathbf{x}_{j_e})\ \omega'_{j_e}, \tag{121}$$

and where the outer sum is over the elements connected to the k-l nodal "edge."

The finite element representation and associated Gauss quadratures allow for a general and flexible means of creating stable, projection-based ROMs. The only requirements are that data are stored at nodes of the mesh and that the mesh can be decomposed into finite elements of the desired order. Higher order representations of the base flow and inner product matrix $\mathbf{H}$ are also possible, given a quadrature rule of sufficient order.

2.8 Numerical Results

ROM generation procedure

For the results presented in this section, the fluid simulation data were generated using the AERO-F simulation code [34]. AERO-F is an Arbitrary Lagrangian-Eulerian code that can be used for high-fidelity aeroelastic analysis. The linearized Euler solver capability of AERO-F was used in the present work; details of the finite volume discretization and linearization can be found in Lieu *et al.* [11].

The fluid ROMs were built using nondimensionalized equations and CFD solutions. The nondimensionalization used was $\zeta^* = \zeta/\zeta_{ref}$, $u^* = u/c_{ref}$, $v^* = v/c_{ref}$, $w^* = w/c_{ref}$, $p^* = p/\rho_{ref}c_{ref}^2$, where * quantities are non-dimensional.

The fluid POD modes are generated by solution of an eigenproblem, as explained in section 2.2. A code was written that reads in the snapshot data written by AERO-F, assembles the necessary finite element representation of the snapshots, and computes the numerical quadrature necessary for evaluation of the inner products. The code performs all the calculations in parallel using distributed matrix and vector data structures and parallel eigensolvers from the Trilinos project [35], allowing for large data sets and a relatively large number of POD modes. The `libmesh` finite element library [36] was used to compute element quadratures. This code also projects the modes onto the linearized Euler equations and outputs the resulting fluid ROM coefficient matrix.

For all examples the weak implementation of the boundary conditions was used.

Test Case: Random Basis

To demonstrate the stability properties of the fluid ROM, we first consider the case where the modal basis is composed of a sequence of random vector fields that decay to zero at the boundary. The spatial domain is a rectangular prism, discretized by tetrahedral elements. The base flow is taken to be spatially uniform; such a flow is physically stable to any linear disturbance. Projecting the linearized Euler equations onto the random basis leads to a linear ROM (53), written here as

$$\dot{a}_j = A_{jk}a_k. \tag{122}$$

The ROM is stable if the maximum real part of the eigenvalues of the matrix A_{jk}, denoted $\lambda_{r_{max}}$, is less than or equal to zero. Figure 1 plots $\lambda_{r_{max}}$ for ROMs consisting of one through eight basis functions. Using the symmetry inner product $(\cdot,\cdot)_{\mathbf{H},\Omega)}$ to construct the ROM results in a $\lambda_{r_{max}}$ of zero to machine precision. This is completely consistent with convection of a neutral disturbance in uniform flow, and confirms that for any modal basis, this property of the linearized Euler equations is preserved by the ROM. For comparison, a second set of ROMs was constructed using the vector form of the unweighted L^2 inner product, equation (23), to project the equations. As seen in the figure, depending on the number of modes used in the ROM, the ROM can be stable or unstable. While this is a somewhat extreme case using "bad" modes, it is often the case that POD modes

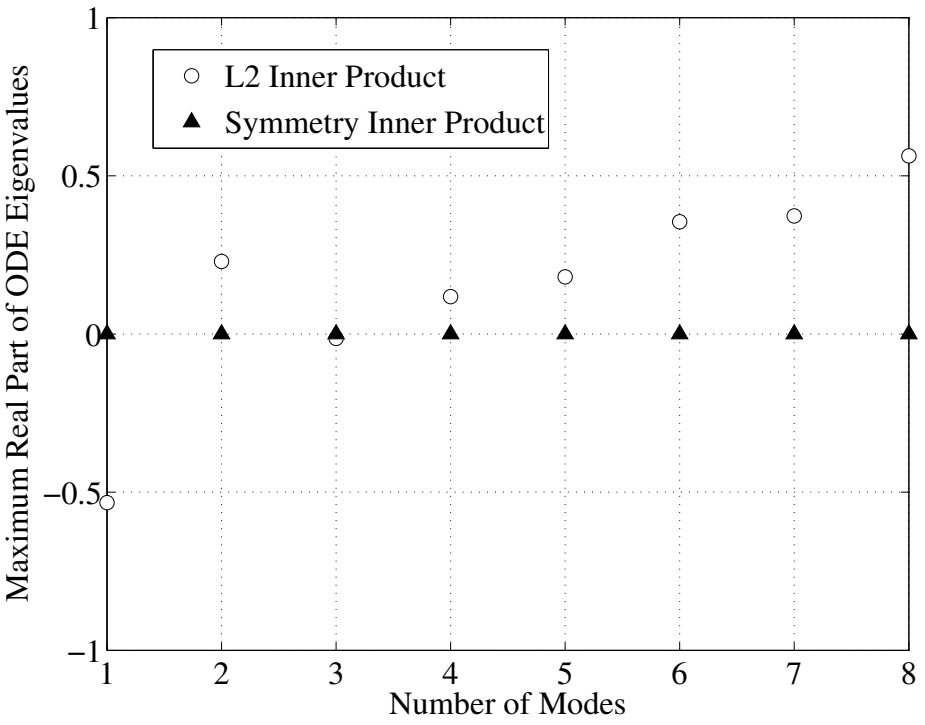

Figure 1. Maximum real part of the eigenvalues of the ROM coefficient matrix A_{jk} for the case of random modes on a uniform base flow.

with small energy are largely comprised of numerical error and other high-frequency "noise." The symmetry inner product method ensures that such modes will not destabilize the ROM.

Two-dimensional Acoustic Pulse

The convergence estimates of Section 2.6 are examined using a ROM constructed from CFD solutions of an IBVP for which an exact solution is known. The problem is the propagation and reflection from two parallel walls of a cylindrical acoustic pulse in a uniform mean flow. The mean flow velocity is taken to be uniform in the x-direction with Mach number $M_\infty \equiv \frac{\bar{u}}{\bar{c}} = 0.25$. The initial condition at time $t = 0$ is

$$\frac{p'}{\bar{\rho}\bar{c}^2} = 0.1M_\infty^2 \exp(-((x-x_0)^2 + (y-y_0)^2)), \quad \frac{\zeta'}{\bar{\zeta}} = -\frac{p'}{\bar{\rho}\bar{c}^2}, \quad u' = v' = w' = 0, \tag{123}$$

with $(x_0, y_0) = (10, -1)$. The exact solution for this IBVP can be found in [37]. The numerical solution was performed on a three-dimensional rectangular prism domain, with extent $0 \le x \le 20$, $-5 \le y \le 5$, $0 \le z \le 1$. The grid was composed of approximately 212,000 nodes that were interconnected to form unstructured tetrahedral elements. Slip wall boundary conditions were

applied on the constant y and z boundaries. The CFD simulation was run for a non-dimensional time of $T_{tot} = 6.4$ using 624 time steps. Snapshots were saved every 4 time steps beginning at time $t = t_0 = 0.57$ and ending at $t = T_{tot}$, and these were used to generate a 14-mode POD basis.

The reduced order models were built by projecting the linearized Euler equations onto the POD basis using the symmetry inner product (24). The CFD snapshots and resulting POD modes were represented using piece-wise linear tetrahedral finite elements and all projection inner products were computed using exact quadratures of these representations. The ROMs were integrated in time using a fourth order Runge-Kutta scheme with the same time step that was used in the CFD computation. It was found through numerical experimentation that this time step was small enough to ensure time step independence of the ROM solutions.

Figure 2 shows the pressure field at time $t - t_0 = 5.0$ for the CFD solution, compared with solutions reconstructed from six- and fourteen-mode ROM solutions. For this solution time the pulse has reflected from the bottom wall and is beginning to reflect from the top wall. The six-mode ROM solution shows significant differences from the CFD solution, while the fourteen-mode ROM solution is very nearly indistinguishable from the CFD solution.

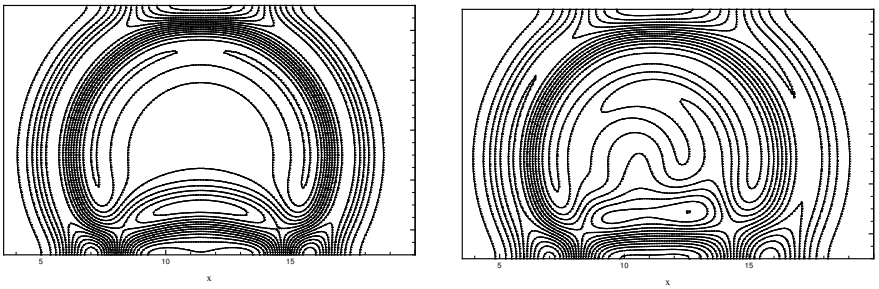

(a) CFD solution. **(b)** Six-mode ROM solution.

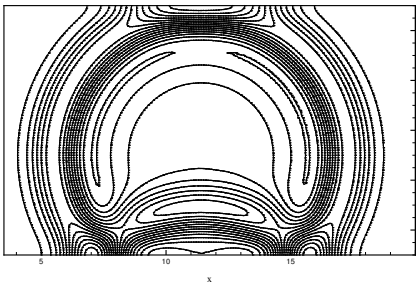

(c) Fourteen-mode ROM solution

Figure 2. Pressure field at time $t - t_0 = 5.0$.

The error terms appearing in (106) were computed using the available exact solution, the CFD solution, and the ROM solution. Terms involving integration in time were approximated using the trapezoidal rule for numerical integration. Figure 3 shows the error estimates for the six-mode ROM and the fourteen-mode ROM, compared with the actual ROM solution error. The ROM solu-

tion error is well below the total error estimate for the entire time history. The conservative nature of the total error estimate is traced primarily to the "operator representation error" term. For the six-mode ROM, the ROM solution error is well above the CFD solution error and tracks reasonably well with the CFD representation error. As the number of basis functions increases to fourteen, the ROM solution error drops below the CFD solution error term. The CFD representation error is reduced by about two orders of magnitude from the six-mode case, while the operator representation error drops only by about a factor of approximately three. The operator representation error evidently does not prohibit the ROM solution error from approaching the CFD solution error, however.

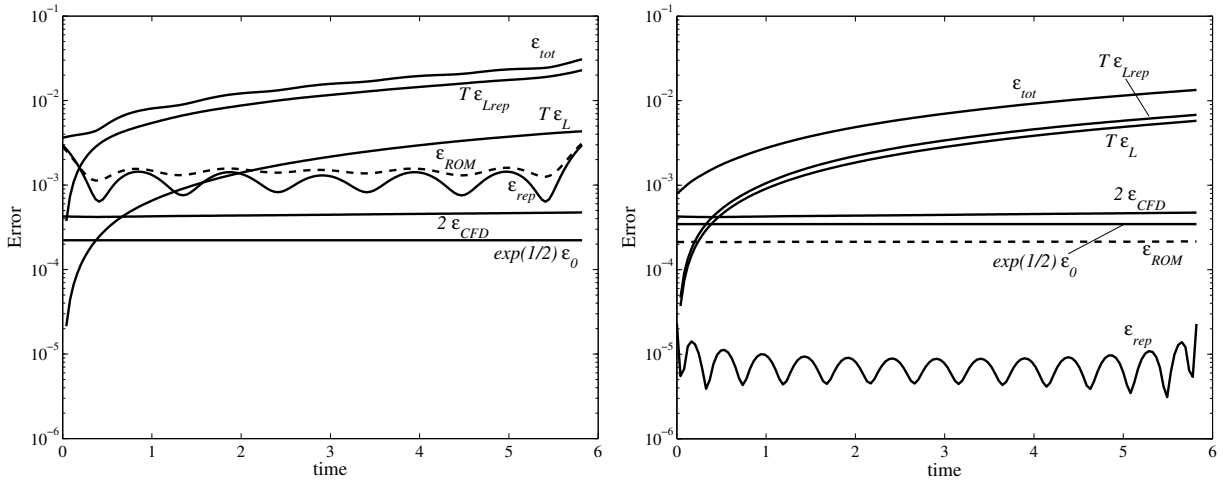

(a) Six-mode ROM.

(b) Fourteen-mode ROM.

Figure 3. Error estimates and ROM solution error (broken line).

Figure 4 shows the average error $\left(\text{expressed in the } ||\cdot||^{avg}_{(\mathbf{H},\Omega)} \text{ norm}\right)$ of the ROM solution as a function of the basis size used to construct the ROM. The ROM solution error approaches the CFD solution error as the basis size increases, levelling out close to the CFD error. This result confirms the intuitive argument that a reduced order model can only be as accurate as the CFD solutions used to construct it. It also demonstrates that, given a sufficiently rich POD basis, the present projection approach is capable of recovering the accuracy of the original CFD model.

Interestingly, the ROM error is slightly lower than the CFD solution error when twelve or fourteen modes are used. This seemingly counterintuitive result is not inconsistent with the POD/Galerkin approach for model reduction. The POD basis forms an approximation for the CFD solution space, and the ROM solution necessarily lies in this space. However, the CFD trajectory through this space is not necessarily the best one. The projection can (and does for a twelve or fourteen mode ROM) give a solution trajectory through the space that is slightly closer to the exact solution. This suggests that a slightly more accurate ROM may result from projecting the original continuous equations rather than projecting the discretized equations. It is not clear, however, whether this result is general or specific to our particular test case.

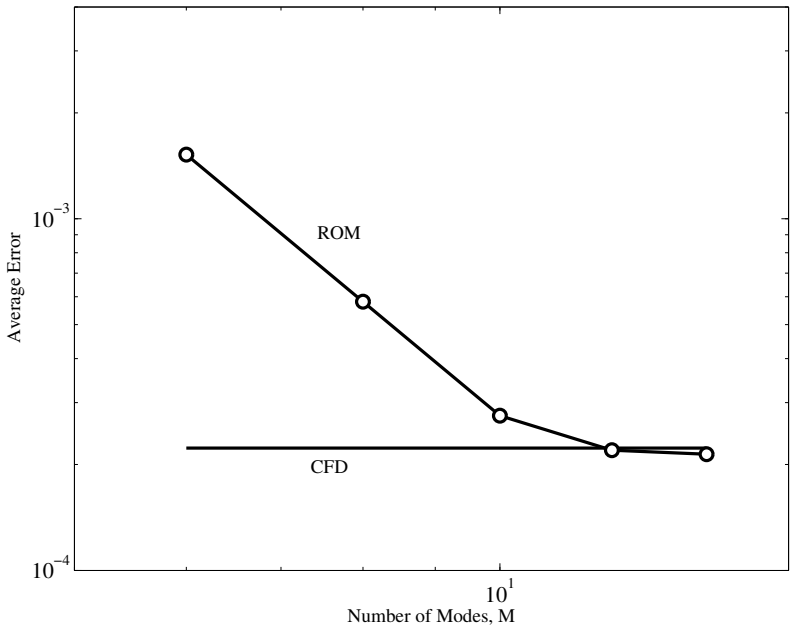

Figure 4. Error $||\mathbf{q}'_M - \mathbf{q}'||^{avg}_{(\mathbf{H},\Omega)}$ in the ROM solution as a function of basis size, compared with the error $||\mathbf{q}'_h - \mathbf{q}'||^{avg}_{(\mathbf{H},\Omega)}$ in the CFD solution error.

3 Reduced Order Models for a Nonlinear Plate with Aerodynamic Forcing

3.1 Introduction

Much like with fluid mechanical systems, first-principles computer simulation of the dynamics of complex structural systems is often prohibitively expensive. Techniques to reduce the number of degrees of freedom of the models, while preserving all of the relevant physics, are needed in order to analyze and optimize the design of complex structures. One approach of model reduction methods for structures is to first develop a full finite element model, then use a component mode synthesis approach to significantly reduce the number of degrees of freedom while incorporating the essential physics of the system including the nonlinearities [38, 39, 40, 41]. Other approaches include the use of a Galerkin approximation based on the results of a finite element analysis [42] or a hierarchical finite element method in which the order of the approximating polynomial is increased while the mesh size is held constant, which allows for meshes with as little as one element for a plate [43, 44]. These methods, however, can not be applied directly to nonlinear problems.

In what follows, von Karman plate theory will be employed to model the structure considered here, namely a panel on an aircraft or other moving body. The von Karman plate theory considers a class of nonlinear plates that takes into account in-plane stretching (a membrane nonlinearity) in the equations of motion, and thus allows for the modeling of large displacements of the plate. A modal expansion solution exists for the case of a cantilevered von Karman plate [45], but analytical, closed form solutions are not available for most other cases with general boundary conditions. A number of approximate methods exist, however, that can accurately model von Karman plates and shells [46]. Approximate methods include finite elements, both spline finite strip methods [47] and hierarchical finite element methods [43, 44], incremental harmonic balance [48], nonlinear normal modes [49], and assumed displacement fields with Taylor series expansions in the normal directions [50].

In this paper, the von Karman plate is coupled to an adjacent supersonic flow via a quasi-steady aerodynamic theory commonly referred to as piston theory. Dowell [51] considered the same problem and used a Galerkin approximation to model the mode shapes of the plate, while introducing an additional basis for the membrane motion that was coupled nonlinearly to the mode shapes through a weighted residuals technique. Other related aero-elastic problems include incompressible flow [52, 53, 54], turbulent flow modeled as a random process [55], reduced order models of the full fluid field [56, 19], and cylindrical bending assumptions for the plate [51, 57, 58], which effectively reduce the problem to that of a beam.

In what follows, the von Karman plate equations are presented in Section 3.2, and are discretized using the method of quadratic components in Section 3.2. A Galerkin method is then applied in Section 3.2 to develop an equation of motion in terms of the modal coefficients, and an implicit integration scheme for solving the coupled, nonlinear differential equations developed in the Galerkin discretization is presented in Section 3.2. An example to validate the discretization of

the plate's equation of motion is presented in Section 3.2 in order to compare the results from an explicit closed form solution for the linear plate to a one-term approximation of the nonlinear plate, a numerical analysis of the nonlinear plate performed in ABAQUS, and the present method with five mode shapes for the nonlinear plate. Finally, in Section 3.3, the coupling of the discretized plate with piston theory is presented, a cyclic method for calculating the limit cycle amplitudes is described, and a comparison to the results of [51, 59, 60, 61] is made.

3.2 The von Karman Plate

For thin plates, the out-of-plane displacement, w, is a function of the planar coordinates $w(x,y,z,t) = w(x,y,t)$ (where x is the direction of the fluid flow and y is the in-plane direction orthogonal to the flow) and time t. With the Kirchhoff assumption [62], the internal strains are

$$\varepsilon_{xx} = \frac{\partial u}{\partial x} + \frac{1}{2}\left(\frac{\partial w}{\partial x}\right)^2 \tag{124}$$

$$\varepsilon_{yy} = \frac{\partial v}{\partial y} + \frac{1}{2}\left(\frac{\partial w}{\partial y}\right)^2 \tag{125}$$

$$\varepsilon_{xy} = \frac{1}{2}\left(\frac{\partial v}{\partial x} + \frac{\partial u}{\partial y} + \frac{\partial w}{\partial x}\frac{\partial w}{\partial y}\right). \tag{126}$$

Following [62], the equations of motion for a thin plate with a membrane nonlinearity can be written in terms of the strains as

$$\rho_s h w_{,tt} + \mathcal{D}\nabla^4 w = g + \frac{12\mathcal{D}}{h^2}\left(\left(\varepsilon_{xx} + \nu\varepsilon_{yy}\right)\frac{\partial^2 w}{\partial x^2} + \left(\varepsilon_{yy} + \nu\varepsilon_{xx}\right)\frac{\partial^2 w}{\partial y^2} + 2\left(1-\nu\right)\varepsilon_{xy}\frac{\partial^2 w}{\partial x \partial y}\right) \tag{127}$$

$$\frac{\partial}{\partial x}\left(\varepsilon_{xx} + \nu\varepsilon_{yy}\right) + \left(1-\nu\right)\frac{\partial \varepsilon_{xy}}{\partial y} = 0 \tag{128}$$

$$\frac{\partial}{\partial y}\left(\varepsilon_{yy} + \nu\varepsilon_{xx}\right) + \left(1-\nu\right)\frac{\partial \varepsilon_{xy}}{\partial x} = 0. \tag{129}$$

with density ρ_s, flexural stiffness $\mathcal{D} = Eh^3/(12(1-\nu^2))$, and Poisson ratio ν. Substitution of Eqs. (124)-(126) into Eqs. (127)-(129) yields the familiar $w-u-v$ formulation [63]

$$\begin{aligned}\rho_s h w_{,tt} + \mathcal{D}\nabla^4 w = g + \frac{12\mathcal{D}}{h^2}\Bigg[&\left(u_{,x} + \frac{1}{2}{w_{,x}}^2\right)\left(w_{,xx} + \nu w_{,yy}\right) \\ &+ \left(v_{,y} + \frac{1}{2}{w_{,y}}^2\right)\left(w_{,yy} + \nu w_{,xx}\right) + \left(1-\nu\right)\left(u_{,y} + v_{,x} + w_{,x}w_{,y}\right)w_{,xy}\Bigg]\end{aligned} \tag{130}$$

$$u_{,xx} + w_{,x}w_{,xx} + \left(\frac{1-\nu}{2}\right)\left(u_{,yy} + w_{,x}w_{,yy}\right) + \left(\frac{1+\nu}{2}\right)\left(v_{,xy} + w_{,y}w_{,xy}\right) = 0 \tag{131}$$

$$v_{,yy} + w_{,y}w_{,yy} + \left(\frac{1-\nu}{2}\right)\left(v_{,xx} + w_{,y}w_{,xx}\right) + \left(\frac{1+\nu}{2}\right)\left(u_{,xy} + w_{,x}w_{,xy}\right) = 0. \tag{132}$$

Model Reduction Using Quadratic Components

The method of quadratic components consists of the selection of a set of basis functions $\{\phi_i\}$ appropriate for the linearized equations and postulating a solution to the nonlinear equation of the form

$$f(t,x) = \sum_i \alpha_i(t)\phi_i(x) + \sum_{i,j\leq i} \alpha_i(t)\alpha_j(t)G_{ij}(x), \tag{133}$$

where the $G_{ij}(x)$ are selected such that the expansion of (133) can solve a quasi-static version of the governing equation correctly to within second order in $\{\alpha_i\}$. The full expansion is then substituted into the dynamic governing differential equations to achieve nonlinear equations for the $\{\alpha_i\}$. Usually, but not always, the $\{\phi_i\}$ are selected to be the eigen solutions to the linearized equations. The method for solving for the $G_{ij}(x)$ is illustrated in the following and is discussed at length in [64, 65].

In the context of the von Karman plate equations, the method of quadratic components begins by identifying the eigenmodes $\underset{\sim}{\phi}_n$ and natural frequencies ω_n of the linearized homogeneous equation of motion

$$\rho_s h w_{,tt} + \mathcal{D}\nabla^4 w = 0. \tag{134}$$

The eigenmodes of the linear plate are then used to construct an orthogonal set of modal forces f_n. In the following discussion, however, the derivation does not necessitate this choice of basis. The forces are applied in an arbitrary linear combination

$$\underset{\sim}{f}(x,y) = \sum_{i=1}^{N} \alpha_i K \underset{\sim}{\phi}_i(x,y) \tag{135}$$

on the nonlinear plate, where K is the stiffness of the linear plate, and the response is numerically calculated. Next, the full kinematics of the plate are postulated as consisting of a linear component and a quadratic component.

The Taylor series expansion for a multivariate expression centered about the origin is given as

$$\begin{aligned}\underset{\sim}{\mathcal{N}}(\alpha_1,\alpha_2,...,\alpha_N) = {} & [\alpha_1 \quad \alpha_2 \quad \cdots \quad \alpha_N] \begin{bmatrix} \partial \underset{\sim}{f}/\partial\alpha_1 \\ \partial \underset{\sim}{f}/\partial\alpha_2 \\ \vdots \\ \partial \underset{\sim}{f}/\partial\alpha_N \end{bmatrix} + \\ & [\alpha_1 \quad \alpha_2 \quad \cdots \quad \alpha_N] \begin{bmatrix} \partial^2 \underset{\sim}{f}/\partial\alpha_1^2 & \partial^2 \underset{\sim}{f}/\partial\alpha_2\partial\alpha_1 & \cdots & \partial^2 \underset{\sim}{f}/\partial\alpha_N\partial\alpha_1 \\ \partial^2 \underset{\sim}{f}/\partial\alpha_1\partial\alpha_2 & \partial^2 \underset{\sim}{f}/\partial\alpha_2^2 & \cdots & \partial^2 \underset{\sim}{f}/\partial\alpha_N\partial\alpha_2 \\ \vdots & \vdots & \ddots & \vdots \\ \partial^2 \underset{\sim}{f}/\partial\alpha_1\partial\alpha_N & \partial^2 \underset{\sim}{f}/\partial\alpha_2\alpha_N & \cdots & \partial^2 \underset{\sim}{f}/\partial\alpha_N^2 \end{bmatrix} \begin{bmatrix} \alpha_1 \\ \alpha_2 \\ \vdots \\ \alpha_N \end{bmatrix} + \cdots . \end{aligned} \tag{136}$$

The response of the structure $\underset{\sim}{\mathcal{W}}$ is thus written in terms of the Taylor series up through quadratic terms

$$\underset{\sim}{\mathcal{W}}\ (x,y) = \underset{\sim}{\mathcal{N}}(\alpha_1,\alpha_2,...,\alpha_N) = \sum_{n=1}^{N} \alpha_n \underset{\sim}{Y_n}(x,y) + \sum_{n=1}^{N}\sum_{m=1}^{N} \alpha_n\alpha_m\, \underset{\sim}{G_{nm}}\,(x,y), \tag{137}$$

where

$$\underset{\sim}{Y_n}(x,y) = \frac{\partial \underset{\sim}{f}}{\partial \alpha_n} \tag{138}$$

and

$$\underset{\sim}{G_{nm}}\,(x,y) = \frac{\partial^2 \underset{\sim}{f}}{\partial\alpha_n \partial\alpha_m}. \tag{139}$$

With this nomenclature, the unit normal vectors are denoted as $\underset{\sim}{i}$, $\underset{\sim}{j}$, and $\underset{\sim}{k}$ in the x, y, and z directions respectively.

The derivatives $\partial \underset{\sim}{f}/\partial\alpha_i$ and $\partial^2 \underset{\sim}{f}/\partial\alpha_i\partial\alpha_j$ are calculated via finite difference approximations. In what follows, third and fifth order finite difference expressions are used; however, higher order expressions may be used. For each quantity, two low order finite difference approximations are constructed and are then used to compose the higher order approximation

$$\underset{\sim}{Y_n^{(a)}} = \frac{\underset{\sim}{\mathcal{N}}(\alpha_n) - \underset{\sim}{\mathcal{N}}(-\alpha_n)}{2\alpha_n} \tag{140}$$

$$\underset{\sim}{Y_n^{(b)}} = \frac{\underset{\sim}{\mathcal{N}}(2\alpha_n) - \underset{\sim}{\mathcal{N}}(-2\alpha_n)}{4\alpha_n} \tag{141}$$

$$\underset{\sim}{Y_n} = (4/3)\,\underset{\sim}{Y_n^{(a)}} - (1/3)\,\underset{\sim}{Y_n^{(b)}} \tag{142}$$

$$\underset{\sim}{G_{nn}^{(a)}} = \frac{\underset{\sim}{\mathcal{N}}(\alpha_n) + \underset{\sim}{\mathcal{N}}(-\alpha_n)}{\alpha_n^2} \tag{143}$$

$$\underset{\sim}{G_{nn}^{(b)}} = \frac{\underset{\sim}{\mathcal{N}}(2\alpha_n) + \underset{\sim}{\mathcal{N}}(-2\alpha_n)}{4\alpha_n^2} \tag{144}$$

$$\underset{\sim}{G_{nn}} = (4/3)\,\underset{\sim}{G_{nn}^{(a)}} - (1/3)\,\underset{\sim}{G_{nn}^{(b)}} \tag{145}$$

$$\underset{\sim}{G_{nm}^{(a)}} = \frac{\underset{\sim}{\mathcal{N}}(\alpha_n,\alpha_m) + \underset{\sim}{\mathcal{N}}(-\alpha_n,-\alpha_m) - \underset{\sim}{\mathcal{N}}(\alpha_n,-\alpha_m) - \underset{\sim}{\mathcal{N}}(-\alpha_n,\alpha_m)}{4\alpha_n\alpha_m} \tag{146}$$

$$\underset{\sim}{G_{nm}^{(b)}} = \frac{\underset{\sim}{\mathcal{N}}(2\alpha_n,2\alpha_m) + \underset{\sim}{\mathcal{N}}(-2\alpha_n,-2\alpha_m) - \underset{\sim}{\mathcal{N}}(2\alpha_n,-2\alpha_m) - \underset{\sim}{\mathcal{N}}(-2\alpha_n,2\alpha_m)}{16\alpha_n\alpha_m} \tag{147}$$

$$\underset{\sim}{G_{nm}} = (4/3)\,\underset{\sim}{G^{(a)}_{nm}} - (1/3)\,\underset{\sim}{G^{(b)}_{nm}}\,. \tag{148}$$

The notation $\underset{\sim}{\mathcal{N}}(\alpha_n)$ and $\underset{\sim}{\mathcal{N}}(\alpha_n,\alpha_m)$ is meant to indicate that the only non-zero elements of $[\alpha_1,\alpha_2,...,\alpha_N]$ are α_n, and α_n and α_m respectively. Because $\underset{\sim}{Y}$ is the linear component of the expansion, a converged solution for the coefficients yields that $\underset{\sim}{Y_n} = c\underset{\sim}{\phi^{(k)}_n}(x,y)$ when $\underset{\sim}{\phi^{(k)}_n}$ is resolved in the $\underset{\sim}{k}$ direction, and c is a constant based on the normalization method. In practice, the values for α are reduced until the coefficients have converged.

The out of plane and in-plane displacements are then expressed as

$$w(x,y,t) = \sum_{n=1}^{N} \alpha_n(t) W^{(n)}(x,y) = \sum_{n=1}^{N} \alpha_n \underset{\sim}{Y_n}(x,y) \tag{149}$$

$$u(x,y,t) = \sum_{n=1}^{N}\sum_{m=1}^{n} \alpha_n(t)\alpha_m(t) U^{(nm)}(x,y) \tag{150}$$

$$v(x,y,t) = \sum_{n=1}^{N}\sum_{m=1}^{n} \alpha_n(t)\alpha_m(t) V^{(nm)}(x,y), \tag{151}$$

with $U^{(nm)}$ and $V^{(nm)}$ being the components of $\underset{\sim}{G_{nm}}$ taken in the $\hat{x}$ and $\hat{y}$ directions respectively. Substitution of Eqs. (149)-(151) into Eqs. (131)-(132) and matching coefficients yields that for each $\alpha_n\alpha_m$,

$$\begin{aligned} 2U^{(mn)}_{,xx} + (1+\nu)V^{(mn)}_{,xy} + (1-\nu)U^{(mn)}_{,yy} &= -2\left(W^{(m)}_{,x}W^{(n)}_{,xx} + W^{(n)}_{,x}W^{(m)}_{,xx}\right) \\ &\quad -(1+\nu)\left(W^{(m)}_{,y}W^{(n)}_{,xy} + W^{(n)}_{,y}W^{(m)}_{,xy}\right) - (1-\nu)\left(W^{(m)}_{,x}W^{(n)}_{,yy} + W^{(n)}_{,x}W^{(m)}_{,yy}\right) \end{aligned} \tag{152}$$

and

$$\begin{aligned} 2V^{(mn)}_{,yy} + (1+\nu)U^{(mn)}_{,xy} + (1-\nu)V^{(mn)}_{,xx} &= -2\left(W^{(m)}_{,y}W^{(n)}_{,yy} + W^{(n)}_{,y}W^{(m)}_{,yy}\right) \\ &\quad -(1+\nu)\left(W^{(m)}_{,x}W^{(n)}_{,xy} + W^{(n)}_{,x}W^{(m)}_{,xy}\right) - (1-\nu)\left(W^{(m)}_{,y}W^{(n)}_{,xx} + W^{(n)}_{,y}W^{(m)}_{,xx}\right). \end{aligned} \tag{153}$$

Equations (152)-(153) are for the quasi-static in-plane displacement when the right hand sides are taken as distributed body forces in the $\underset{\sim}{i}$ and $\underset{\sim}{j}$ directions respectively. For any m, n, and appropriate in-plane boundary conditions, it is possible to solve for $U^{(mn)}$ and $V^{(mn)}$ in terms of $W^{(m)}$, $W^{(n)}$, and their derivatives.

Galerkin Formulation

With $U^{(mn)}$ and $V^{(mn)}$ known in terms of $W^{(m)}$, $W^{(n)}$, and their derivatives, substitution of Eqs. (149)-(151) into Eq. (130) yields the equation of motion in terms of α

$$\begin{aligned}
&\alpha_{s,tt}\rho_s h W^{(s)} + \alpha_s \mathcal{D}\nabla^4 W^{(s)} \\
&\quad - \frac{12\mathcal{D}}{h^2}\sum_{r=1}^{N}\sum_{n=1}^{N}\sum_{m=1}^{N}\left[\left(\alpha_n\alpha_m U_{,x}^{(nm)} + \frac{1}{2}\alpha_n W_{,x}^{(n)}\alpha_m W_{,x}^{(m)}\right)\left(\alpha_r W_{,xx}^{(r)} + \alpha_r \nu W_{,yy}^{(r)}\right)\right. \\
&\qquad + \left(\alpha_n\alpha_m V_{,y}^{(nm)} + \frac{1}{2}\alpha_n W_{,y}^{(n)}\alpha_m W_{,y}^{(m)}\right)\left(\alpha_r W_{,yy}^{(r)} + \alpha_r \nu W_{,xx}^{(r)}\right) \\
&\qquad \left. + (1-\nu)\left(\alpha_n\alpha_m U_{,y}^{(nm)} + \alpha_n\alpha_m V_{,x}^{(nm)} + \alpha_n W_{,x}^{(n)}\alpha_m W_{,y}^{(m)}\right)\alpha_r W_{,xy}^{(r)}\right] = g. \quad (154)
\end{aligned}$$

Contracting both sides with $W^{(s)}$ yields the Galerkin formulation, which is cubic in α. Because $W^{(s)}$ is proportional to the s^{th} eigenvector of the linearized problem,

$$\alpha_{s,tt} + \omega_s^2\alpha_s + \sum_{r=1}^{N}\sum_{n=1}^{N}\sum_{m=1}^{N} P_{srnm}\alpha_r\alpha_n\alpha_m = G_s(t), \quad (155)$$

where

$$\omega_s^2 = \int W^{(s)}\mathcal{D}\nabla^4 W^{(s)} dA, \quad (156)$$

$$G_s(t) = \int W^{(s)} g dA, \quad (157)$$

and

$$\begin{aligned}
P_{srnm} = -\frac{12\mathcal{D}}{h^2}\int W^{(s)}&\left[\left(U_{,x}^{(nm)} + \frac{1}{2}W_{,x}^{(n)}W_{,x}^{(m)}\right)\left(W_{,xx}^{(r)} + \nu W_{,yy}^{(r)}\right)\right. \\
&\left. + \left(V_{,y}^{(nm)} + \frac{1}{2}W_{,y}^{(n)}W_{,y}^{(m)}\right)\left(W_{,yy}^{(r)} + \nu W_{,xx}^{(r)}\right) + (1-\nu)\left(U_{,y}^{(nm)} + V_{,x}^{(nm)} + W_{,x}^{(n)}W_{,y}^{(m)}\right)W_{,xy}^{(r)}\right] dA. \quad (158)
\end{aligned}$$

In practice, only half of the elements of P need to be calculated as $P_{srnm} = P_{srmn}$. The corresponding matrix form of Eq. (155) is written as

$$\mathbb{I}\underset{\sim}{\ddot{\alpha}} + \mathrm{diag}\left(\omega_s^2\right)\underset{\sim}{\alpha} + \begin{bmatrix} \underset{\sim}{\alpha}^T\mathbb{P}_{11}\underset{\sim}{\alpha} & \cdots & \underset{\sim}{\alpha}^T\mathbb{P}_{1N}\underset{\sim}{\alpha} \\ \vdots & \ddots & \vdots \\ \underset{\sim}{\alpha}^T\mathbb{P}_{N1}\underset{\sim}{\alpha} & \cdots & \underset{\sim}{\alpha}^T\mathbb{P}_{NN}\underset{\sim}{\alpha} \end{bmatrix}\underset{\sim}{\alpha} = \underset{\sim}{G}(t). \quad (159)$$

Here, $\mathbb{I}$ denotes the identity matrix, $\mathrm{diag}\left(\omega_s^2\right)$ indicates a diagonal matrix with nonzero values corresponding to the squares of the natural frequencies in order of $s = 1$ to N, and

$$\mathbb{P}_{ab} = \begin{bmatrix} P_{ab11} & \cdots & P_{ab1N} \\ \vdots & \ddots & \vdots \\ P_{abN1} & \cdots & P_{abNN} \end{bmatrix}. \quad (160)$$

The advantage of this system of coupled, nonlinear differential equations is that there are only as many degrees of freedom as there are transverse modes. Additionally, no further spatial integrations must be performed once the coefficients and $\underset{\sim}{G}(t)$ are calculated.

Implicit Time Integration Method

Solutions of the nonlinear equation for α (155) are available through power series methods, harmonic balance/Fourier series methods, and other approximate solutions. However, in order to efficiently account for an arbitrary applied pressure g, an implicit integration method, the Hilber-Hughes-Taylor (HHT) method [66, 67], is applied. Due to the nonlinearities of (155), the first step in the solution is to guess a solution at the next time step $\underset{\sim}{\chi} = \underset{\sim}{\alpha}(t_{n+1})$. The mass and stiffness matrices for the system can then be defined as

$$\mathbb{M} = \mathbb{I} \tag{161}$$

and

$$\mathbb{K}(\underset{\sim}{\chi}) = \text{diag}\left(\omega_s^2\right) + \begin{bmatrix} \underset{\sim}{\chi}^T \mathbb{P}_{11} \underset{\sim}{\chi} & \cdots & \underset{\sim}{\chi}^T \mathbb{P}_{1N} \underset{\sim}{\chi} \\ \vdots & \ddots & \vdots \\ \underset{\sim}{\chi}^T \mathbb{P}_{N1} \underset{\sim}{\chi} & \cdots & \underset{\sim}{\chi}^T \mathbb{P}_{NN} \underset{\sim}{\chi} \end{bmatrix}. \tag{162}$$

From the HHT method, with modal acceleration $\underset{\sim}{\xi}$, and modal velocity $\underset{\sim}{\zeta}$,

$$\mathbb{M}\underset{\sim}{\xi}(t_{n+1}) + (1+\lambda)\,\mathbb{K}(\underset{\sim}{\chi})\underset{\sim}{\alpha}(t_{n+1}) - \lambda\mathbb{K}(\underset{\sim}{\chi})\underset{\sim}{\alpha}(t_n) = \underset{\sim}{G}(t_{n+1+\lambda}), \tag{163}$$

where

$$t_{n+1+\lambda} = t_{n+1} + \lambda\Delta t, \tag{164}$$

$$\beta = \frac{1-\lambda^2}{4}, \tag{165}$$

$$\gamma = \frac{1-2\lambda}{2}, \tag{166}$$

$$\underset{\sim}{\alpha}(t_{n+1}) = \underset{\sim}{\alpha}(t_n) + \Delta t\,\underset{\sim}{\zeta}(t_n) + \frac{\Delta t^2}{2}\left[(1-2\beta)\underset{\sim}{\xi}(t_n) + 2\beta\underset{\sim}{\xi}(t_{n+1})\right], \tag{167}$$

$$\underset{\sim}{\zeta}(t_{n+1}) = \underset{\sim}{\zeta}(t_n) + \Delta t\left[(1-\gamma)\underset{\sim}{\xi}(t_n) + \gamma\underset{\sim}{\xi}(t_{n+1})\right], \tag{168}$$

and

$$\begin{aligned}\underset{\sim}{\xi}(t_{n+1}) = &\left[\mathbb{M} + (1+\lambda)\Delta t^2\beta\mathbb{K}(\underset{\sim}{\chi})\right]^{-1} \\ &\times\left[\underset{\sim}{G}(t_{n+1+\lambda}) - \left((1+\lambda)\frac{\Delta t^2}{2}(1-2\beta)\mathbb{K}(\underset{\sim}{\chi})\right)\underset{\sim}{\xi}(t_n)\right. \\ &\left. - \left((1+\lambda)\Delta t\,\mathbb{K}(\underset{\sim}{\chi})\right)\underset{\sim}{\zeta}(t_n) - \mathbb{K}(\underset{\sim}{\chi})\underset{\sim}{\alpha}(t_n)\right].\end{aligned} \tag{169}$$

In practice, Eq. (169) is solved via LU-decomposition, and a typical value for $\lambda = 0.05$. Next, the residual $R = \underset{\sim}{\alpha}(t_{n+1}) - \underset{\sim}{\chi}$ is calculated, and the procedure is repeated with a new guess for $\underset{\sim}{\chi}$ until $R \to 0$.

Static Pressure Validation Example

In Figure 5, a plate with simply supported conditions at $x = 0$ and $x = L_x$, and free boundary conditions at $y = 0$ and $y = L_y$ is modeled. The material properties are based on aluminum, and are listed in Table 2 along with the geometric properties. Four different solutions for the displacement of this plate are considered: an explicit, closed form solution for the linear plate [68], a one term approximation for the nonlinear plate, the numerical results calculated using the ABAQUS software package for the nonlinear plate, and the nonlinear model discretized in the previous sections using five mode shapes. The applied pressure in all cases is a constant, uniform pressure with magnitude F.

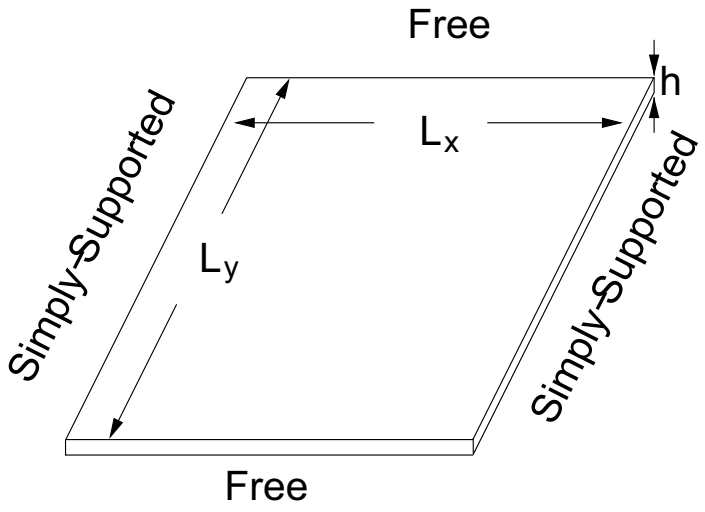

Figure 5. Geometry of the rectangular plate.

Variable	Value
Plate modulus of elasticity, E	75.378 GPa
Plate thickness, h	4.6 mm
Plate length in the downstream direction, L_x	1 m
Plate length in the cross-stream direction, L_yx	1 m
Plate density, ρ_s	2770 kg/m^3
Poisson's ratio of the plate, ν	0.33
Mach number, M	2

Table 2. System parameters for the comparison with [51].

One Term Approximation

The one term approximation is developed with the assumption that the displacement does not vary in y. In this case, the problem is reduced to that of a beam. The eigenmodes for this problem are

$$W^{(n)}(x) = c_0 \sin\frac{n\pi x}{L_x} \tag{170}$$

where $c_0 = \sqrt{\frac{2}{L_x\rho_s h L_y}}$. Taking only the first mode, the equation for the lateral deformation $U^{(11)}$ is

$$U^{(11)}_{,xx} = -W^{(1)}_{,x}W^{(1)}_{,xx}. \tag{171}$$

Substitution into Eq. (170) yields the in-plane displacement

$$U^{(11)} = -\frac{c_0^2\pi}{8L_x}\sin\left(\frac{2\pi x}{L_x}\right). \tag{172}$$

With a lateral deflection of $w(x) = \alpha W^{(1)}(x)$, the longitudinal strain due to the lateral deformation and the strain of the corresponding longitudinal displacement are

$$\varepsilon_w = \frac{1}{2}w^2_{,x} = \frac{\alpha^2\pi^2}{L_x^4\rho_s h}\cos^2\left(\frac{\pi x}{L_x}\right) \tag{173}$$

$$\varepsilon_u = \alpha^2\frac{\partial U^{11}}{\partial x} = -\alpha^2\frac{\pi^2}{2L_x^4\rho_s h}\cos^2\left(\frac{2\pi x}{L_x}\right). \tag{174}$$

Combining these two strain components and substituting into the governing equation yields the one term approximation for α

$$\ddot{\alpha} + \omega^2\alpha + \alpha^3\left[\left(\frac{12\mathcal{D}}{h^2}\right)\left(\frac{\pi^4}{2L_x^5}\right)\left(\frac{1}{\rho_s h L_x}\right)^3\right] = \int_0^{L_x} g(x)W^{(1)}dx. \tag{175}$$

For the present quasi-static problem, solution of (175) reduces to determining the roots of a polynomial.

Results

The results for the four solution methods are shown in Figure 6 on a logarithmic plot and Figure 7 on a linear plot. For pressures below $F = 100$, all four solutions show good agreement. Above $F = 100$, the linear solution diverges from the three nonlinear solutions. While the one term approximation exhibits the stiffening behavior associated with the von Karman plate equations, there is a 30% relative error, with respect to the numerical solution, in the maximum deflection of the plate for $F = 1000$, and for the discretization method presented in the previous sections with $N \geq 3$, a 5.0% relative error is observed with respect to the numerical solution. Additionally, the present method is found to yield converged results with only 3 modes.

In terms of computational efficiency, the linear and one term solution both were completed in under one second. The numerical solution in ABAQUS with three modes and 2601 elements, the minimum needed for convergence, required 27.5 minutes while the present method with three modes took 2.65 minutes using a simplex algorithm [69] to efficiently minimize the residuals R once the coefficients $\underset{\sim}{G_{nm}}$ and $\underset{\sim}{Y_n}$ had been calculated. All simulations were calculated using a single processor.

3.3 Fluid-Structure Interaction

With the matrix form of the equation of motion now specified in terms of one variable (159), the fluid model can be introduced via the forcing function $\underset{\sim}{G}(t)$. The "full" quasi-steady pressure relationship of piston theory for a flow with speed Υ, density ρ_f, and Mach number M is given as [51]

$$p - p_\infty = w_{,t}\frac{\rho_f \Upsilon}{\rho_s h}\frac{M^2-2}{(M^2-1)^{3/2}} + w_{,x}\frac{\rho_f \Upsilon^2}{(M^2-1)^{1/2}}. \tag{176}$$

In terms of the Galerkin formulation (155), the applied force becomes

$$\begin{aligned} G_s &= -\int W^{(s)}\,(p - p_\infty)\,dA \\ &= -\zeta_s\frac{\rho_f \Upsilon}{\rho_s h}\frac{M^2-2}{(M^2-1)^{3/2}} - \frac{\rho_f \Upsilon^2}{(M^2-1)^{1/2}}\sum_{n=1}^{N}\alpha_n\int W^{(s)}W_{,x}^{(n)}dA. \end{aligned} \tag{177}$$

In order to find the amplitudes and periods of the limit cycles excited by the fluid flow over the plate, a cyclic method similar to [70, 71] is employed. In this method, the modal amplitudes α_n and period of vibration for the system T are sought such that

$$\begin{aligned} \alpha_n(t) &= \alpha_n(t+T) \\ \zeta_n(t) &= \zeta_n(t+T) \\ \xi_n(t) &= \xi_n(t+T). \end{aligned} \tag{178}$$

The period T is found by simulating the response over a time long enough to include several periods, then choosing the T that minimizes the residuals of (3.3). For cases that do not converge after one simulation, a simplex algorithm is employed to minimize both T and α_n, ζ_n, and ξ_n efficiently. Once T is found, the modal periods are found by calculating the number of periods for each mode per period of the system. In practice, once α_n, ζ_n, and ξ_n and T are found for one value of a parameter being varied, either by a transient analysis or minimization algorithm, the α_n, ζ_n, and ξ_n and T are quickly found for an adjacent value of the parameter being studied by using the previous value's results as an initial value for the next value.

Comparison to Classical Results

For the present analysis, the Mach number is held constant while the speed of sound in the fluid μ is varied, with the fluid speed

$$\Upsilon = \mu M, \tag{179}$$

and fluid density

$$\rho_f = \frac{\rho_s h M}{10}. \tag{180}$$

This allows for the direct comparison to the results of Dowell [51] and more recent studies [59, 60, 61]. The relationship between Dowell's nondimensionalized nomenclature and the variables in the present analysis are given for the dynamic pressure and period

$$\lambda^* = \frac{3\rho_f \Upsilon^2 L_x^3}{2\mathcal{D}\sqrt{M^2-1}} \tag{181}$$

$$\tau = T\sqrt{\frac{\mathcal{D}}{\rho_s h L_x^4}} \tag{182}$$

respectively. The plate is modeled with the material properties of aluminum and geometrical properties listed in Table 2. In keeping with the analysis of [51], the first six mode shapes that have no variation in y are used in what follows. Defining the quantities

$$\psi_n = \max \frac{\alpha_n(t) W^{(n)}(x,y)}{h} \qquad \forall x \in [0, L_x], \quad \forall y \in [0, L_y], \quad \forall t \tag{183}$$

$$\Psi = \max \frac{w(\frac{3}{4}L_x, \frac{1}{2}L_y, t)}{h} \qquad \forall t \tag{184}$$

$$\Psi_D = \Psi_{Classical} - \Psi_{Present}, \tag{185}$$

the modal limit cycle amplitudes ψ_n and periods τ are calculated as a function of λ^*, and are shown in Figure 8. Below the onset of flutter, at $\lambda^* \approx 530$, the τ do not converge to any particular limit cycle period as the modal amplitudes are approximately zero. Above the onset of flutter, though, the τ are convergent to the same value for all modes at a given λ^* as the plate undergoes forced vibration. The mode number for each modal limit cycle amplitude is indicated on the right side of Figure 8(a). While the modal coefficient for the first mode α_1 is higher than the other five modes, the product $\alpha_j W^{(j)}$ is greater for modes 2 through 4.

The range over which the onset of flutter occurs varied from $\lambda^* = 522$ to 545, depending on initial conditions, though in each case the flutter amplitude after onset converged over a short range of λ^*. Between λ^*=480 and the onset of the primary limit cycle, a second, non-zero limit cycle was observed with an amplitude that is 8 orders of magnitude below the limit cycle amplitudes reported here. The present analysis is compared to the results of [51] in Figure 9. The multiple points for the present result over the range of $\lambda^* \in [522, 545]$ indicate the range of onset of the limit cycle determined by the initial conditions of the simulation. The onset of flutter predicted by [51] occurs at the extremum of the range of λ^* calculated here (at $\lambda^* \approx 545$). Overall there is good agreement between the two models, though there is some discrepancy at lower values of λ^*.

The more recent analyses [59, 60, 61] of the same system are compared to the results of the model developed in this paper and [51] in Figure 10. Each of these analyses utilizes a finite element method; [60], in particular, studies two types of elements, a rectangular element and a higher order discrete Kirchhoff theory triangular element, and also takes into account thermal effects. While the simulation results using the rectangular element have higher agreement with [51] near the onset of flutter, the triangular element is shown to be significantly better for $\lambda^* \geq 600$. A triangular element with the same number of degrees of freedom is also employed in the finite element analysis performed in [59], but the predicted limit cycle amplitudes with this element are appreciably below those predicted in [60]. The finite element analysis of [61] uses a rectangular four-node Bogner-Fox-Schmidt C^1 conforming element. The relative difference between [61] and [51] is greater than any of the other studies reported, but the modeling of [61] also takes into account acoustical and thermal loading. By contrast, the present analysis develops a reduced order model that incorporates higher order effects for the entire plate, which is a much more computationally efficient approach than what is reported in the literature, and it does not sacrifice accuracy.

For all results shown in Figure 10, the disagreement is highest at the onset of flutter, but the results tend to converge to those of the present model away from onset. The onset of flutter is highly dependent on the initial conditions, thus the reported results and discrepancies in that region is not a significant concern. The difference in limit cycle amplitudes between the present method and [51, 59, 60, 61] is further analyzed in Figure11. The analysis of [59], in particular, is shown to converge to the same limit cycle amplitude as λ^* increases, and the most recent study [61] is shown to be consistently higher than all other reported results. Possible variance between [51] and the present method include [51] reporting values that had converged to within 5% of the $N \to \infty$ solution, which could account for all of the variance for $\lambda > 560$. Second, and to a lesser extent than the previous explanation, the values from [51, 59, 60, 61] were interpolated from plots using electronic copies of the original papers. Overall, though, there is reasonable agreement between the methods.

3.4 Conclusions

A reduced order model for von Karman plates was developed and discretized in both space by a Galerkin approximation and time with an implicit integration scheme. The model developed here is at least as computationally efficient and as accurate as the other models described in the literature. The reduced order model of the von Karman plate is subsequently validated using a

numerical analysis for the case of a static plate, and by comparison to the classic results of [51] for the case of a plate under quasi-steady pressure fluid flow. The primary results and contributions of this paper are

1. The full kinematics of a von Karman plate can be postulated as consisting of both linear and quadratic components. These are found by first identifying the eigenmodes and natural frequencies of the linear plate, then using them in a multivariate expansion to find the response of the nonlinear plate.

2. The reduced order modeling method developed in this paper is validated for a plate with a uniform load using both numerical and classical results, and it is shown that the computational time required for it is significantly less than that of other numerical methods.

3. The application of the model developed in this paper to the problem of quasi-steady fluid flow shows that the predicted results are in good agreement with results previously reported in [51, 59, 60, 61].

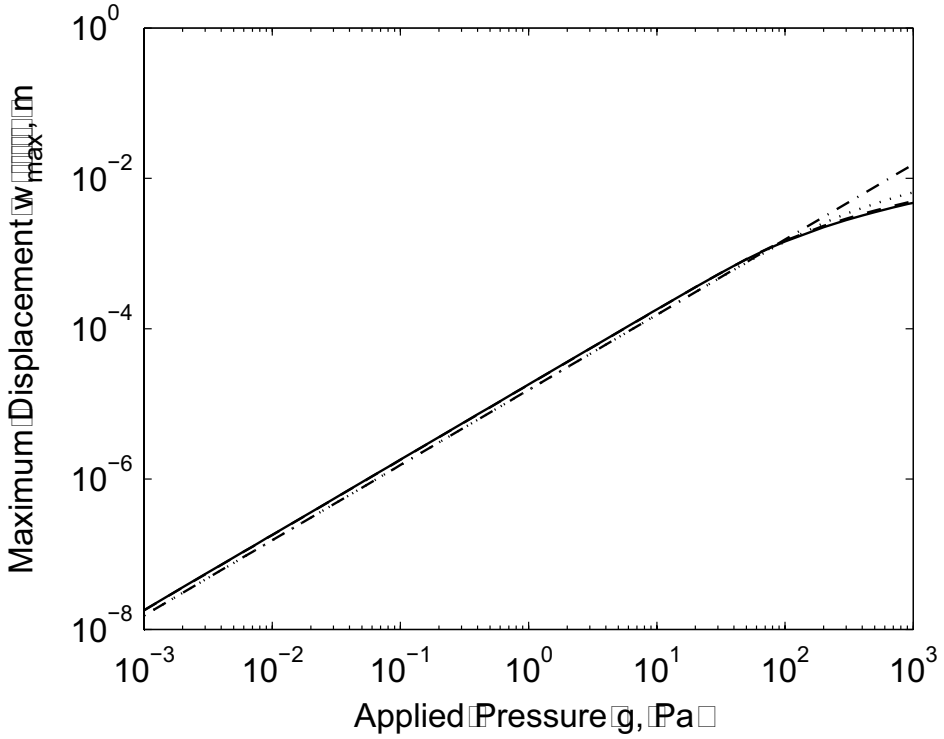

Figure 6. Log plot of the four solutions to the quasi-static example; (—) the present method, (– –) numerical results from ABAQUS, $(\cdots)$ the one term approximation, $(-\cdot-)$ the explicit linear solution [68].

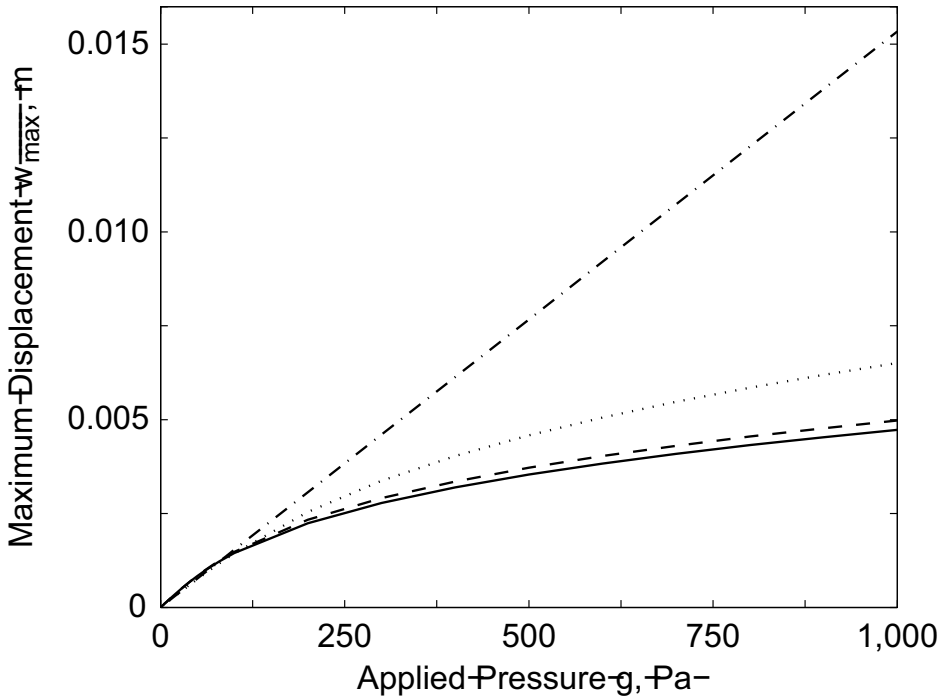

Figure 7. Linear plot of the four solutions to the quasi-static example; (—) the present method, (– –) numerical results from ABAQUS, $(\cdots)$ the one term approximation, $(- \cdot -)$ the explicit linear solution [68].

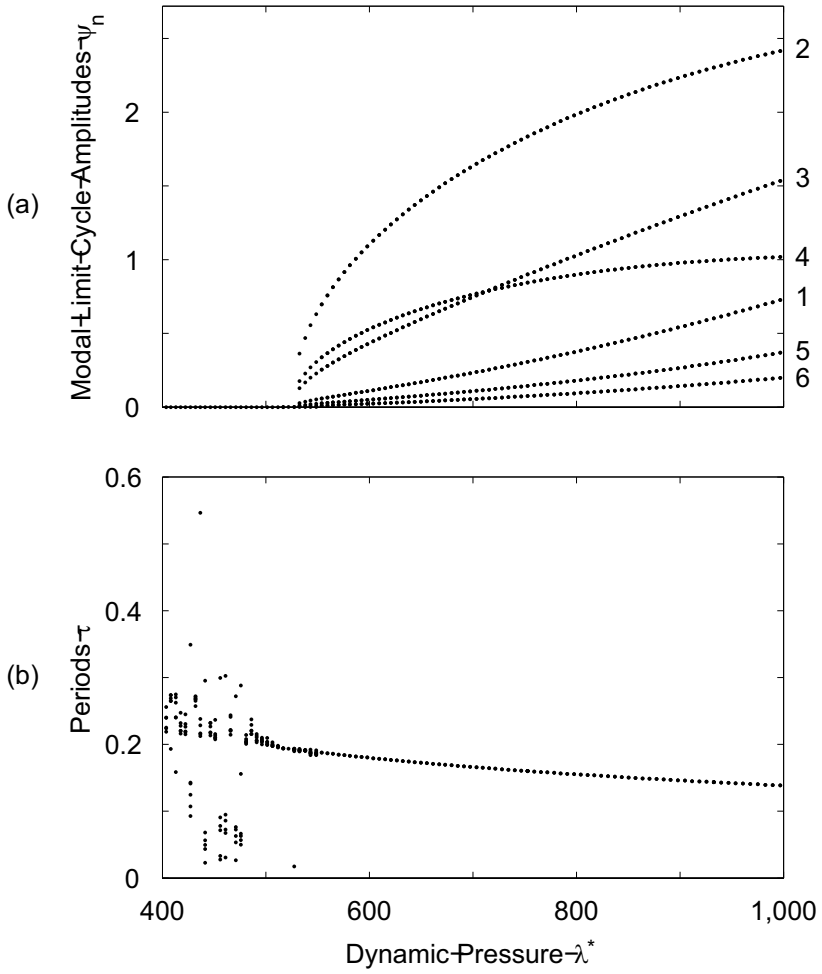

Figure 8. The limit cycle (a) amplitudes and (b) periods for each mode included in the analysis as a function of the nondimensional dynamic pressure. Mode numbers are indicated on the right side of the figure.

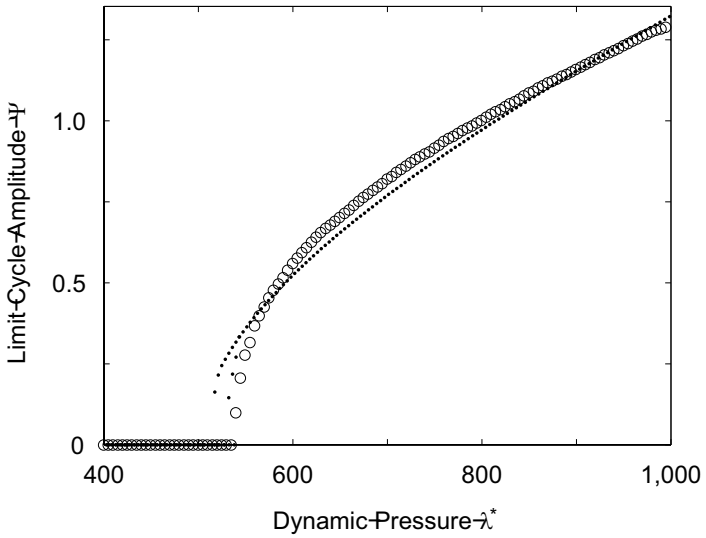

Figure 9. The limit cycle amplitudes for the total plate response at $x = 0.75L_x$ and $y = 0.5L_y$ as a function of the nondimensional dynamic pressure for the present work (•) and [51] (◯).

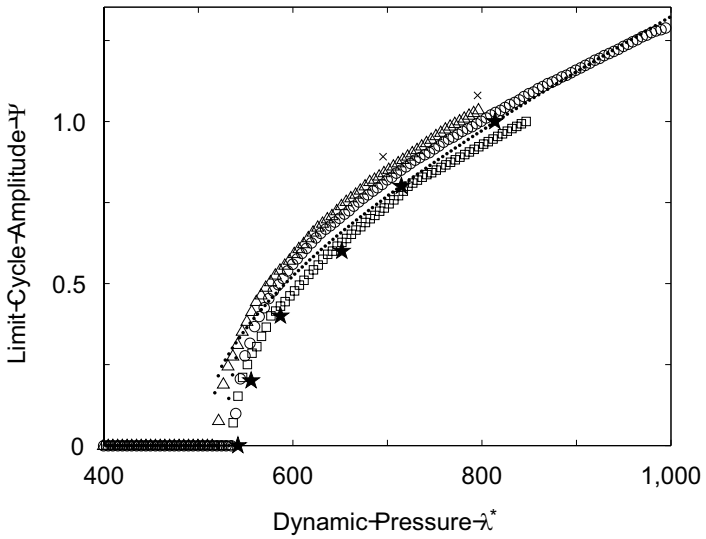

Figure 10. The limit cycle amplitudes for the total plate response at $x = 0.75L_x$ and $y = 0.5L_y$ as a function of the nondimensional dynamic pressure for the present work (•), [51] (◯), [59] (★), [60] using rectangular (□) and triangular (△) elements, and [61] (x).

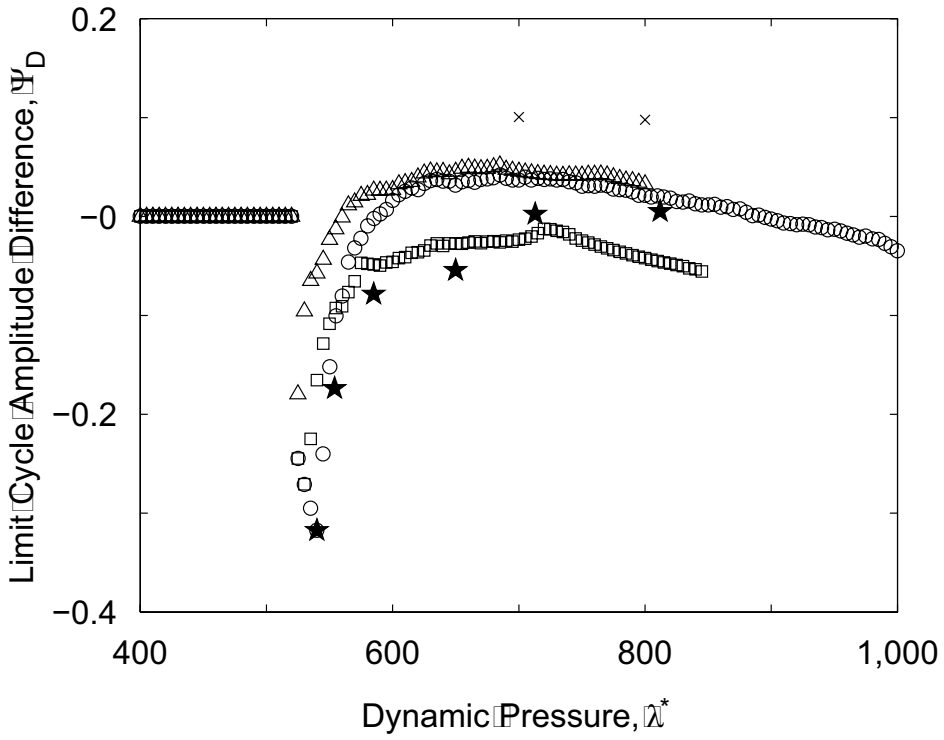

Figure 11. The difference in limit cycle amplitudes for the total plate response at $x = 0.75L_x$ and $y = 0.5L_y$ as a function of the nondimensional dynamic pressure between the present work and [51] (◯), [59] (★), [60] using rectangular (□) and triangular (△) elements, and [61] (x).

4 Coupled Fluid/Structure Reduced Order Models

4.1 Introduction

The main goal of this section is to tie together the discussion of the fluid (Section 2) and structure (Section 3) reduced order models (ROMs), and to prove numerical stability of the coupled linearized fluid/structure Galerkin ROM.

Recall that the governing fluid equations are the linearized compressible Euler equations (10) in some open bounded domain $\Omega \subset \mathbb{R}^3$. In the fluid ROM, the primal unknown, namely the vector of fluctuating state variables $\mathbf{q}'^T = \begin{pmatrix} u'_1 & u'_2 & u'_3 & \zeta' & p' \end{pmatrix}$ is expanded in an orthonormal, vector modal basis $\{\boldsymbol{\phi}_m\}_{m=1}^M \subset \mathbb{R}^5$ as in (31):

$$\mathbf{q}'_M(\mathbf{x},t) = \sum_{m=1}^{m} a_m(t)\boldsymbol{\phi}_m(\mathbf{x}) \tag{186}$$

To generate a simple linear coupled fluid/structure ROM, let us assume that the domain Ω contains a linear, rectangular plate of dimensions $L_x \times L_y$, located in the $z = 0$ plane, allowed to move in the positive or negative z–coordinate direction only. Denoting the z–displacement of this plate by $w(x,y,t)$, the governing structure equations are the linearized von Karman equations (Section 3.2) for the z–displacement of the plate, with appropriate boundary conditions applied along the plate edges (e.g., simply supported or clamped edges):

$$\rho_s h w_{,tt} + \mathcal{D}\nabla^4 w = g(x,y,t) \tag{187}$$

where

$$\nabla^4 w \equiv \frac{\partial^4 w}{\partial x^4} + 2\frac{\partial^4 w}{\partial x^2 \partial y^2} + \frac{\partial^4 w}{\partial y^4} \tag{188}$$

The physical properties that appear in (187) are described in Section 3.2. Letting $\{W^{(k)}(x,y) : k = 1,2,\ldots,N\}$ be the orthonormal (scalar) modal basis, the z-displacement w can be expanded in this basis as

$$w_N(x,y,t) = \sum_{n=1}^{N} \alpha_n(t) W^{(n)}(x,y) \tag{189}$$

as in (149).

In (187), $g(x,y,t)$ is the applied fluid loading, assumed to be free of shear components and thus consists only of the static pressure. Physically, g will represent the fluid pressure loading on the structure (in this case, the linear plate):

$$g(x,y,t) = -p'_N(x,y,0,t) = -\sum_{k=1}^{M} a_k(t)\phi_k^5(x,y,0) \tag{190}$$

One can see that with the source g in (187) defined by (190), the structure equations (187) are coupled to the fluid equations (10). Additional coupling terms will arise when one considers the

boundary conditions on the fluid variables at the plate boundary. Recall from Section 2.5 that we have prescribed a linearized acoustically-reflecting (or no-penetration) boundary condition on $\partial\Omega_W$ (58):

$$V_5' = V_4' - 2u_w' \quad \text{on} \quad \partial\Omega_W \tag{191}$$

where $\mathbf{V}' \equiv \mathbf{S}^{-1}\mathbf{q}'$ is the primal fluid unknown in the characteristic variables, and u_w' is the fluid velocity at the wall. In terms of the displacement w:

$$u_w'(x,y,t) = -\dot{w} - \bar{\mathbf{u}} \cdot \nabla w \tag{192}$$

Thus, the boundary condition on the fluid equations (191) is coupled to the structure ROM, as the structure displacement appears in (192).

Letting $\{\alpha_n(t)\}_{n=1}^N$ be the structure ROM coefficients (189) and $\{a_n(t)\}_{n=1}^M$ be the fluid ROM coefficients (186) and denoting

$$\mathbf{S}^T \equiv \begin{pmatrix} \alpha_1(t) & \cdots & \alpha_N(t) & \dot{\alpha}_1(t) & \cdots & \dot{\alpha}_N(t) \end{pmatrix} \in \mathbb{R}^{2N} \tag{193}$$

$$\mathbf{F}^T \equiv \begin{pmatrix} a_1(t) & \cdots & a_M(t) \end{pmatrix} \in \mathbb{R}^M \tag{194}$$

the coupled fluid/structure system can be written in the form

$$\begin{pmatrix} \dot{\mathbf{F}} \\ \dot{\mathbf{S}} \end{pmatrix} = \begin{pmatrix} \mathbf{A} & \mathbf{B} \\ \mathbf{C} & \mathbf{D} \end{pmatrix} \begin{pmatrix} \mathbf{F} \\ \mathbf{S} \end{pmatrix} \tag{195}$$

The $\mathbf{A}$ and $\mathbf{B}$ matrices come from the fluid ROM for (10), whereas the $\mathbf{C}$ and $\mathbf{D}$ matrices come from the structure ROM for (187). The entries $\mathbf{A}$ and $\mathbf{B}$ depend on the boundary conditions on $\partial\Omega_W$ and $\partial\Omega_F$, and were derived earlier, namely in (53). Assuming the so-called acoustically-reflecting boundary condition (191) plate boundary $\partial\Omega_W$, the matrix system coming from the fluid equations is

$$\dot{\mathbf{F}} = \mathbf{A}\mathbf{F} + \mathbf{B}\mathbf{S} \tag{196}$$

where

$$A(i,j) = -\int_{\partial\Omega_W} \phi_i^n(\phi_j^5 + \bar{\rho}c\phi_j^n)dS - \int_{\partial\Omega_F} h_j(\boldsymbol{\phi}_i)dS + \int_\Omega \frac{\partial}{\partial x_i}(\boldsymbol{\phi}_j^T \mathbf{H}\mathbf{A}_i)\mathbf{q}'d\Omega, \quad 1 \le i,j \le M \tag{197}$$

$$B(i,j) = \begin{cases} \left(\phi_i^5, \bar{\mathbf{u}} \cdot \nabla W^{(j)}\right)_{L^2(\partial\Omega_W)}, & 1 \le i \le M, \;\; 1 \le j \le N \\ \int_{\partial\Omega_W} W^{(j-N)}(\phi_i^5 - \bar{\rho}c\phi_i^n)dS, & 1 \le i \le M, \;\; (N+1) \le j \le 2N \end{cases} \tag{198}$$

In (197), $h_j(\boldsymbol{\phi}_i)$ is determined by the far-field boundary conditions[6]. Note that, under the uniform base flow assumption $\bar{\mathbf{u}} = \mathbf{0}$, the $\mathbf{B}$ matrix (198) reduces to

$$B(i,j) = \begin{cases} 0, & 1 \le i \le M, \;\; 1 \le j \le N \\ \int_{\partial\Omega_W} W^{(j-N)}(\phi_i^5 - \bar{\rho}c\phi_i^n)dS, & 1 \le i \le M, \;\; (N+1) \le j \le 2N \end{cases} \tag{199}$$

[6]See the Appendix of [31] for a detailed discussion of the implementation of the far-field boundary conditions.

To arrive at the structure ROM, one substitutes the modal expansion (189) into (187). Doing so gives the following system for the structure ROM modes

$$(\rho_s h)\ddot{\alpha}_k + \omega_k^2 \alpha_k = G_k(t), \quad k = 1, ..., N \tag{200}$$

where, as in (156) and (157) respectively,

$$\omega_k^2 \equiv \mathcal{D}(\nabla^4 W^{(k)}, W^{(k)})_{L^2(\partial\Omega_W)} \tag{201}$$

$$G_k(t) = (g, W^{(k)})_{L^2(\partial\Omega_W)} \tag{202}$$

Substituting (190) into (200) gives rise to the following matrix system:

$$\dot{\mathbf{S}} = \mathbf{CF} + \mathbf{DS} \tag{203}$$

where

$$\mathbf{C} \equiv \left(\begin{array}{c} \mathbf{0}_{N\times M} \\ \hline \frac{1}{\rho_s h}\tilde{\mathbf{C}}_{N\times M} \end{array} \right), \quad \mathbf{D} \equiv \left(\begin{array}{c|c} \mathbf{0}_{N\times N} & \mathbf{I}_{N\times N} \\ \hline -\frac{1}{\rho_s h}\tilde{\mathbf{L}}_{N\times N} & \mathbf{0}_{N\times N} \end{array} \right) \tag{204}$$

and

$$\tilde{\mathbf{C}}_{N\times M} \equiv \begin{pmatrix} \left(\phi_1^5, W^{(1)}\right)_{L^2(\partial\Omega_W)} & \cdots & \left(\phi_M^5, W^{(1)}\right)_{L^2(\partial\Omega_W)} \\ \vdots & \ddots & \vdots \\ \left(\phi_1^5, W^{(N)}\right)_{L^2(\partial\Omega_W)} & \cdots & \left(\phi_M^5, W^{(N)}\right)_{L^2(\partial\Omega_W)} \end{pmatrix} \tag{205}$$

$$\tilde{\mathbf{L}}_{N\times N} \equiv \begin{pmatrix} \mathcal{D}\left(\nabla^4 W^{(1)}, W^{(1)}\right)_{L^2(\partial\Omega_W)} & 0 & \cdots \\ \vdots & \ddots & \vdots \\ 0 & \cdots & \mathcal{D}\left(\nabla^4 W^{(N)}, W^{(N)}\right)_{L^2(\partial\Omega_W)} \end{pmatrix} \tag{206}$$

The augmented linear system (195) with the matrices **A**, **B**, **C** and **D** given by (197), (198), and (204) respectively define the coupled linearized fluid/structure ROM in which our fluid is assumed to flow over a linear rectangular plate with non-zero z–displacement. As expected, the fluid and structure systems are coupled by the boundary conditions at the solid wall (or plate) boundary $\partial\Omega_W$, contained in the coupling matrices **B** and **C**.

Given the theoretical analysis of the well-posedness and stability of the fluid ROM in Sections 2.4–2.6, it is natural to ask whether anything can be proven about the full fluid/structured ROM with boundary coupling terms. It turns out that numerical stability of the coupled system with the acoustically-reflecting boundary condition (191) can be enforced by adding a stabilization term to the prescribed fluid pressure load on the structure side (Section 4.2). Adding this perturbation can be interpreted as damping the original structure equations (187).

4.2 Numerical Stability of Coupled Linearized Fluid/Structure System

We now prove stability of the coupled fluid/structure system (187) assuming the acoustically-reflecting boundary condition (191) is imposed at the plate (solid wall) boundary. In the subsequent analysis, we assume that the base flow is uniform ($\nabla\bar{\mathbf{q}} \equiv \mathbf{0}$) and that the base flow velocity is zero ($\bar{\mathbf{u}} = 0$). Under these conditions, there should be no physical instability of the coupled system, allowing the analysis to isolate the numerical stability of the ROM technique. It is found that with the boundary condition (191), standard energy matrix techniques [72] (Section B.2 of Appendix B) do not yield a clean analysis of the stability of the coupled system. One therefore seeks an alternate analysis tool to attempt to try to prove stability of the new coupled system (195).

It turns out that stability of the coupled system (195) *can* be shown using a direct energy method, i.e., by showing that the total energy E (207) is non-decreasing, assuming a perturbed pressure loading g on the plate. Recalling the definition of $\mathbf{q}'_M$ in Section 2.3 and defining $\mathbf{r}_N$ as in (209), define the total energy of the coupled system as

$$E \equiv \frac{1}{2}||\mathbf{q}'_M||^2_{(\mathbf{H},\Omega)} + \frac{1}{2}||\mathbf{r}_N||^2_{L^2(\partial\Omega_W)} = \begin{pmatrix} \mathbf{q}'^T_M & \mathbf{r}^T_N \end{pmatrix} \begin{pmatrix} \frac{1}{2}\mathbf{H} & 0 \\ 0 & \frac{1}{2}\mathbf{I}_2\delta_{\partial\Omega_W} \end{pmatrix} \begin{pmatrix} \mathbf{q}'_M \\ \mathbf{r}_N \end{pmatrix} \tag{207}$$

We begin by showing that the Galerkin method for the linearized von Karman equations (187) without fluid coupling is stable. We then show that the coupled fluid/structure system (195) under the acoustically-reflecting boundary condition (191) may be stable if $g = -p'_M$. This leads to the main result (Theorem 4.2.2), namely a proof of stability for the coupled system (195) under the acoustically-reflecting boundary condition (191) when a perturbed fluid pressure loading is prescribed on the structure equations: $g = -p'_M + O(u'_{n,M} - u'_w)$.

Numerical Stability of Galerkin-Projected Structure Equations

Before studying the stability of the coupled system (195), one needs to make sure the ROMs for the fluid-only and structure-only systems ($\dot{\mathbf{F}} = \mathbf{AF}$ and $\dot{\mathbf{S}} = \mathbf{CS}$ respectively) are numerically stable. Stability of the fluid equations under the condition (191) and assuming uniform base flow ($\nabla\bar{\mathbf{q}} \equiv \mathbf{0}$) that satisfies the no-penetration boundary condition $\bar{u}_n = 0$ was shown in Section 2.5 (Theorem 2.5.1). For the sake of rigor, we formally prove stability of Galerkin discretization of the structure system here (Theorem 4.2.1).

Theorem 4.2.1. *The Galerkin discretization of the linearized von Karman equations governing the z-displacement of the plate* (187) *is numerically stable.*

Proof. It is sufficient to show stability for $g = 0$, which will imply stability for all $g \neq 0$ by Section A.4 of Appendix A. Dividing both sides of (187) by $\rho_s h$ and setting $g = 0$, the z-displacement equation is

$$\ddot{w} + \frac{\mathcal{D}}{\rho_s h}(\nabla^4 w) = 0 \tag{208}$$

Let

$$\mathbf{r} \equiv \begin{pmatrix} w \\ \dot{w} \end{pmatrix}, \quad \mathbf{r}_N \equiv \sum_{k=1}^{N} \begin{pmatrix} \alpha_k \\ \dot{\alpha}_k \end{pmatrix} W^{(k)} \tag{209}$$

Then (208) can be written as

$$\dot{\mathbf{r}} + \underbrace{\begin{pmatrix} 0 & -1 \\ \frac{\mathcal{D}}{\rho_s h}\nabla^4 & 0 \end{pmatrix}}_{\equiv \mathbf{P}} \mathbf{r} = 0 \tag{210}$$

or, substituting $\mathbf{r} \leftarrow \mathbf{r}_N$ and projecting onto $W^{(k)}$,

$$\begin{pmatrix} \dot{\alpha}_k \\ \ddot{\alpha}_k \end{pmatrix} + \underbrace{\begin{pmatrix} 0 & -1 \\ \frac{\mathcal{D}}{\rho_s h}(W^{(k)}, \nabla^4 W^{(k)})_{L^2(\partial\Omega_W)} & 0 \end{pmatrix}}_{\equiv \mathbf{P}_k} \begin{pmatrix} \alpha_k \\ \dot{\alpha}_k \end{pmatrix} = 0 \tag{211}$$

Now, the rate of change in energy of the solid-only system is

$$\begin{aligned}
\tfrac{1}{2}\tfrac{d}{dt}||\mathbf{r}_N||^2_{L^2(\partial\Omega_W)} &= \tfrac{1}{2}\tfrac{d}{dt}\textstyle\int_{\partial\Omega_W} \mathbf{r}_N^T \mathbf{r}_N dS \\
&= \tfrac{1}{2}\tfrac{d}{dt}\textstyle\int_{\partial\Omega_W} \left\{ \sum_{k=1}^N \sum_{l=1}^N (W^{(k)}, W^{(l)})_{L^2(\partial\Omega_W)} \begin{pmatrix} \alpha_k & \dot{\alpha}_k \end{pmatrix} \begin{pmatrix} \alpha_l \\ \dot{\alpha}_l \end{pmatrix} \right\} dS \\
&= \tfrac{1}{2}\tfrac{d}{dt}\textstyle\int_{\partial\Omega_W} \left\{ \sum_{k=1}^N \sum_{l=1}^N \delta_{kl} \begin{pmatrix} \alpha_k & \dot{\alpha}_k \end{pmatrix} \begin{pmatrix} \alpha_l \\ \dot{\alpha}_l \end{pmatrix} \right\} dS \\
&= \tfrac{1}{2}\tfrac{d}{dt}\textstyle\int_{\partial\Omega_W} \left\{ \sum_{k=1}^N \begin{pmatrix} \alpha_k & \dot{\alpha}_k \end{pmatrix} \begin{pmatrix} \alpha_k \\ \dot{\alpha}_k \end{pmatrix} \right\} dS \\
&= \textstyle\int_{\partial\Omega_W} \sum_{k=1}^N \begin{pmatrix} \alpha_k & \dot{\alpha}_k \end{pmatrix} \begin{pmatrix} \dot{\alpha}_k \\ \ddot{\alpha}_k \end{pmatrix} dS \\
&= \textstyle\sum_{k=1}^N \begin{pmatrix} \alpha_k & \dot{\alpha}_k \end{pmatrix} \underbrace{\begin{pmatrix} 0 & 1 \\ -\frac{\omega_k^2}{\rho_s h} & 0 \end{pmatrix}}_{-\mathbf{P}_k} \begin{pmatrix} \alpha_k \\ \dot{\alpha}_k \end{pmatrix} dS
\end{aligned} \tag{212}$$

using the definition $\omega_k^2 \equiv \mathcal{D}\left(W^{(k)}, \nabla^4 W^{(k)}\right)_{L^2(\partial\Omega_W)}$. The Lyapunov condition for stability (see Section B.1 in Appendix B) is that the real parts of the eigenvalues of the matrices $\{-\mathbf{P}_k : k = 1, 2, \ldots, N\}$ be non-positive. The eigenvalues of these matrices are $\pm\sqrt{-\frac{\omega_k^2}{\rho_s h}} = \pm\sqrt{\frac{\omega_k^2}{\rho_s h}}i$, since $\omega_k^2 \geq 0$ for all k, and $\rho_s, h > 0$ (recall that h is the thickness of the plate and ρ_s is the density of the plate material). Since the eigenvalues are all pure imaginary or 0, the Lyapunov condition holds, implying the last line of (212) is ≤ 0, as desired. It follows that the structure system is stable. □

Numerical Stability of Coupled Fluid/Structure System

As defined in (187), the function g represents the fluid pressure loading on the structure or plate, i.e., $g = -p'_M$ on $\partial\Omega_W$. Since u'_w is the total derivative of the plate's displacement, in the case

when the plate has a non-zero displacement only in the z-direction and $\bar{\mathbf{u}} \equiv \mathbf{0}$, one has that $\dot{w} = -u'_w$ so that $\mathbf{r}^T = \begin{pmatrix} w & -u'_w \end{pmatrix}$. Denoting $\mathbf{e}_2^T \equiv \begin{pmatrix} 0 & 1 \end{pmatrix}$, it follows from (62) and the fact that $\mathbf{q}_M'^T \mathbf{H}\mathbf{A}_n \mathbf{q}'_M = 2p'_M u_{n,M}$ that the fluid contribution to the energy estimate (207) is:

$$\begin{aligned} \tfrac{1}{2}\tfrac{d}{dt}||\mathbf{q}'_M||^2_{(\mathbf{H},\Omega)} &= \int_{\partial\Omega_W} \mathbf{q}_M'^T \mathbf{H}\mathbf{A}_n \left[\tfrac{1}{2}\,\mathbf{q}'_M - \mathbf{q}'_w\right] dS \\ &= \int_{\partial\Omega_W} [-\bar{\rho} c u'_{n,M}(u'_{n,M} - u'_w) - u'_w p'_M] dS \\ &= \int_{\partial\Omega_W} [-\bar{\rho} c u'^2_{n,M} + (\bar{\rho} c u'_{n,M} - p'_M)] dS \\ &= \int_{\partial\Omega_W} \left[-\bar{\rho} c u'^2_{n,M} - \left(\bar{\rho} c u'_{n,M} - p'_M\right) \mathbf{r}_N^T \mathbf{e}_2\right] dS \end{aligned} \tag{213}$$

With pressure loading $g = -p_M$, the structure system (210) takes the form $\dot{\mathbf{r}} = -\mathbf{P}\mathbf{r} - p_M \mathbf{e}_2$, so that the structure contribution to the energy estimate (207) is:

$$\tfrac{1}{2}\tfrac{d}{dt}||\mathbf{r}_N||^2_{L^2(\partial\Omega_W)} = \int_{\partial\Omega_W} \mathbf{r}_N^T \left[-\mathbf{P}\mathbf{r}_N - p'_M \mathbf{e}_2\right] dS \tag{214}$$

Now, the rate of change in the total energy is:

$$\begin{aligned} \tfrac{dE}{dt} &= \tfrac{1}{2}\tfrac{d}{dt}||\mathbf{q}'_M||^2_{(\mathbf{H},\Omega)} + \tfrac{1}{2}\tfrac{d}{dt}||\mathbf{r}_N||^2_{L^2(\partial\Omega_W)} \\ &= \int_{\partial\Omega_W} \left[-\bar{\rho} c u'^2_{n,M} - \left(\bar{\rho} c u'_{n,M} - p'_M\right) \mathbf{r}_N^T \mathbf{e}_2\right] dS + \int_{\partial\Omega_W} \mathbf{r}_N^T (-\mathbf{P}\mathbf{r}_N - p'_M \mathbf{e}_2) dS \\ &= \int_{\partial\Omega_W} \left[\mathbf{e}_2^T \left(-\bar{\rho} c u'^2_{n,M}\right) \mathbf{e}_2 - \mathbf{r}_N^T \mathbf{P}\mathbf{r}_N - \mathbf{r}_N^T \bar{\rho} c u'_{n,M} \mathbf{e}_2\right] dS \\ &= \tfrac{d}{dt}(E_{\text{fluid only}}) + \tfrac{d}{dt}(E_{\text{structure only}}) + \int_{\partial\Omega_W} \bar{\rho} c u'_{n,M} u'_w dS \end{aligned} \tag{215}$$

By Section A.4 of Appendix A, a sufficient condition for stability is that $\frac{dE}{dt} \leq 0$. (215) implies that if there is a "stability margin" in the fluid-only and/or structure-only systems (that is, if $\frac{d}{dt}E_{\text{fluid only}} + \frac{d}{dt}E_{\text{structure only}} < 0$), the coupled system can still be stable as long as

$$\int_{\partial\Omega_W} \bar{\rho} c u'_{n,M} u'_w dS \leq -\frac{d}{dt}(E_{\text{fluid only}}) - \frac{d}{dt}(E_{\text{structure only}}) \tag{216}$$

Numerical Stability of Coupled Fluid/Structure System with Perturbed Fluid Pressure Loading

While the above analysis is promising, we now seek a stronger stability result. It turns out that it *can* be shown that $\frac{dE}{dt} \leq 0$ necessarily, which implies stability for the coupled fluid/structure system (195) with the acoustically-reflecting boundary condition (191), if a perturbed fluid pressure loading of the form

$$g = -p'_M + O(u'_{n,M} - u'_w) \quad \text{on} \quad \partial\Omega_W \tag{217}$$

is prescribed. Since one expects $u'_{n,M} \to u'_w$ on $\partial\Omega_W$, $g = -p'_M + O(u'_{n,M} - u'_w) \approx -p'_M$, with $|g - (-p'_M)| \to 0$ as the error in enforcement of the wall boundary condition decreases to zero. Thus, the pressure loading increment to be added, which amounts to a stabilization term, is bounded by the error in the weak boundary condition enforcement.

The main stability result of this section is stated and proven in the following theorem, Theorem 4.2.2.

Theorem 4.2.2. *Assume* $\bar{\mathbf{u}} = 0$, $\nabla\bar{\mathbf{q}} = \mathbf{0}$ *and we enforce the acoustically-reflecting boundary condition* (191) *on* $\partial\Omega_W$. *Suppose the fluid pressure loading is* $g = -p'_M + K(u'_{n,M} - u'_w)$ *on* $\partial\Omega_W$, *with* $K = -\bar{\rho}c$. *Then* $\frac{dE}{dt} \leq 0$ *(with* $\frac{dE}{dt}$ *defined in* (215)*), so that the coupled fluid/structure Galerkin ROM for* (195) *with the entries of* $\mathbf{A}$ *given by* (197) *and the entries of* $\mathbf{B}$ *given by* (199) *is numerically stable.*

Proof. First, observe that

$$-\bar{\rho}cu'^2_{n,M} = -\bar{\rho}c(u'_{n,M} - u'_w)^2 - 2\bar{\rho}cu'_w(u'_{n,M} - u'_w) - \bar{\rho}cu'^2_w \tag{218}$$

With the new structure loading and using this relation, line 2 of (215) is

$$\begin{aligned}
\tfrac{dE}{dt} &= \int_{\partial\Omega_W}\left[-\bar{\rho}c(u'_{n,M} - u'_w)^2 - 2\bar{\rho}cu'_w(u'_{n,M} - u'_w) - \bar{\rho}cu'^2_w - \left(\bar{\rho}cu'_{n,M} - p'_M\right)\mathbf{r}_N^T\mathbf{e}_2\right]dS \\
&+ \int_{\partial\Omega_W}\mathbf{r}_N^T(-\mathbf{P}\mathbf{r}_N + [-p'_M + K(u'_{n,M} - u'_w)]\mathbf{e}_2)dS \\
&= \int_{\partial\Omega_W}\left[-\bar{\rho}c(u'_{n,M} - u'_w)^2 - 2\bar{\rho}cu'_w(u'_{n,M} - u'_w) - \bar{\rho}cu'^2_w - \bar{\rho}cu'_{n,M}u'_w - \mathbf{r}_N^T\mathbf{P}\mathbf{r}_N\right. \\
&\qquad \left. -K(u'_{n,M} - u'_w)u'_w\right]dS \\
&= \int_{\partial\Omega_W}\left[-\mathbf{r}_N^T\mathbf{P}\mathbf{r}_N - \bar{\rho}c(u'_{n,M} - u'_w)^2 - 2\bar{\rho}cu'_w(u'_{n,M} - u'_w) + \bar{\rho}cu'_w(u'_{n,M} - u'_w)\right. \\
&\qquad \left. -K(u'_{n,M} - u'_w)u'_w\right]dS \\
&= \int_{\partial\Omega_W}\left[-\mathbf{r}_N^T\mathbf{P}\mathbf{r}_N - \bar{\rho}c(u'_{n,M} - u'_w)^2 - \bar{\rho}cu'_w(u'_{n,M} - u'_w) - K(u'_{n,M} - u'_w)u'_w\right]dS
\end{aligned} \tag{219}$$

If $K = -\bar{\rho}c$, the $u'_w(u'_{n,N} - u'_w)$ terms cancel. Then

$$\begin{aligned}
\tfrac{dE}{dt} &= \int_{\partial\Omega_W}\left[-\mathbf{r}_N^T\mathbf{P}\mathbf{r}_N - \bar{\rho}c(u'_{n,M} - u'_w)^2\right]dS \\
&= \tfrac{d}{dt}(E_{\text{structure only}}) - \int_{\partial\Omega_W}\bar{\rho}c(u'_{n,M} - u'_w)^2 dS \\
&\leq 0
\end{aligned} \tag{220}$$

provided the structure-only system is stable, which it is by Theorem 4.2.1. □

The implication of Theorem 4.2.2 is that, to ensure stability of the coupled fluid/structure system (195) with the acoustically-reflecting boundary condition (191), one must add a sort of penalty to the source (pressure load) on the right-hand-side of the structure equations (187), that is, implement

$$\rho_s h\ddot{w} + \mathcal{D}\nabla w = g(x,y,t) = -p'_M(x,y,0,t) - \bar{\rho}c(u'_{n,M} - u'_w) \tag{221}$$

Note that $u'_w = -\dot{w}$ when $\bar{\mathbf{u}} = 0$, so that (221) is equivalent to

$$\rho_s h\ddot{w} + \bar{\rho}c\dot{w} + \mathcal{D}\nabla w = -p'_M(x,y,0,t) - \bar{\rho}cu'_{n,M} \tag{222}$$

The analog to (200) is

$$(\rho_s h)\ddot{\alpha}_k + \bar{\rho}c\dot{\alpha}_k + \omega_k^2\alpha_k = \hat{G}_k(t) \tag{223}$$

where

$$\hat{G}_k(t) = (\hat{g}, W^{(k)})_{L^2(\partial\Omega_W)} \tag{224}$$

and

$$\hat{g}(x,y,t) = -p'_M(x,y,0,t) - \bar{\rho}cu'_{n,M} = -\sum_{k=1}^{M} a_k(t)[\phi_k^5(x,y,0) + \bar{\rho}c\phi_k^n(x,y,0)] \tag{225}$$

It follows that the modified structure equations, i.e., the analogs to (203) but with the perturbed pressure loading (221) are:

$$\dot{\mathbf{S}} = \hat{\mathbf{C}}\mathbf{F} + \hat{\mathbf{D}}\mathbf{S} \tag{226}$$

where

$$\hat{\mathbf{C}} \equiv \begin{pmatrix} \mathbf{0}_{N\times M} \\ \hline \frac{1}{\rho_s h}\bar{\mathbf{C}}_{N\times M} \end{pmatrix}, \quad \hat{\mathbf{D}} \equiv \left(\begin{array}{c|c} \mathbf{0}_{N\times N} & \mathbf{I}_{N\times N} \\ \hline -\frac{1}{\rho_s h}\tilde{\mathbf{L}}_{N\times N} & -\frac{\bar{\rho}c}{\rho_s h}\mathbf{I}_{N\times N} \end{array}\right) \tag{227}$$

and

$$\bar{\mathbf{C}}_{N\times M} \equiv \begin{pmatrix} \left(\phi_1^5 + \bar{\rho}c\phi_1^n, W^{(1)}\right)_{L^2(\partial\Omega_W)} & \cdots & \left(\phi_M^5 + \bar{\rho}c\phi_M^n, W^{(1)}\right)_{L^2(\partial\Omega_W)} \\ \vdots & \ddots & \vdots \\ \left(\phi_1^5 + \bar{\rho}c\phi_1^n, W^{(N)}\right)_{L^2(\partial\Omega_W)} & \cdots & \left(\phi_M^5 + \bar{\rho}c\phi_M^n, W^{(N)}\right)_{L^2(\partial\Omega_W)} \end{pmatrix} \tag{228}$$

with $\tilde{\mathbf{L}}_{N\times N}$ as in (206).

Comparing (222) with (187), remark that the modified pressure loading g (222) has given rise to an additional term on the left-hand-side of the structure equations, namely $\frac{\bar{\rho}c}{\rho_s h}\dot{w}$. One may recognize from classical mechanics (Newton's Second Law of Motion applied to e.g., a mass-spring-damper system) that this first order derivative term represents damping. Thus, (222) is a damped variant of the original equations (187). The natural question to ask is whether the result of Theorem 4.2.1 can be extended to the modified structure equations (222). Intuitively, one would expect the additional damping to improve stability. It is shown in Theorem 4.2.1 that the structure-only Galerkin ROM for the modified equations (222) is indeed numerically stable.

Theorem 4.2.1. *Assume the base flow satisfies:* $\bar{\mathbf{u}} \equiv 0$ *and* $\nabla\bar{\mathbf{q}} \equiv \mathbf{0}$*. Then the modified linearized von Karman equations governing the z-displacement of the plate* (222) *with damping are stable.*

Proof. As in the proof of Theorem 4.2.1, it is sufficient to show stability for 0 right-hand-side (refer also to Section A.4 of Appendix A). With zero right-hand-side, the damped structure equation (222) is:

$$\ddot{w} + \frac{\bar{\rho}c}{\rho_s h}\dot{w} + \frac{\mathcal{D}}{\rho_s h}(\nabla^4 w) = 0 \tag{229}$$

Defining $\mathbf{r}$ and $\mathbf{r}_N$ as in (209), (229) can be written as

$$\dot{\mathbf{r}} + \underbrace{\begin{pmatrix} 0 & -1 \\ \frac{\mathcal{D}}{\rho_s h}\nabla^4 & \frac{\bar{\rho}c}{\rho_s h} \end{pmatrix}}_{\equiv\bar{\mathbf{P}}}\mathbf{r} = 0 \tag{230}$$

or, substituting $\mathbf{r} \leftarrow \mathbf{r}_N$, projecting onto $W^{(k)}$, and employing the fact that $\bar{\rho}$ and c are constant when $\nabla\bar{\mathbf{q}} \equiv \mathbf{0}$ and the orthonormality of the $W^{(k)}$, so that $\left(\frac{\bar{\rho}c}{\rho_s h}W^{(n)}, W^{(k)}\right)_{L^2(\partial\Omega_W)} = \frac{\bar{\rho}c}{\rho_s h}\delta_{nk}$, one obtains:

$$\begin{pmatrix} \dot{\alpha}_k \\ \ddot{\alpha}_k \end{pmatrix} + \underbrace{\begin{pmatrix} 0 & -1 \\ \frac{\mathcal{D}}{\rho_s h}(W^{(k)}, \nabla^4 W^{(k)})_{L^2(\partial\Omega_W)} & \frac{\bar{\rho}c}{\rho_s h} \end{pmatrix}}_{\equiv \bar{\mathbf{P}}_k} \begin{pmatrix} \alpha_k \\ \dot{\alpha}_k \end{pmatrix} = 0 \tag{231}$$

Now, the rate of change in energy of the solid-only system, following the energy estimate in (212),

$$\frac{1}{2}\frac{d}{dt}||\mathbf{r}_N||^2_{L^2(\partial\Omega_W)} = \sum_{k=1}^N \begin{pmatrix} \alpha_k & \dot{\alpha}_k \end{pmatrix} \underbrace{\begin{pmatrix} 0 & 1 \\ -\frac{\omega_k^2}{\rho_s h} & -\frac{\bar{\rho}c}{\rho_s h} \end{pmatrix}}_{-\bar{\mathbf{P}}_k} \begin{pmatrix} \alpha_k \\ \dot{\alpha}_k \end{pmatrix} dS \tag{232}$$

The Lyapunov condition for stability (see Section B.1 in Appendix B) is that the real parts of the eigenvalues of the matrices $\{-\bar{\mathbf{P}}_k : k = 1, 2, \ldots, N\}$ be non-positive. One can easily show that:

$$\lambda_\pm(\bar{\mathbf{P}}_k) = \frac{-\bar{\rho}c}{2\rho_s h} \pm \frac{\sqrt{\bar{\rho}^2c^2 - 4\rho_s h\omega_k^2}}{2\rho_s h} \tag{233}$$

First, suppose $\bar{\rho}^2c^2 - 4\rho_s h\omega_k^2 < 0$. Then

$$\lambda_\pm(\bar{\mathbf{P}}_k) = \frac{-\bar{\rho}c}{2\rho_s h} \pm \frac{\sqrt{-\bar{\rho}^2c^2 + 4\rho_s h\omega_k^2}}{2\rho_s h} i \tag{234}$$

where $i = \sqrt{-1}$, so that $\Re\{\lambda_\pm(\bar{\mathbf{P}}_k)\} = \frac{-\bar{\rho}c}{2\rho_s h} < 0$, i.e., the Lyapunov condition for stability holds. Now, suppose $\bar{\rho}^2c^2 - 4\rho_s h\omega_k^2 \geq 0$, so that $\lambda_\pm(\bar{\mathbf{P}}_k) \in \mathbb{R}$. It is clear that $\lambda_-(\bar{\mathbf{P}}_k) \leq 0$. Let us look at the other eigenvalue. Suppose $\lambda_+(\bar{\mathbf{P}}_k) > 0$. Then

$$\sqrt{\bar{\rho}^2c^2 - 4\rho_s h\omega_k^2} > \bar{\rho}c \tag{235}$$

or

$$-4\rho_s h\omega_k^2 > 0 \tag{236}$$

But this is a contradiction, as $\rho_s, h\omega_k^2 \geq 0$. It follows that the real parts of the eigenvalues of $\bar{\mathbf{P}}_k$ in (230) are necessarily non-positive, meaning the Lyapunov condition holds. Thus, the left-hand-side of (231) is ≤ 0, from which the numerical stability of the modified structure equations (222) with damping follows. □

We have thus shown that, assuming a uniform base flow $\nabla\bar{\mathbf{q}} \equiv \mathbf{0}$, not only is the fluid-only Galerkin ROM with the acoustically-reflecting solid wall boundary condition stable (Section 2.5) and the structure-only Galerkin ROM (187) stable, numerical stability of the boundary-condition coupled linear system (195) can be ensured with a simple alteration to the structure ROM, namely (226). This modification gives rise to a damping term that appears in the structure equations (187) that does not affect the numerical stability of the damped structure-only ROM (222).

Numerical Example: Supersonic Panel Flutter

A coupled fluid/structure ROM was constructed for the problem of inviscid, supersonic flow past a thin, square, elastic rectangular $L_x \times L_y$ plate that is aligned with the flow. The z–displacement of the plate, $w(x,y,t)$ is governed by the linearized von Karman equation (187) The fore and aft edges of the plate are clamped to the surrounding flat surface, which is considered rigid; the side edges are simply supported. For a given flow Mach number, the panel will undergo flutter once the non-dimensional dynamic pressure parameter λ exceeds a threshold [73].

A POD basis was obtained by running the AERO-F simulation code with a free stream Mach number of 2.0. The motion of the plate was described by four linear eigenmodes, which were computed using the ABAQUS code. A series of solutions for the fluid motion were obtained in the frequency domain, assuming time harmonic oscillation of each of the plate modes over a range of discrete frequencies. The non-dimensional frequencies for the computations were equally spaced from 0 to 8.0 at intervals of 0.04. The AERO-F code was run in 'Linearized Euler' mode, with linear perturbations of the plate eigenmodes providing forcing for the solution in the fluid domain. The computational fluid mesh is shown in Figure 12, while a particular solution for oscillatory plate motion is shown in Figure 13. The POD was then computed on the resulting complex-valued solutions using the frequency domain POD algorithm described in [11].

A coupled ROM was constructed by projecting the linearized Euler equations onto the POD basis and incorporating the boundary coupling terms using the methods described in Section 2 and the present section. Note that the stabilization term was not added to the pressure loading for this example. A stability analysis was performed by computing the eigenvalues of the resulting ROM system matrix, and examining the maximum real component of the eigenvalues. Figure 14 compares the results of this analysis for 32, 48, and 64-mode ROMs and for the theoretical result using quasi-steady aerodynamic theory, also called 'piston theory'. The ROM is seen to have converged by 48 modes, giving a result for the flutter dynamic pressure within 5 percent of the theoretical value. With sufficient resolution, the ROM also properly predicts the maintenance of stability below the boundary and a reasonable prediction for the instability growth rate above the flutter boundary.

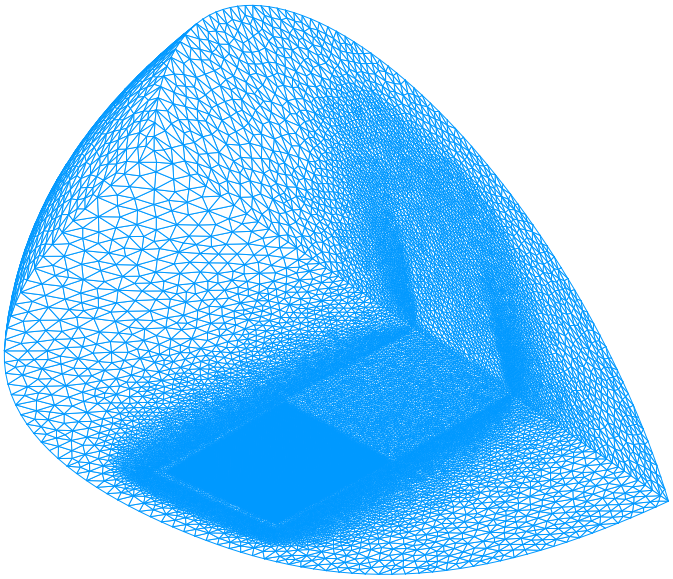

Figure 12. Computational mesh for the supersonic panel flutter problem. Grid nodes are clustered around the square panel location on the bottom surface of the mesh.

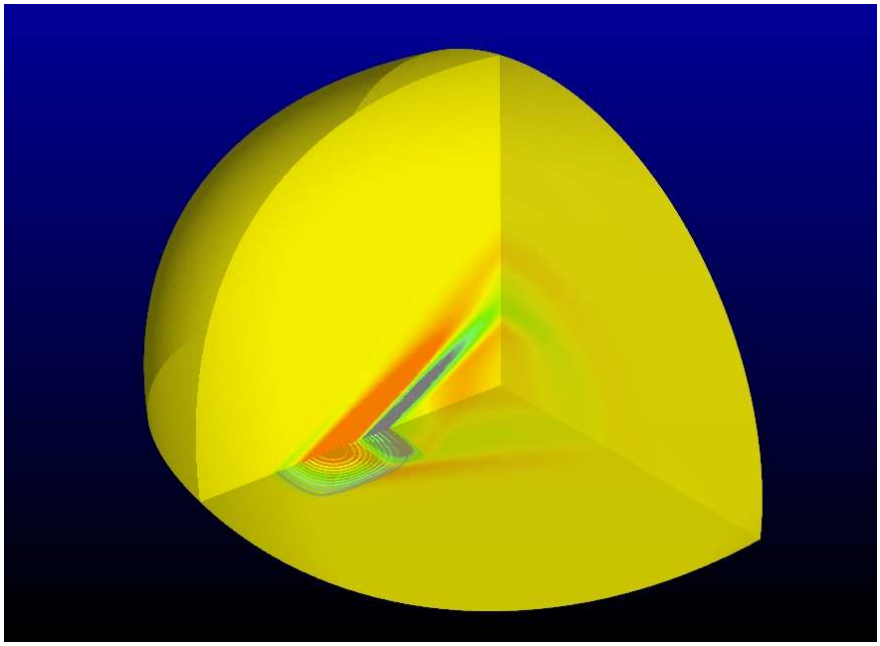

Figure 13. The continuous contours show the pressure perturbation field for harmonic oscillation of the first panel eigenmode. The line contours show the plate deflection.

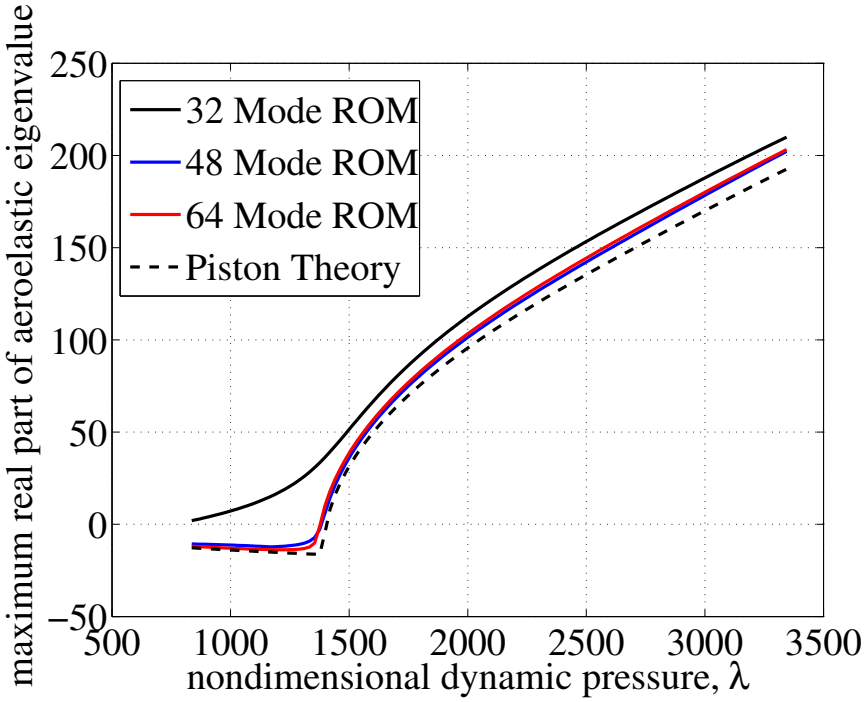

Figure 14. Panel flutter analysis using the coupled ROM, compared with predictions using aerodynamic piston theory.

5 Reduced Order Models for Non-linear Fluid Flow

5.1 Introduction

Having formulated and analyzed a linear fluid reduced order model (Section 2), the goal now is to build a ROM for the non-linear equations of fluid mechanics, namely the 3D compressible Navier-Stokes equations. The challenges in addressing the non-linear equations include maintenance of numerical stability of the ROM scheme as well as preservation of computational efficiency of the ROM. As with the linearized fluid equations, stability of the Galerkin projection of the non-linear equations can be ensured by defining a transformation that essentially symmetrizes these equations. Following appropriate symmetrization, one can use entropy estimates, namely the Clausius-Duhem entropy inequality, to show *ab initio* satisfaction of the second law of thermodynamics by all numerical solutions to the ROM. We will term this notion of numerical stability "entropy-stability".

The other issue that must be addressed is efficiency. As discussed in [74] and illustrated herein, for general non-linear partial differential equations (PDEs), the standard Galerkin projection method is no longer efficient in generating reduced order models. This is because the integrals involving the non-linear terms can no longer be precomputed, as in the case for a set of linear equations, but must instead by recomputed at each time or Newton step. The key in circumventing this difficulty is finding a way to handle the Galerkin projection of the non-linear terms without having to recompute these projections (inner products). To do this, we employ the so-called "best" points interpolation technique [75, 74]. The basic idea is, given a non-polynomial, non-linear function $f(\mathbf{u})$, we wish to represent it efficiently by expanding the function itself in an orthonormal basis.

The "best" points interpolation procedure, adapted from [75, 74], is outlined in Section 5.2 in the context of a one-dimensional (1D) non-linear convection-diffusion-reaction system of PDEs describing non-adiabatic flow through a tubular reactor. We give some results for the tubular reactor ROM with interpolation and a Fourier cosine basis and discuss some difficulties encountered when attempting to employ a POD basis on this problem. In Section 5.3, we proceed to the 3D compressible Navier-Stokes equations. A change of variables that ensures entropy-stability of the Galerkin projection of the equations *with* appropriate boundary treatment (no-slip and adiabatic wall) is defined using entropy principles [76, 77, 78]. A procedure to interpolate the non-linear terms that appear in these projected equations is formulated. Conclusions are offered in Section 5.4.

5.2 "Best" Points Interpolation Procedure: Illustration on a 1D Non-Linear Reduced Order Model of a Tubular Reactor

To demonstrate and better understand the properties of the "best" points interpolation [75, 74] prior to formulating its application to the full compressible 3D Navier-Stokes equations, we first illustrate the general interpolation procedure on a simpler one-dimensional (1D) non-linear system of two coupled equations. Given this discussion, it is straightforward to extend the interpolation to

each of the non-linear terms in the Navier-Stokes equations (Section 5.3).

Model 1D Nonlinear Convection-Diffusion-Reaction System of Equations

The problem of interest is a model of a non-adiabatic tubular reactor with a single $A \rightarrow B$ reaction [79]. In dimensionless form, the governing equations, describing the conservation of reactant A and energy for the nonadiabatic tubular reactor with axial mixing, are:

$$\left\{ \begin{array}{ll} \frac{\partial y}{\partial \tau} & = \frac{1}{Pe_m}\frac{\partial^2 y}{\partial s^2} - \frac{\partial y}{\partial s} - Dye^{\gamma - \frac{\gamma}{\theta}}, \qquad s \in (0,1), \tau \in (0,\infty) \\ \frac{\partial \theta}{\partial \tau} & = \frac{1}{Pe_h}\frac{\partial^2 \theta}{\partial s^2} - \frac{\partial \theta}{\partial s} - \beta(\theta - \theta_0) + BDye^{\gamma - \frac{\gamma}{\theta}}, \quad s \in (0,1), \tau \in (0,\infty) \end{array} \right. \tag{237}$$

subject to boundary conditions

$$\left\{ \begin{array}{ll} \frac{\partial y}{\partial s}\Big|_{s=0} & = Pe_m(y-1)|_{s=0}, \quad \tau \in (0,\infty) \\ \frac{\partial \theta}{\partial s}\Big|_{s=0} & = Pe_h(\theta-1)|_{s=0}, \quad \tau \in (0,\infty) \end{array} \right. \tag{238}$$

$$\left\{ \begin{array}{ll} \frac{\partial y}{\partial s}\Big|_{s=1} & = 0, \quad \tau \in (0,\infty) \\ \frac{\partial \theta}{\partial s}\Big|_{s=1} & = 0, \quad \tau \in (0,\infty) \end{array} \right. \tag{239}$$

and initial condition

$$y|_{\tau=0} = y_{in}, \quad \theta|_{\tau=0} = \theta_{in}, \quad s \in (0,1). \tag{240}$$

Here, y is the concentration, θ is the temperature, s is the axial distance, τ is the time, β is the heat transfer coefficient, γ is the activation energy, D is the Damkohler number, B is the heat of reaction, and Pe_m and Pe_h are the Peclet numbers for mass and heat transfer respectively[7]. All variables have been non-dimensionalized. It is convenient to write (237)–(240) in vector form, as follows:

$$\begin{array}{rll} \frac{\partial \mathbf{u}}{\partial \tau} & = \mathbf{A}^{-1}\frac{\partial^2 \mathbf{u}}{\partial s^2} - \frac{\partial \mathbf{u}}{\partial s} - \mathbf{B}(\mathbf{u}-\mathbf{u}_0) - \mathbf{C}f(\mathbf{u}), & s \in (0,1), \tau \in (0,\infty) \\ \frac{\partial \mathbf{u}}{\partial s}\Big|_{s=0} & = \mathbf{A}(\mathbf{u}-\mathbf{1})\big|_{s=0}, & \tau \in (0,\infty) \\ \frac{\partial \mathbf{u}}{\partial s}\Big|_{s=1} & = \mathbf{0}, & \tau \in (0,\infty) \\ \mathbf{u} & = \mathbf{u}_{in}, & s \in (0,1) \end{array} \tag{241}$$

where

$$\mathbf{u} \equiv \begin{pmatrix} y \\ \theta \end{pmatrix}, \quad \mathbf{u}_0 \equiv \begin{pmatrix} y_0 \\ \theta_0 \end{pmatrix} \tag{242}$$

$$\mathbf{A} \equiv \begin{pmatrix} Pe_m & 0 \\ 0 & Pe_h \end{pmatrix}, \quad \mathbf{B} \equiv \begin{pmatrix} 0 & 0 \\ 0 & \beta \end{pmatrix}, \quad \mathbf{C} \equiv \begin{pmatrix} D \\ -BD \end{pmatrix}, \quad \mathbf{1} \equiv \begin{pmatrix} 1 \\ 1 \end{pmatrix} \tag{243}$$

and

$$f(\mathbf{u}) \equiv ye^{\gamma - \frac{\gamma}{\theta}} \tag{244}$$

Classical numerical techniques [79] illustrate periodic solutions which possess Hopf bifurcations. Figure 15 shows the existence of stable oscillatory solutions as a function of the Damkohler number D when $Pe_m = Pe_h = 5$, $B = 0.50$, $\gamma = 25$, $\beta = 2.5$ and $\theta_0 = 1$. In particular, one can see from this plot that there is a stable solution that bifurcates into a limit cycle at the lower Hopf point, $D = 0.165$.

[7] For more on these parameters, the reader is referred to the "Notation" section of [79].

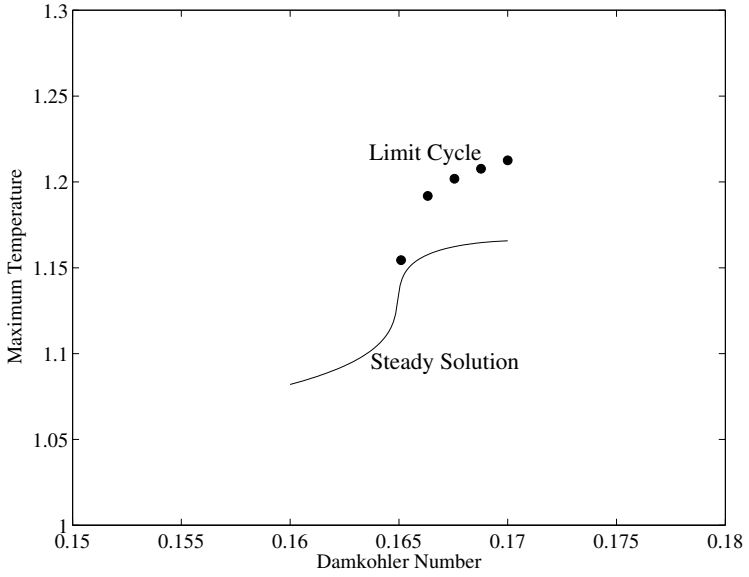

Figure 15. Existence of stable oscillatory solutions to the convection-diffusion-reaction system when $Pe_h = Pe_m = 5$, $B = 0.50$, $\gamma = 25$, $\beta = 2.5$, $\theta_0 = 1$.

Weak Formulation and Reduced Order Approximation

To formulate a reduced order approximation of the solution of (237), begin by expanding $\mathbf{u}$ in an orthonormal vector[8] basis $\{\boldsymbol{\phi}_m^u\}_{m=1}^M \in \mathbb{R}^2$:

$$\mathbf{u}(s,\tau) \approx \mathbf{u}_M(s,\tau) \equiv \sum_{m=1}^{M} a_m(\tau)\boldsymbol{\phi}_m^u(s) \tag{245}$$

where M is the size of the reduced basis. The basis functions $\boldsymbol{\phi}_m^u$ are chosen such that they are orthonormal in some inner product $(\cdot,\cdot)$ (to be specified given the choice of basis), so that $(\boldsymbol{\phi}_i, \boldsymbol{\phi}_j) = \delta_{ij}$, the Dirac delta function.

To obtain the weak form of the equations (241), we project them onto the j^{th} mode $\boldsymbol{\phi}_j^u$ in the $(\cdot,\cdot)$ inner product, perform an integration by parts on the diffusion term, and substitute the

[8]Alternatively, one may expand each y and θ in their own scalar, orthonormal bases. This is in fact what is done later when using a Fourier cosine basis. The result is a ROM ODE system involving a total of $2M$ ROM coefficients.

boundary conditions (238) and (239) into the boundary integral that arises. Doing so gives:

$$\begin{aligned}
0 &= \left(\frac{\partial \mathbf{u}}{\partial \tau} - \mathbf{A}^{-1}\frac{\partial^2 \mathbf{u}}{\partial s^2} + \frac{\partial \mathbf{u}}{\partial s} + \mathbf{B}(\mathbf{u}-\mathbf{u}_0) + \mathbf{C}f(\mathbf{u}), \boldsymbol{\phi}_j^u\right) \\
&= \left(\frac{\partial \mathbf{u}}{\partial \tau}, \boldsymbol{\phi}_j^u\right) + \left(\mathbf{A}^{-1}\frac{\partial \mathbf{u}}{\partial s}, \frac{\partial \boldsymbol{\phi}_j^u}{\partial s}\right) - \langle \mathbf{A}^{-1}\frac{\partial \mathbf{u}}{\partial s}\mathbf{n}, \boldsymbol{\phi}_j^u\rangle + \left(\frac{\partial \mathbf{u}}{\partial s}, \boldsymbol{\phi}_j^u\right) + \left(\mathbf{B}(\mathbf{u}-\mathbf{u}_0), \boldsymbol{\phi}_j^u\right) + \left(\mathbf{C}f(\mathbf{u}), \boldsymbol{\phi}_j^u\right) \\
&= \left(\frac{\partial \mathbf{u}}{\partial \tau}, \boldsymbol{\phi}_j^u\right) + \left(\mathbf{A}^{-1}\frac{\partial \mathbf{u}}{\partial s}, \frac{\partial \boldsymbol{\phi}_j^u}{\partial s}\right) - \mathbf{A}^{-1}\frac{\partial \mathbf{u}}{\partial s}\cdot\boldsymbol{\phi}_j^u\big|_{s=1} + \mathbf{A}^{-1}\frac{\partial \mathbf{u}}{\partial s}\cdot\boldsymbol{\phi}_j^u\big|_{s=0} + \left(\frac{\partial \mathbf{u}}{\partial s}, \boldsymbol{\phi}_j^u\right) + \left(\mathbf{B}(\mathbf{u}-\mathbf{u}_0), \boldsymbol{\phi}_j^u\right) + \left(\mathbf{C}f(\mathbf{u}), \boldsymbol{\phi}_j^u\right) \\
&= \left(\frac{\partial \mathbf{u}}{\partial \tau}, \boldsymbol{\phi}_j^u\right) + \left(\mathbf{A}^{-1}\frac{\partial \mathbf{u}}{\partial s}, \frac{\partial \boldsymbol{\phi}_j^u}{\partial s}\right) + \mathbf{A}^{-1}\mathbf{A}(\mathbf{u}-\mathbf{1})\big|_{s=0}\cdot\boldsymbol{\phi}_j^u + \left(\frac{\partial \mathbf{u}}{\partial s}, \boldsymbol{\phi}_j^u\right) + \left(\mathbf{B}(\mathbf{u}-\mathbf{u}_0), \boldsymbol{\phi}_j^u\right) + \left(\mathbf{C}f(\mathbf{u}), \boldsymbol{\phi}_j^u\right) \\
&= \left(\frac{\partial \mathbf{u}}{\partial \tau}, \boldsymbol{\phi}_j^u\right) + \left(\mathbf{A}^{-1}\frac{\partial \mathbf{u}}{\partial s}, \frac{\partial \boldsymbol{\phi}_j^u}{\partial s}\right) + (\mathbf{u}-\mathbf{1})\big|_{s=0}\cdot\boldsymbol{\phi}_j^u + \left(\frac{\partial \mathbf{u}}{\partial s}, \boldsymbol{\phi}_j^u\right) + \left(\mathbf{B}(\mathbf{u}-\mathbf{u}_0), \boldsymbol{\phi}_j^u\right) + \left(\mathbf{C}f(\mathbf{u}), \boldsymbol{\phi}_j^u\right)
\end{aligned} \tag{246}$$

Substituting (245) into (246) and invoking orthonormality of the basis functions $\{\boldsymbol{\phi}_m^u\}_{m=1}^M$ yields the following system of ordinary differential equations (ODEs) for the time-dependent ROM coefficients a_j, $j = 1,...,M$:

$$\begin{aligned}
\dot{a}_j &= -\textstyle\sum_{m=1}^M a_m \mathbf{A}^{-1}\left[\int_0^1 \frac{\partial \boldsymbol{\phi}_m^u}{\partial s}\cdot\frac{\partial \boldsymbol{\phi}_j^u}{\partial s}ds\right] - \sum_{m=1}^M a_m[\boldsymbol{\phi}_m^u(0)\boldsymbol{\phi}_j^u(0)] + \mathbf{1}\cdot\boldsymbol{\phi}_j^u(0) - \textstyle\sum_{m=1}^M a_m\int_0^1 \frac{\partial \boldsymbol{\phi}_m^u}{\partial s}\cdot\boldsymbol{\phi}_j^u ds \\
&\quad - \textstyle\sum_{m=1}^M a_m \mathbf{B}\left[\int_0^1 \boldsymbol{\phi}_m^u\cdot\boldsymbol{\phi}_j^u ds\right] + \int_0^1 \mathbf{B}\mathbf{u}_0\cdot\boldsymbol{\phi}_j^u ds - \int_0^1 \mathbf{C}f(\mathbf{u}_M)\cdot\boldsymbol{\phi}_j^u ds
\end{aligned} \tag{247}$$

Here, $\dot{a}_j \equiv \frac{da_j}{d\tau}$.

The last term in (247) contains the function $f(\mathbf{u}_M)$, which is non-linear in $\mathbf{u}_M$. In vector form, (247) can be written as:

$$\boxed{\dot{\mathbf{a}}_M = \mathbf{F} - \mathbf{L}\mathbf{a}_M - \mathbf{N}(\mathbf{a}_M)} \tag{248}$$

where

$$\mathbf{a}_M^T \equiv \begin{pmatrix} a_1 & \cdots & a_M \end{pmatrix} \tag{249}$$

$$F_i = \mathbf{1}\cdot\boldsymbol{\phi}_i^u(0) + \int_0^1 \mathbf{B}\mathbf{u}_0\cdot\boldsymbol{\phi}_i^u ds \tag{250}$$

$$L_{ij} = \boldsymbol{\phi}_j^u(0)\boldsymbol{\phi}_i^u(0) + \int_0^1 \left[\mathbf{A}^{-1}\frac{\partial \boldsymbol{\phi}_i^u}{\partial s}\cdot\frac{\partial \boldsymbol{\phi}_j^u}{\partial s} + \frac{\partial \boldsymbol{\phi}_j^u}{\partial s}\cdot\boldsymbol{\phi}_i^u + \mathbf{B}\boldsymbol{\phi}_j^u\cdot\boldsymbol{\phi}_i^u\right] ds \tag{251}$$

$$N_i(\mathbf{a}_M) = \int_0^1 \mathbf{C}f\left(\sum_{m=1}^M a_m\boldsymbol{\phi}_m^u\right)\cdot\boldsymbol{\phi}_i^u ds \tag{252}$$

for $i, j = 1,...,M$. In the simpler case when $Pe_h = Pe_m = Pe$, (250) and (251) simplify to:

$$F_i = [\phi_i^u(0)]^1 + [\phi_i^u(0)]^2 + \int_0^1 \beta\theta_0[\phi_i^u]^2 ds \tag{253}$$

$$\begin{aligned}
L_{ij} &= [\phi_i^u(0)]^1[\phi_j^u(0)]^2 + [\phi_i^u(0)]^2[\phi_j^u(0)]^2 \\
&\quad + \textstyle\int_0^1 \left\{\frac{1}{Pe}\left[\frac{\partial[\phi_i^u]^1}{\partial s}\frac{\partial[\phi_j^u]^1}{\partial s} + \frac{\partial[\phi_i^u]^2}{\partial s}\frac{\partial[\phi_j^u]^2}{\partial s}\right] + \left[\frac{\partial[\phi_j^u]^1}{\partial s}[\phi_i^u]^1 + \frac{\partial[\phi_j^u]^2}{\partial s}[\phi_i^u]^2\right] + \beta[\phi_j^u]^2[\phi_i^u]^2\right\} ds
\end{aligned} \tag{254}$$

where $[\phi_i^u]^k$ denotes the k^{th} component of $\boldsymbol{\phi}_i^u$, for $k = 1,2$. For clarification of the notation in (252), for the function f in (244):

$$f\left(\sum_{m=1}^M a_m\boldsymbol{\phi}_m^u\right) \equiv f\left(\sum_{m=1}^M a_m^y[\phi_m^u]^1, \sum_{m=1}^M a_m^\theta[\phi_m^u]^2\right) = \left(\sum_{m=1}^M a_m^y[\phi_m^u]^1\right)\exp\left[\gamma - \gamma\left(\sum_{m=1}^M a_m^\theta[\phi_m^u]^2\right)^{-1}\right] \tag{255}$$

Since the vector stemming from the non-linear function $f(\mathbf{u})$ (244) depends on $\mathbf{a}_M$, the inner products in (252) *cannot* be pre-computed prior to time-integration of the ROM system (248), as would be done in the case of linear equations. This greatly reduces the efficiency of this ROM, and motivates one to consider some alternative way to handle the nonlinearity in (252), so that inner products involving $f(\mathbf{u}_M)$ need not be recomputed at each time step.

Solution for the Interpolation Points: "Best" Points vs. Hierarchical Points

In order to recover efficiency, let us develop the coefficient function approximation for the non-linear terms in (237) by employing the "best" points interpolation of [75, 74]. We outline the general procedure below.

Suppose K snapshots have been taken of the (vector-valued) primal unknown field, at K different times:

$$\mathcal{S}^u \equiv \{\boldsymbol{\xi}_k^u(s) = \mathbf{u}_h^k(s) : 1 \leq k \leq K\} \tag{256}$$

Here, the $\mathbf{u}_h^k(s)$ are vectors of state variables at grid point locations, each containing a single solution (snapshot) from the numerical simulation.

Given this set of snapshots of the primal unknown field $\mathbf{u}$, one can construct the following set of snapshots of the non-linear (scalar-valued) function f defined in (244):

$$\mathcal{S}^f \equiv \{\xi_k^f(s) = f(\mathbf{u}_h^k(s)) : 1 \leq k \leq K\} \tag{257}$$

The snapshot sets are assumed to be spanned by an orthonormal basis, $\{\phi_m^f\}_{m=1}^M$. A coefficient-function approximation of f is defined as

$$f_M = \sum_{m=1}^{M} \beta_m \phi_m^f. \tag{258}$$

Here, the coefficients β_m are solved from

$$\sum_{m=1}^{M} \phi_m^f(z_i)\beta_m = f(\mathbf{u}(z_i)), \qquad i = 1,\ldots,M \tag{259}$$

and $\{z_i\}_{i=1}^M$ is a set of interpolation points.

We now define the best approximations of the elements in the snapshot set as:

$$f_M^*(\mathbf{u}_h^k(\cdot)) = \arg \min_{w_M \in \text{span}\{\phi_1^f,\ldots,\phi_M^f\}} ||f(\mathbf{u}_h^k(\cdot)) - w_M||, \quad 1 \leq k \leq K \tag{260}$$

Orthonormality of the ϕ_m^f implies that

$$f_M^*(\mathbf{u}_h^k(x)) = \sum_{m=1}^{M} \alpha_m^k \phi_m^f(s), \quad 1 \leq k \leq K \tag{261}$$

where

$$\alpha_m^k = (\phi_m^f, f(\mathbf{u}_h^k(\cdot))), \quad m = 1,...,M, 1 \le k \le K \tag{262}$$

The "best" interpolation points [75, 74] $\{s_m^{bp}\}_{m=1}^M$ are defined as the solution to the following optimization problem:

$$\begin{array}{c} \min_{s_1^{bp},...,s_M^{bp} \in \Omega} \sum_{k=1}^K \left|\left| f_M^*(\mathbf{u}_h^k(\cdot)) - \sum_{m=1}^M \beta_m^k(s_1^{bp},...,s_M^{bp}) \phi_m^f \right|\right|^2 \\ \sum_{n=1}^M \phi_n^f(s_m^{bp}) \beta_n^k(s_1^{bp},...,s_M^{bp}) = f(\mathbf{u}_h^k(s_m^{bp})), \quad 1 \le m \le M, 1 \le k \le K \end{array} \tag{263}$$

Substituting (261) into (263) and invoking the orthonormality of the $\{\phi_m^f\}_{m=1}^M$, we obtain:

$$\boxed{\begin{array}{c} \min_{s_1^{bp},...,s_M^{bp} \in \Omega} \sum_{k=1}^K \sum_{m=1}^M (\alpha_m^k - \beta_m^k(s_1^{bp},...,s_M^{bp}))^2 \\ \sum_{n=1}^M \phi_n^f(s_m^{bp}) \beta_n^k(s_1^{bp},...,s_M^{bp}) = f(\mathbf{u}_h^k(s_m^{bp})), \quad 1 \le m \le M, 1 \le k \le K \end{array}} \tag{264}$$

i.e., the set of points $\{s_m^{bp}\}_{m=1}^M$ is determined to minimize the average error between the interpolants $f_M(\cdot)$ and the best approximations $f_M^*(\cdot)$. For implementational purposes, it is useful to rewrite (264) as

$$\begin{array}{c} \min_{s_1^{bp},...,s_M^{bp} \in \Omega} \sum_{q=1}^Q (\tilde{\alpha}_q - \tilde{\beta}_q(s_1^{bp},...,s_M^{bp}))^2 \\ \sum_{n=1}^M \phi_n^f(s_m^{bp}) \tilde{\beta}_{(k-1)M+m}(s_1^{bp},...,s_M^{bp}) = f(\mathbf{u}_h^k(s_m^{bp})), \quad 1 \le m \le M, 1 \le k \le K \end{array} \tag{265}$$

where $Q = MK$ and, for $1 \le m \le M$, $1 \le k \le K$,

$$\begin{array}{c} \alpha_m^k = \tilde{\alpha}_{(k-1)M+m} \\ \beta_m^k = \tilde{\beta}_{(k-1)M+m} \end{array} \tag{266}$$

The solution to the least-square optimization problem (265) can be found using the Levenberg-Marquardt (LM) algorithm[9]. According to [74], the optimal solution is typically reached in less than fifteen iterations of the LM algorithm.

As noted in [75], the solutions to (265) are in general non-unique, as the objective function defining the "best" points is usually non-convex. As a consequence, any iterative minimization algorithm used to solve (265) is very sensitive to the initial guess.

One systematic approach that works well for selecting the initial guess for (265) is to first compute the so-called "hierarchical" interpolation points[10], $\{s_m^{hp}\}_{m=1}^M$ and then use these as the initial guess in finding the "best" points. The hierarchical points are less expensive to construct than the "best" points $\{s_m^{bp}\}_{m=1}^M$, as they are computed one at a time by solving a sequence of univariate optimization problems. They also exhibit the nice property that $\{s_1^{hp},...,s_m^{hp}\} \subset \{s_1^{hp},...,s_{m+1}^{hp}\}$ for $m = 1,...,M-1$.

[9] E.g., by employing the `lsqnonlin` function in MATLAB's optimization toolbox.

[10] For more on the hierarchical points, the reader is referred to Section 2.2.3 of [75].

The solution procedure for the hierarchical points is as follows. To obtain the first hierarchical point, s_1^{hp} one computes the minimizer of the following (univariate, or 1D) optimization problem:

$$\begin{aligned} &\min_{s_1^{hp}\in\Omega} \sum_{k=1}^{K} (\alpha_1^k - \beta_1^k(s_1^{hp}))^2 \\ &\phi_1^f(s_1^{hp})\beta_1^k(s_1^{hp}) = f(\mathbf{u}_h^k(s_1^{hp})), \quad 1 \le k \le K \end{aligned} \tag{267}$$

Then, for $L = 2, ..., M$, one finds s_L^{hp} and appends it to the sequence $\{s_1^{hp}, ..., s_{L-1}^{hp}\}$ already computed, where s_L^{hp} is defined as the minimizer of

$$\begin{aligned} &\min_{s_L^{hp}\in\Omega} \sum_{k=1}^{K} \sum_{l=1}^{L} (\alpha_l^k - \beta_l^k(s_L^{hp}))^2 \\ &\sum_{l=1}^{L} \phi_l^f(s_m^{hp})\beta_l^k(s_m^{hp}) = f(\mathbf{u}_h^k(s_m^{hp})), \quad 1 \le m \le L-1, 1 \le k \le K \\ &\sum_{l=1}^{L} \phi_l^f(s_L^{hp})\beta_l^k(s_L^{hp}) = f(\mathbf{u}_h^k(s_L^{hp})), \quad 1 \le k \le K \end{aligned} \tag{268}$$

where $L = 2, ..., M$ and α_l^k is as defined in (262).

As will be illustrated in Section 5.2, the objective functions in (268) are, like the objective function in (265), in general non-convex, meaning they possess multiple local minima. However, as each minimization (268) is univariate, one could, rather than using an iterative optimization procedure to obtain local minima, compute the global minimizers that solve (268). This idea is explored further in Section 5.2.

Reduced Order Approximation to (237) **with Interpolation**

Given the "best" points for f, i.e., the solutions to (265) (or any set of interpolation points), call them $\{s_m^f\}_{m=1}^M$, it is straight-forward to apply the interpolation outlined in Section 5.2 to the non-linear function $f(\mathbf{u})$ (244). We begin by computing snapshots for the non-linear function f in (244). From these snapshots we compute the interpolation points $\{s_m^f\}_{m=1}^M$ following the approach outlined in Section 5.2 (see also Section 2 of [74]). Given $\{s_m^f\}_{m=1}^M$ and $\{\phi_m^f\}_{m=1}^M$, one obtains the so-called "cardinal functions" $\{\psi_m^f\}_{m=1}^M$ by solving the following linear system

$$\boldsymbol{\phi}_M^f(s) = \mathbf{A}\boldsymbol{\psi}_M^f(s) \tag{269}$$

where $\boldsymbol{\phi}_M^f(s) = (\phi_1^f(s), ..., \phi_M^f(s))^T$ and $\boldsymbol{\psi}_M^f(s) = (\psi_1^f(s), ..., \psi_M^f(s))^T$, and $A_{ij} = \phi_j^f(s_i^f)$. Note that (269) is well-defined, as the basis for f, like f itself, is *scalar*. Note also that the cardinal functions satisfy $\psi_j(s_i^f) = \delta_{ij}$.

Given the interpolation points $\{s_m^f\}$ and the cardinal functions $\{\psi_m^f\}$, one can approximate f as:

$$f(\mathbf{u}) \approx f_M(\mathbf{u}) = \sum_{m=1}^{M} f(\mathbf{u}(s_m^f))\psi_m^f \in \mathbb{R} \tag{270}$$

so that

$$f_M = \sum_{m=1}^{M} f\left(\sum_{n=1}^{M} a_n(t)\boldsymbol{\phi}_n^u(s_m^f)\right)\psi_m^f \tag{271}$$

The projection of f_M onto the l^{th} POD mode for $\mathbf{u}$ can be written in matrix/vector form. To do this, note that, for a general function $f_M(\mathbf{a}_M)$ and for $l = 1, ..., M$, we have that:

$$\begin{aligned}(\boldsymbol{\phi}_l^u, \mathbf{C} f_M(\mathbf{a}_N)) &= \left(\boldsymbol{\phi}_l^u, \sum_{m=1}^M \mathbf{C} f\left(\sum_{n=1}^M a_n \boldsymbol{\phi}_n^u(s_m^f)\right) \psi_m^f\right) \\ &= \sum_{m=1}^M \left[\int_\Omega \boldsymbol{\phi}_l^u \cdot \mathbf{C}\psi_m^f d\Omega\right] f\left(\sum_{n=1}^M a_n \boldsymbol{\phi}_n^u(s_m^f)\right)\end{aligned} \tag{272}$$

Remark that (272) is a matrix/vector product of the form $\mathbf{G} f\left(\sum_{n=1}^M a_n \boldsymbol{\phi}_n^u(s_m^f)\right)$ where

$$G_{nm} = \int_\Omega \boldsymbol{\phi}_n^u \cdot \mathbf{C}\psi_m^f d\Omega \tag{273}$$

for $1 \leq m, n \leq M$ (so that $\mathbf{G} \in \mathbb{R}^{M \times M}$).

It follows that, with the interpolation procedure employed here, our ODE system for the ROM coefficients is now

$$\boxed{\dot{\mathbf{a}}_M = \mathbf{F} - \mathbf{L}\mathbf{a}_M - \mathbf{G} f(\mathbf{D}^f \mathbf{a}_M)} \tag{274}$$

where $\mathbf{F}$ and $\mathbf{L}$ are defined in (250) and (251) respectively, the entries of $\mathbf{G}$ are given by (273), and

$$\mathbf{D}^f \equiv \begin{pmatrix} \boldsymbol{\phi}_1^u(s_1^f) & \cdots & \boldsymbol{\phi}_M^u(s_1^f) \\ \vdots & \ddots & \vdots \\ \boldsymbol{\phi}_1^u(s_M^f) & \cdots & \boldsymbol{\phi}_M^u(s_M^f) \end{pmatrix} \in \mathbb{R}^{2M \times M} \tag{275}$$

To clarify the notation in (274), namely what is meant by a function f of a vector:

$$f(\mathbf{D}^f \mathbf{a}_M) \equiv f\begin{pmatrix} \sum_{m=1}^M \boldsymbol{\phi}_m^u(s_1^f) a_m \\ \vdots \\ \sum_{m=1}^M \boldsymbol{\phi}_m^u(s_M^f) a_m \end{pmatrix} \equiv \begin{pmatrix} f\left(\sum_{m=1}^M \boldsymbol{\phi}_m^u(s_1^f) a_m\right) \\ \vdots \\ f\left(\sum_{m=1}^M \boldsymbol{\phi}_m^u(s_M^f) a_m\right) \end{pmatrix} \in \mathbb{R}^M \tag{276}$$

where $f\left(\sum_{m=1}^M \boldsymbol{\phi}_m^u(s_i^f) a_m\right)$ is defined as in (255).

Essentially, in the interpolation procedure outlined here, recomputation of inner products (projection) of the nonlinear terms at each time (or Newton) step is replaced by evaluation of the basis functions at the pre-computed interpolation points (275). There is also a matrix inversion (269) involved in solving for the cardinal functions $\{\psi_m^f\}_{m=1}^M$ (269). This is the key difference between the ROM with interpolation (274) and the ROM without interpolation (248), and what makes (274) far more efficient. The formulation and solution of the ROM with interpolation, including computation of the "best" points and time-integration, is summarized in Algorithm 1.

Some Numerical Results for (244) **with a Fourier Cosine Reduced Basis**

Since we are interested in formulating a *Galerkin* Reduced Order Model (ROM), we seek a basis that satisfies the boundary conditions, namely (238) and (239). It turns out that a Fourier cosine basis, defined by

$$\phi_m(s) = \cos(\pi(m-1)s), \quad m = 1, ..., M \tag{283}$$

Algorithm 1 Summary of ROM solution procedure of (237) with "best" points interpolation

1. Compute a set of K snapshots for the primal unknown field $\mathbf{u}$:

$$\mathcal{S}^u \equiv \{\boldsymbol{\xi}_k^u(s) = \mathbf{u}_h^k(s) : 1 \leq k \leq K\} \tag{277}$$

2. Given this set of snapshots of the primal unknown field $\mathbf{u}$, compute the following set of snapshots of the non-linear function f (244) from (277):

$$\mathcal{S}^f \equiv \{\xi_k^f(s) = f(\mathbf{u}_h^k(x)) : 1 \leq k \leq K\} \tag{278}$$

3. Compute an orthonormal basis $\{\phi_1^f, ..., \phi_M^f\}$ for f.
4. For the nonlinear function $f(\mathbf{u})$ in (244), apply (for instance) the Levenberg-Marquandt (LM) algorithm to solve (265) for the "best" points $\mathbf{s}^{bp} = \{s_1^{bp}, ..., s_M^{bp}\}$.
5. Compute an orthonormal basis $\{\phi_1^u, ..., \phi_M^u\}$ for $\mathbf{u}$.
6. Compute the matrix $\mathbf{L}$ and vector $\mathbf{F}$ from (251) and (252) respectively.
7. Compute $\mathbf{A} \equiv \mathbf{A}(\mathbf{s}^{bp})$ at the best points, with:

$$A_{mn} = \phi_n^f(s_m^f) \tag{279}$$

8. Compute the set of cardinal functions $\{\psi_1^f, ..., \psi_M^f\}$ by solving $\boldsymbol{\phi}_M^f = \mathbf{A}\boldsymbol{\psi}_M^f$.
9. Compute $\mathbf{G}$ from

$$G_{nm} = \int_\Omega \boldsymbol{\phi}_n^u \cdot \mathbf{C}\psi_m^f d\Omega \tag{280}$$

10. Compute $\mathbf{D}^f$ from

$$D_{mn}^f = \phi_n^u(z_m^f) \tag{281}$$

11. Advance the following ODE system forward in time using a standard time-integration scheme (e.g., Euler, Runge-Kutta, etc.).

$$\dot{\mathbf{a}}_N + \mathbf{L}\mathbf{a}_N - \mathbf{F} + \mathbf{G}f(\mathbf{D}^f\mathbf{a}_N) = \mathbf{0} \tag{282}$$

(Note that Newton's method is not required if an explicit scheme is employed.)

for $0 \leq s \leq 1$ satisfies these boundary conditions. To generate some preliminary numerical results, we will therefore employ a scalar Fourier cosine basis for each y and θ:

$$y(\tau, s) \approx y_M(\tau, s) = \sum_{m=1}^{M} a_m^y(\tau)\cos(\pi(m-1)s) \tag{284}$$

$$\theta(\tau, s) \approx \theta_M(\tau, s) = \sum_{m=1}^{M} a_m^\theta(\tau)\cos(\pi(m-1)s) \tag{285}$$

It is well-known that the Fourier cosine basis is orthonormal in the L_2 inner product; hence, we will take as $(\cdot,\cdot)$ the $L_2([0,1])$ inner product. It follows that the coefficients in (284) and (285) are given by

$$a_m^y(\tau) = (y(\tau, s), \cos(\pi(m-1)s)_{L_2([0,1])} \equiv \int_0^1 y(\tau, s)\cos(\pi(m-1)s)ds \tag{286}$$

and

$$a_m^{\theta}(\tau) = (\theta(\tau,s), \cos(\pi(m-1)s)_{L_2([0,1])} \equiv \int_0^1 \theta(\tau,s)\cos(\pi(m-1)s)ds \tag{287}$$

respectively.

For concreteness and to generate some numerical results, we fix the properties in the equations (237) to those summarized in Table 3. As one can infer from Figure 15, the solution exhibits a limit cycle for $D = 0.170$. One of our goals is to see if the ROM solution with interpolation captures this limit cycle correctly.

Table 3. Fluid properties used in the numerical solution of (237)

Property	Symbol	Value
Peclet number for heat transfer	Pe_h	5.00
Peclet number for mass transfer	Pe_m	5.00
Dimensionless heat of reaction	B	0.50
Dimensionless activation energy	γ	25.0
Dimensionless heat transfer coefficient	β	2.50
Reference dimensionless temperature	θ_0	1.00
Damkohler number	D	0.17

The reduced order model for which we give numerical results was generated by taking $K = 701$ snapshots of the solution fields y and θ, at time increments $d\tau = 0.25$ apart. The solution fields were generated using a fourth order finite difference approximation to the spatial derivative terms in (241) and a fourth order Runge-Kutta time-integration method. Numerical tests reveal that, to capture the correct limit cycle, a reduced basis Fourier cosine basis of size at least $M = 6$ modes is required. Below, we give some results for $M = 6$ and $M = 10$.

Tables 4 and 5 give the uniform, hierarchical and "best" points for a basis of size $M = 6$ and $M = 10$ respectively, and the nonlinear function (244). The "best" points are computed by solving the optimization problem (265) using the `lsqnonlin` function in MATLAB's optimization toolbox, and with the hierarchical points as the initial guess. We note that the objective function in (265) is not necessarily convex, so it may possess multiple local minima, which implies that the "best" points are non-unique. The same is true for the objective function that defines the hierarchical points. Since in this latter case of the hierarchical points, the minimization is univariate, it is possible to obtain hierarchical points that are global minima of the relevant objective function (third column of Tables 4 and 5). These points can be quite different, as one can see by comparing columns two and three of Tables 4 and 5. Indeed, Figure 16 shows that the objective function defining the second and third hierarchical points (and subsequent hierarchical points) possesses multiple local minima. A surprising observation is that it turns out not to matter which hierarchical points, the local minimizers (column two of Tables 4 and 5) or the global minimizers (column three of Tables 4 and 5), are used as the initial guess to obtain the "best" points in column four of these tables. Selecting s^{unif} (the uniform points) as the initial guess produces in general a different set of "best" points, however.

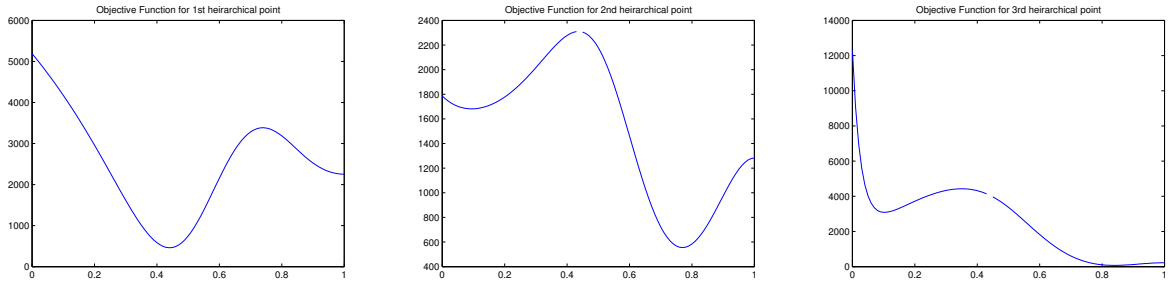

(a) s_1^{hp} **(b)** s_2^{hp} **(c)** s_3^{hp}

Figure 16. Objective functions defining the first three hierarchical points s_1^{hp}, s_2^{hp} and s_3^{hp}

The ROM ODE system resulting from the discretization (274) was advanced forward in time using a nonlinear fourth order Runge-Kutta (RK-4) time integration scheme, with time step $\Delta\tau = 10^{-3}$.

Figures 17 and 19 show the $L_2([0,1])$ errors in the ROM solutions computed using $M = 6$ and $M = 10$ Fourier cosine modes respectively with the interpolation outlined in Section 5.2. Errors are computed relative to the snapshots for uniformly spaced interpolation points versus the "best" points. It is found that using the "best" points reduces the error by an order of magnitude for $M = 6$. One can also see by comparing Figures 17 and 19 that there is greater payoff in using the "best" points for smaller M.

Figures 18 and 20 depict the limit cycle computed by the 6 and 10 mode ROMs (respectively) with "best" points interpolation. There is a slight phase error when $M = 6$ because so few modes are employed; nonetheless, it is clear that the nonlinear behavior, namely the limit cycle, is captured. There is excellent agreement between the ROM limit cycle and the snapshot limit cycle for $M = 10$ (Figure 20): the non-linear behavior is captured with the correct phase/magnitude.

Table 4. Uniform (s^{unif}), hierarchical (s^{hp}) and "best" (s^{bp}) points for $M = 6$

s^{unif}	s^{hp} (local minimizer)	s^{hp} (global minimizer)	s^{bp}
0.0000	0.0291	0.20	0.0572
0.2000	0.1202	0.25	0.2465
0.4000	0.2211	0.44	0.4203
0.6000	0.3252	0.72	0.5909
0.8000	0.4311	0.77	0.7578
1.0000	0.5378	0.78	0.9211

Table 5. Uniform (s^{unif}), hierarchical (s^{hp}) and "best" (s^{bp}) points for $M = 10$

s^{unif}	s^{hp} (local minimizer)	s^{hp} (global minimizer)	s^{bp}
0.0000	0.0945	0.01	0.0291
0.1111	0.1021	0.04	0.1202
0.2222	0.2568	0.20	0.2211
0.3333	0.3355	0.25	0.3252
0.4444	0.4407	0.42	0.4311
0.5556	0.5490	0.44	0.5378
0.6667	0.6659	0.50	0.6443
0.7778	0.7014	0.77	0.7504
0.8889	0.8529	0.78	0.8560
1.0000	0.9157	0.87	0.9564

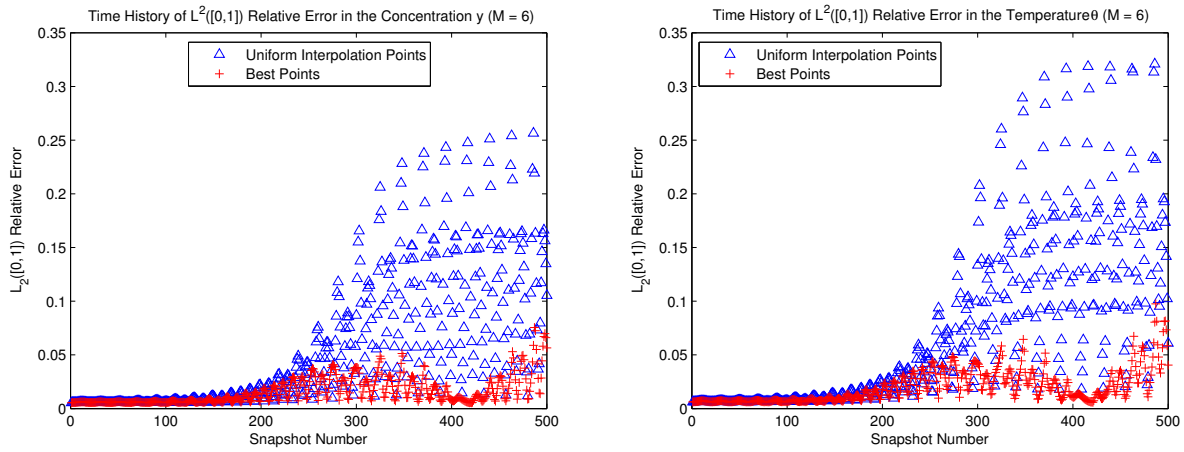

(a) Concentration y **(b)** Temperature θ

Figure 17. Time history of $L^2([0,1])$ relative errors in 6 mode ROM solution with interpolation using uniform points vs. "best" points

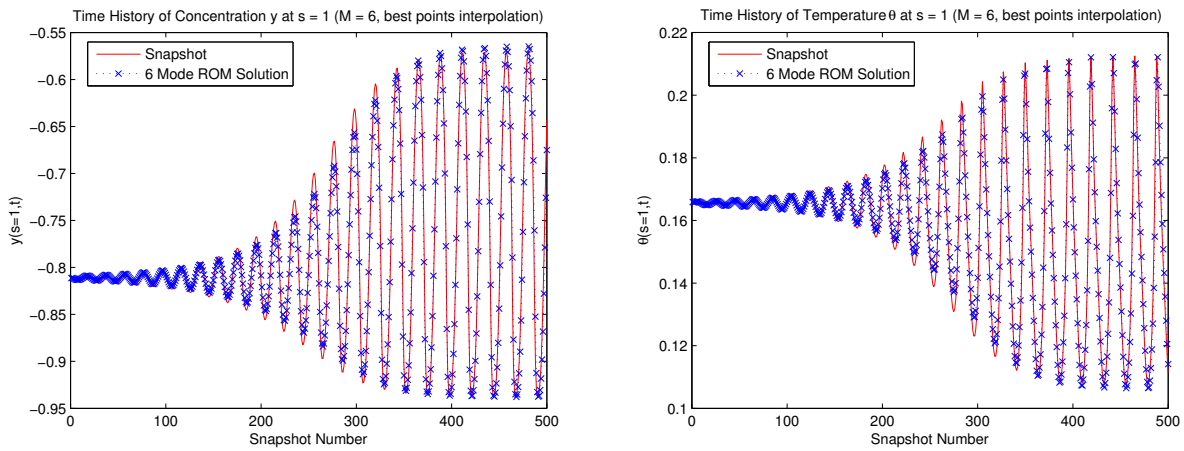

(a) Concentration y **(b)** Temperature θ

Figure 18. Correct computation of limit cycles by a 6 mode ROM with "best" points interpolation

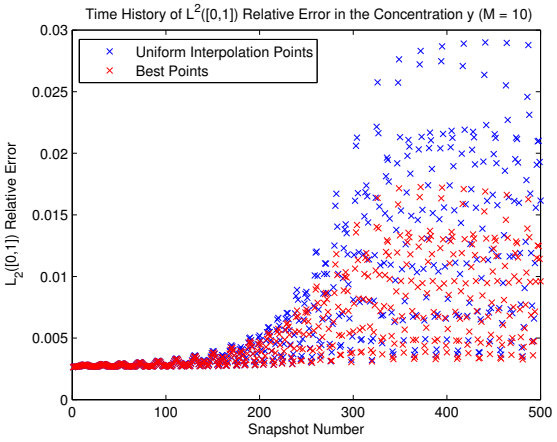

(a) Concentration y

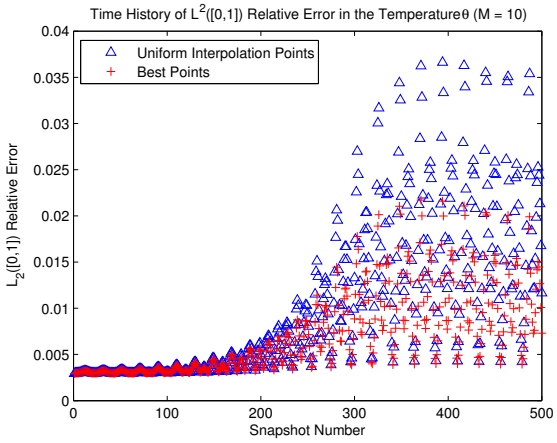

(b) Temperature θ

Figure 19. Time history of $L^2([0,1])$ relative errors in 10 mode ROM solution with interpolation using uniform points vs. "best" points

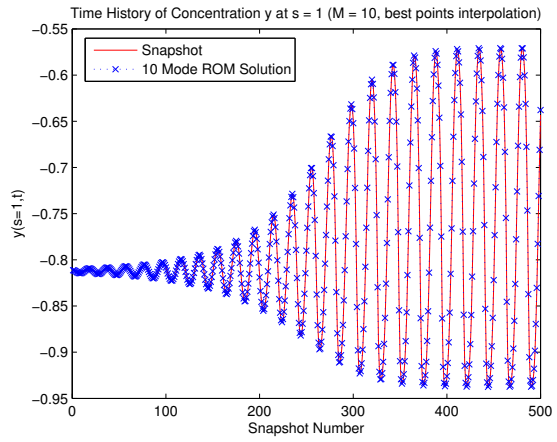

(a) Concentration y

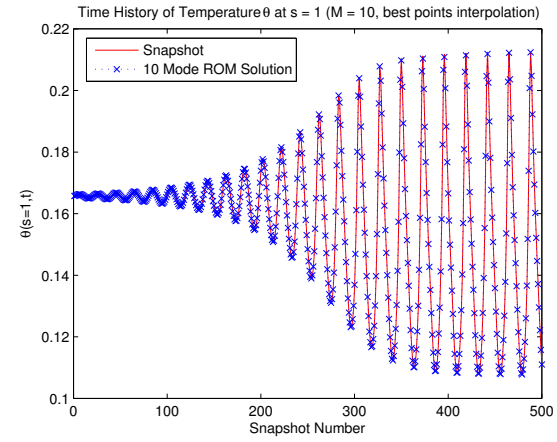

(b) Temperature θ

Figure 20. Correct computation of limit cycles by a 10 mode ROM with "best" points interpolation

Other Orthogonal Bases: Some Difficulties with a Proper Orthogonal Decomposition (POD) Basis for the Tubular Reactor ROM

We end the discussion of the 1D non-linear tubular rector ROM with some comments regarding the performance of the ROM with a Proper Orthogonal Decomposition (POD) basis[11], instead of a spectral basis like the Fourier cosine basis (283).

Numerical experiments with a POD basis suggest that POD is a poor choice of ROM basis for this problem. In particular, it is observed that:

- The method of snapshots appears to break down when computing bases of M greater than approximately 30 for the $K = 700$ snapshots of the field $\mathbf{u}$. Non-orthogonal modes begin to appear.
- The Fourier basis seems to be much more efficient at representing the nonlinear function $f(\mathbf{u})$ (244) than the POD basis.

The second point is likely the primary cause of the trouble. Indeed, POD is optimal in representing $\mathbf{u}$ but not necessarily $f(\mathbf{u})$, so its inadequacy is not entirely surprising. The excellent results with a Fourier basis can further be attributed to the smoothness of this basis, as well as the fact that the exact derivatives of the basis functions are available.

5.3 An Entropy-Stable and Efficient Reduced Order Model (ROM) for the 3D Compressible Navier-Stokes Equations

Having formulated the "best" points interpolation of [75, 74] in the context of a non-linear Galerkin reduced order model, and demonstrated its application to a simple 1D non-linear convection-diffusion-reaction system (Section 5.2), let us now turn our attention to the equations of interest, namely the three-dimensional (3D) compressible Navier-Stokes equations. Following a discussion of the fluid variables, the governing equations and the boundary conditions , we exhibit an entropy-stable inner product for the Galerkin projection step , and formulate the "best" points interpolation procedure outlined in Section 5.2 to handle the non-linear terms present in these equations.

Notation and Governing Equations

In terms of the conservation variables $\mathbf{U}$, the Navier-Stokes equations can be written as[12] [78]:

$$\mathbf{U}_{,t} + \mathbf{F}_{i,i} = \mathbf{F}^v_{i,i} + \mathbf{F}^h_{i,i} \tag{288}$$

[11] The reader is referred to Section 2.2 for an overview of Proper Orthogonal Decomposition (POD).

[12] Note that we are employing the so-called Einstein notation, or implied summation on repeated indices, so that, e.g., $\mathbf{F}_{i,i} \equiv \frac{\partial \mathbf{F}_1}{\partial x_1} + \frac{\partial \mathbf{F}_2}{\partial x_2} + \frac{\partial \mathbf{F}_3}{\partial x_3}$.

where, in three-dimensions (3D):

$$\mathbf{U} \equiv \begin{pmatrix} U_1 \\ U_2 \\ U_3 \\ U_4 \\ U_5 \end{pmatrix} \equiv \begin{pmatrix} \rho \\ \rho u_1 \\ \rho u_2 \\ \rho u_3 \\ \rho e \end{pmatrix} \tag{289}$$

$$\mathbf{F}_i = u_i \mathbf{U} + p \begin{pmatrix} 0 \\ \delta_{1i} \\ \delta_{2i} \\ \delta_{3i} \\ u_i \end{pmatrix}, \quad \mathbf{F}_i^v = \begin{pmatrix} 0 \\ \tau_{1i} \\ \tau_{2i} \\ \tau_{3i} \\ \tau_{ij} u_j \end{pmatrix}, \quad \mathbf{F}_i^h = \begin{pmatrix} 0 \\ 0 \\ 0 \\ 0 \\ -q_i \end{pmatrix} \tag{290}$$

for $i = 1,2,3$. $\mathbf{F}_i$ is known as the convective or Euler flux, $\mathbf{F}_i^v$ is the viscous flux, and $\mathbf{F}_i^h$ is the heat flux. The variables and parameters appearing in (289)–(290) are defined in Table 6. The specific heats are assumed to be positive constants. Moreover, we require that

$$\mu \geq 0, \quad \lambda + \frac{2}{3}\mu \geq 0, \quad \kappa \geq 0 \tag{291}$$

Table 6. Fluid variables

Variable	Physical Meaning	Expression
ρ	fluid density	
u_i	fluid velocity in the i^{th} direction	
δ_{ij}	Kronecker delta	$\delta_{ij} = \begin{cases} 1, & \text{if } i = j \\ 0, & \text{otherwise} \end{cases}$
e	total energy density	$e = \iota + \frac{1}{2}u^2$
ι	internal energy density	$\iota = c_v \theta$
θ	absolute temperature	
c_v	specific heat at constant volume	
c_p	specific heat at constant pressure	
γ	ratio of specific heats	$\gamma = c_p / c_v$
p	fluid pressure	$p = (\gamma - 1)\rho\iota$
τ_{ij}	viscous stress	$\tau_{ij} = \lambda u_{k,k}\delta_{ij} + \mu(u_{i,j} + u_{j,i})$
λ, μ	viscosity coefficients	
q_i	heat flux	$q_i = -\kappa\theta_{,i}$
κ	conductivity	
η	thermodynamic entropy density per unit mass	
s	nondimensional entropy	$s \equiv \eta / c_v = \ln(p\rho^{-\gamma})$ [Gibbs' equation]
t	time	
$\mathbf{x}$	position vector in Cartesian coordinates	$\mathbf{x}^T = (x_1, x_2, x_3)$

(288) is the conservative form of the 3D compressible Navier-Stokes equations. These equations can also be written in non-conservative form as

$$\mathbf{U}_{,t} + \mathbf{A}_i \mathbf{U}_{,i} = (\mathbf{K}_{ij}\mathbf{U}_{,j})_{,i} \tag{292}$$

where $\mathbf{A}_i \equiv \mathbf{A}_i(\mathbf{U})$, $\mathbf{K}^v_{ij} \equiv \mathbf{K}^v_{ij}(\mathbf{U})$ and $\mathbf{K}^h_{ij} \equiv \mathbf{K}^h_{ij}(\mathbf{U})$ are defined by

$$\mathbf{F}_{i,i} = \mathbf{F}_{i,\mathbf{U}}\mathbf{U}_{,i} \equiv \mathbf{A}_i \mathbf{U}_{,i} \tag{293}$$

$$\mathbf{F}^v_i \equiv \mathbf{K}^v_{ij}\mathbf{U}_{,j} \tag{294}$$

$$\mathbf{F}^h_i \equiv \mathbf{K}^h_{ij}\mathbf{U}_{,j} \tag{295}$$

and

$$\mathbf{K}_{ij} \equiv \mathbf{K}^v_{ij} + \mathbf{K}^h_{ij} \tag{296}$$

Let us for now neglect the far-field boundary conditions, so that we consider only the solid wall boundary conditions, denoting the solid wall boundary of the domain Ω by $\partial\Omega_W \equiv \partial\Omega$. The relevant boundary conditions at the solid wall are:

$$\begin{array}{lll} \text{no slip BC:} & \mathbf{u} = \mathbf{0}, & \text{on } \partial\Omega_W \\ \text{adiabatic wall BC:} & \nabla\theta \cdot \mathbf{n} = 0, & \text{on } \partial\Omega_W \end{array} \tag{297}$$

This document (Section 5.3) also includes a discussion of the no-penetration boundary condition:

$$\text{no-penetration BC:} \quad \mathbf{u} \cdot \mathbf{n} = 0, \quad \text{on } \partial\Omega_W \tag{298}$$

which it may be desirable to implement, for instance, if the basis functions employed do not satisfy the no-slip condition at the wall.

Clausius-Duhem Inequality, Entropy Variables and Symmetrization of the Navier-Stokes Equations

In designing a Galerkin Reduced Order Model (ROM) for the compressible Navier Stokes equations (288), we are interested in defining an inner product in which the Galerkin projection will be stable. As discussed in [76, 78], stability can be ensured by the energy method.

For the full (non-linear) Euler or Navier-Stokes equations, the energy method can be closely related to the second law of thermodynamics, or the Clausius-Duhem inequality, namely

$$\frac{d}{dt}\int_\Omega \rho\eta d\Omega \geq -\int_{\partial\Omega_W} \frac{q_i n_i}{\theta} dS \tag{299}$$

where η is the thermodynamic entropy density per unit mass (Table 6). (299) essentially states that the entropy of the system is non-decreasing. For (288), energy estimates, or the satisfaction of the entropy inequality (299), imply that the semi-discrete solutions possess stability properties akin to those of the exact solutions of the governing equations [76, 78]. We will call solutions that satisfy

(299) "entropy-stable". Our aim here is to develop a transformation (symmetrization) and define an inner product such that the Clausius-Duhem inequality (299) is necessarily satisfied for the Galerkin ROM we will build for the compressible Navier-Stokes equations (288) with boundary conditions (297).

To develop a Clausius-Duhem inequality-preserving Galerkin projection of the equations (292), let us introduce a change of variables $\mathbf{U} \rightarrow \mathbf{V}$:

$$\mathbf{U} = \mathbf{U}(\mathbf{V}) \tag{300}$$

We will refer to $\mathbf{V}$ as the "entropy variables". In terms of the entropy variables $\mathbf{V}$, the equations of interest (292) are:

$$\mathbf{A}_0 \mathbf{V}_{,t} + \tilde{\mathbf{A}}_i \mathbf{V}_{,i} - (\tilde{\mathbf{K}}_{ij} \mathbf{V}_{,j})_{,i} = \mathbf{0} \tag{301}$$

where[13]

$$\mathbf{A}_0 \equiv \mathbf{U}_{,\mathbf{V}} \tag{302}$$

$$\tilde{\mathbf{A}}_i \equiv \mathbf{A}_i \mathbf{A}_0 \tag{303}$$

$$\tilde{\mathbf{K}}_{ij} \equiv \mathbf{K}_{ij} \mathbf{A}_0 \tag{304}$$

It is well-known that the matrices $\mathbf{A}_i$ in (292) are non-symmetric. However, it is also well-known that all linear combinations of the $\mathbf{A}_i$ possess real eigenvalues and a complete set of eigenvectors, meaning $\mathbf{U}_{,t} + \mathbf{A}_i \mathbf{U}_{,i} = \mathbf{0}$ constitutes a hyperbolic system of conservation laws. We seek a change of variables (300) such that:

1. The matrices $\mathbf{A}_0$ and $\tilde{\mathbf{A}}_i$ are symmetric, and
2. The matrix

$$\tilde{\mathbf{K}} \equiv \begin{pmatrix} \tilde{\mathbf{K}}_{11} & \tilde{\mathbf{K}}_{12} & \tilde{\mathbf{K}}_{13} \\ \tilde{\mathbf{K}}_{21} & \tilde{\mathbf{K}}_{22} & \tilde{\mathbf{K}}_{23} \\ \tilde{\mathbf{K}}_{31} & \tilde{\mathbf{K}}_{32} & \tilde{\mathbf{K}}_{33} \end{pmatrix} \tag{305}$$

   is symmetric positive semi-definite.

If the transformation (300) is defined such that these properties hold, the resulting system in the entropy variables will be a symmetric hyperbolic system.

Following the symmetrization approaches of [76, 78], we define the change of variables (300) with the help of so-called generalized entropy functions. A generalized entropy function $H \equiv H(\mathbf{U})$ is by definition a function that satisfies the following two conditions [78]:

1. H is convex[14].

[13] The reader is referred to Section C.1 of Appendix C for explicit expressions of the symmetrized matrices (302)–(304).

[14] The convexity of H is equivalent to the positive-definiteness of $\mathbf{A}_0$, since $\mathbf{A}_0^{-1} = \mathbf{V}_{,\mathbf{U}} = H_{,\mathbf{UU}}$.

2. There exist scalar-valued functions $\sigma_i \equiv \sigma_i(\mathbf{U})$, $i = 1,2,3$, referred to as entropy fluxes, such that

$$H_{,\mathbf{U}}\mathbf{A}_i = \sigma_{i,\mathbf{U}} \tag{306}$$

The following theorems, quoted from [77], delineate the relationship between symmetric hyperbolic systems and generalized entropy functions, and will be employed in our symmetrization of the equations (293):

Theorem 3.2.1 (Mock). *A hyperbolic system of conservation laws possessing a generalized entropy function becomes symmetric under the change of variables*

$$\mathbf{V}^T = H_{,\mathbf{U}} \tag{307}$$

Theorem 3.2.2 (Godunov). *If a hyperbolic system can be symmetrized by introducing a change of variables, then a generalized entropy function and corresponding entropy fluxes exist for this system.*

It is shown in [77, 78] that for the compressible Navier-Stokes equations (292), appropriate choices for the entropy flux and entropy function are

$$\sigma_i = Hu_i, \quad H = -\rho g(s) \equiv -\rho s \tag{308}$$

respectively. Here s is the non-dimensional entropy, $s = \eta/c_v$ (Table 6), which satisfies $s = \ln(p\rho^{-\gamma}) + \text{const}$.

With the choice of affine entropy flux (308), the transformation $\mathbf{U} \rightarrow \mathbf{V}$ (307) is given by

$$\mathbf{V} = \frac{1}{\rho\iota}\begin{pmatrix} -U_5 + \rho\iota(\gamma + 1 - s) \\ U_2 \\ U_3 \\ U_4 \\ -U_1 \end{pmatrix} \tag{309}$$

where

$$s = \ln\left[\frac{(\gamma-1)\rho\iota}{U_1^\gamma}\right] \tag{310}$$

$$\rho\iota = U_5 - \frac{1}{2U_1}(U_2^2 + U_3^2 + U_4^2) \tag{311}$$

The inverse mapping $\mathbf{V} \rightarrow \mathbf{U}$ is given by

$$\mathbf{U} = \rho\iota\begin{pmatrix} -V_5 \\ V_2 \\ V_3 \\ V_4 \\ 1 - \frac{1}{2V_5}(V_2^2 + V_3^2 + V_4^2) \end{pmatrix} \tag{312}$$

where

$$\rho\iota = \left[\frac{\gamma-1}{(-V_5)^\gamma}\right]^{1/(\gamma-1)} \exp\left(\frac{-s}{\gamma-1}\right) \tag{313}$$

$$s = \gamma - V_1 + \frac{1}{2V_5}(V_2^2+V_3^2+V_4^2) \tag{314}$$

We conclude the discussion by calling attention to the fact that the affine entropy flux (308) is *not* homogeneous. To be called a homogeneous flux function [76], H must be selected such that:

$$\mathbf{U}_{,\mathbf{V}}\mathbf{V} = \beta\mathbf{U} \tag{315}$$

$$\tilde{\mathbf{F}}_{i,\mathbf{V}}\mathbf{V} = \beta\tilde{\mathbf{F}}_i \tag{316}$$

for some $\beta \in \mathbb{R}$, where $\tilde{\mathbf{F}}_i \equiv \mathbf{F}_i(\mathbf{V}(\mathbf{U}))$ (the Euler fluxes in the transformed entropy variables). As shown in [77], the *viscous* terms in the Navier-Stokes equations will be symmetric and positive definite after symmetrization for any member $H = -\rho g(s)$ of Harten's generalized entropy functions, in particular the following family of exponential *homogeneous* flux functions:

$$h(s) = Ke^{\kappa s} = K(p\rho^{-\gamma}), \quad K, \kappa \neq 0 \tag{317}$$

However, as proven in Section C.5 of Appendix C, if the heat flux term $\mathbf{F}^h_{i,i}$ is present in the equations (288), the only way for the augmented heat flux matrix (305) to remain positive semi-definite is if H is affine in s, i.e., if H has the form (308). It is for this reason that we have selected the *inhomogeneous* entropy flux function (308) for the compressible Navier-Stokes equations (288) instead of the *homogeneous* flux function (317). The latter could be used for the Euler equations or the Navier-Stokes equations with $\mathbf{F}^h_{i,i} \equiv \mathbf{0}$. In our case, since $\mathbf{F}^h_{i,i} \neq \mathbf{0}$, we select (308) to obtain the entropy-stability result in Theorem 5.3.1.

Entropy Stable Galerkin Projection of the Symmetrized Compressible Navier-Stokes Equations with Boundary Conditions

Let us now examine the stability of the Galerkin projection in the $L_2(\Omega)$ inner product of the symmetrized compressible Navier-Stokes equations (301) with boundary conditions (297). We will say that the Galerkin projection is "entropy-stable" if it satisfies the Clausius-Duhem entropy inequality (299), or the second law of thermodynamics. Per the discussion in [76, 78], we aim to show that the change of variables (309) is such that when the transformed equations (301) are projected onto an approximation mode, the Clausius-Duhem inequality is respected *ab initio* for all numerical solutions.

Assume the entropy variables have been expanded in a vector basis $\{\boldsymbol{\phi}_i\}_{i=1}^M \in \mathbb{R}^5$:

$$\mathbf{V}(\mathbf{x},t) \approx \mathbf{V}_M(\mathbf{x},t) = \sum_{m=1}^{M} a_m(t)\boldsymbol{\phi}_m(\mathbf{x}) \tag{318}$$

where the $a_m(t)$ are the modal amplitudes (or ROM coefficients) to be solved for. Assume the basis is orthonormal in the $L_2(\Omega)$ inner product, so that $(\boldsymbol{\phi}_i, \boldsymbol{\phi}_j) = \delta_{ij}$ for all $i, j = 1, ..., M$.

Theorem 5.3.1. *Consider the symmetrized compressible 3D Navier-Stokes equations* (301) *in an open bounded domain $\Omega \subset \mathbb{R}^3$, with the no-slip and adiabatic wall boundary condition* (297) *on the boundary $\partial\Omega_W$. Define the transformation $\mathbf{U} \rightarrow \mathbf{V}$ given by the entropy flux* (308)*, so that the relationship between $\mathbf{U}$ and the entropy variables $\mathbf{V}$ is* (309)*. Then the Galerkin projection of* (301) *with boundary conditions* (297) *onto an approximation mode $\boldsymbol{\phi}_j$ in the $L^2(\Omega)$ inner product is "entropy stable" (i.e.., satisfies the entropy estimate* (299)*) if the approximation modes $\boldsymbol{\phi}_j$ satisfy the no-slip condition on $\partial\Omega_W$, i.e., if*

$$\phi_j^2 = \phi_j^3 = \phi_j^4 = 0 \tag{319}$$

for $j = 1, ..., M$ where ϕ_j^i denotes the i^{th} component of $\boldsymbol{\phi}_j$ for $i = 1, ..., 5$.

Proof. Let us work out the projection of each of the terms at (301), one at a time. Premultiplying (301) by $\mathbf{V}^T$ and integrating over Ω, we have:

$$\begin{aligned} \int_\Omega \mathbf{V}^T \mathbf{A}_0 \mathbf{V}_{,t} d\Omega &= \int_\Omega H_{,\mathbf{U}} \mathbf{U}_{,\mathbf{V}} \mathbf{V}_{,t} d\Omega \\ &= \int_\Omega H_{,\mathbf{U}} \mathbf{U}_{,t} d\Omega \\ &= \int_\Omega H_{,t} d\Omega \end{aligned} \tag{320}$$

Note that

$$\mathbf{V}^T \tilde{\mathbf{A}}_i = (H_{,\mathbf{U}} \mathbf{A}_i) \mathbf{A}_0 = \sigma_{i,\mathbf{U}} \mathbf{U}_{,\mathbf{V}} = \sigma_{i,\mathbf{V}} \tag{321}$$

Now, for the convection term:

$$\int_\Omega \mathbf{V}^T \tilde{\mathbf{A}}_i \frac{\partial \mathbf{V}}{\partial x_i} d\Omega = \int_\Omega \underbrace{\sigma_{i,\mathbf{V}} \frac{\partial \mathbf{V}}{\partial x_i}}_{\sigma_{i,i}} d\Omega = \int_\Omega (H u_i)_{,i} d\Omega \tag{322}$$

Moving on to the diffusion term:

$$\begin{aligned} \int_\Omega \mathbf{V}^T (\tilde{\mathbf{K}}_{ij} \mathbf{V}_{,j})_{,i} d\Omega &= -\int_\Omega \mathbf{V}_{,i}^T \tilde{\mathbf{K}}_{ij} \mathbf{V}_{,j} d\Omega + \int_\Omega (\mathbf{V}^T \tilde{\mathbf{K}}_{ij} \mathbf{V}_{,j})_{,i} d\Omega \\ &= -\int_\Omega \mathbf{V}_{,i}^T \tilde{\mathbf{K}}_{ij} \mathbf{V}_{,j} d\Omega + \int_{\partial\Omega_W} \mathbf{V}^T \tilde{\mathbf{K}}_{ij} \mathbf{V}_{,j} dS \\ &= -\int_\Omega \mathbf{V}_{,i}^T \tilde{\mathbf{K}}_{ij} \mathbf{V}_{,j} d\Omega + \int_{\partial\Omega_W} \mathbf{V}^T \mathbf{K}_{ij} \mathbf{n}_i \mathbf{A}_0 \mathbf{V}_{,j} dS \\ &= -\int_\Omega \mathbf{V}_{,i}^T \tilde{\mathbf{K}}_{ij} \mathbf{V}_{,j} d\Omega + \int_{\partial\Omega_W} \mathbf{V}^T (\mathbf{K}_{ij}^v + \mathbf{K}_{ij}^h) \mathbf{n}_i \mathbf{U}_{,\mathbf{V}} \mathbf{V}_{,j} dS \\ &= -\int_\Omega \mathbf{V}_{,i}^T \tilde{\mathbf{K}}_{ij} \mathbf{V}_{,j} d\Omega + \int_{\partial\Omega_W} \mathbf{V}^T (\mathbf{K}_{ij}^v + \mathbf{K}_{ij}^h) \mathbf{n}_i \mathbf{U}_{,j} dS \\ &= -\int_\Omega \mathbf{V}_{,i}^T \tilde{\mathbf{K}}_{ij} \mathbf{V}_{,j} d\Omega + \int_{\partial\Omega_W} \mathbf{V}^T (\mathbf{F}_i^v + \mathbf{F}_i^h) \mathbf{n}_i dS \\ &= -\int_\Omega \mathbf{V}_{,i}^T \tilde{\mathbf{K}}_{ij} \mathbf{V}_{,j} d\Omega + \int_{\partial\Omega_W} \mathbf{V}^T \mathbf{F}_i^v n_i dS + \tfrac{1}{c_v} \int_{\partial\Omega_W} \tfrac{\mathbf{q}_i \mathbf{n}_i}{\theta} dS \end{aligned} \tag{323}$$

The integrand in the first boundary integral in (323) becomes, after the application of the no-slip condition (see (415))

$$[\mathbf{F}_i^v n_i]^{ns} = \frac{\mu}{V_5^2} \begin{pmatrix} 0 \\ (-V_5 V_{i+1,1} + V_{i+1} V_{5,1} - V_5 V_{2,i} + V_2 V_{5,i}) n_i \\ (-V_5 V_{i+1,2} + V_{i+1} V_{5,2} - V_5 V_{3,i} + V_3 V_{5,i}) n_i \\ (-V_5 V_{i+1,3} + V_{i+1} V_{5,3} - V_5 V_{4,i} + V_4 V_{5,i}) n_i \\ 0 \end{pmatrix} + \lambda \left[\frac{-V_5 V_{i+1,i} + V_{i+1} V_{5,i}}{V_5^2} \right] \begin{pmatrix} 0 \\ n_1 \\ n_2 \\ n_3 \\ 0 \end{pmatrix} \tag{324}$$

Let $\boldsymbol{\phi}_j \in \mathbb{R}^5$ be an approximation mode for the primal unknown field in the entropy variables, $\mathbf{V}$, and assume that $\boldsymbol{\phi}_j$ satisfies the no-slip condition (e.g., assume $\phi_j^2, \phi_j^3, \phi_j^4$ on $\partial\Omega_W$ is zero-ed out *a posteriori* in the implementation to ensure that it satisfies no-slip). Then, it follows from (324) that $[\boldsymbol{\phi}_j^T \mathbf{F}_i^v n_i]^{ns} = 0$ necessarily for all j, meaning $[\mathbf{V}^T \mathbf{F}_i^v n_i]^{ns} = 0$.

Putting (320), (322) and (323) together, we obtain:

$$\begin{aligned}
\tfrac{1}{c_v}\textstyle\int_\Omega (\rho\eta)_{,t} d\Omega &= \textstyle\int_\Omega c_v \mathbf{V}_{,i}^T \tilde{\mathbf{K}}_{ij} \mathbf{V}_{,j} d\Omega + \tfrac{1}{c_v}\int_\Omega \left[-(Hu_i)_{,i} - \left(\tfrac{q_i}{\theta}\right)_{,i}\right] d\Omega \\
&= \textstyle\int_\Omega c_v \mathbf{V}_{,i}^T \tilde{\mathbf{K}}_{ij} \mathbf{V}_{,j} d\Omega + \tfrac{1}{c_v}\int_{\partial\Omega_W} \left[-H \underbrace{u_i n_i}_{=0 \text{ (by no-slip BC)}} - \left(\tfrac{q_i}{\theta}\right) n_i\right] dS \\
&= \textstyle\int_\Omega c_v \mathbf{V}_{,i}^T \tilde{\mathbf{K}}_{ij} \mathbf{V}_{,j} d\Omega - \tfrac{1}{c_v}\int_{\partial\Omega_W} \underbrace{\left(\frac{q_i n_i}{\theta}\right)}_{=0 \text{ (by adiabatic wall BC)}} dS \\
&\geq 0
\end{aligned} \tag{325}$$

or

$$\frac{d}{dt}\int_\Omega \rho\eta d\Omega \geq 0 \tag{326}$$

which implies non-decreasing entropy (299), and therefore entropy-stability of the Galerkin projection. □

Weak Formulation and Implementation of Boundary Conditions (297) **and** (298)

Let us now formulate a weak implementation of the boundary conditions (297), using the viscous fluxes to implement the no-slip condition. We also formulate the implementation of the no-penetration boundary condition (298) using the convection term, which may be required for the numerics if the basis functions $\boldsymbol{\phi}_m$ do *not* satisfy the no-slip condition on $\partial\Omega_W$. Projecting (292) onto the mode $\boldsymbol{\phi}_m$, gives:

$$\begin{aligned}
\textstyle\int_\Omega \boldsymbol{\phi}_m^T \mathbf{A}_0 \mathbf{V}_{,t} d\Omega &= -\textstyle\int_\Omega \boldsymbol{\phi}_m^T \tilde{\mathbf{A}}_i \mathbf{V}_{,i} d\Omega + \int_\Omega \boldsymbol{\phi}_m^T ([\tilde{\mathbf{K}}_{ij}^v + \tilde{\mathbf{K}}_{ij}^h]\mathbf{V}_{,j})_{,i} d\Omega \\
&= \textstyle\int_\Omega (\boldsymbol{\phi}_m^T \tilde{\mathbf{A}}_i)_{,i} \mathbf{V} d\Omega - \int_\Omega \boldsymbol{\phi}_{m,i}^T \tilde{\mathbf{K}}_{ij} \mathbf{V}_{,j} d\Omega \\
&\quad \underbrace{-\int_{\partial\Omega_W} \boldsymbol{\phi}_m^T [\tilde{\mathbf{A}}_i n_i \mathbf{V}]^{np} dS}_{=I_m^{np}} + \underbrace{\int_{\partial\Omega_W} \boldsymbol{\phi}_m^T [\tilde{\mathbf{K}}_{ij}^v n_i \mathbf{V}_{,j}]^{ns} dS}_{=I_m^{ns}} + \underbrace{\int_{\partial\Omega_W} \boldsymbol{\phi}_m^T [\tilde{\mathbf{K}}_{ij}^h n_i \mathbf{V}_{,j}]^{ad} dS}_{=I_m^{ad}}
\end{aligned} \tag{327}$$

From Sections C.2–C.4 of Appendix C, we have that:

$$[\tilde{\mathbf{A}}_i n_i \mathbf{V}]^{np} = \begin{pmatrix} 0 \\ -\rho\iota s n_1 \\ -\rho\iota s n_2 \\ -\rho\iota s n_3 \\ 0 \end{pmatrix} \tag{328}$$

$$[\tilde{\mathbf{K}}^v_{ij} n_i \mathbf{V}_{,j}]^{ns} = \frac{\mu}{V_5^2} \begin{pmatrix} 0 \\ (-V_5 V_{i+1,1} + V_{i+1} V_{5,1} - V_5 V_{2,i} + V_2 V_{5,i}) n_i \\ (-V_5 V_{i+1,2} + V_{i+1} V_{5,2} - V_5 V_{3,i} + V_3 V_{5,i}) n_i \\ (-V_5 V_{i+1,3} + V_{i+1} V_{5,3} - V_5 V_{4,i} + V_4 V_{5,i}) n_i \\ 0 \end{pmatrix} + \lambda \left[\frac{-V_5 V_{i+1,i} + V_{i+1} V_{5,i}}{V_5^2} \right] \begin{pmatrix} 0 \\ n_1 \\ n_2 \\ n_3 \\ 0 \end{pmatrix} \tag{329}$$

and

$$[\tilde{\mathbf{K}}^h_{ij} n_i \mathbf{V}_{,j}]^{ad} = \mathbf{0} \tag{330}$$

Denoting

$$[\phi_m]_n \equiv \phi^2_m n_1 + \phi^3_m n_2 + \phi^4_m n_3 \tag{331}$$

we obtain the following expressions for the boundary integrals in (327) (Table 7).

Table 7. Boundary integrals arising from the weak implementation of the BCs (297)

Boundary Integral	Expression
I^{np}_m	$\int_{\partial\Omega_W} \left[\frac{\gamma-1}{(-V_5)^2}\right]^{\frac{1}{\gamma-1}} \exp\left(\frac{-\gamma+V_1-\frac{1}{2V_5}(V_2^2+V_3^2+V_4^2)}{\gamma-1}\right) [\gamma - V_1 + \frac{1}{2V_5}(V_2^2+V_3^2+V_4^2)][\phi_m]_n dS$
I^{ns}_m	$\int_{\partial\Omega_W} \frac{1}{V_5^2} \left[-\mu(V_5 V_{i+1,j} - V_{i+1} V_{5,j} + V_5 V_{j+1,i} - V_{j+1} V_{5,i}) n_i \phi^{m+1} - \lambda (V_5 V_{i+1,i} - V_{i+1} V_{5,i}) [\phi_m]_n\right] dS$
I^{ad}_m	0

Note that if the approximation modes $\boldsymbol{\phi}_m$ satisfy the no-slip condition on $\partial\Omega_W$, i.e., $\phi^2_m = \phi^3_m = \phi^4_m = 0$, then the integrals I^{np}_m and I^{ns}_m in Table 7 are identically 0: $I^{np}_m = I^{ns}_m \equiv 0$.

The non-linearity in the full Navier-Stokes equations (288) is in the advection term, or Euler fluxes $\mathbf{A}_i$. Note, however, that the diffusive terms in the entropy variable analog of (288), namely (301), are also non-linear, due to the fact that the symmetrizing matrix (Jacobian) $\mathbf{A}_0 \equiv \mathbf{U}_{,\mathbf{V}}$ is a function of $\mathbf{V}$. Hence, *all* the symmetrized matrices, namely $\tilde{\mathbf{A}}_i$ and $\tilde{\mathbf{K}}_{ij}$ will be non-linear in $\mathbf{V}$; in the ROM with boundary conditions, the boundary integrals (Table 7) will contain non-linearities as well if the basis functions do not satisfy no-slip. Moreover, since $\mathbf{A}_0 \equiv \mathbf{A}_0(\mathbf{V})$, while one has that $(\boldsymbol{\phi}_j, \boldsymbol{\phi}_i) = \delta_{ij}$ for any two basis functions $\boldsymbol{\phi}_j, \boldsymbol{\phi}_i$,

$$(\boldsymbol{\phi}_i, \mathbf{A}_0 \boldsymbol{\phi}_j) \neq \delta_{ij} \tag{332}$$

A consequence of (332) is a mass matrix will appear in the semi-discrete ROM to be advanced forward in time (see e.g., (366)).

Introducing the shorthand, for $\mathbf{V}_1, \mathbf{V}_2 \in \mathbb{R}^5$:

$$(\mathbf{V}_1, \mathbf{V}_2) \equiv \int_\Omega \mathbf{V}_1^T \mathbf{V}_2 d\Omega, \quad \langle \mathbf{V}_1, \mathbf{V}_2 \rangle_{\partial\Omega_W} \equiv \int_{\partial\Omega_W} \mathbf{V}_1^T \mathbf{V}_2 dS \tag{333}$$

the governing equations (301) projected onto an approximation mode $\boldsymbol{\phi}_m$ are

$$(\boldsymbol{\phi}_m, \mathbf{A}_0 \mathbf{V}_{,t}) - \big((\boldsymbol{\phi}_m \tilde{\mathbf{A}}_i)_{,i}, \mathbf{V}\big) + (\boldsymbol{\phi}_{m,i}, \tilde{\mathbf{K}}_{ij}\mathbf{V}_{,j}) \underbrace{-\langle \boldsymbol{\phi}_m, [\tilde{\mathbf{A}}_i n_i \mathbf{V}]^{np}\rangle_{\partial\Omega_W}}_{=I_m^{np}} + \underbrace{\langle \boldsymbol{\phi}_m, [\tilde{\mathbf{K}}^v_{ij} n_i \mathbf{V}_{,j}]^{ns}\rangle_{\partial\Omega_W}}_{=I_m^{ns}} + \underbrace{\langle \boldsymbol{\phi}_m, [\tilde{\mathbf{K}}^h_{ij} n_i \mathbf{V}_{,j}]^{ad}\rangle_{\partial\Omega_W}}_{=I_m^{ad}=0} = 0 \tag{334}$$

or (setting $I_{ad} = 0$; see Table 7)

$$(\boldsymbol{\phi}_m, \mathbf{A}_0 \mathbf{V}_{,t}) = \big(\boldsymbol{\phi}_{m,i}, \tilde{\mathbf{A}}_i \mathbf{V}\big) + \big(\boldsymbol{\phi}_m, \tilde{\mathbf{A}}_{i,i}\mathbf{V}\big) - (\boldsymbol{\phi}_{m,i}, \tilde{\mathbf{K}}_{ij}\mathbf{V}_{,j}) \underbrace{+\langle \boldsymbol{\phi}_m, [\tilde{\mathbf{A}}_i n_i \mathbf{V}]^{np}\rangle_{\partial\Omega_W}}_{=I_m^{np}} \underbrace{-\langle \boldsymbol{\phi}_m, [\tilde{\mathbf{K}}^v_{ij} n_i \mathbf{V}_{,j}]^{ns}\rangle_{\partial\Omega_W}}_{=I_m^{ns}} \tag{335}$$

Substituting the modal expansion (318) into (335), one obtains

$$\begin{aligned}\textstyle\sum_{n=1}^M (\boldsymbol{\phi}_m, [\mathbf{A}_0]_M \boldsymbol{\phi}_n)\, \dot{a}_n \;&= \big(\boldsymbol{\phi}_{m,i}, [\tilde{\mathbf{A}}_i]_M \mathbf{V}_M\big) + \big(\boldsymbol{\phi}_m, [\tilde{\mathbf{A}}_{i,i}]_N \mathbf{V}_M\big) - (\boldsymbol{\phi}_{m,i}, [\tilde{\mathbf{K}}_{ij}]_M \mathbf{V}_{M,j}) \\ &\quad + \langle \boldsymbol{\phi}_m, [\tilde{\mathbf{A}}_i n_i \mathbf{V}]^{np}_M\rangle_{\partial\Omega_W} - \langle \boldsymbol{\phi}_m, [\tilde{\mathbf{K}}^v_{ij} n_i \mathbf{V}_{,j}]^{ns}_M\rangle_{\partial\Omega_W}\end{aligned} \tag{336}$$

where $[\mathbf{A}_0]_M \equiv \mathbf{A}_0(\mathbf{V}_M) = \mathbf{A}_0\left(\sum_{n=1}^M a_n(t)\boldsymbol{\phi}_n\right)$ and similarly for the other matrices with "M" subscripts in (336).

All the terms in the projected equations (335) contain non-linearities[15], including the term on the left-hand side. We will denote the non-linear terms as follows:

$$[\mathbf{f}_0(\mathbf{V}_M)]_n = [\mathbf{A}_0]_M \boldsymbol{\phi}_n, \quad n = 1, ..., M \tag{337}$$

$$\mathbf{f}_i(\mathbf{V}_M) \equiv [\tilde{\mathbf{A}}_i]_M \mathbf{V}_M, \quad i = 1,2,3 \tag{338}$$

$$\mathbf{f}_4(\mathbf{V}_M) \equiv [\tilde{\mathbf{A}}_{i,i}]_M \mathbf{V}_M \tag{339}$$

$$\mathbf{f}_i(\mathbf{V}_M) \equiv [\tilde{\mathbf{K}}_{ij}]_M \mathbf{V}_{M,j}, \quad i = 5,6,7 \tag{340}$$

$$\mathbf{f}_8(\mathbf{V}_M) \equiv [\tilde{\mathbf{A}}_i n_i \mathbf{V}]^{np}_M \tag{341}$$

$$\mathbf{f}_9(\mathbf{V}_M) \equiv [\tilde{\mathbf{K}}^v_{ij} n_i \mathbf{V}_{,j}]^{ns}_M \tag{342}$$

Then (336) takes the form (for $i = 1,2,3$)

$$\begin{aligned}\textstyle\sum_{n=1}^M (\boldsymbol{\phi}_m, [\mathbf{f}_0(\mathbf{V}_M)]_n)\, \dot{a}_n \;&= \big(\boldsymbol{\phi}_{m,i}, \mathbf{f}_i(\mathbf{V}_M)\big) + (\boldsymbol{\phi}_m, \mathbf{f}_4(\mathbf{V}_M)) - (\boldsymbol{\phi}_{m,i}, \mathbf{f}_{i+4}(\mathbf{V}_M)) + \langle \boldsymbol{\phi}_m, \mathbf{f}_8(\mathbf{V}_M)\rangle_{\partial\Omega_W} \\ &\quad - \langle \boldsymbol{\phi}_m, \mathbf{f}_9(\mathbf{V}_M)\rangle_{\partial\Omega_W}\end{aligned} \tag{343}$$

for $t \in (0,T]$ subject to the initial condition $\mathbf{V}(0,\mathbf{x}) = \mathbf{V}_0(\mathbf{x})$. Once discretized in time, (343) will yield a non-linear discrete system of equations that can be advanced in time using an explicit time integration scheme, or by combining an implicit scheme with Newton's method at each time step. Note that, unlike in the case of a ROM for linear equations, the left-hand side of (343) will contain a mass matrix that will need to be inverted during the time-integration of the ROM.

[15] As discussed in Section 5.3, if the approximation modes $\boldsymbol{\phi}_m$ satisfy the no-slip condition at $\partial\Omega_W$ the boundary integrals I_m^{ns} and I_m^{np} vanish.

"Best Points" Interpolation for Non-Linear Projected Terms

As in the 1D tubular reactor problem of Section 5.2, applying the standard Galerkin reduced-order model to (343) is inefficient due to the presence of the non-linear terms. To recover efficiency, let us develop the coefficient function approximation (Section 5.2) to the non-linear terms in this expression.

As outlined in Algorithm 1, one begins by computing snapshots K for the primal unknown field $\mathbf{V}$, at K different times t_k:

$$\mathcal{S}^{\mathbf{V}} \equiv \{\boldsymbol{\xi}_k^{\mathbf{V}}(\mathbf{x}) = \mathbf{V}_h^k(\mathbf{x}) : 1 \leq k \leq K\} \tag{344}$$

Given this set of snapshots of the flow field, one then computes snapshots for each of the non-linear functions in (337) – (342):

$$\mathcal{S}^{[\mathbf{f}_0]_n} \equiv \{\boldsymbol{\xi}_k^{[\mathbf{f}_0]_n}(\mathbf{x}) = [\mathbf{f}_0(\mathbf{V}_h^k(\mathbf{x}))]_n : 1 \leq k \leq K\}, \quad n = 1,...,M \tag{345}$$

$$\mathcal{S}^{\mathbf{f}_j} \equiv \{\boldsymbol{\xi}_k^{\mathbf{f}_j}(\mathbf{x}) = \mathbf{f}_j(\mathbf{V}_h^k(\mathbf{x})) : 1 \leq k \leq K\}, \quad j = 1,...,9 \tag{346}$$

From these snapshots, one solves for the "best" interpolation points for each of the non-linear functions (337)–(342), denoted here by:

$$\{\mathbf{z}_m^{[\mathbf{f}_0]_n}\}_{m=1}^M : \quad \text{"best" (or any) interpolation points for } [\mathbf{f}_0]_n, n = 1,...,M \tag{347}$$

$$\{\mathbf{z}_m^{\mathbf{f}_j}\}_{m=1}^M : \quad \text{"best" (or any) interpolation points for } \mathbf{f}_j, j = 1,...,9 \tag{348}$$

following the approach outlined above in Section 5.2 and in [74].

We note that the main difference between the non-linear functions that appear in the projected Navier-Stokes equations (343) and the projected equations for the tubular reactor (247) is that the non-linear functions in the former are vector-valued. However, in practice, this poses no difficulty for the solution procedure of Section 5.2, as this exact procedure can be applied to each *component* of each of the non-linear vector-valued function in (337)–(342). For concreteness, let $\mathbf{f}_j \in \mathbb{R}^5$ be any of the vector-valued functions in (337)–(342), and let f_j^i denote the i^{th} component of $\mathbf{f}_j$ for $j = 0,1...,9$, $i = 1,...,5$. Then, each of the components of each of the functions $\mathbf{f}_j$ can be expanded in an orthonormal (scalar) basis as, denoted here by $\{\phi_m^{f_j^i}\}_{m=1}^M$. Now, we can define the best approximations of the elements in the snapshot set as:

$$[f_j^i]_M^*(\mathbf{V}_h^k) = \sum_{m=1}^M \alpha_m^{f_j^i} \phi_m^{f_j^i}(\mathbf{x}), \quad 1 \leq k \leq K \tag{349}$$

where

$$\alpha_m^{f_j^i} = (\phi_m, f_j^i(\mathbf{V}_h^k(\cdot))), \quad m = 1,...,M, 1 \leq k \leq K \tag{350}$$

for $i = 1,...,5$, $j = 0,1,...,9$. Now, the interpolation points for each component of each nonlinear function $\{\mathbf{z}_m^{f_j^i}\}_{m=1}^M \in \Omega \subset \mathbb{R}^3$ are defined as the solution to the following optimization problem:

$$\begin{aligned} &\min_{\mathbf{z}_1,...,\mathbf{z}_M \in \Omega} \left|\left| [f_j^i]_M^*(\cdot) - \textstyle\sum_{m=1}^M \beta_m^{f_j^i}(\mathbf{z}_1,...,\mathbf{z}_M)\phi_m^{f_j^i} \right|\right|^2 \\ &\textstyle\sum_{n=1}^M \phi_n^{f_j^i}(\mathbf{z}_m)\beta_n^{f_j^i}(\mathbf{z}_1,...,\mathbf{z}_M) = f_j^i(\mathbf{z}_m), \quad 1 \leq m \leq M \end{aligned} \tag{351}$$

Substituting (349) into (351) and invoking the orthonormality of the $\{\phi_m^{f_j^i}\}_{m=1}^M$, we obtain:

$$\begin{array}{c} \min_{\mathbf{z}_1,...,\mathbf{z}_M \in \Omega} \sum_{m=1}^M (\alpha_m^{f_j^i} - \beta_m^{f_j^i}(\mathbf{z}_1,...,\mathbf{z}_M))^2 \\ \sum_{n=1}^M \phi_n^{f_j^i}(\mathbf{z}_m)\beta_n^{f_j^i}(\mathbf{z}_1,...,\mathbf{z}_M) = f_j^i(\mathbf{z}_m), \quad 1 \le m \le M \end{array} \tag{352}$$

i.e., the set of points $\{\mathbf{z}_m^{f_j^i}\}_{m=1}^M$ is determined to minimize the average error between the interpolants $[f_j^i]_M(\cdot)$ and the best approximations $[f_j^i]_M^*(\cdot)$. Comparing the optimization problems (352) and (263), one can see that these are identical, with the general function f in (263) replaced by f_j^i, the i^{th} component of $\mathbf{f}_j$, one of the non-linear functions in (337)–(342), and so we refer the reader to Section 5.2 for details of the solution procedure for the "best" (or, hierarchical, if desired) interpolation points.

Given a set of interpolation points $\mathbf{z}_m^{f_j^i}$ for f_j^i, one can define the cardinal function $\{\psi_m^{f_j^i}\}$ for f_j^i by

$$\boldsymbol{\phi}_M^{f_j^i}(\mathbf{x}) = \mathbf{A}^{f_j^i} \boldsymbol{\psi}_M^{f_j^i}(\mathbf{x}) \tag{353}$$

where $\boldsymbol{\phi}_M^{f_j^i}(\mathbf{x}) = (\phi_1^{f_j^i}(\mathbf{x}),...,\phi_M^{f_j^i}(\mathbf{x}))^T$ and $\boldsymbol{\psi}_M^{f_j^i}(\mathbf{x}) = (\psi_1^{f_j^i}(\mathbf{x}),...,\psi_M^{f_j^i}(\mathbf{x}))^T$, and $A_{mn}^{f_j^i} = \phi_n^{f_j^i}(\mathbf{z}_m^{f_j^i})$. As before, the (scalar) cardinal functions $\psi_m^{f_j^i}$ satisfy $\psi_m^{f_j^i}(\mathbf{z}_n^{f_j^i}) = \delta_{mn}$. Given the interpolation points $\{\mathbf{z}_m^{f_j^i}\}_{m=1}^M$ and cardinal functions $\{\psi_m^{f_j^i}\}$ (353), one can approximate the i^{th} component ($i = 1,...,5$) of $\mathbf{f}_j$ (337) – (342) by

$$[f_0^i(\mathbf{V})]_n \approx [[f_0^i]_M(\mathbf{V})]_n = \sum_{m=1}^M [f_0^i]_n(\mathbf{V}(\mathbf{z}_m^{[f_0^i]_n}))\psi_m^{[f_0^i]_n} \in \mathbb{R}, \quad n = 1,...,M \tag{354}$$

$$f_j^i(\mathbf{V}) \approx [f_j^i]_M(\mathbf{V}) = \sum_{m=1}^M f_j^i(\mathbf{V}(\mathbf{z}_m^{f_j^i}))\psi_m^{f_j^i} \in \mathbb{R}, \quad i = 1,..,5, j = 1,...,9 \tag{355}$$

Reduced Order Approximation to the Symmetrized Compressible Navier-Stokes Equations with Interpolation

Our reduced-order approximation, (343) but now with interpolation, is obtained from (354) and (355) and takes the following form

$$\begin{array}{rl} \sum_{n=1}^M (\boldsymbol{\phi}_m, [\mathbf{f}_0(\mathbf{a}_M)]_n)\dot{a}_n & = \big(\boldsymbol{\phi}_{m,i}, \mathbf{f}_i(\mathbf{a}_M)\big) + (\boldsymbol{\phi}_m, \mathbf{f}_4(\mathbf{a}_M)) - (\boldsymbol{\phi}_{m,i}, \mathbf{f}_{i+4}(\mathbf{a}_M)) \\ & \quad - \langle \boldsymbol{\phi}_m, \mathbf{f}_8(\mathbf{a}_M)\rangle_{\partial\Omega_W} - \langle \boldsymbol{\phi}_m, \mathbf{f}_9(\mathbf{a}_M)\rangle_{\partial\Omega_W} \end{array} \tag{356}$$

for $m = 1,...,M$, where $\mathbf{a}_M^T \equiv (a_1,...,a_M) \in \mathbb{R}^M$ and

$$[f_0^i]_n \approx [f_0^i(\mathbf{a}_M)]_n = \sum_{m=1}^M [f_0^i]_n \left(\sum_{m=1}^m a_m(t)\boldsymbol{\phi}_m(\mathbf{z}_m^{[f_0^i]_n}) \right) \psi_m^{[f_0^i]_n}(\mathbf{x}), \quad n = 1,...,M \tag{357}$$

$$f_j^i \approx f_j^i(\mathbf{a}_M) = \sum_{m=1}^{M} f_j^i \left(\sum_{m=1}^{m} a_m(t) \boldsymbol{\phi}_m(\mathbf{z}_m^{f_j^i}) \right) \psi_m^{f_j^i}(\mathbf{x}), \quad j = 1, ..., 9 \tag{358}$$

It is convenient to write (356) in matrix/vector form, as would be required for numerical implementation. To do this, note that, for the i^{th}, $i = 1, ..., 5$ component of $\mathbf{f}_j(\mathbf{a}_M)$ and for $l = 1, ..., M$, we have that (implied summation on the $i = 1, ..., 5$, and letting ϕ_l^i denote the i^{th} component of $\boldsymbol{\phi}_l$):

$$\begin{aligned}
(\boldsymbol{\phi}_l, \mathbf{f}_j(\mathbf{a}_M)) &= \left(\phi_l^i, f_j^i(\mathbf{a}_M) \right) \\
&= \left(\phi_l^i, \sum_{m=1}^{M} f_j^i \left(\sum_{n=1}^{M} a_n \boldsymbol{\phi}_n(\mathbf{z}_m^{f_j^i}) \right) \psi_m^{f_j^i} \right) \\
&= \int_\Omega \phi_l^i \left[\sum_{m=1}^{M} \left\{ f_j^i \left(\sum_{n=1}^{M} a_n \boldsymbol{\phi}_n(\mathbf{z}_m^{f_j^i}) \right) \right\} \psi_m^{f_j^i} \right] d\Omega \\
&= \sum_{m=1}^{M} \underbrace{\left[\int_\Omega (\phi_l^1 \psi_m^{f_j^1}, \phi_l^2 \psi_m^{f_j^2}, \phi_l^3 \psi_m^{f_j^3}, \phi_l^4 \psi_m^{f_j^4}, \phi_l^5 \psi_m^{f_j^5}) d\Omega \right]}_{\in \mathbb{R}^{1\times 5}} \underbrace{\mathbf{f}_j \left(\sum_{n=1}^{M} a_n \boldsymbol{\phi}_n(\mathbf{z}_m^{\mathbf{f}_j}) \right)}_{\in \mathbb{R}^{5\times 1}}
\end{aligned} \tag{359}$$

where, to further clarify the notation:

$$\mathbf{f}_j \left(\sum_{n=1}^{N} a_n \boldsymbol{\phi}_n(\mathbf{z}_m^{\mathbf{f}_j}) \right) \equiv \begin{pmatrix} f_j^1 \left(\sum_{n=1}^{m} a_n \boldsymbol{\phi}_n(\mathbf{z}_m^{f_j^1}) \right) \\ f_j^2 \left(\sum_{n=1}^{M} a_n \boldsymbol{\phi}_n(\mathbf{z}_m^{f_j^2}) \right) \\ f_j^3 \left(\sum_{n=1}^{M} a_n \boldsymbol{\phi}_n(\mathbf{z}_m^{f_j^3}) \right) \\ f_j^4 \left(\sum_{n=1}^{M} a_n \boldsymbol{\phi}_n(\mathbf{z}_m^{f_j^4}) \right) \\ f_j^5 \left(\sum_{n=1}^{m} a_n \boldsymbol{\phi}_n(\mathbf{z}_m^{f_j^5}) \right) \end{pmatrix} \in \mathbb{R}^5 \tag{360}$$

(359) is a matrix/vector product of the form $\mathbf{G}^{\mathbf{f}_j} \mathbf{f}_j(\mathbf{D}^{\mathbf{f}_j} \mathbf{a}_M)$ where

$$\mathbf{G}^{\mathbf{f}_j}_{l,[5(m-1)+1:5m]} = \int_\Omega (\phi_l^1 \psi_m^{f_j^1}, \phi_l^2 \psi_m^{f_j^2}, \phi_l^3 \psi_m^{f_j^3}, \phi_l^4 \psi_m^{f_j^4}, \phi_l^5 \psi_m^{f_j^5}) d\Omega \in \mathbb{R}^{1\times 5} \tag{361}$$

for $1 \leq l, m \leq M$ (so that $\mathbf{G}^{\mathbf{f}_j} \in \mathbb{R}^{M\times 5M}$), and

$$\mathbf{D}^{\mathbf{f}_j} \equiv \begin{pmatrix} \boldsymbol{\phi}_1(\mathbf{z}_1^{\mathbf{f}_j}) & \dots & \boldsymbol{\phi}_N(\mathbf{z}_1^{\mathbf{f}_j}) \\ \vdots & \ddots & \vdots \\ \boldsymbol{\phi}_1(\mathbf{z}_M^{\mathbf{f}_j}) & \dots & \boldsymbol{\phi}_N(\mathbf{z}_M^{\mathbf{f}_j}) \end{pmatrix} \in \mathbb{R}^{5M\times N} \tag{362}$$

By $\boldsymbol{\phi}_m(\mathbf{z}_n^{\mathbf{f}_j})$ we mean

$$\boldsymbol{\phi}_m(\mathbf{z}_n^{\mathbf{f}_j}) \equiv \begin{pmatrix} \phi_m^1(\mathbf{z}_n^{f_j^1}) \\ \phi_m^2(\mathbf{z}_n^{f_j^2}) \\ \phi_m^3(\mathbf{z}_n^{f_j^3}) \\ \phi_m^4(\mathbf{z}_n^{f_j^4}) \\ \phi_m^5(\mathbf{z}_n^{f_j^5}) \end{pmatrix} \in \mathbb{R}^5, \quad 1 \le m,n \le M \tag{363}$$

$\mathbf{f}_j(\mathbf{D}^{\mathbf{f}_j}\mathbf{a}_M) \in \mathbb{R}^{5M}$ is defined analogously to (276).

Similarly, turning one's attention to the left-hand side of (356) (with implied summation on $i = 1,...,5$ as in (359)):

$$\begin{aligned} \textstyle\sum_{k=1}^M (\boldsymbol{\phi}_l, [\mathbf{f}_0(\mathbf{a}_M)]_k)\dot{a}_k &= \textstyle\sum_{k=1}^M \left(\phi_l^i, [f_0^i(\mathbf{a}_M)]_k\right)\dot{a}_k \\ &= \textstyle\sum_{k=1}^M \left(\phi_l^i, \sum_{m=1}^M \left[f_0^i\left(\sum_{n=1}^M a_n \boldsymbol{\phi}_n(\mathbf{z}_m^{[f_0^i]_k})\right)\right]_k \psi_m^{[f_0^i]_k}\right)\dot{a}_k \\ &= \textstyle\sum_{k=1}^M \dot{a}_k \int_\Omega \phi_l^i \left\{\sum_{m=1}^M \left[f_0^i\left(\sum_{n=1}^M a_n \boldsymbol{\phi}_n(\mathbf{z}_m^{[f_0^i]_k})\right)\right]_k \psi_m^{[f_0^i]_k}\right\} d\Omega \\ &= \textstyle\sum_{k=1}^M \Bigg\{ \sum_{m=1}^M \underbrace{\left[\int_\Omega (\phi_l^1\psi_m^{[f_0^1]_k}, \phi_l^2\psi_m^{[f_0^2]_k}, \phi_l^3\psi_m^{[f_0^3]_k}, \phi_l^4\psi_m^{[f_0^4]_k}, \phi_l^5\psi_m^{[f_0^5]_k}) d\Omega\right]}_{\in\mathbb{R}^{1\times 5}} \cdot \\ &\qquad \underbrace{\left[\mathbf{f}_0\left(\sum_{n=1}^M a_n \boldsymbol{\phi}_n(\mathbf{z}_m^{[\mathbf{f}_0]_k})\right)\right]_k}_{\in\mathbb{R}^{5\times 1}} \Bigg\} \dot{a}_k \end{aligned} \tag{364}$$

The entries of the mass matrix can be "read off" from (364), namely

$$\mathbf{M}_{[1:M],k} = \mathbf{G}^{[\mathbf{f}_0]_k}[\mathbf{f}_0]_k \left(\mathbf{D}^{[\mathbf{f}_0]_k}\mathbf{a}_M\right) \in \mathbb{R}^M \tag{365}$$

for $1 \le k \le M$, where $\mathbf{G}^{[\mathbf{f}_0]_k}$ and $\mathbf{D}^{[\mathbf{f}_0]_k}$ are defined analogously to (361) and (362) respectively.

With this notation in place, (356) can be written in matrix/vector form as

$$\boxed{\mathbf{M}\dot{\mathbf{a}}_M = \mathbf{G}^{\mathbf{f}_i}\mathbf{f}_i(\mathbf{D}^{\mathbf{f}_i}\mathbf{a}_M) + \mathbf{G}^4\mathbf{f}_4(\mathbf{D}^{\mathbf{f}_4}\mathbf{a}_M) - \mathbf{G}^{\mathbf{f}_{i+4}}\mathbf{f}_{i+4}(\mathbf{D}^{\mathbf{f}_{i+4}}\mathbf{a}_M) - \mathbf{G}^{\mathbf{f}_8}\mathbf{f}_8(\mathbf{D}^{\mathbf{f}_8}\mathbf{a}_M) - \mathbf{G}^{\mathbf{f}_9}\mathbf{f}_9(\mathbf{D}^{\mathbf{f}_9}\mathbf{a}_M)} \tag{366}$$

(implied summation on $i = 1,2,3$). (366) can be integrated in time using a standard explicit time-integration scheme, or an implicit time-integration scheme, with the application of Newton's method at each time step. We emphasize again that the result of formulating the ROM *with* interpolation is all the inner-products are contained in the $\mathbf{G}^{\mathbf{f}_j}$ matrices (361), which can be pre-computed prior to time integration of and/or application of Newton's method to the ROM ODE system (366). Similarly, the interpolated mass matrix (365) can also be pre-computed. The time-integration of the ROM ODE system (366) will require inversion of this matrix, but since the number of modes M will in general be quite small, the relative cost of this inversion is small.

5.4 Conclusions

The present work has focused on techniques for building entropy-stable reduced order models (ROMs) governed by non-linear partial differential equations (PDEs) in fluid mechanics. It turns out that one can bypass the need to recompute inner products involving the non-linear terms at each time or Newton step, thereby reducing the on-line computational complexity of the ROM, by handling the nonlinearities using a "best" points interpolation algorithm [75, 74].

The said "best" points interpolation approach was tested on a model one-dimensional (1D) convection-diffusion-reaction system of equations representing the flow through a non-adiabatic tubular reactor [79]. Numerical tests on this simple non-linear problem revealed that the interpolation procedure successfully captures the non-linear behavior (e.g., limit cycles) of the solution when a spectral basis is employed. It also revealed some shortcomings of the Proper Orthogonal Decomposition (POD) basis that one may wish to examine further in future work.

Following this preliminary testing of the interpolation, attention was turned to the key equations in fluid dynamics, namely the compressible three-dimensional (3D) Navier-Stokes equations. The nonlinearity present in these equations presents a challenge for developing provably stable ROMs. This challenge was addressed with the help of a transformation that effectively symmetrizes these equations. The Galerkin projection of these equations gives a discrete model that obeys the second law of thermodynamics. Following a proof of the entropy-stability of the ROM solution with appropriate boundary condition, an efficient "best" points interpolation procedure was formulated to handle the non-linear terms in the symmetrized equations. Given this formulation, it should be straight forward to implement the Navier-Stokes ROM with the proposed interpolation, and to test the performance of this solution under different choices of bases.

Appendix A Mathematical Details for Numerical Analysis of the Fluid ROM

A.1 Projection Operator

Let $\mathcal{V}$ and $\mathcal{V}^M$ be vector spaces. By definition, a projection operator $\Pi_M : \mathcal{V} \to \mathcal{V}^M$ has the following properties:

1. For all $u \in \mathcal{V}$, $\Pi_M(\Pi_M u) = \Pi_M u$ (that is, Π_M is *idempotent*).

2. For all $u, v \in \mathcal{V}$, $\Pi_M(u+v) = \Pi_M u + \Pi_M v$ (that is, Π_M is *linear*).

3. $||\Pi_M|| = 1$ for any norm $||\cdot||$ on $\mathcal{V}$ (a consequence 1. above).

4. For all $u \in \mathcal{V}$, $\frac{\partial(\Pi_M u)}{\partial t} = \Pi_M \left(\frac{\partial u}{\partial t}\right)$ (that is, Π_M is a spatial-only operator, so time-differentiation commutes with projection).

5. For all $v \in \mathcal{V}^M$, $\Pi_M v = v$.

6. For all $v \in (\mathcal{V}^M)^\perp$, $\Pi_M v = 0$ (here $(\mathcal{V}^M)^\perp$ denotes the subspace orthogonal to $\mathcal{V}^M$).

A.2 Diagonalization of $\mathbf{A}_n$

Let $\mathbf{A}_n \equiv \mathbf{A}_1 n_1 + \mathbf{A}_2 n_2 + \mathbf{A}_3 n_3$. The matrices $\mathbf{S}$ that diagonalize $\mathbf{A}_n$ (so that $\mathbf{A}_n = \mathbf{S}\mathbf{\Lambda}_n\mathbf{S}^{-1}$, with $\mathbf{\Lambda}_n$ given in (15)) are:

$$\mathbf{S} = \begin{pmatrix} 0 & n_3 & n_2 & \frac{1}{2}n_1 & -\frac{1}{2}n_1 \\ n_3 & 0 & -n_1 & \frac{1}{2}n_2 & -\frac{1}{2}n_2 \\ -n_2 & -n_1 & 0 & \frac{1}{2}n_3 & -\frac{1}{2}n_3 \\ n_1 & -n_2 & n_3 & -\frac{\zeta}{2\bar{c}} & -\frac{\zeta}{2\bar{c}} \\ 0 & 0 & 0 & \frac{\gamma\bar{p}}{2\bar{c}} & \frac{\gamma\bar{p}}{2\bar{c}} \end{pmatrix}, \quad \mathbf{S}^{-1} = \begin{pmatrix} 0 & n_3 & -n_2 & n_1 & \frac{\bar{\zeta}}{\gamma\bar{p}}n_1 \\ n_3 & 0 & -n_1 & -n_2 & -\frac{\bar{\zeta}}{\gamma\bar{p}}n_2 \\ n_2 & -n_1 & 0 & n_3 & \frac{\bar{\zeta}}{\gamma\bar{p}}n_3 \\ n_1 & n_2 & n_3 & 0 & \frac{\bar{c}}{\gamma\bar{p}} \\ -n_1 & -n_2 & -n_3 & 0 & \frac{\bar{c}}{\gamma\bar{p}} \end{pmatrix} \tag{367}$$

It follows that

$$\mathbf{V}' \equiv \mathbf{S}^{-1}\mathbf{q}' = \begin{pmatrix} (n_3u_2' - n_2u_3' + n_1\zeta') + \frac{\bar{\zeta}}{\gamma\bar{p}}n_1p' \\ (n_3u_1' - n_1u_3' - n_2\zeta') - \frac{\bar{\zeta}}{\gamma\bar{p}}n_2p' \\ (n_2u_1' - n_1u_2' + n_3\zeta') + \frac{\bar{\zeta}}{\gamma\bar{p}}n_3p' \\ u_n' + \frac{\bar{\zeta}}{\bar{c}}p' \\ -u_n' + \frac{\bar{\zeta}}{\bar{c}}p' \end{pmatrix}$$

$$= \begin{pmatrix} \sum_{k=1}^{M}\left[n_1\left(\phi_k^4 + \left(\frac{\bar{\zeta}}{\bar{c}}\right)^2\phi_k^5\right) - n_2\phi_k^3 + n_3\phi_k^2\right]a_k(t) \\ \sum_{k=1}^{M}\left[-n_1\phi_k^3 - n_2\left(\phi_k^4 + \left(\frac{\bar{\zeta}}{\bar{c}}\right)^2\phi_k^5\right) + n_3\phi_k^1\right]a_k(t) \\ \sum_{k=1}^{M}\left[-n_1\phi_k^2 + n_2\phi_k^1 + n_3\left(\phi_k^4 + \left(\frac{\bar{\zeta}}{\bar{c}}\right)^2\phi_k^5\right)\right]a_k(t) \\ \sum_{k=1}^{M}\left[n_1\phi_k^1 + n_2\phi_k^2 + n_3\phi_k^3 + \frac{\bar{\zeta}}{\bar{c}}\phi_k^5\right]a_k(t) \\ \sum_{k=1}^{M}\left[-n_1\phi_k^1 - n_2\phi_k^2 - n_3\phi_k^3 + \frac{\bar{\zeta}}{\bar{c}}\phi_k^5\right]a_k(t) \end{pmatrix} \tag{368}$$

where $\boldsymbol{\phi}_k^T \equiv \begin{pmatrix} \phi_k^1 & \phi_k^2 & \phi_k^3 & \phi_k^4 & \phi_k^5 \end{pmatrix} \in \mathbb{R}^5$ is the ROM basis vector.

A.3 Well-Posedness

Consider a general initial-boundary value problem (IBVP) of the form

$$\begin{aligned} \tfrac{\partial u}{\partial t} &= Pu + F, \quad t \geq 0 \\ Bu &= g \\ u &= f, \qquad t = 0 \end{aligned} \tag{369}$$

Here, P is a differential operator in space, and B is a boundary operator acting on the solution at the spatial boundary.

Definition 2.8 in [30]: The IBVP (369) is *well-posed* if for $F = 0$, $g = 0$, there is a unique solution satisfying

$$||u(\cdot,t)|| \leq Ke^{\beta t}||f(\cdot)|| \tag{370}$$

where K and β are constants independent of $f(x)$.

A.4 Stability

Consider the following semi-discrete problem:

$$\begin{aligned} \tfrac{du_j}{dt} &= Qu_j + F_j, \quad j = 1,2,\ldots,N-1 \\ B_h u &= g(t) \\ u_j(0) &= f_j, \qquad j = 1,2,\ldots,N \end{aligned} \tag{371}$$

where Q is a discretizing operator, F_j and f_j are the discretized version of F and f respectively, and $B_h u$ denotes the complete set of discretized boundary conditions. Let $||\cdot||_h$ be a discrete norm.

Definition 2.11 in [30]: The semi-discrete IBVP (371) is *stable* if there is a unique solution satisfying

$$||u(\cdot,t)||_h \leq Ke^{\beta t}||f(\cdot)||_h \tag{372}$$

where K and β are constants independent of f and g.

Appendix B Mathematical Details for Numerical Analysis of the Coupled Fluid/Structure ROM

B.1 Lyapunov Stability Condition

A continuous-time linear time-invariant system $\dot{X} = AX$ is Lyapunov stable if and only if all the eigenvalues of A have real parts less than or equal to 0, and those with real parts equal to 0 are non-repeated.

B.2 Energy Matrix Stability Analysis Techniques for Coupled Systems [72]

In trying to study the stability of the coupled system (195), the following theorems, proven in [72], can be useful. First, a definition, quoted from [72]:

Definition 3.1 in [72]. *We say that a matrix* $\mathbf{K}$ *is 'stable' if and only if:*

1. $\mathbf{K}$ *is diagonalizable in* $\mathbb{C}$.
2. $\forall \lambda \in Sp(\mathbf{K}), \mathcal{R}(\lambda) \leq 0$.

Theorem 3.1 in [72]. *A real, symmetric positive definite (RSPD) matrix* $\mathbf{E}_K$ *is an energy matrix for* $\mathbf{K}$ *if and only if for all* $\mathbf{X}$ *that solve* $\dot{\mathbf{X}} = \mathbf{K}\mathbf{X}$, $\frac{1}{2}\frac{d}{dt}\left(\mathbf{X}^T\mathbf{E}_K\mathbf{X}\right) \leq 0$.

Theorem 3.4 in [72]. *If* $\mathbf{A}$ *and* $\mathbf{D}$ *are two real, stable matrices with energy matrices* $\mathbf{E}_A$ *and* $\mathbf{E}_D$, *then*

$$\left\{\mathbf{E}_A\mathbf{B} + (\mathbf{E}_D\mathbf{C})^T = \mathbf{0}\right\} \Rightarrow \left\{\mathbf{K} = \begin{pmatrix} \mathbf{A} & \mathbf{B} \\ \mathbf{C} & \mathbf{D} \end{pmatrix} \text{ is a stable matrix.}\right\} \tag{373}$$

Appendix C Mathematical Expressions and Details for the Non-Linear Fluid ROM

C.1 Euler Fluxes in the Entropy Variables and Symmetrized Matrices

To simplify the notation, let us introduce the following variables[16]:

$$\begin{array}{lll} \bar{\gamma} = \gamma - 1, & k_1 = \frac{1}{2V_5}(V_2^2 + V_3^2 + V_4^2), & k_2 = k_1 - \gamma, \\ k_3 = k_1^2 - 2\gamma k_1 + \gamma, & k_4 = k_2 - \bar{\gamma}, & k_5 = k_2^2 - \bar{\gamma}(k_1 + k_2), \\ c_1 = \bar{\gamma}V_5 - V_2^2, & d_1 = -V_2V_3, & e_1 = V_2V_5, \\ c_2 = \bar{\gamma}V_5 - V_3^2, & d_2 = -V_2V_4, & e_2 = V_3V_5, \\ c_3 = \bar{\gamma}V_5 - V_4^2, & d_3 = -V_3V_4, & e_3 = V_4V_5. \end{array} \tag{374}$$

In the entropy variables $\mathbf{V}$, the Euler fluxes $\mathbf{F}_i(\mathbf{V})$ are given by:

$$\mathbf{F}_1(\mathbf{V}) = \frac{\rho\iota}{V_5}\begin{pmatrix} e_1 \\ c_1 \\ d_1 \\ d_2 \\ k_2V_2 \end{pmatrix}, \quad \mathbf{F}_2(\mathbf{V}) = \frac{\rho\iota}{V_5}\begin{pmatrix} e_2 \\ d_1 \\ c_2 \\ d_3 \\ k_2V_3 \end{pmatrix}, \quad \mathbf{F}_3(\mathbf{V}) = \frac{\rho\iota}{V_5}\begin{pmatrix} e_3 \\ d_2 \\ d_3 \\ c_3 \\ k_2V_4 \end{pmatrix} \tag{375}$$

The symmetrizing matrix $\mathbf{A}_0$ and its inverse are given by

$$\mathbf{A}_0 = \mathbf{U}_{,\mathbf{V}} = \frac{\rho\iota}{\bar{\gamma}V_5}\begin{pmatrix} -V_5^2 & e_1 & e_2 & e_3 & V_5(1-k_1) \\ & c_1 & d_1 & d_2 & V_2k_2 \\ & & c_2 & d_3 & V_3k_2 \\ & & & c_3 & V_4k_2 \\ \text{symm.} & & & & -k_3 \end{pmatrix} \tag{376}$$

and

$$\mathbf{A}_0^{-1} = \mathbf{V}_{,\mathbf{U}} = -\frac{1}{\rho\iota V_5}\begin{pmatrix} k_1^2+\gamma & k_1V_2 & k_1V_3 & k_1V_4 & (k_1+1)V_5 \\ & V_2^2 - V_5 & -d_1 & -d_2 & e_1 \\ & & V_3^2 - V_5 & -d_3 & e_2 \\ & & & V_4^2 - V_5 & e_3 \\ \text{symm.} & & & & V_5^2 \end{pmatrix} \tag{377}$$

The Jacobians of the Euler fluxes are:

$$\tilde{\mathbf{A}}_1 = \mathbf{F}_{1,\mathbf{V}} = \frac{\rho\iota}{\bar{\gamma}V_5^2}\begin{pmatrix} e_1V_5 & c_1V_5 & d_1V_5 & d_2V_5 & k_2e_1 \\ & -(c_1+2\bar{\gamma}V_5)V_2 & -c_1V_3 & -c_1V_4 & c_1k_2 + \bar{\gamma}V_2^2 \\ & & -c_2V_2 & -d_1V_4 & k_4d_1 \\ & & & -c_3V_2 & k_4d_2 \\ \text{symm.} & & & & k_5V_2 \end{pmatrix} \tag{378}$$

[16] This section is repeated here from the Appendix of [78] to make this document self-contained.

$$\tilde{\mathbf{A}}_2 = \mathbf{F}_{2,\mathbf{V}} = \frac{\rho\iota}{\bar{\gamma}V_5^2}\begin{pmatrix} e_2V_5 & d_1V_5 & c_2V_5 & d_3V_5 & k_2e_2 \\ & -c_1V_3 & -c_2V_2 & -d_1V_4 & k_4d_1 \\ & & -(c_2+2\bar{\gamma}V_5)V_3 & -c_2V_4 & c_2k_2+\bar{\gamma}V_3^2 \\ & & & -c_3V_3 & k_4d_3 \\ \text{symm.} & & & & k_5V_3 \end{pmatrix} \tag{379}$$

$$\tilde{\mathbf{A}}_3 = \mathbf{F}_{3,\mathbf{V}} = \frac{\rho\iota}{\bar{\gamma}V_5^2}\begin{pmatrix} e_3V_5 & d_2V_57d_3V_5 & c_3V_5 & k_2e_3 & \\ & -c_1V_4 & -d_2V_3 & -c_3V_2 & k_4d_2 \\ & & -c_2V_4 & -c_3V_3 & k_4d_3 \\ & & & -(c_3+2\bar{\gamma}V_5)V_4 & c_3k_2+\bar{\gamma}V_4^2 \\ \text{symm.} & & & & k_5V_4 \end{pmatrix} \tag{380}$$

The velocity and temperature can be written in the entropy variables as:

$$u_i(\mathbf{V}) = -\frac{V_{i+1}}{V_5}, \;\; i = 1,2,3 \tag{381}$$

$$\theta(\mathbf{V}) = -\frac{1}{c_v V_5} \tag{382}$$

The gradients of the viscous and heat fluxes are given by:

$$u_{i,j} = \frac{-V_5V_{i+1,j} + V_{i+1}V_{5,j}}{V_5^2} \tag{383}$$

$$\kappa\theta_{,i} = \frac{\gamma\mu}{Pr}\frac{1}{V_5^2}V_{5,i} \tag{384}$$

where $Pr \equiv \mu c_p/\kappa$ is the Prandtl number.

Finally, the symmetrized viscous and heat flux matrices $\tilde{\mathbf{K}}_{ij} \equiv \tilde{\mathbf{K}}_{ij}^v + \tilde{\mathbf{K}}_{ij}^h$ are given by:

$$\tilde{\mathbf{K}}_{11} = \frac{1}{V_5^3}\begin{pmatrix} 0 & 0 & 0 & 0 & 0 \\ 0 & -(\gamma-2\mu)V_5^2 & 0 & 0 & (\lambda+2\mu)e_1 \\ 0 & 0 & -\mu V_5^2 & 0 & \mu e_2 \\ 0 & 0 & 0 & -\mu V_5^2 & \mu e_3 \\ 0 & (\lambda+2\mu)e_1 & \mu e_2 & \mu e_3 & -\left[(\lambda+2\mu)V_2^2+\mu(V_3^2+V_4^2)-\frac{\gamma\mu V_5}{Pr}\right] \end{pmatrix} \tag{385}$$

$$\tilde{\mathbf{K}}_{12} = \frac{1}{V_5^3}\begin{pmatrix} 0 & 0 & 0 & 0 & 0 \\ 0 & 0 & -\lambda V_5^2 & 0 & \lambda e_2 \\ 0 & -\mu V_5^2 & 0 & 0 & \mu e_1 \\ 0 & 0 & 0 & 0 & 0 \\ 0 & \mu e_2 & \lambda e_1 & 0 & (\lambda+\mu)d_1 \end{pmatrix} \tag{386}$$

$$\tilde{\mathbf{K}}_{13} = \frac{1}{V_5^3}\begin{pmatrix} 0 & 0 & 0 & 0 & 0 \\ 0 & 0 & 0 & -\lambda V_5^2 & \lambda e_3 \\ 0 & 0 & 0 & 0 & 0 \\ 0 & -\mu V_5^2 & 0 & 0 & \mu e_1 \\ 0 & \mu e_3 & 0 & \lambda e_1 & (\lambda+\mu)d_2 \end{pmatrix} \tag{387}$$

$$\tilde{\mathbf{K}}_{22} = \frac{1}{V_5^3}\begin{pmatrix} 0 & 0 & 0 & 0 & 0 \\ 0 & -\mu V_5^2 & 0 & 0 & \mu e_1 \\ 0 & 0 & -(\lambda+2\mu)V_5^2 & 0 & (\lambda+2\mu)e_2 \\ 0 & 0 & 0 & -\mu V_5^2 & \mu e_3 \\ 0 & \mu e_1 & (\lambda+2\mu)e_2 & \mu e_3 & -\left[(\lambda+2\mu)V_3^2+\mu(V_2^2+V_4^2)-\frac{\gamma\mu V_5}{Pr}\right] \end{pmatrix} \tag{388}$$

$$\tilde{\mathbf{K}}_{23} = \frac{1}{V_5^3}\begin{pmatrix} 0 & 0 & 0 & 0 & 0 \\ 0 & 0 & 0 & 0 & 0 \\ 0 & 0 & 0 & -\lambda V_5^2 & \lambda e_3 \\ 0 & 0 & -\mu V_5^2 & 0 & \mu e_2 \\ 0 & 0 & \mu e_3 & \lambda e_2 & (\lambda+\mu)d_3 \end{pmatrix} \tag{389}$$

$$\tilde{\mathbf{K}}_{33} = \frac{1}{V_5^3}\begin{pmatrix} 0 & 0 & 0 & 0 & 0 \\ 0 & -\mu V_5^2 & 0 & 0 & \mu e_1 \\ 0 & 0 & -\mu V_5^2 & 0 & \mu e_2 \\ 0 & 0 & 0-(\lambda+2\mu)V_5^2 & (\lambda+2\mu)e_3 & \\ 0 & \mu e_1 & \mu e_2 & (\lambda+2\mu)e_3 & -\left[(\lambda+2\mu)V_4^2+\mu(V_2^2+V_3^2)-\frac{\gamma\mu V_5}{Pr}\right] \end{pmatrix} \tag{390}$$

with

$$\tilde{\mathbf{K}}_{21} = \tilde{\mathbf{K}}_{12}^T, \quad \tilde{\mathbf{K}}_{31} = \tilde{\mathbf{K}}_{13}^T, \quad \tilde{\mathbf{K}}_{32} = \tilde{\mathbf{K}}_{23}^T \tag{391}$$

C.2 The Matrix $\tilde{\mathbf{A}}_i n_i$ and Application of No-Penetration Boundary Condition

Given the symmetrized Euler flux matrices (378)–(380), and letting $\mathbf{n}^T = (n_1, n_2, n_3)$ denote an outward normal vector to some boundary $\partial\Omega_W$ in the domain, one has that:

$$\tilde{\mathbf{A}}_i n_i = \begin{pmatrix} \frac{\rho}{\gamma-1}(\mathbf{u}\cdot\mathbf{n}) & \rho\iota n_1 + \frac{\rho}{\gamma-1}(\mathbf{u}\cdot\mathbf{n})u_1 & \rho\iota n_2 + \frac{\rho}{\gamma-1}(\mathbf{u}\cdot\mathbf{n})u_2 \\ & \rho\iota(\mathbf{u}\cdot\mathbf{n}) + 2\rho\iota u_1 n_1 + \frac{\rho}{\gamma-1}u_1^2(\mathbf{u}\cdot\mathbf{n}) & \rho\iota\left(u_2 n_1 + u_1 n_2\right) + \frac{\rho}{\gamma-1}u_1 u_2(\mathbf{u}\cdot\mathbf{n}) \\ & & \rho\iota(\mathbf{u}\cdot\mathbf{n}) + 2\rho\iota u_2 n_2 + \frac{\rho}{\gamma-1}u_2^2(\mathbf{u}\cdot\mathbf{n}) \\ & \text{symm.} & \end{pmatrix}$$

$$\begin{pmatrix} \rho\iota n_3 + \frac{\rho}{\gamma-1}(\mathbf{u}\cdot\mathbf{n})u_3 & \frac{\rho}{\gamma-1}(\mathbf{u}\cdot\mathbf{n})\left[\frac{1}{2}u^2+\gamma\iota\right] \\ \rho\iota\left[u_3 n_1 + u_1 n_3\right] + \frac{\rho}{\gamma-1}u_1 u_3(\mathbf{u}\cdot\mathbf{n}) & \rho\iota\left(\frac{1}{2}u^2+\gamma\iota\right)n_1 + \frac{\rho}{\gamma-1}\left[\left(\frac{1}{2}u^2+\iota\gamma\right)+\iota(\gamma-1)\right]u_1(\mathbf{u}\cdot\mathbf{n}) \\ \frac{\rho}{\gamma-1}u_2 u_3(\mathbf{u}\cdot\mathbf{n}) + \rho\iota(u_3 n_2 + u_2 n_3) & \rho\iota\left(\frac{1}{2}u^2+\iota\gamma\right)n_2 + \frac{\rho}{\gamma-1}\left[\left(\frac{1}{2}u^2+\iota\gamma\right)+\iota\left(\gamma-1\right)\right]u_2(\mathbf{u}\cdot\mathbf{n}) \\ \rho\iota(\mathbf{u}\cdot\mathbf{n}) + 2\rho\iota u_3 n_3 + \frac{\rho}{\gamma-1}u_3^2(\mathbf{u}\cdot\mathbf{n}) & \left(\frac{1}{2}u^2+i\gamma\right)\rho\iota n_3 + \frac{\rho}{\gamma-1}\left(\left[\frac{1}{2}u^2+\iota\gamma\right]+\iota\left[\gamma-1\right]\right)u_3(\mathbf{u}\cdot\mathbf{n}) \\ & \frac{\rho}{\gamma-1}\left[\frac{1}{4}u^4+\iota(u^2+\gamma\iota)(2\gamma-1)\right](\mathbf{u}\cdot\mathbf{n}) \end{pmatrix} \tag{392}$$

It is straight forward to apply the no-penetration boundary condition, $\mathbf{u}\cdot\mathbf{n}=0$ on $\partial\Omega_W$ to (392):

$$[\tilde{\mathbf{A}}_i n_i]^{np} = \begin{pmatrix} 0 & \rho\iota n_1 & \rho\iota n_2 & \rho\iota n_3 & 0 \\ & 2\rho\iota u_1 n_1 & \rho\iota\left(u_2 n_1 + u_1 n_2\right) & \rho\iota\left[u_3 n_1 + u_1 n_3\right] & \rho\iota\left(\frac{1}{2}u^2 + \gamma\iota\right) n_1 \\ & & 2\rho\iota u_2 n_2 & \rho\iota(u_3 n_2 + u_2 n_3) & \rho\iota\left(\frac{1}{2}u^2 + \iota\gamma\right) n_2 \\ & & & 2\rho\iota u_3 n_3 & \left(\frac{1}{2}u^2 + \iota\gamma\right)\rho\iota n_3 \\ & & & & 0 \end{pmatrix} \tag{393}$$

so that

$$[\tilde{\mathbf{A}}_i n_i \mathbf{V}]^{np} = \begin{pmatrix} 0 \\ -\rho\iota s n_1 \\ -\rho\iota s n_2 \\ -\rho\iota s n_3 \\ 0 \end{pmatrix} \tag{394}$$

and

$$\begin{aligned} \mathbf{V}^T[\mathbf{A}_i n_i \mathbf{V}]^{np} &= -\rho s(\mathbf{u}\cdot\mathbf{n}) \\ &= H u_i n_i \\ &= \sigma_i n_i \end{aligned} \tag{395}$$

Note that by the divergence theorem,

$$\int_\Omega (Hu_i), i d\Omega = \int_\Omega \sigma_{i,i} d\Omega = \int_{\partial\Omega_W} \sigma_i n_i dS \tag{396}$$

C.3 The Matrices $\tilde{\mathbf{K}}^v_{ij} n_i$ and Application of No-Slip Boundary Condition

From (385)–(391), letting $\mathbf{n}^T = (n_1, n_2, n_3)$ denote the outward unit normal vector to some relevant boundary $\partial\Omega_W$:

$$\tilde{\mathbf{K}}^v_{11}\mathbf{V}_{,1} = \begin{pmatrix} 0 \\ (\lambda+2\mu)u_{1,1} \\ \mu u_{2,1} \\ \mu u_{3,1} \\ -(\lambda+2\mu)\frac{V_2}{V_5}u_{1,1} - \mu\frac{V_3}{V_5}u_{2,1} - \mu\frac{V_4}{V_5}u_{3,1} \end{pmatrix} \tag{397}$$

$$\tilde{\mathbf{K}}^v_{12}\mathbf{V}_{,2} = \begin{pmatrix} 0 \\ \lambda u_{2,2} \\ \mu u_{1,2} \\ 0 \\ -\mu\frac{V_3}{V_5}u_{1,2} - \lambda\frac{V_2}{V_5}u_{2,2} \end{pmatrix} \tag{398}$$

$$\tilde{\mathbf{K}}^v_{13}\mathbf{V}_{,3} = \begin{pmatrix} 0 \\ \lambda u_{3,3} \\ 0 \\ \mu u_{1,3} \\ -\mu\frac{V_4}{V_5}u_{1,3} - \lambda\frac{V_2}{V_5}u_{3,3} \end{pmatrix} \tag{399}$$

So that

$$\tilde{\mathbf{K}}_{1j}\mathbf{V}_{,j} = \begin{pmatrix} 0 \\ (\lambda+2\mu)u_{1,1}+\lambda u_{2,2}+\lambda u_{3,3} \\ \mu u_{2,1}+\mu u_{1,2} \\ \mu u_{3,1}+\mu u_{1,3} \\ -(\lambda+2\mu)\frac{V_2}{V_5}u_{1,1}-\mu\frac{V_3}{V_5}u_{2,1}-\mu\frac{V_4}{V_5}u_{3,1}-\mu\frac{V_3}{V_5}u_{1,2}-\lambda\frac{V_2}{V_5}u_{2,2}-\mu\frac{V_4}{V_5}u_{1,3}-\lambda\frac{V_2}{V_5}u_{3,3} \end{pmatrix} \tag{400}$$

meaning

$$\begin{aligned} \mathbf{V}^T\tilde{\mathbf{K}}_{1j}\mathbf{V}_{,j} &= (\lambda+2\mu)u_{1,1}V_2+\lambda u_{2,2}V_2+\lambda u_{3,3}V_2+\mu u_{2,1}V_3+\mu u_{1,2}V_3+\mu u_{3,1}V_4+\mu u_{1,3}V_4 \\ &-(\lambda+2\mu)V_2u_{1,1}-\mu V_3u_{2,1}-\mu V_4u_{3,1}-\mu V_3u_{1,2}-\lambda V_2u_{2,2}-\mu V_4u_{1,3}-\lambda V_2u_{3,3} \\ &= 0 \end{aligned} \tag{401}$$

(as asserted by Hughes in [78]). Moreover, applying the no-slip condition $\mathbf{u}=\mathbf{0}$ on $\partial\Omega_W$, one has that

$$[\tilde{\mathbf{K}}_{1j}\mathbf{V}_{,j}]^{ns} = \begin{pmatrix} 0 \\ 2\mu u_{1,1}+\lambda(u_{1,1}+u_{2,2}+u_{3,3}) \\ \mu(u_{2,1}+u_{1,2}) \\ \mu(u_{3,1}+u_{1,3}) \\ 0 \end{pmatrix} \tag{402}$$

Next:

$$\tilde{\mathbf{K}}^v_{21}\mathbf{V}_{,1} = \frac{1}{V_5^3}\begin{pmatrix} 0 \\ \mu V_5[-V_5V_{3,1}+\mu V_3V_{5,1}] \\ \lambda V_5[-V_5V_{2,1}+V_2V_{5,1}] \\ 0 \\ -\lambda V_3[-V_5V_{2,1}+V_2V_{5,1}]+\mu V_2[V_5V_{3,1}-V_3V_{5,1}] \end{pmatrix} \tag{403}$$

$$\tilde{\mathbf{K}}^v_{22}\mathbf{V}_{,2} = \begin{pmatrix} 0 \\ \mu u_{1,2} \\ (\lambda+2\mu)u_{2,2} \\ \mu u_{3,2} \\ -\mu\frac{V_2}{V_5}u_{1,2}-\mu\frac{V_4}{V_5}u_{3,2}-(\lambda+2\mu)\frac{V_3}{V_5}u_{2,2} \end{pmatrix} \tag{404}$$

$$\tilde{\mathbf{K}}^v_{23}\mathbf{V}_{,3} = \begin{pmatrix} 0 \\ 0 \\ \lambda u_{3,3} \\ \mu u_{2,3} \\ -\mu\frac{V_4}{V_5}u_{2,3}-\lambda\frac{V_3}{V_5}u_{3,3} \end{pmatrix} \tag{405}$$

It follows that

$$\mathbf{K}_{2j}\mathbf{V}_{,j} = \begin{pmatrix} 0 \\ \mu u_{2,1}+\mu u_{1,2} \\ \lambda u_{1,1}+(\lambda+2\mu)u_{2,2}+\lambda u_{3,3} \\ \mu u_{3,2}+\mu u_{2,3} \\ -\lambda\frac{V_3}{V_5}u_{1,1}-\mu\frac{V_2}{V_5}u_{2,1}-\mu\frac{V_4}{V_5}u_{2,3}-\lambda\frac{V_3}{V_5}u_{3,3}-\mu\frac{V_2}{V_5}u_{1,2}-\mu\frac{V_4}{V_5}u_{3,2}-(\lambda+2\mu)\frac{V_3}{V_5}u_{2,2} \end{pmatrix} \tag{406}$$

so that

$$\begin{aligned}\mathbf{V}^T\mathbf{K}_{2j}\mathbf{V}_{,j} &= \mu u_{2,1}V_2 + \mu u_{1,2}V_2 + \lambda u_{1,1}V_3 + (\lambda+2\mu)u_{2,2}V_3 + \lambda u_{3,3}V_3 + \mu u_{3,2}V_4 + \mu u_{2,3}V_4 \\ &-\lambda V_3 u_{1,1} - \mu V_2 u_{2,1} - \mu V_4 u_{2,3} - \lambda V_3 u_{3,3} - \mu V_2 u_{1,2} - \mu V_4 u_{3,2} - (\lambda+2\mu)V_3 u_{2,2} \\ &= 0\end{aligned} \tag{407}$$

(also as Hughes asserts [78]). Then, applying the no-slip condition, $\mathbf{u} = \mathbf{0}$ on $\partial\Omega_W$:

$$[\mathbf{K}_{2j}\mathbf{V}_{,j}]^{ns} = \begin{pmatrix} 0 \\ \mu(u_{2,1}+u_{1,2}) \\ \lambda(u_{1,1}+u_{2,2}+u_{3,3})+2\mu u_{2,2} \\ \mu(u_{3,2}+u_{2,3}) \\ 0 \end{pmatrix} \tag{408}$$

Finally:

$$\tilde{\mathbf{K}}^v_{31}\mathbf{V}_{,1} = \frac{1}{V_5^3}\begin{pmatrix} 0 \\ \mu u_{3,1} \\ 0 \\ \lambda u_{1,1} \\ -\lambda\frac{V_4}{V_5}u_{1,1} - \mu\frac{V_2}{V_5}u_{3,1} \end{pmatrix} \tag{409}$$

$$\tilde{\mathbf{K}}^v_{32}\mathbf{V}_{,2} = \begin{pmatrix} 0 \\ 0 \\ \mu u_{3,2} \\ \lambda u_{2,2} \\ -\lambda\frac{V_4}{V_5}u_{2,2} - \mu\frac{V_3}{V_5}u_{3,2} \end{pmatrix} \tag{410}$$

$$\tilde{\mathbf{K}}^v_{33}\mathbf{V}_{,3} = \begin{pmatrix} 0 \\ \mu u_{1,3} \\ \mu u_{2,3} \\ (\lambda+2\mu)u_{3,3} \\ -\mu\frac{V_2}{V_5}u_{1,3} - \mu\frac{V_3}{V_5}u_{2,3} - (\lambda+2\mu)\frac{V_4}{V_5}u_{3,3} \end{pmatrix} \tag{411}$$

so that

$$\tilde{\mathbf{K}}^v_{3j}\mathbf{V}_{,j} = \begin{pmatrix} 0 \\ \mu(u_{3,1}+u_{1,3}) \\ \mu(u_{3,2}+u_{2,3}) \\ \lambda(u_{1,1}+u_{2,2}+u_{3,3})+2\mu u_{3,3} \\ -\lambda\frac{V_4}{V_5}u_{1,1} - \mu\frac{V_2}{V_5}u_{3,1} - \lambda\frac{V_4}{V_5}u_{2,2} - \mu\frac{V_3}{V_5}u_{3,2} - \mu\frac{V_2}{V_5}u_{1,3} - \mu\frac{V_3}{V_5}u_{2,3} - (\lambda+2\mu)\frac{V_4}{V_5}u_{3,3} \end{pmatrix} \tag{412}$$

which confirms that

$$\begin{aligned}\mathbf{V}^T\tilde{\mathbf{K}}^v_{3j}\mathbf{V}_{,j} &= \mu u_{3,1}V_2 + \mu u_{1,3}V_2 + \mu u_{3,2}V_3 + \mu u_{2,3}V_3 + \lambda u_{1,1}V_4 + \lambda u_{2,2}V_4 + (\lambda+2\mu)u_{3,3}V_4 \\ &-\lambda V_4 u_{1,1} - \mu V_2 u_{3,1} - \lambda V_4 u_{2,2} - \mu V_3 u_{3,2} - \mu V_2 u_{1,3} - \mu V_3 u_{2,3} - (\lambda+2\mu)V_4 u_{3,3} \\ &= 0\end{aligned} \tag{413}$$

As for the application of the no-slip condition ($\mathbf{u} = \mathbf{0}$ on $\partial\Omega_W$):

$$[\tilde{\mathbf{K}}^v_{3j}\mathbf{V}_{,j}]^{ns} = \begin{pmatrix} 0 \\ \mu(u_{3,1}+u_{1,3}) \\ \mu(u_{3,2}+u_{2,3}) \\ \lambda(u_{1,1}+u_{2,2}+u_{3,3})+2\mu u_{3,3} \\ 0 \end{pmatrix} \tag{414}$$

Putting everything together, we obtain the matrix stemming from the application of the no-slip condition $\mathbf{u} = \mathbf{0}$ on $\partial\Omega_W$:

$$[\tilde{\mathbf{K}}_{ij}n_i\mathbf{V}_{,j}]^{ns} = \frac{\mu}{V_5^2}\begin{pmatrix} 0 \\ (-V_5V_{i+1,1}+V_{i+1}V_{5,1}-V_5V_{2,i}+V_2V_{5,i})n_i \\ (-V_5V_{i+1,2}+V_{i+1}V_{5,2}-V_5V_{3,i}+V_3V_{5,i})n_i \\ (-V_5V_{i+1,3}+V_{i+1}V_{5,3}-V_5V_{4,i}+V_4V_{5,i})n_i \\ 0 \end{pmatrix} + \lambda\left[\frac{-V_5V_{i+1,i}+V_{i+1}V_{5,i}}{V_5^2}\right]\begin{pmatrix} 0 \\ n_1 \\ n_2 \\ n_3 \\ 0 \end{pmatrix} \tag{415}$$

An interesting observation is that components $(2:4)$ of $[\tilde{\mathbf{K}}_{ij}n_i\mathbf{V}_{,j}]^{ns}$ are

$$[\tilde{\mathbf{K}}_{ij}n_i\mathbf{V}_{,j}]^{ns}_{2:4} = [2\mu\mathbf{S}+\lambda\nabla\cdot\mathbf{u}\mathbf{I}]\mathbf{n} \tag{416}$$

where $\mathbf{S}$ is the strain tensor, with components given by

$$S_{ij} = \frac{1}{2}(u_{i,j}+u_{j,i}) \tag{417}$$

Recall that the general deformation law for a Newtonian viscous fluid is (see equation (11) in [78]):

$$\tau_{ij} = 2\mu S_{ij} + \delta_{ij}\lambda\nabla\cdot\mathbf{u} \tag{418}$$

Moreover, the governing momentum equations have the form:

$$\rho\frac{D\mathbf{u}}{Dt} = \nabla\cdot\tau_{ij} \tag{419}$$

If we set $\frac{D\mathbf{u}}{Dt} = \mathbf{0}$ at the wall (i.e., assume the fluid is at rest at the wall), then (419) implies that $\nabla\cdot\tau_{ij} = 0$ at the wall, or $\tau_{ij}\cdot\mathbf{n} = 0$ at the wall (by the divergence theorem). Then (418) implies that $[2\mu\mathbf{S}+\lambda\nabla\cdot\mathbf{u}\mathbf{I}]\mathbf{n} = \mathbf{0}$ at the wall.

C.4 The Matrices $\tilde{\mathbf{K}}^h_{ij}n_i$ and Application of the Adiabatic-Wall Boundary Condition

Let θ denote the absolute temperature. Then, from (45) in [78],

$$\tilde{\mathbf{K}}^h_{ij}n_i\mathbf{V}_{,j} = \mathbf{F}^h_i n_i = \begin{pmatrix} 0 \\ 0 \\ 0 \\ 0 \\ \kappa\theta_{,i}n_i \end{pmatrix} \tag{420}$$

Suppose the wall is adiabatic, i.e., $\theta_{,i} n_i = 0$. Then

$$[\tilde{\mathbf{K}}^h_{ij} n_i \mathbf{V}_{,j}]^{ad} = 0 \tag{421}$$

C.5 Proof of Indefiniteness of Heat Flux Matrix $\tilde{\mathbf{K}}^h_{ij}$ with Harten's Family of Homogeneous Generalized Entropy Flux Functions

Suppose we wish to use a homogeneous entropy flux function, from Harten's family of homogeneous generalized entropy flux functions [77]:

$$H(s) = Ke^{\frac{s}{\alpha+\gamma}} \tag{422}$$

where $\alpha, K \in \mathbb{R}$.

Without loss of generality, consider the 1D case. Refer to [76]. In particular, we have:

$$\mathbf{U} = \begin{pmatrix} \rho \\ \rho u \\ E \end{pmatrix} \equiv \begin{pmatrix} U_1 \\ U_2 \\ U_3 \end{pmatrix} \tag{423}$$

where

$$p = (\gamma - 1)\left(E - \frac{1}{2}\rho u^2\right) \tag{424}$$

It is shown in [76] that with the generalized entropy flux function (422), the entropy variables in terms of the primitive variables are:

$$\mathbf{V} = \frac{p^*}{p}\begin{pmatrix} U_3 + \frac{\alpha-1}{\gamma-1}p \\ -U_2 \\ U_1 \end{pmatrix} \equiv \begin{pmatrix} V_1 \\ V_2 \\ V_3 \end{pmatrix} \tag{425}$$

where

$$p^* = \frac{\gamma-1}{\alpha}\left(V_1 - \frac{1}{2}\frac{V_2^2}{V_3}\right) \tag{426}$$

The inverse transformation is given by:

$$\mathbf{U} = \frac{p}{p^*}\begin{pmatrix} V_3 \\ -V_2 \\ V_1 - \frac{\alpha-1}{\gamma-1}p^* \end{pmatrix} \tag{427}$$

Assuming a calorically-perfect gas,

$$E = \rho\left(c_v T - \frac{1}{2}u^2\right) \tag{428}$$

where T is the temperature (denoted θ in [78]) . Let us work this out in terms of the variables $\mathbf{U}$ and $\mathbf{V}$:

$$\begin{array}{rcl} E & = & \rho c_v T + \frac{\rho u^2}{2} \\ U_3 & = & U_1 c_v T + \frac{U_2^2}{2U_1} \\ V_1 - \frac{\alpha-1}{\gamma-1} p^* & = & V_3 c_v T + \frac{1}{2}\frac{V_2^2}{V_3} \\ V_1 - \frac{\alpha-1}{\gamma-1}\frac{\gamma-1}{\alpha}\left(V_1 - \frac{1}{2}\frac{V_2^2}{V_3}\right) & = & V_3 c_v T + \frac{1}{2}\frac{V_2^2}{V_3} \\ \left(V_1 - \frac{1}{2}\frac{V_2^2}{V_3}\right) - \frac{\alpha-1}{\alpha}\left(V_1 - \frac{1}{2}\frac{V_2^2}{V_3}\right) & = & V_3 c_v T \\ \frac{1}{\alpha}\left(V_1 - \frac{1}{2}\frac{V_2^2}{V_3}\right) & = & V_3 c_v T \end{array} \tag{429}$$

Rearranging,

$$c_v T = \frac{1}{\alpha}\left(\frac{V_1}{V_3} - \frac{1}{2}\frac{V_2^2}{V_3^2}\right) \tag{430}$$

Now, the heat flux is given by: $q_i = -\kappa T_{,i}$. Therefore, we must differentiate T with respect to x_i:

$$\begin{array}{rl} c_v \frac{\partial T}{\partial x_i} & = \frac{1}{\alpha}\left(\frac{V_3 V_{1,i} - V_1 V_{3,i}}{V_3^2} - \frac{V_3^2 V_2 V_{2,i} - V_2^2 V_3 V_{3,i}}{V_3^4}\right) \\ & = \frac{1}{\alpha}\left(\frac{1}{V_3}V_{1,i} - \frac{V_2}{V_3}V_{2,i} + \left(\frac{V_3 - V_1}{V_3^2}\right)V_{3,i}\right) \\ & = \frac{1}{\alpha}\begin{pmatrix} \frac{1}{V_3} & -\frac{V_2}{V_3} & \frac{V_3-V_1}{V_3^2} \end{pmatrix}\mathbf{V}_{,i} \end{array} \tag{431}$$

so that, in the notation of [78], the heat flux matrix is:

$$\tilde{\mathbf{K}}_{11}^h = -\frac{\kappa}{\alpha c_v}\begin{pmatrix} 0 & 0 & 0 \\ 0 & 0 & 0 \\ \frac{1}{V_3} & -\frac{V_2}{V_3} & \frac{V_3-V_1}{V_3^2} \end{pmatrix} \tag{432}$$

The matrix (432) is asymmetric, as Hughes asserts; but that in itself is not a problem, since the stability proof (Theorem 5.3.1) simply requires $\tilde{\mathbf{K}}_{11}^h$ to be positive semi-definite. Note that, for any $\mathbf{x} \in \mathbb{R}^3$:

$$\mathbf{x}^T \tilde{\mathbf{K}}_{11} \mathbf{x} = \mathbf{x}^T \left(\underbrace{\frac{\tilde{\mathbf{K}}_{11}^h + (\tilde{\mathbf{K}}_{11}^h)^T}{2}}_{\equiv (\mathbf{K}_{11}^h)^{symm}} \right) \mathbf{x} \tag{433}$$

Therefore, $\mathbf{x}^T \tilde{\mathbf{K}}_{11} \mathbf{x} \geq 0$ if the symmetric part of $\tilde{\mathbf{K}}_{11}^h$ is positive semidefinite. From (432),

$$\left(\tilde{\mathbf{K}}_{11}^h\right)^{symm} = -\frac{\kappa}{\alpha c_v}\begin{pmatrix} 0 & 0 & \frac{1}{2V_3} \\ 0 & 0 & -\frac{V_2}{2V_3} \\ \frac{1}{2V_3} & -\frac{V_2}{2V_3} & \frac{V_3-V_1}{V_3^2} \end{pmatrix} \tag{434}$$

The eigenvalues of this matrix are:

$$\{\lambda_1, \lambda_2, \lambda_3\} = \left\{ 0, \frac{\kappa}{\alpha c_v}\left(\frac{V_1 - V_3 \pm \sqrt{V_1^2 - 2V_1V_3 + 2V_3^2 + V_3^2 V_2^2}}{2V_3^2}\right) \right\} \tag{435}$$

The first eigenvalue is 0, so we are good to go with that one. Let us look at λ_1. It is non-negative is $V_1 - V_3 \geq 0$.

$$\begin{aligned} V_1 - V_3 &= \frac{p^*}{p}\left(U_3 + \frac{\alpha-1}{\gamma-1}p - U_1\right) \\ &= \frac{p^*}{p}\left(E + \frac{\alpha-1}{\gamma-1}p - \rho\right) \\ &= \frac{p^*}{p}\left(\frac{1}{\gamma-1}p + \frac{1}{2}\rho u^2 + \frac{\alpha-1}{\gamma-1}p - \rho\right) \\ &= \frac{p^*}{p}\left(\frac{1}{2}\rho u^2 + \frac{\alpha}{\gamma-1}p - \rho\right) \end{aligned} \tag{436}$$

Now, we desire $-\rho + \frac{\alpha}{\gamma-1}p + \frac{1}{2}\rho u^2 \geq 0$. Let us see what requirements on α this constraint places:

$$\begin{aligned} -\rho + \frac{\alpha}{\gamma-1}p + \frac{1}{2}\rho u^2 &\geq 0 \\ \frac{\alpha}{\gamma-1}p &\geq \rho\left(1 - \frac{1}{2}u^2\right) \\ &\geq -\rho\frac{1}{2}u^2 \\ \alpha &\geq -\frac{\rho}{p}\frac{1}{2}u^2(\gamma-1) \end{aligned} \tag{437}$$

The right-hand side of (437) is necessarily negative given the physics ($p, \rho > 0$, $\gamma > 1$); therefore if $\alpha > 0$, then $\lambda_2 \geq 0$. Harten has already placed this constraint on α so in fact it is nothing new. Therefore $\lambda_2 \geq 0$ for $\alpha > 0$.

Let us examine the last eigenvalue λ_3. For it to be non-negative, we must have:

$$\begin{aligned} V_1 - V_3 &\geq \sqrt{V_1^2 - 2V_1V_3 + 2V_3^2 + V_3^2V_2^2} \\ V_1^2 - 2V_1V_3 + V_3^2 &\geq V_1^2 - 2V_1V_3 + 2V_3^2 + V_3^2V_2^2 \\ 0 &\geq V_3^2 + V_3^2V_2^2 \\ 0 &\geq V_3^2(1 + V_2^2) \end{aligned} \tag{438}$$

The only way for (438) to hold is if $V_3 = 0$. Let us see if this is possible:

$$V_3 = \frac{p^*}{p}U_1 = \frac{p^*}{p}\rho \tag{439}$$

But requiring this to be zero would amount to requiring $\rho = 0$, which is non-physical. Therefore the last eigenvalue λ_3 will necessarily be negative, unfortunately. The heat flux matrix $\tilde{\mathbf{K}}_{11}$ is *not* positive semi-definite with the choice of Harten's homogeneous generalized entropy flux function (422).

References

[1] L. Sirovich. Turbulence and the dynamics of coherent structures, Part III: Dynamics and scaling. *Quarterly of Applied Mathematics*, 45(3):583–590, 1987.

[2] N. Aubry, P. Holmes, J. Lumley, and E. Stone. The dynamics of coherent structures in the wall region of a turbulent boundary layer. *J. Fluid Mech.*, 192:115–173, 1988.

[3] P. Holmes, J.L. Lumley, and G. Berkooz. *Turbulence, coherent structures, dynamical systems and symmetry*. Cambridge University Press, 1996.

[4] K. Veroy and A.T. Patera. Certified real-time solution of the parametrized steady incompressible Navier-Stokes equations: rigorous reduced-basis *a posteriori* error bounds. *Int. J. Num. Meth. Fluids*, 47:773–788, 2005.

[5] K. Willcox and J. Peraire. Balanced model reduction via the proper orthogonal decomposition. *AIAA J.*, 40(11):2323–2330, 2002.

[6] C.W. Rowley. Model reduction for fluids, using balanced proper orthogonal decomposition. *Int. J. Bifurcation and Chaos*, 15(3):997–1013, 2005.

[7] T. Bui-Thanh, K. Willcox, O. Ghattas, and B. van Bloemen Waanders. Goal-oriented, model-constrained optimization for reduction of large-scale systems. *J. Comp. Phys.*, 224:880–896, 2007.

[8] J.A. Taylor and M.N. Glauser. Towards practical flow sensing and control via POD and LSE based low-dimensional tools. *J. Fluids Eng.*, 126(3):337–345, 2003.

[9] P.A. LeGresley and J.J. Alonso. Investigation of non-linear projection for POD based reduced order models for aerodynamics. AIAA Paper 2001-0926, 39th AIAA Aerospace Sciences Meeting & Exhibit, 2001.

[10] K.C. Hall, J.P. Thomas, and E.H. Dowell. Proper orthogonal decomposition technique for transonic unsteady aerodynamic flows. *AIAA J.*, 38(10), 2000.

[11] T. Lieu, C. Farhat, and M. Lesoinne. Reduced-order fluid/structure modeling of a complete aircraft configuration. *Comput. Methods Appl. Mech. Engrg.*, 195:5730–5742, 2006.

[12] T. Lieu and C. Farhat. Aerodynamic parameter adaptation of CFD-based reduced-order models. AIAA Paper 2007-328, 45th Aerospace Sciences Meeting and Exhibit, 2007.

[13] Z. Bai, P.M. Dewilde, and R.W. Freund. Reduced order modeling. In W.H.A. Schilders and E.J.W. ter Maten, editors, *Numerical Methods in Electromagnetics, Handbook of Numerical Analysis, Volume XIII*, pages 825–895. Elsevier, Amsterdam, 2005.

[14] F. Kwasniok. Empirical low-order models of barotropic flow. *Journal of the Atmospheric Sciences*, 61(2):235–245, 2004.

[15] C.W. Rowley, T. Colonius, and R.M. Murray. Model reduction for compressible flows using POD and Galerkin projection. *Physica D*, 189:115–129, 2004.

[16] T. Bui-Thanh, K. Willcox, and O. Ghattas. Model reduction for large-scale systems with high-dimensional parametric input space. *SIAM J. Sci. Comput.*, 30(6):3270–3288, 2008.

[17] M. Rathinam and L.R. Petzold. A new look at proper orthogonal decomposition. *SIAM J. Numer. Anal.*, 41(5):1893–1925, 2003.

[18] K. Kunisch and S. Volkwein. Galerkin proper orthogonal decomposition for a general equation in fluid dynamics. *SIAM J. Numer. Anal.*, 40(2):492–515, 2002.

[19] M.F. Barone, I. Kalashnikova, D.J. Segalman, and H.K. Thornquist. Stable Galerkin reduced order models for linearized compressible flow. *Journal of Computational Physics*, 228:1932–1946, 2009.

[20] I. Kalashnikova and M.F. Barone. On the stability and convergence of a galerkin reduced order model (rom) for coupled fluid/structure interaction problems. *Int. J. Numer. Meth. Engng.* (submitted), 2009.

[21] J.L. Lumley. *Stochastic tools in turbulence*. Academic Press, New York, 1971.

[22] A. Harten. On the symmetric form of systems of conservation laws with entropy. *J. Comp. Physics*, 49:151–164, 1983.

[23] T.J.R. Hughes, L.P. Franca, and M. Mallet. A new finite element formulation for computational fluid dynamics: I. Symmetric forms of the compressible Euler and Navier-Stokes equations and the second law of thermodynamics. *Comput. Methods Appl. Mech. Engrg.*, 54:223–234, 1986.

[24] S.W. Bova and G.F. Carey. An entropy variable formulation and applications for the two-dimensional shallow water equations. *Int. J. Num. Meth. Fluids*, 23:29–46, 1996.

[25] A. Greven, G. Keller, and G. Warnecke. *Entropy*. Princeton University Press, Princeton, NJ, 2003.

[26] B. Gustafsson and A. Sundström. Incompletely parabolic problems in fluid dynamics. *SIAM J. Appl. Math.*, 35(2):343–357, 1978.

[27] B. Gustaffson, H.O. Kreiss, and J. Oliger. *Time Dependent Problems and Difference Methods*. John Wiley & Sons, New York, NY, 1995.

[28] J. Oliger and A. Sundström. Theoretical and practical aspects of some initial boundary-value problems in fluid dynamics. *SIAM J. Appl. Math.*, 35(3):419–446, 1978.

[29] S. Abarbanel and D. Gottlieb. Optimal time splitting for two- and three-dimensional Navier-Stokes equations with mixed derivatives. *J. Comp. Phys*, 35:1–33, 1981.

[30] B. Gustafsson. *High Order Difference Methods for Time Dependent PDE*. Springer-Verlag, Leipzig, Germany, 2008.

[31] M.F. Barone, I. Kalashnikova, D.J. Segalman, and H.K. Thornquist. Galerkin reduced order models for compressible flow with structural interaction. AIAA Paper 2008-0612, presented at the AIAA 46th Aerospace Sciences Meeting and Exhibit, 2008.

[32] J.S. Hesthaven and D. Gottlieb. A stable penalty method for the compressible Navier-Stokes equations: I. Open boundary conditions. *SIAM J. Sci. Comput.*, 17(3):579–612, 1996.

[33] D. Funaro and D. Gottlieb. Convergence results for pseudospectral approximations of hyperbolic systems by a penalty-type boundary treatment. *Math of Comput.*, 57(196):585–596, 1991.

[34] C. Farhat, P. Geuzaine, and G. Brown. Application of a three-field nonlinear fluid-structure formulation to the prediction of the aeroelastic parameters of an F-16 fighter. *Computers & Fluids*, 32:3–29, 2003.

[35] M.A. Heroux, R.A. Bartlett, V.E. Howle, R.J. Hoekstra, J.J. Hu, T.G. Kolda, R.B. Lehoucq, K.R. Long, R.P. Pawlowski, E.T. Phipps, A.G. Salinger, H.K. Thornquist, R.S. Tuminaro, J.M. Willenbring, A. Williams, and K.S. Stanley. An overview of the trilinos project. *ACM Trans. Math. Softw.*, 31(3), 2005.

[36] B. Kirk, J. W. Peterson, R. H. Stogner, and G. F. Carey. `libMesh`: A C++ Library for Parallel Adaptive Mesh Refinement/Coarsening Simulations. *Engineering with Computers*, 22(3–4):237–254, 2006.

[37] C.K.W. Tam and J.C. Webb. Dispersion-relation-preserving finite difference schemes for computational acoustics. *J. Comput. Phys.*, 107:262–281, 1993.

[38] M.H. Milman and C.-C. Chu. Optimization methods for passive damper placement and tuning. *Journal of Guidance, Control, and Dynamics*, 17:848–856, 1994.

[39] M.P. Castanier, Y.-C. Tan, and C. Pierre. Characteristic constraint modes for component mode synthesis. *AIAA Journal*, 39:1182–1187, 2001.

[40] Y.-C. Tan, M.P. Castanier, and C. Pierre. Power flow analysis of complex structures using characteristic constraint modes. *AIAA Journal*, 43:1360–1370, 2005.

[41] D.J. Segalman. Model reduction of systems with localized nonlinearities. *ASME Journal of Computational and Nonlinear Dynamics*, 2:249–266, 2007.

[42] E.S. Hung and S.D. Senturia. Generating efficient dynamical models for microelectromechanical systems from a few finite-element simulation runs. *IEEE Journal of Microelectromechanical Systems*, 8:280–289, 1999.

[43] P. Ribeiro and M. Petyt. Nonlinear vibration of plates by the hierarchical finite element and continuation methods. *International Journal of Mechanical Sciences*, 41:437–459, 1999.

[44] X. Zhao, E. M. Abdel-Rahman, and A.H. Nayfeh. A reduced-order model for electrically actuated microplates. *Journal of Micromechanics and Microengineering*, 14:900–906, 2004.

[45] H.S. Lim and H.H. Yoo. Modal analysis of cantilever plates undergoing accelerated in-plane motion. *Journal of Sound and Vibration*, 297:880–894, 2006.

[46] F. Moussaoui and R. Benamar. Non-linear vibrations of shell-type structures: A review with bibliography. *Journal of Sound and Vibration*, 255:161–184, 2002.

[47] A.H. Sheikh and M. Hukhopadhyay. Large amplitude free flexural vibration of stiffened plates. *AIAA Journal*, 34:2377–2383, 1996.

[48] A.Y.T. Leung and S.K. Chui. On the non-linear vibration of the von karman square plate by the ihb method. *Journal of Sound and Vibration*, 204:239–247, 1997.

[49] C. Touzé, O. Thomas, and A. Chaigne. Hardening/softening behaviour in non-linear oscillations of structural systems using non-linear normal modes. *Journal of Sound and Vibration*, 273:77–101, 2004.

[50] A.C.J. Luo. An approximate theory for geometrically nonlinear thin plates. *International Journal of Solids and Structures*, 37:7655–7670, 2000.

[51] E.H. Dowell. Nonlinear oscillations of a fluttering plate. *AIAA Journal*, 4:1267–1275, 1966.

[52] B.H.K. Lee, L.Y. Jiang, and Y.S. Wong. Flutter of an airfoil with a cubic restoring force. *Journal of Fluids and Structures*, 13:75–101, 1999.

[53] L. Liu, E. H. Dowell, and J.P. Thomas. A high dimensional harmonic balance approach fo an aeroelastic airfoil with cubic restoring forces. *Journal of Fluids and Structures*, 23:351–363, 2007.

[54] B. Ghadiri and M. Razi. Limit cycle oscillations of rectangular cantilever wings containing cubic nonlinearity in an incompressible flow. *Journal of Fluids and Structures*, 23:665–680, 2007.

[55] D.C. Poirel and S.J. Price. Structurally nonlinear fluttering airfoil in turbulent flow. *AIAA Journal*, 39:1960–1968, 2001.

[56] P.S. Beran, D.J. Lucia, and C.L. Pettit. Reduced-order modelling of limit-cycle oscillation for aeroelastic systems. *Journal of Fluids and Structures*, 19:575–590, 2004.

[57] S.A. Mortara, J. Slater, and P.S. Beran. Analysis of nonlinear aeroelastic panel response using proper orthogonal decomposition. *ASME Journal of Vibration and Acoustics*, 126:416–4221, 2004.

[58] B.I. Epureanu, L.S. Tang, and M.P. Païdoussis. Coherent structures and their influence on the dynamics of aeroelastic panels. *International Journal of Non-linear Mechanics*, 39:977–991, 2004.

[59] A.D. Han and T.Y. Yang. Nonlinear panel flutter using high-order triangular finite elements. *AIAA Journal*, 21:1453–1461, 1983.

[60] D.Y. Xue and C. Mei. Finite element nonlinear panel flutter with arbitrary temperatures in supersonic flow. *AIAA Journal*, 31:154–162, 1993.

[61] H.H. Ibrahim, H.H. Yoo, and K.-S. Lee. Supersonic flutter of functionally graded panels subject to acoustic and thermal loads. *Journal of Aircraft*, 46:593–600, 2009.

[62] F. Ziegler. *Mechanics of Solids and Fluids*. Springer, 1998.

[63] J. Lee. Comparison of the two formulations of $w-u-v$ and $w-f$ in nonlinear plate analysis. *ASME Journal of Applied Mechanics*, 69:547–552, 2002.

[64] D. J. Segalman and C. R. Dohrmann. A method for calculating the dynamics of rotating flexible structures, part 1: Derivation. *ASME Journal of Vibration and Acoustics*, 118:313–317, 1996.

[65] D. J. Segalman, C. R. Dohrmann, and A. M. Slavin. A method for calculating the dynamics of rotating flexible structures, part 2: Example calculations. *ASME Journal of Vibration and Acoustics*, 118:318–322, 1996.

[66] H.M. Hilber, T.J.R. Hughes, and R.L. Taylor. Improved numerical dissipation for time integration algorithms in structural dynamics. *Earthquake Engineering and Structural Dynamics*, 5:283–292, 1977.

[67] T.J.R. Hughes. *The Finite Element Method; Linear Static and Dynamic Finite Element Analysis*. Dover Publications, Inc., 2000.

[68] S.P. Timoshenko and S. Woinowsky-Krieger. *Theory of Plates and Shells*. McGraw-Hill International Book Company, 1959.

[69] J.C. Lagarias, J.A. Reeds, M.H. Wright, and P.E. Wright. Convergence properties of the Nelder-Mead simplex method in low dimensions. *SIAM Journal on Optimization*, 9:112–147, 1998.

[70] P.S. Beran and D.J. Lucia. A reduced order cyclic method for computation of limit cycles. *Nonlinear Dynamics*, 39:143–158, 2005.

[71] A.K. Gopinath, P.S. Beran, and A. Jameson. Comparative analysis of computational methods for limit-cycle oscillations. *47th AIAA/ASME/ASCE/AHS/ASC Structures, Structural Dynamics and materials Conference*, Newport, RI, May 1-4, 2006, 2006.

[72] S. Piperno, C. Farhat, and B. Larroututou. Partitioned procedure for the transient solution of coupled aeroelastic problems. *Comp. Methods Appl. Mech. Engrg.*, 124:79–112, 1995.

[73] E.H. Dowell. Nonlinear oscillations of a fluttering plate. *AIAA Journal*, 7:1267–1275, 1966.

[74] N.C. Nguyen and J. Peraire. An efficient reduced-order modeling approach for non-linear parametrized partial differential equations. *Int. J. Numer. Meth. Engng.*, 76:27–55, 2008.

[75] N.C. Nguyen, A.T. Patera, and J. Peraire. A 'best points' interpolation method for efficient approximatio of parametrized functions. *Int. J. Numer. Meth. Engng.*, 73:521–543, 2008.

[76] M. Gerritsen and P. Olsson. Designing an efficient solution strategy for fluid flows: 1. a stable high order finite difference scheme and sharp shock resolution for the euler equations. *Journal of Computational Physics*, 129:245–262, 1996.

[77] A. Harten. On the symmetric form of systems of conservation laws with entropy. *Journal of Computational Physics*, 49:151–164, 1983.

[78] T.J.R. Hughes, L.P. Franca, and M. Mallet. A new finite element formulation for computational fluid dynamics: I. symmetric forms of the compressible euler and navier-stokes equations and the second law of thermodynamics. *Computational Methods in Applied Mechanical Engineering*, 54:223–234, 1996.

[79] R.F. Heinemann and A.B. Poore. Multiplicity, stability, and oscillatory dynamics of the tubular reactor. *Chem. Engng. Sci.*, 36:1411–1419, 1981.

DISTRIBUTION:

5	MS 1124	Matthew Barone, 6333
1	MS 0899	Technical Library, 9536 (electronic)
1	MS 0123	D. Chavez, LDRD Office, 1011

Sandia National Laboratories